Università degli Studi di Salerno

Dipartimento di Ingegneria Civile

Dottorato in Rischio e Sostenibilità nei Sistemi dell'Ingegneria Civile, Edile ed Ambientale

XXXV Ciclo (2020-2022)

Fotografia digitale per il rilievo e la rappresentazione di dettaglio

Processi image-based per la digitalizzazione a scala sub-millimetrica

Sara Antinozzi

Tutor
Prof. Salvatore Barba

Co-tutor
Dott. Massimo Leserri

Coordinatore
Prof. Fernando Fraternali

Università degli Studi di Salerno
Dipartimento di Ingegneria Civile

Corso di Dottorato in

"Rischio e sostenibilità nei Sistemi dell'Ingegneria Civile, Edile ed Ambientale" XXXV Ciclo (2020-2022)

Fotografia digitale per il rilievo e la rappresentazione di dettaglio

Processi image-based per la digitalizzazione

a scala sub-millimetrica

Sara Antinozzi

Tutor
Prof. Salvatore Barba

Coordinatore
Prof. Fernando Fraternali

Co-tutor
Dott. Massimo Leserri

Dipartimento di *Ingegneria Civile*

Rischio e Sostenibilità *nei Sistemi dell'Ingegneria Civile, Edile ed Ambientale*

Indice

Abstract

The widespread popularity of digital photography and the ongoing implementation of equipment with an extremely high processing power are among the main reasons for the extensive and popular use of image-based surveying techniques. However, especially in extreme conditions, such as activities involving the representation of sub-millimetre details, the systematisation of photogrammetric applications at relatively low costs, as well as the methodological rigour imposed on the technique, generally constitute exceptions to widespread practice. Nevertheless, such circumstances are not to be considered as exceptions in the museum digitisation context, as in cases of accurate representations of numerous small artefacts; moreover, the demand also has a metrological character, as the level of accuracy of the generated models may allow experts to verify or formulate key hypotheses for the valorisation of the asset. The result is an unbalanced scenario, due to the presence of an offer limited both by application specificity and by best practices, thus creating a clear gap with the growing emerging demand catalysed by recent European actions for heritage digitisation. The reasons for a certain mistrust in the use of very close-range photogrammetry are mainly due to the necessary specialist knowledge and the costs, which are not always low, in addition to the further difficulties posed to the surveyor in situ, including the unfavourable context for complex survey campaigns.

Through a necessary in-depth study of the topic and an examination of the instrumentation that can be used, the overall objective of the thesis work can be summarised as the proposal of innovative solutions for the accurate, descriptive and metric representation of objects with millimetre and sub-millimetre characteristics. The specific aim was to close a gap in the representation of objects that were too small for ordinary close-range workflows, or too large for the instruments used in precision micromechanics or microscopy of microorganisms. Hence, the key to this work lies in the systematisation of – truly accessible – approaches for the acquisition and restitution of digital models with a high power of detail, making

it possible to reveal material characteristics, textures and morphologies that were hitherto not always perceptible and/or representable, and do it cost-effectively. In other words, the possibility of representing more data and on a larger scale.
This aim is pursued both by codifying the use of: (i) apparatus commonly used for detailed photogrammetric applications, such as professional cameras with specific optics, but combined with ad hoc designed accessories; (ii) devices born in different fields and subsequently adapted for the purpose, e.g., portable USB microscopes. In this sense, the customisation of specifically designed accessories for the integration of USB microscopes in the photogrammetric process constitutes the innovative part of the experiment.
This scenario will be dealt with by means of a compendium of ten articles written during the doctoral years, which place the purpose and results of the work in the broader context of the current state of international research and manifest the intention to conduct constant research work and continuous scientific verification and dissemination. The introduction to this context and the development of the research activity – a deliberately non-technical and/or specialised approach, connotations for which, otherwise, please refer to the following chapters – is geared towards outlining the motivations behind the thesis work, to promote and encourage reading. Following the contributions, technical considerations (see § *Approfondimenti*) contain more detailed analyses of the photographic and photogrammetric process and a description of the latest activities conducted, followed by a section of concluding considerations and observations on potential future developments.

Sintesi

La grande diffusione della fotografia digitale e la continua implementazione di attrezzature dalla capacità di elaborazione estremamente elevata costituiscono tra le principali ragioni dell'ampio e diffuso impiego di tecniche di rilievo image-based. Tuttavia, specialmente in condizioni limite, come attività di rappresentazione di dettagli sub-millimetrici, la sistematizzazione di applicazioni fotogrammetriche a costi relativamente contenuti, così come il rigore metodologico a cui la tecnica deve soggiacere, generalmente, costituiscono un'eccezione alla pratica comune. Eppure, tali circostanze non sono da considerarsi eccezionali nell'ambito della digitalizzazione museale, come nel caso di rappresentazioni accurate di numerosi piccoli reperti; la domanda, inoltre, ha anche un carattere metrologico, dal momento che il livello di accuratezza dei modelli generati può consentire agli esperti di verificare o formulare ipotesi chiave per la messa in valore del bene. Ne risulta un quadro sbilanciato, per la presenza di un'offerta limitata sia dalla particolarità delle applicazioni che dalle buone prassi, creando, quindi, un'evidente divergenza con la domanda emergente sempre più ampia, mobilitata dalle recenti azioni europee per la digitalizzazione del patrimonio. Le motivazioni di una certa sfiducia nell'utilizzo della fotogrammetria very close-range sono da imputare principalmente alle necessarie conoscenze specialistiche e ai costi, non sempre contenuti, oltre alle ulteriori difficoltà poste al rilevatore in situ, tra le quali l'incertezza del contesto adeguato a campagne di rilievo complesso.
Attraverso un necessario approfondimento del tema e una disamina delle strumentazioni vagliabili, l'obiettivo generale del lavoro di tesi si può sintetizzare nella proposta di nuove soluzioni per una rappresentazione accurata, descrittiva e metrica, di oggetti con caratteristiche millimetriche e sub-millimetriche. Il fine specifico è stato quello di colmare un gap nella rappresentazione di oggetti che risultavano troppo piccoli per gli ordinari workflow close-range, o troppo grandi per le strumentazioni impiegate nel settore della micromeccanica di precisione o della microscopia di microrganismi. Per cui la chiave di lettura del lavoro è nella sistematizzazione di

approcci – veramente accessibili – per l'acquisizione e la restituzione di modelli digitali con un elevato potere di dettaglio, consentendo di rivelare caratteristiche di materiali, texture e morfologie fino a ora non sempre percepibili e/o rappresentabili, e a costi perdipiù abbastanza contenuti. In altre parole, la possibilità di rappresentare un numero maggiore di dati e a una scala più grande. Tale scopo è perseguito sia con la codifica dell'impiego di apparati già utilizzati per applicazioni fotogrammetriche di dettaglio, quali fotocamere professionali con ottiche specifiche, però abbinate ad accessori progettati ad hoc, sia con dispositivi nati in ambiti differenti e successivamente adattati allo scopo, quali i microscopi portatili USB. In tal senso, la customizzazione di accessori ideati appositamente per l'inserimento dei microscopi USB nel procedimento fotogrammetrico costituisce la parte innovativa della sperimentazione.
Questo scenario verrà trattato attraverso un compendio di dieci articoli scritti durante gli anni del dottorato, che collocano lo scopo e i risultati del lavoro nel più ampio contesto dello stato attuale della ricerca internazionale e manifestano il proposito di condurre un lavoro di ricerca costante e una continua verifica e divulgazione scientifica. L'introduzione a questo contesto e allo sviluppo dell'attività di ricerca – una presentazione volutamente di natura non tecnica e/o specialistica, connotazioni per le quali, diversamente, si rimanda ai successivi capitoli – è orientata a delineare le motivazioni sottese al lavoro di tesi, al fine di agevolarne e invogliarne la lettura. A valle dei contributi, considerazioni di carattere tecnico (cfr. § *Approfondimenti*) contengono delle analisi più dettagliate del processo fotografico e fotogrammetrico e la descrizione delle ultime attività condotte, a cui fa seguito una sezione di considerazioni conclusive e riflessioni sui possibili sviluppi futuri.

Introduzione

1. Generalità

Le trasformazioni digitali hanno profondamente rivoluzionato i settori disciplinari che concorrono alla formazione di ingegneri e architetti, senza escludere le procedure di rilievo e di rappresentazione nelle loro diverse applicazioni sia di misura che di conoscenza.

Nel 1995 la celebre pubblicazione *Being Digital* di Nicholas Negroponte profetizzava uno sviluppo digitale 'irreversibile e inarrestabile'[1] di cui oggi sembra essere giunta la fase più matura, caratterizzata dalla presenza imprescindibile delle tecnologie emergenti e della loro più consapevole comprensione.

A poco più di un ventennio dalla diffusione su larga scala della tecnologia digitale, non solo la produzione di strumenti al servizio dei tecnici, ma anche il loro utilizzo è cambiato e spesso influenzato e assorbito da diverse discipline[2], a testimonianza della natura transdisciplinare della società odierna. La rivoluzione compiuta dal digitale risiede, infatti, anche nella progressiva interazione-integrazione di settori che per molto tempo si sono sviluppati separatamente, convergendo verso un insieme di prodotti e di servizi che hanno trasformato professioni e stili di vita.

All'interno di uno scenario così avanguardistico, non è insolito ritrovare una disciplina di vecchia data come la fotografia, anche se qualcuno potrebbe senz'altro affermare che la fotografia abbia già raggiunto il suo apice e che possa essere difficile prevederne importanti sviluppi futuri.

La fotografia sopravvive a sé stessa, nel sostanziale passaggio dall'analogico al digitale e lo fa nelle forme e nei modi più svariati, ramificando e ampliando straordinariamente il suo utilizzo. Sono probabilmente le sue capacità di adattarsi al progresso ad averla

[1] Negroponte, N. *Being Digital*. Vintage Book: New York, New York, Stati Uniti, 1995.

[2] Carpiceci, M. *Fotografia digitale e architettura*. Aracne: Roma, Italia, 2012.

trasformata a tal punto da incorporarla nei più recenti processi di rappresentazione[3], consacrandola, con sempre maggior risalto, a strumento di indagine scientifica.

Dal principio, in effetti, e relativamente all'ambito del disegno, la vocazione tecnica della fotografia l'ha asservita a quella branca del rilievo oggi ben conosciuto come fotogrammetrico.

Il processo tecnico su cui la fotogrammetria si basa – il risalire alle coordinate spaziali di un punto a partire da immagini fotografiche – ha avuto uno sviluppo lungo e complesso, che ha origine nell'invenzione della fotografia stessa[4] e prosegue ininterrotto pressoché fino ai giorni nostri.

Successivamente, l'avvento della fotografia digitale e il superamento di un periodo pioneristico caratterizzato da macchine con scarsa potenza di calcolo, nonché il proficuo contributo dell'informatica, hanno determinato un approccio moderno alla fotogrammetria che potremmo definire 'allargato' e 'non convenzionale'. Nel 2004 già cominciava a circolare il termine "Fotogrammetria 2.0"[5], volendo rimarcare la portata di questa trasformazione che si giovava di apparecchiature dai costi più accessibili, del controllo automatizzato delle procedure fotografiche e del trattamento dei dati, consentendone l'impiego anche in ambiti dove raramente era utilizzata in passato.

La fotogrammetria non ha conosciuto l'obsolescenza nonostante l'emergere di tecnologie che nel corso degli ultimi anni si sono proposte come valide alternative, tra cui l'arrivo e l'impressionante crescita prestazionale del laser scanning. Quindi, le previsioni iniziali di un tramonto della fotogrammetria in favore del laser scanning hanno ceduto il passo a una esaltazione dell'integrazione e complementarità dei dati, rivelando la flessibilità e l'adattabilità del metodo fotogrammetrico, che attualmente, rimane ancora uno dei più completi e versatili. Peraltro, i progressi nella fotogrammetria sono intrecciati a tal punto con quelli della computer vision che a oggi

[3] Rodríguez-Navarro, P. Alcune riflessioni sul "Disegno con la fotografia digitale". *DISEGNARECON, Disegnare con la Fotografia Digitale* 2013, *6(12),* 1-7.

[4] Guidi, G., Russo, M., Beraldin, J.A. Acquisizione 3D e modellazione poligonale.

[5] Paris, L. Photogrammetry 2.0. *DISEGNARECON* 2015, *8(14)*, 1-9.

è difficile immaginare una separazione delle due discipline, così come un rallentamento della ricerca in tal senso. Ciò potrà avere un duplice risvolto: (i) vantaggio per il rilevatore, che assisterà a una crescita del proprio rendimento grazie alle evidenti implementazioni software; (ii) spunti di riflessione per la ricerca in ambito fotogrammetrico, orientata al confronto e all'interscambio con competenze informatiche sulla base di gruppi di lavoro congiunti[6].

2. Dal close-range al very close-range: cenni sullo stato dell'arte

La ormai ampia diffusione e accessibilità della fotogrammetria, nonché il consistente materiale presente in letteratura, renderebbe lo studio delle sue applicazioni non necessariamente un'attività innovativa in sé. Tuttavia, la fotogrammetria è solitamente votata a scale di restituzione territoriale, solo più di recente ad attività a distanza più ravvicinata, a fronte di un numero ancora esiguo di applicazioni sub-millimetriche[7]. La distanza dal soggetto costituisce, come noto, la discriminante tra le diverse applicazioni fotogrammetriche[8]. In particolare, nel segmento della fotogrammetria very close-range, caratterizzata da distanze di acquisizione inferiori al metro, si inserisce la fotogrammetria macro, definita da un rapporto di riproduzione (scala della rappresentazione / scala reale) di 1:1[9].

La riduzione della distanza dal soggetto è motivata da un aumento della richiesta di modelli tridimensionali caratterizzati da elevata accuratezza; difatti, in diversi ambiti altamente specifici – ad esempio con applicazioni di ispezione dimensionale, controllo qualità, progettazione industriale, collaudo e reverse engineering di micro

[6] Forlani, G., Roncella, R., Nardinocchi, C. Where is photogrammetry heading to? State of the art and trends. *Rend. Fis. Acc. Lincei* 2015, *26(1)*, 85-96.

[7] Galantucci, M.L., Guerra, M.G., Lavecchia, F. Photogrammetry Applied to Small and Micro Scaled Objects: A Review. In *Proceedings of 3rd International Conference on the Industry 4.0 Model for Advanced Manufacturing*, Ni, J., Majstorovic, V., Djurdjanovic, D. (eds); Lecture Notes in Mechanical Engineering. Springer, Cham, 2018.

[8] Luhmann, T., Robson, S., Kyle, S., Harley, I. *Close Range Photogrammetry. Principles, techniques and applications.* Whittles Publishing: Dunbeath, Scotland, UK, 2011.

[9] Verdiani, G., Formaglini, P., Giansanti, F., Giraudeau, S. Close-Up, Macro and Micro Photogrammetry and Image Perspective: A Comparative Studio on Different Lenses at Work with Small and Medium Size Objects. *Computer Reviews Journal* 2018, *2*, 235-248.

componenti – si sono individuate e consolidate nel tempo tecniche e strumentazioni appropriate per una descrizione rigorosa di piccoli oggetti e per una loro rappresentazione virtuale 3D (digitalizzazione). Tali approcci, quando senza contatto[10], generalmente si basano sull'acquisizione dell'informazione tridimensionale attraverso due tipologie di sensori, comunemente definiti attivi o passivi, in base al ruolo che la radiazione elettromagnetica recita nel processo di misurazione.
La fotogrammetria macro (anche detta macro-fotogrammetria) rientra nella casistica dei sensori passivi e di rado è impiegata negli ambiti applicativi della metrologia industriale, che giovandosi generalmente di budget cospicui, si orienta su tecnologie a sensori attivi perché considerati strumenti più user-friendly, accurati e/o più rapidi. Fra questi, molto diffusi nella micro-meccanica, i sistemi laser a triangolazione, attrezzature costituite da un emettitore laser che proietta un fascio sull'oggetto mentre una camera, che funge da sensore, rileva la componente riflessa; conoscendo le relative posizioni (baseline), gli orientamenti del sensore e del laser e il modello geometrico si può determinare la posizione spaziale del punto illuminato (o della linea nel caso dei cosiddetti *profilers*). Basati sul medesimo principio, ma proiettando un pattern, rientrano in questa categoria anche i sistemi laser a triangolazione *multi-lines* o *grid-models*. Questi strumenti possono arrivare ad accuratezze nell'ordine del micrometro e risoluzioni del decimo di micrometro.
Una soluzione che ha avuto un ampio riscontro in ambiti meno specifici, grazie alla sua versatilità e facilità d'uso, riguarda gli scanner a luce strutturata, strumenti ottici che consentono la ricostruzione tridimensionale grazie alla proiezione di pattern di luce sugli oggetti da rilevare. Il costo di queste strumentazioni è variabile in funzione delle caratteristiche tecniche dichiarate dal produttore, nonché del software proprietario abbinato, o da abbinare, per il processamento dei dati grezzi (Tabella 1).

[10] I sistemi di misurazione 3D a contatto comprendono le cosiddette macchine di misurazione delle coordinate o CMM: si tratta, generalmente, di un sensore costituito da uno stilo rigido alla cui estremità è posta una piccola sfera che agisce da sonda. La misura CMM avviene 'toccando' il punto o la superficie di interesse e acquisendo la terna di coordinate corrispondenti. Per tale ragione questi sistemi sono anche noti nome "tastatori" (Guidi, G., Russo, M., Beraldi, J. Acquisizione 3D e modellazione poligonale. The McGraw-Hill Companies: New York, NY, USA, 2010).

Tabella 1. Scanner commerciali a luce strutturata appartenenti a differenti fasce di prezzo in funzione delle specifiche tecniche dichiarate dai produttori.

Modello	Accuratezza	Risoluzione	Campo utile	Software	Prezzo
Creaform Handy SCAN 3D	0,03 mm	0,03 mm	310×350 mm^2	non incluso	€ 49.000
Artec Micro	0,01 mm	0,03 mm	90×60×60 mm^3	non incluso	€ 40.000
Artec Spider	0,05 mm	0,10 mm	90×70 mm^2 180×140 mm^2	non incluso	€ 30.000
LMI Tech Gocator 3504	0,01 mm	0,007 mm	12,1×13,2 mm^2	incluso	€ 26.000
EinScan PRO HD	0,04 mm	0,20 mm	310×240 mm^2	incluso	€ 7.700
Scan in a Box	0,04 mm	0,08 mm	100×75 mm^2 600×480 mm^2	incluso	€ 5.500
SOL 3D Scan PRO	0,05 mm	0,30 mm	up to 170×170 mm^2	incluso	€ 2.400
Creality CR Scan01	0,10 mm	0,50 mm	536×738 mm^2	non incluso	€ 700
Revopoint POP 3D Scanner	0,30 mm	0,20 mm	130×210 mm^2	incluso	€ 400

Le specifiche strumentali, che tendono a incidere sul rapporto qualità-prezzo delle apparecchiature, si circoscrivono all'accuratezza, che indica quanto la misurazione effettuata si avvicina al valore vero e alla risoluzione, il grado di apprezzamento della minima variazione di grandezza.
Gli scanner a luce strutturata più performanti, disponibili attualmente sul mercato, sono configurati come scanner da tavolo, raggiungono accuratezze di 0,01 millimetri, risoluzione fino a 0,03 millimetri, sono

dotati di rilevazione del colore e non necessitano obbligatoriamente dell'utilizzo di target per facilitare il processo di registrazione. Il loro costo può superare i 40.000 euro; con prestazioni leggermente inferiori il costo medio può attestarsi intorno ai 15.000 euro. Analogamente, ci si può imbattere in scanner a basso costo, ovvero a partire da 500/1.000 euro, progettati per applicazioni non professionali, con accuratezza e risoluzione conseguentemente molto più basse, non all'altezza dei requisiti richiesti per applicazioni micro-metrologiche (caratterizzazione di dettagli inferiori al decimo di millimetro), ma pur sempre interessanti per un utilizzo didattico e/o per ricostruzioni meno dettagliate.

È possibile che in un prossimo futuro, abbattuti i costi strumentali, hardware il cui impiego è a oggi infrequente saranno utilizzati abitualmente per il rilievo dettagliato. A questa corsa all'ultima e più performante strumentazione non sempre corrispondono riflessioni sulla capacità di individuare lo strumento più adatto alla portata del progetto, al personale tecnico, ai tempi e ai vincoli di budget. Si tratta di sollecitare il dibattito verso l'innovazione, ma anche verso la determinazione di alternative valide dal punto di vista del rapporto costi-benefici, nel tentativo di bilanciare la qualità metrica e descrittiva della rappresentazione con l'ambito applicativo, mettendo al centro il ricercatore e non il solo rilevatore.

Adottando un approccio combinato di teoria e pratica, la ricerca può svolgere un ruolo significativo, trascendendo inoltre la mera tendenza del momento. In tal senso, la versatilità della fotogrammetria consente di valutare alternative competitive anche rispetto alle soluzioni a luce strutturata più recenti. Nell'ottica di voler, dunque, superare coscientemente le problematiche, uno sguardo è da rivolgere alle sfide uniche, ma anche ai vantaggi unici che la fotogrammetria, in particolare quella di piccoli oggetti, pone innanzi al rilevatore. Tra questi, il primo vantaggio riguarda l'indipendenza dell'acquisizione fotogrammetrica dal processo di modellazione tridimensionale, intesa come la possibilità di controllare, ed eventualmente implementare la fase di cattura – nettamente scissa dalla fase di gestione del dato – sulla base di fattori propri del sistema ottico (ad esempio tipologia di sensore, tipologia di obiettivo, coefficienti di distorsione, distanza principale, posizione del punto principale) e di fattori di imaging (ad

esempio, distanze di ripresa, baselines, percentuale di sovrapposizione delle foto, numero di foto sovrapposte, angoli di intersezione della fotocamera)[11]. Ciò comporta, in aggiunta, la possibilità di progettare il rilievo ad una risoluzione variabile (funzione dell'ingrandimento raggiungibile e della conseguente distanza dal soggetto) e quindi selezionabile in funzione delle necessità del rilevatore. Essendo, inoltre, il processamento dei dati grezzi una fase disgiunta e operabile in ambienti software differenti, la qualità della modellazione risulterà soggetta a continue implementazioni ad ogni nuova generazione di software, piuttosto che ad ogni nuova generazione strumentale. Inoltre, non è banale, soprattutto nell'ambito di applicazioni di diffusione dei beni culturali, l'implementazione di modelli veramente realistici con la presenza di un dato texture ad alta definizione, basato sulla mappatura spaziale delle immagini fotografiche sul modello tridimensionale. Un altro aspetto non trascurabile è la flessibilità della strumentazione, intesa come la possibilità di generare da fonti diverse, e in maniera più o meno automatizzata, immagini digitali da impiegare per la fotogrammetria. Infatti, chiunque ormai porta con sé una fotocamera ad alta risoluzione, banalmente integrata nel proprio smartphone – c'è da ammettere neanche dal costo molto contenuto – potenzialmente idonea allo scopo. La diffusione di fotocamere compatte e leggere, come le action camera, contribuisce allo scopo, così come la divulgazione single board computer delle dimensioni di una carta di credito (Raspberry Pi), combinabili con sensori fotografici e corpi ottici sia entry-level che professionali.

Sebbene strumentazioni fotografiche differenti si prestino a raggiungere livelli di dettaglio sufficiente per ricostruzioni sub-millimetriche, gli oggetti piccoli con caratteristiche micrometriche devono essere acquisiti con un alto livello di ingrandimento e ad una risoluzione elevatissima, parametri che influenzano restrittivamente accuratezza e livello di dettaglio del modello finale.

Compatibilmente con gli scopi mensori sopracitati, si può quindi

[11] Dai, F., Feng, Y., Hough, R. Photogrammetric error sources and impacts on modeling and surveying in construction engineering applications. *Visualization in Engineering* 2014, *2(2)*, 1-14.

ricorrere come input fotogrammetrico alla cosiddetta macro-fotografia che, come anticipato, vede un più largo impiego per settori che si sono affacciati recentemente al rilievo very close-range e che giovano maggiormente di tecniche a costi contenuti; tra questi, com'è facile immaginare, particolarmente attivo risulta essere il settore museale. Dal punto di vista delle specifiche della strumentazione adottata si predilige l'impiego di obiettivi fotografici "macro", che, come noto, offrono capacità di ingrandimento prossime al rapporto di riproduzione unitario, garantendo grande incisività e una quasi totale assenza di aberrazioni e distorsioni. In alternativa alle ottiche macro, obiettivi comuni possono essere adattati con dispositivi specifici, i tubi di prolunga, composti da anelli spessi che vengono inseriti tra l'obiettivo e il corpo macchina, modificando la distanza minima di messa a fuoco e quindi consentendo un ingrandimento maggiore con costi minori[12]; tuttavia, ciò può comportare effetti peggiorativi[13], e a volte imprevedibili, sulla qualità dell'immagine, sulla profondità di campo e sulla luminosità dell'ottica.

Adottano la succitata strategia operativa alcuni dei principali studi disponibili in letteratura che affrontano l'acquisizione di piccoli oggetti, con livelli di dettaglio e accuratezza necessariamente elevati (rispettivamente centesimi e decimi di millimetro).

Ad esempio, Arrianza et al.[14], Mate-González et al.[15] e Thompson et al.[16] evidenziano come la fotogrammetria ad elevati ingrandimenti, se correttamente condotta, possa fornire un valido sostituto – e più

[12] Gajski, D., Solter, A., Gašparović, M. Application of macro photogrammetry in archaeology. *The International Archives of the Photogrammetry, Remote Sensing and Spatial Information Sciences* 2016, *XLI-B5*, 263-266.

[13] Rodríguez-Martín, M., Rodríguez-Gonzálvez, P. Suitability of Automatic Photogrammetric Reconstruction Configurations for Small Archaeological Remains. *Sensors* 2020, *20*, 2936-2955.

[14] Arriaza, M.C., Yravedra, J., Domínguez-Rodrigo, M., Ángel Mate-González, M., Vargas, E. G., Palomeque-González, J. F., Aramendi, J., González-Aguilera, D., Baquedano, E. Applications of Micro-Photogrammetry and Geometric Morphometrics to Studies of Tooth Mark Morphology: The Modern Olduvai Carnivore Site (Tanzania). *Palaeogeography, Palaeoclimatology, Palaeoecology* 2017, *488*, 103-112.

[15] Maté-González, M.Á., González-Aguilera, D., Linares-Matás, G., Yravedra, J. New Technologies Applied to Modelling Taphonomic Alterations. *Quaternary International* 2019, *517*, 4-15.

[16] Thompson, J.C., Tyler Faith, J., Cleghorn, N., Hodgkins, J. Identifying the Accumulator: Making the Most of Bone Surface Modification Data. *Journal of Archaeological Science*, 2017, *85*, 105-113.

economico – sulla base di confronti con apparecchiature più costose e meno trasportabili, come i microscopi elettronici a scansione[17]. Atre applicazioni riguardano invece test sui flussi di lavoro fotogrammetrici nel tentativo di snellire le procedure, mantenendo al contempo un'alta affidabilità metrica. In particolare, Collins et al.[18], Menna et al.[19], De Paolis et al.[20] ed Eastwood et al.[21] adottano diverse soluzioni basate sulla stabilizzazione della fotocamera, sull'impiego di basi rotanti e target codificati, su un maggiore controllo delle impostazioni della fotocamera e sull'illuminazione, evidenziando i miglioramenti della qualità del modello e sottolineando il vantaggio di protocolli più controllati.

Ulteriori studi si concentrano sulla gestione della ridotta profondità di campo, caratteristica delle ottiche macro – tuttavia riscontrabile, seppur con effetti minori, in tutte le tipologie di obbiettivi – al fine di limitare i possibili effetti diffrattivi causati dalla estrema chiusura del diaframma, scelta obbligata al fine di estendere la nitidezza (cfr. § *Approfondimenti*). In particolare, questi lavori propongono il focus stacking come soluzione efficace e alternativa alla eccessiva chiusura del diaframma. Questa tecnica, che afferisce alla fotografia computazionale, sfrutta una sequenza di immagini – uno stack – scattate dal medesimo angolo di osservazione, ma catturate con diverse distanze di messa a fuoco (crescenti o decrescenti) al fine di

[17] González, E.R., Pastor, S.C., Casals, J. R. Lost Colours: Photogrammetry, Image Analysis Using the DStretch Plugin, and 3-D Modelling of Post-Firing Painted Pottery from the Southwest Iberian Peninsula. *Digital Applications in Archaeology and Cultural Heritage* 2019, *13*.

[18] Collins, T., Woolley, S.I., Gehlken, E., Ch'ng, E. Automated Low-Cost Photogrammetric Acquisition of 3D Models from Small Form-Factor Artefacts. *Electronics* 2019, *8*, 1441-1458.

[19] Menna, F., Nocerino, E., Morabito, D., Farella, E.M., Perini, M., Remondino, F. An open source low-cost automatic system for image-based 3D digitization. *The International Archives of the Photogrammetry, Remote Sensing and Spatial Information Sciences* 2017, *XLII-2/W8*, 155-162.

[20] De Paolis, L.T., De Luca, V., Gatto, C., D'Errico, G., Paladini, G.I. Photogrammetric 3D Reconstruction of Small Objects for a Real-Time Fruition. *Lecture Notes in Computer Science: Lecture Notes in Artificial Intelligence* 2020, *12242*, 375-394.

[21] Eastwood, J., Sims-Waterhouse, D., Piano, S., Weir, R., Leach, R. Towards automated Photogrammetry. In *Proceedings of the 21st International conference of the European Society for Precision Engineering and Nanotechnology (euspen)*, Technical University of Denmark, Copenhagen, Denmark, 2021.

ottenere un immagine singola con una profondità di campo estesa[22]. Gallo et al.[23], Clini et al.[24] e Kontogianni et al.[25] applicano il focus stacking con un buon successo alla modellazione fotogrammetrica 3D di piccoli reperti, raggiungendo un'accuratezza dell'ordine dei decimi di millimetro. Tuttavia, ci sono alcuni aspetti che dovrebbero essere attentamente considerati sia prima che durante il processo di cattura delle immagini quando si combina fotogrammetria e focus stacking. Infatti, il focus stacking può avere un effetto sulla stima dei parametri di calibrazione, considerando che l'allineamento delle immagini di un singolo stack esegue trasformazioni interne allo specifico algoritmo[26] di stacking utilizzato. Infatti, in relazione alle scelte software di individuazione e successiva generazione dei nuovi pixel, è complesso quantificare il rigore della corrispondenza tra l'immagine finale prodotta e le proiezioni prospettiche originarie. Un'altra più banale considerazione in merito ai limiti del focus stacking riguarda l'aumento del tempo necessario per completare le acquisizioni, strettamente dipendente dal numero di scatti da realizzare per ciascuna angolazione della camera (una circostanza quest'ultima che può andare in contrasto a un processo che possa definirsi 'ottimizzato').
Tomas Luhmann, che nel 2006 aveva pubblicato la prima edizione di "Close Range Photogrammetry" – con l'obiettivo di trasferire le conoscenze su un tema ancora poco discusso[27] – recentemente, nel 2020 ha avuto la necessità di aggiornare per la terza volta i contenuti del

[22] Lastilla, L., Ravanelli, R., Ferrara, S. Modellazione 3D di alta qualità di oggetti inscritti archeologici piccoli e complessi: questioni rilevanti e metodologia proposta. *The International Archives of the Photogrammetry, Remote Sensing and Spatial Information Sciences* 2019, *XLII-2/W11*, 699-706.
[23] Gallo, A., Muzzupappa, M., Bruno, F. 3D reconstruction of small sized objects from a sequence of multi-focused images. *Journal of Cultural Heritage* 2014, *15(2)*, 173-182.
[24] Clini, P., Frapiccini, N., Mengoni, M., Nespeca, R., Ruggeri, L. SfM Technique And Focus Stacking for Digital Documentation of Archaeological Artifacts. *The International Archives of the Photogrammetry, Remote Sensing and Spatial Information Sciences* 2016, *XLI-B5*, 229-236.
[25] Kontogianni, G., Chliverou, R., Koutsoudis, A., Pavlidis, G., Georgopoulos, A. Enhancing close-up image based 3D digitisation with focus stacking. *The International Archives of the Photogrammetry, Remote Sensing and Spatial Information Sciences* 2017, *42*, 421-425.
[26] Sono molte le tecniche e gli algoritmi offerti come soluzioni software che consentono di creare immagini a fuoco sovrapposte. Alcune delle tecniche più diffuse sono l'approccio piramidale, l'approccio a mappa di profondità e l'approccio a pixel ponderati.
[27] Luhmann, T., Robson, S., Kyle, S., Boehm, J. *Close-Range Photogrammetry and 3D Imaging*, De Gruyter: Berlin, Boston, 2020.

proprio saggio, con il fine di porre l'accento su nuova sensoristica low-cost e creare un ponte con aree che non avevano un legame con la fotogrammetria. È stato così evidenziato quanto il campo della fotogrammetria, della metrologia ottica 3D e dell'imaging 3D sia ancora in crescita; un campo, inoltre, in cui la formalizzazione di pratiche di rilievo per oggetti di piccole dimensioni, generalmente compresi tra i 5 e i 50 millimetri, rimangono comunque limitatamente affrontate.
In sintesi, ciò è da imputare a due ragioni significative di cui la prima, come discusso, riguarda i costi elevati delle nuove tecnologie, frutto delle recenti ricerche in campo micrometrico e di conseguenza l'impossibilità di investire in strumentazioni così costose e generalmente poco versatili in contesti che differiscono da quello nativo (CMM, triangolatori laser, olografia conoscopica, interferometria, tomografia assiale computerizzata a raggi-x, microscopia confocale, etc.). La seconda ragione afferisce alla difficoltà di riuscire a ottenere il risultato atteso con alternative relativamente più economiche. Nel caso della tecnica fotogrammetrica, inoltre, c'è da sottolineare il sostanziale contributo di vive competenze specialistiche, oltre che una certa dose di pazienza e perseveranza, necessarie per la ripetitività e il dispendio di tempo che ragionevolmente possono caratterizzare un processo a costi hardware contenuti.
Recentemente, un'altra tipologia di dispositivi compatti, portatili e accessibili, si è affacciata per soddisfare questa esigenza di ingrandire il soggetto, nascendo più come prodotti di consumo che come strumenti specialistici: trattasi di microscopi portatili USB, nati per l'ispezione, l'analisi metrologica bidimensionale e già diffusi nell'industria manifatturiera per il controllo qualità e in campo medico. Si configurano come degli zoom ottici piccoli e maneggevoli, progettati per visualizzare immagine output direttamente a monitor.
Quello che incuriosisce di questi dispositivi è che, a fronte di una spesa di poche centinaia di euro, i produttori offrano un articolo caratterizzato da capacità di ingrandimento elevate, abbinate a dimensioni ridotte. In realtà, va considerato che l'immagine prodotta da un microscopio USB è visualizzata direttamente su un monitor elettronico per l'osservazione (assenza di oculari come nei microscopi tradizionali). Ciò comporta la dipendenza dell'ingrandimento dalla dimensione dell'immagine a monitor, oltre che dalle specifiche del

monitor stesso e dal sensore della camera incorporata. In tal senso, la valutazione dell'ingrandimento implica forme di ingrandimento digitale (interpolazioni), che modificano sensibilmente il suo potere risolutivo. Nonostante la risoluzione (fino a 5MP per i modelli ammiragli) e le dimensioni ridotte del sensore (1/4"), le immagini prodotte sono da considerare di alta qualità per il segmento commerciale in cui si inseriscono. Tuttavia, anche a causa dell'assenza di componenti accessorie come supporti e calibratori che li adattino a scopi fotogrammetrici, sono sporadiche le applicazioni che vedono i microscopi portatili USB impiegati per ricostruzioni tridimensionali dell'intero volume del campione in esame. Meno insolite sono invece modellazioni parziali di oggetti la cui bidimensionalità sia prevalente. Esmaeili et al.[28] sono tra i primi, se non i primi, a suggerire l'impiego fotogrammetrico di questa peculiare strumentazione, con la ricostruzione di una impronta digitale e di un'unghia a partire da una serie di scatti ad assi paralleli ricavati da una sequenza video effettuata con microscopi USB Coolingtech e Medic. Le loro applicazioni, condotte nel 2017, dimostravano che era possibile generare modelli tridimensionali da catture eseguite con microscopi USB, ma non ne analizzavano le accuratezze. Tema, recente e poco discusso in letteratura, che rende da un lato complessi gli sviluppi della ricerca di dottorato, ma dall'altro li connota di una potenziale originalità. Quindi, da queste prime intuizioni si sono poste le basi per immaginare un inserimento dei microscopi USB nel processo fotogrammetrico, con un'accuratezza e precisione adeguate e verificate, secondo un processo ottimizzato per un loro uso diffuso, anche oltre il mero lavoro di tesi.

La valutazione dell'accuratezza può essere condotta attraverso il confronto di modelli omologhi, prodotti con tecniche diverse la cui affidabilità sia ritenuta maggiore in base a specifiche strumentali e a workflow operativi, adottati come riferimento per poi condurre analisi comparative basate sulle distanze tra i modelli. L'ottimizzazione dei processi è da considerarsi sia in termini di rapidità dei flussi di lavoro che di robustezza del modello prodotto.

[28] Esmaeili, F., Ebadi, H. Handy Microscopic Close-Range Videogrammetry. *The International Archives of the Photogrammetry, Remote Sensing and Spatial Information Sciences* 2017, *XLII-4*, 65-67.

La prima accezione si può avvalere dell'implementazione custom delle componenti hardware del sistema, attraverso la sistematizzazione di: accessori per il posizionamento relativo vantaggioso di soggetto e ottica al fine di ridurre al minimo necessario il numero di scatti; di riferimenti metrici per la definizione di un sistema di coordinate locali, messa in scala del modello e miglioramento della procedura di allineamento delle catture.
La seconda accezione riguarda i processi in ambiente Structure from Motion (SfM), da finalizzare ad attributi della modellazione che non siano solo rappresentativi, ma anche affidabili. Ciò con una riduzione dell'errore attraverso processi iterativi di filtraggio della nuvola sparsa (Tie Points filtering) e un controllo del perfezionamento del modello di camera stimato (Sigma0 and Root Mean Square (RMS) Reprojection Errors checking). La prospettiva futura riguarda l'automazione della geometria di presa, attraverso un controllo remoto delle inclinazioni e delle rotazioni frutto di una progettazione a monte, fattore che potrà aggiungersi ai precedenti, semplificando il compito dell'operatore e abbattendo i tempi di acquisizione.
Pertanto, i microscopi portatili USB possono rappresentare una alternativa low cost molto valida sia a strumentazioni convenzionali, ormai consolidate per applicazioni di macro-fotogrammetria, sia a tecniche competitor, soprattutto se le loro prestazioni sono suscettibili di sensibili miglioramenti in fase di acquisizione, sia in termini di qualità del dato, che di tempo richiesto alla campagna di rilievo.

3. Cultural Heritage e digitalizzazione: le motivazioni

Tra i segmenti di mercato che principalmente risentono della mancanza di strumenti flessibili per la rappresentazione dettagliata di piccoli oggetti emerge quello dei musei e delle piccole e medie imprese che afferiscono al settore dei Beni Culturali. Il censimento ISTAT 2020 ha evidenziato una peculiarità distintiva che caratterizza il nostro paese rispetto alle altre nazioni, attestando la grande disseminazione del patrimonio sul territorio e la prevalenza di strutture medio-piccole afferenti a enti locali[29].

[29] Benedetti, D. L'uso dei media da parte dei musei nell'era della pandemia Covid-19: criticità e potenzialità. *Media Education* 2020, *11(2)*, 199-205.

Le ripercussioni di questa frammentazione sulle risorse economiche – e quindi sulla presenza e differenziazione di strumenti e competenze professionali nel settore – accentuano un certo ritardo rispetto al resto d'Europa nella digitalizzazione e nella condivisione online dei beni. Tuttavia, guardando alle opportunità di collaborazione pubblico-private offerte dall'Unione Europea a supporto di musei e collezioni, per lo sviluppo delle politiche sul patrimonio e/o a tutela dello stesso, si palesa un'occasione certamente unica per la realtà italiana, a determinazione dei cospicui investimenti del nuovo programma Ricerca e Innovazione Horizon Europe 2021-2027, il principale programma di finanziamento dell'Unione Europea per la ricerca e l'innovazione, con un budget di 95,5 miliardi di euro[30].

Promuovere la diffusione della conoscenza attraverso una comunicazione 'digital-based' è tra gli aspetti cardine della "vision" del programma e, oltre alla promozione della "Eccellenza scientifica", Pilastro I di Horizon Europe, ben due poli tematici del Pilastro II, "Sfide globali e competitività industriale europea", sono dedicati alla cultura e al digitale, nonché le azioni del Pilastro III, "Europa Innovativa" si confermano a sostegno dell'innovazione[31]. Inoltre, sulla scorta della programmazione precedente (2014-2020), si noti anche il consistente impegno della comunità accademica, con la partecipazione di 87 università italiane al Programma europeo Horizon 2020 e un contributo di 1,8 miliardi di euro[32]. A livello di coordinamento nazionale e nell'ambito della valorizzazione e gestione del patrimonio culturale, tra i numerosi progetti finanziati, solo per annoverarne alcuni, si notino: INCEPTION (2015-2019), per la ricostruzione 3D dinamica nel tempo di manufatti, ambienti costruiti e sociali; PROMETHEUS (2019-2023), con la generazione di un sistema informatico/cognitivo tridimensionale per la digitalizzazione dell'architettura; HERACLES (2016-2019), con lo sviluppo di una piattaforma ICT per la raccolta e l'integrazione di informazioni a

[30] Horizone Europe: research-and-innovation.ec.europa.eu/funding/funding-opportunities/funding-programmes-and-open-calls/horizon-europe_it

[31] Horizon Europe - Investire per plasmare il nostro futuro: research-and-innovation.ec.europa.eu/document/9224c3b4-f529-4b48-b21b-879c442002a2_it

[32] Partecipazione delle Università Italiane ad HORIZON 2020: emiliaromagnainnodata.art-er.it/partecipazione-delle-universita-italiane-ad-horizon-2020/

supporto delle decisioni sul patrimonio; 4CH (2021-2023), per la costituzione di una infrastruttura virtuale del patrimonio digitalizzato con accesso ad archivi di dati, metadati, standard e linee guida; RePAIR (2021-2025), per lo sviluppo di un sistema robotico intelligente in grado di elaborare, abbinare e assemblare in modo autonomo reperti frammentati.

Un altro attualissimo programma, parte del fondo "Next Generation EU", noto anche come "recovery found", è il Piano Nazionale di Ripresa e Resilienza (PNRR), approvato nel 2021 per uno sviluppo verde e digitale del Paese[33].

Uno degli assi strategici del piano è, infatti, la "digitalizzazione e innovazione" di processi, prodotti e servizi, fattori riconosciuti come fondamentali per il miglioramento della competitività italiana. Inoltre, la prima delle sei componenti specifiche del piano (gli ambiti in cui aggregare progetti di investimento e riforma), denominata "Digitalizzazione, innovazione, competitività, cultura e turismo", propone la transizione digitale rilanciando due settori caratterizzanti dell'Italia: il turismo e la cultura.

Ciò evidenzia una volontà di recuperare il terreno perduto in termini di adozione digitale e innovazione tecnologica, come rimarcato dallo stesso piano: l'Italia si collocherebbe al 24° posto fra i 27 Stati membri dell'UE in base all'indice DESI (Digital Economy and Society Index) che monitora a livello europeo le prestazioni digitali e i progressi dei paesi membri UE in termini di competitività digitale.

Da un lato, orbene, gli investimenti europei nello sviluppo di strumenti digitali e tecnologie a sostegno del patrimonio culturale possono oggi consentire a molte realtà differenti di cimentarsi nell'implementazione della rappresentazione dei manufatti conservati ed esposti ai visitatori. Dall'altro, l'interruzione delle attività con il pubblico, e più in generale di quelle finalizzate alla disseminazione del patrimonio, causate come ben noto dalla recente emergenza sanitaria, ha spontaneamente spinto musei, biblioteche, archivi, teatri a produrre un'ondata di contenuti digitali, molti dei quali autoprodotti, che, nello smarrimento generale, hanno costituito un

[33] Piano Nazionale di Ripresa e Resilienza #nextgenerationitalia: www.governo.it/ sites/ governo.it /files/PNRR_0.pdf

appiglio identitario per la collettività. Ciò ha fatto emergere i limiti progettuali di operazioni talvolta considerate banali, ma soprattutto ha delineato un panorama vasto e diversificato, ricco di spunti, riflessioni e idee sulle motivazioni della digitalizzazione.
Le motivazioni della digitalizzazione, tuttavia, non sono vincolate solo a momenti di emergenza eccezionali o a settori specialistici, che piuttosto possono costituire una spinta propulsiva all'attivazione di nuove forme di accesso e fruizione dei dati relativi ai beni culturali. Uno dei principali obiettivi è, infatti, il riconnettere le generazioni giovani e meno giovani al patrimonio, facendo leva sull'attrattività che emerge dalle esperienze ad alto contenuto digitale. Il ruolo del visitatore è, infatti, cambiato significativamente nel corso degli ultimi anni. Si richiede una fruizione dinamica dei beni, coadiuvata dalla trasmissione visiva e sensoriale dei risultati scientifici, con una partecipazione attiva all'Offerta culturale e un contatto dialettico positivo con il patrimonio.
Anche il bacino di utenza risulta ampliato, con destinatari su larga scala che guardano alle caratteristiche del bene in una forma di comprensione immediata, senza necessarie qualifiche specialistiche. Questo, nell'ottica più ampia di un trasferimento delle risorse culturali a un senso di proprietà comunitaria del patrimonio, che contribuisca ad avvicinare il pubblico ai beni e definisca un'Offerta culturale innovativa.

4. Verso la sistematizzazione di un metodo: struttura del lavoro

Le considerazioni su esposte sono state la base di partenza del percorso di Dottorato svolto presso l'Università degli Studi di Salerno, cominciato sul finire del 2019 con il rilievo di una laminetta orfica del V-IV secolo a.C., conservata al Museo Nazionale di Vibo Valentia, un reperto delicato e prezioso in quanto costituisce una delle poche testimonianze del culto delle religioni misteriche in Calabria. Le sue piccole dimensioni, la presenza di un testo realizzato con microincisioni con depressioni che difficilmente giungono ai 2 mm e il materiale altamente riflettente (oro) di cui è costituito, lo rendevano particolarmente ostico da acquisire.
La questione si fece cogente quando l'eccezionalità del manufatto mise in crisi una delle strumentazioni all'epoca più performante e

disponibile. Infatti, un primo tentativo di acquisire l'oggetto fu condotto con lo scanner VIVID 910, un sistema senza contatto della KONIKA-MINOLTA basato sulla triangolazione laser, che a causa dell'elevata riflettanza superficiale dell'oro, restituì risultati insoddisfacenti, soprattutto per quanto riguardava il dettaglio delle microincisioni. Inoltre, pur volendo procedere con la fotogrammetria, le condizioni al contorno complicavano ulteriormente la situazione. L'illuminazione era scarsa: la laminetta è conservata in una sala che dispone solo di un faretto puntuale e indiretto, sfortunatamente insufficiente per lo scopo. Ciò non dava adito a improvvisazioni: acquisire senza supporti ad hoc sarebbe stato impossibile, causa le lunghe esposizioni richieste dalla penuria di luce.

Queste circostanze posero l'accento sull'importanza della pianificazione della campagna di rilievo, finalizzata non solo a raccogliere informazioni sull'oggetto da rilevare, ma anche sul contesto in cui si trova inserito. Come accade spesso, infatti, non ci sono alternative vagliabili se non quella, di riuscire a organizzare lo spostamento di reperti fragili in un ambiente più 'comodo' come, ad esempio, un laboratorio attrezzato. Tuttavia, questi costituiscono casi non banali e, soprattutto, di eccezionale rarità.

Nel caso della laminetta, ulteriori difficoltà erano rappresentate dalla necessità di includere riferimenti metrici nella scena e dall'impossibilità di apporli direttamente su un oggetto così piccolo (larghezza massima di 59 mm, minima di 49 mm e altezza pari a 32 mm) – oltre che così delicato. E, pur risolvendo tale difficoltà, non risultava scontato riuscire a produrre un oggetto calibrato – da impiegare come riferimento metrico – sufficientemente piccolo e quindi adeguato alla scala dell'oggetto da rilevare.

Infine, la questione più spinosa: la gestione dell'area nitida – area entro cui i soggetti ripresi appaiono sufficientemente chiari e i dettagli visibili – che, come noto, si riduce all'aumentare dell'ingrandimento richiesto. Questo comportava l'avere a fuoco solo una piccola porzione dell'artefatto, implicando che solo una modesta percentuale dell'immagine apparisse nitida abbastanza da poter essere utilizzata per la ricostruzione tridimensionale.

I test condotti in quella occasione e le prime soluzioni adottate hanno permesso di collezionare una serie di dati per successivi sviluppi.

I risultati iniziali sono così stati oggetto di una pubblicazione dal titolo *Macro e micro fotogrammetria per la virtualizzazione della laminetta orfica (V-IV a.C.) del Museo Nazionale di Vibo Valentia*, contenuta negli atti del "Convegno Internazionale dei Docenti delle Discipline della Rappresentazione" - UID 2020.
Gli open issue lasciati aperti da questo primo approccio hanno evidenziato quattro componenti hardware da sviluppare per concorrere a configurare un sistema di micro-scansione[34] tridimensionale image-based efficiente:

(i) le caratteristiche del sistema ottico e il sensore, da cui dipenderà il calcolo della profondità di campo in funzione dell'ingrandimento progettato sulla base di lunghezza focale, distanza dal soggetto, distanza principale, apertura di diaframma e diametro del cerchio di confusione;
(ii) un calibratore che funga da riferimento metrico, opportunamente dimensionato, per risultati sufficientemente robusti durante la fase di allineamento, di scala e di ottimizzazione del modello;
(iii) una serie di supporti a sostegno dell'oggetto da rilevare, con possibilità di rotazione a 360°, per posizionare agilmente e vantaggiosamente il soggetto rispetto al sistema ottico;
(iv) infine, un sistema di illuminazione che garantisca condizioni di luce diffusa, così da minimizzare variazioni in intensità delle ombre, luci e colori a seconda delle diverse posizioni che l'oggetto assume durante la fase di acquisizione.

Quest'ultima componente ha da subito registrato la necessità di approfondire e sviluppare soluzioni innovative, con l'adozione di una specifica tecnica di illuminazione, da noi denominata "Ring Reflection Lighting" - RRL. Trattandosi di piccoli oggetti, si è immaginato, per

[34] Si chiarisce che in questo lavoro che il termine 'micro' (utilizzato come: 'micro-scansione', 'micro-fotogrammetria', 'micro-metrologia', etc.) fa riferimento alla risoluzione del rilievo in termini di GSD – la distanza, espressa in multipli o sottomultipli di lunghezza, tra i centri di due pixel adiacenti dell'immagine (Orych, A. Review of methods for determining the spatial resolution of UAV sensors. *The International Archives of the Photogrammetry, Remote Sensing and Spatial Information Sciences* 2015, *Volume XL-1/W4,* 391-395) – che nelle applicazioni tende a essere nell'ordine dei micrometri; 'micro' è inoltre utilizzato nella medesima funzione del termine 'very close-range' che, però, fa riferimento a ridotte distanze dall'oggetto.

una più efficiente acquisizione, una collocazione su base rotante con condizioni di luce vantaggiose in termini di ripresa fotografica e che, al contempo, non comprometta – anzi eventualmente migliori – la ricostruzione della geometria. A questo fine è necessario impiegare un tipo di luce che non incida direttamente sull'oggetto: a tale scopo l'oggetto, assieme a una base rotante, è posto su un pannello orizzontale costituito da un materiale diffusore, un pannello in plexiglas, retroilluminato da una torcia flash. La luce proveniente dal basso è riflessa sull'oggetto grazie all'impiego di un cilindro in forex bianco, concentrico alla base rotante, ma di diametro maggiore, cosicché la differenza fra i diametri determini un anello di luce che rimbalza sulla superficie cilindrica – che funge, quindi, da pannello riflettente – illuminando uniformemente l'oggetto.
Agli elencati quattro fattori strumentali, si aggiungono fattori tipologici intrinsechi del vastissimo e variegato patrimonio culturale a scala di dettaglio. Nello specifico, la selezione di oggetti, che per dimensioni e per complessità permettessero di stressare il sistema facendone emergere i punti deboli, si è basata su una valutazione delle caratteristiche sia superficiali che morfologiche[35].
Tali features consentono di identificare il livello di complessità di un oggetto e la conseguente definizione del progetto di rilievo.
Il fine è stato quello di individuare un approccio versatile, che, con minime variazioni in strumentazioni e accessori, si adattasse alle differenti casistiche, sulla base di una riflessione progettuale condotta sull'analisi di fattori caratterizzanti. Fattori che possiamo così identificare:

- comparabilità dimensionale, ovvero la distribuzione delle masse e il rapporto delle dimensioni X, Y o Z dell'oggetto. Gli scenari peggiori riguardano oggetti sottili, a sviluppo prevalentemente longitudinale o piano;
- complessità topologica, relativa alle proprietà geometriche del manufatto e in particolare alla presenza di buchi o di fori ciechi che non lo configurano come uno spazio semplicemente connesso;

[35] Apollonio, F.I., Fantini, F., Garagnani, S.; Gaiani, M. A Photogrammetry-Based Workflow for the Accurate 3D Construction and Visualization of Museums Assets. *Remote Sensing* 2021, *13*, 486-515.

- libertà logistica, che riguarda le condizioni al contorno con riferimento alla possibilità di lavorare senza ostacoli orbitando attorno a esso e/o di spostarlo liberamente;
- rapporto di risoluzione, il rapporto tra la dimensione massima dell'oggetto e la risoluzione del modello digitale (distanza media tra i vertici del modello); a valori elevati corrisponde un maggiore dettaglio richiesto e quindi una maggiore complessità del rilievo;
- complessità superficiale, influenzata da fattori geometrici (micro-depressioni, rugosità, incisioni, ecc.), dalla caratterizzazione radiometrica del materiale e dalla omogeneità della texture;
- limite visivo, che dipende dalla presenza di parti non osservabili direttamente per questioni morfologiche dello stesso oggetto e dalla conseguente impossibilità di acquisirle perché strumentalmente non sempre visibili.

Sulla base di questi fattori sono stati individuati altri piccoli manufatti che rispecchiassero una complessità accentuata e che consentissero di avere contezza della qualità descrittiva del processo fotogrammetrico attraverso un confronto con strumentazioni a luce strutturata. Una nuova occasione ci è stata offerta da un'epigrafe funeraria (di dimensioni leggermente maggiori, 31×20 cm con uno spessore di 3,5 cm) realizzata in marmo pario e proveniente da Velia, antica polis della Magna Grecia parte dal Parco Archeologico di Paestum e Velia. Questo manufatto riporta un'iscrizione poco leggibile, perché erosa nel tempo dagli agenti atmosferici: le incisioni non superano una profondità di 2 mm. In questo caso, l'implementazione di tecniche sia image-based che range-based ha contribuito alla lettura delle iscrizioni, permettendo di recuperare molte informazioni superficiali non visibili a occhio nudo. Tali approfondimenti sono confluiti nell'articolo *Digital survey and reconstruction for enhancing epigraphic readings with erode surface*, pubblicato nell'ambito di METROARCHEO 2021 - "The International Conference on Metrology for Archaeology and Cultural Heritage".
Con l'intenzione di raggiungere ingrandimenti maggiori, la possibilità di utilizzare i microscopi USB nei processi image-based di ricostruzione tridimensionale, come già emerso in maniera empirica, è stata successivamente codificata. Così, accanto alla sistematizzazione di pratiche fotogrammetriche con l'impiego di strumentazioni fotografiche

più o meno convenzionali, gli studi successivi sono stati orientati a una sorta di processo di avvicinamento all'impiego di nuovi hardware, in particolare i microscopi USB, a fini fotogrammetrici.
La collaborazione con la Dino-lite[36], leader nel mercato industriale dei microscopi portatili digitali, ha consentito di sperimentarne diversi modelli (AM 4113 ZT Universal, AM 73915 MZTL High Speed, AM 7013 MZT Universal), potendone studiare le differenti caratteristiche. Grazie a questo sodalizio, nel corso delle ricerche sono state condotte diverse applicazioni, proponendo l'uso di questi strumenti – a oggi con risultati più che apprezzabili – nel processo fotogrammetrico. Non ideati come strumenti per ricostruzioni tridimensionali image-based, questi microscopi USB, per quanto semplici e intuitivi, hanno destato non poche difficoltà d'uso, principalmente afferenti alla necessità di limitare le vibrazioni durante lo scatto e garantire una inquadratura sufficiente alla sovrapposizione per una corretta ricostruzione.
I successivi adattamenti, quali la produzione di una serie di calibratori e supporti sia per gli oggetti che per le ottiche, resisi via via necessari sulla base delle evidenze sperimentali sono sempre stati condotti con l'obiettivo di mantenere contenuti i costi per rimanere nell'ambito delle strumentazioni di tipo low-cost. I relativi test eseguiti su alcune monete con un primo allestimento strumentale hanno condotto alla pubblicazione dal titolo *3Dino System, Shortening Distances in Precision Surveys*, contenuta negli atti del "Convegno Internazionale dei Docenti delle Discipline della Rappresentazione" - UID 2021. Lo studio, quindi, ha perseguito lo scopo di determinare una iniziale configurazione low-cost, completa e portatile, basata sull'impiego dei microscopi USB per la scansione image-based e verificato la possibilità di raccogliere in un unico sistema, da noi denominato "3Dino", le diverse componenti hardware messe in luce durante il primo anno.
L'oggetto selezionato per stabilire se il sistema di registrazione digitale potesse supportare le esigenze di una ricerca condotta con tutti i crismi, è stato una moneta bronzea del diametro di circa 1,2 cm proveniente, ancora una volta, da Velia. Il reperto fa parte di un gruppo di oltre mille esemplari simili, riferibili alla stessa produzione databili alla seconda metà del I secolo a.C. Nel caso specifico, inoltre,

[36] Dino-lite homepage: www.dino-lite.com

particolare attenzione è stata riposta nella progettazione di un calibratore piano, in analogia a simili casi studio e che consentisse un uso combinato e agile con il microscopio.
Il primo calibratore, da noi denominato "3Dino Plate", è costituito da una piastra in PLA ottenuta con una stampa 3D a filamento, delle dimensioni di 18×15 cm e caratterizzata da un pattern ortogonale di 99 fori troncoconici, con un angolo di svasatura di 60° e diametro della base minore pari a 0,35 mm. L'accuratezza del calibratore, in base ai settaggi della stampa 3D e alle valutazioni dei relativi scarti, ovvero alla conformità della posizione effettiva dei fori rispetto al file di progetto, è stata stimata in 0,1 mm, assunto come valore dell'errore strumentale del sistema (ossia l'accuratezza dei markers). Le coordinate di ciascun foro – rispetto a un sistema di riferimento locale – sono note all'operatore e possono essere facilmente importate nel progetto fotogrammetrico: ciò ha consentito di utilizzare il pattern forato come una griglia di punti di controllo (GCP), omogeneamente distribuita su tutta l'area di interesse per l'ottimizzazione dei parametri che governano l'orientamento. Per garantire risultati più robusti nella fase di allineamento è stato poi disegnato un pattern adesivo applicato sul calibratore, geometricamente e cromaticamente non ripetitivo, dotato di target codificati. Il sistema ha previsto, infine, l'alloggiamento del "3Dino Plate" su un binario a scorrimento, che permettesse la traslazione, manuale in questa prima sperimentazione, della piastra di calibrazione rispetto al microscopio USB. Questo era alloggiato su una staffa verticale, con l'asse ottico ortogonale al calibratore (acquisizioni parallele), consentendo di scattare una serie di immagini con sufficiente sovrapposizione in maniera agile semplicemente facendo scorrere la piastra calibrata sotto l'ottica. Il sistema permetteva di acquisire, nel caso di oggetti di dimensioni massime inferiore ai 2 cm, circa 400 scatti all'ora con ingrandimenti digitali moderati di 20×. Si precisa che per ingrandimento digitale si intende la capacità di un microscopio di produrre un'immagine di un oggetto a una scala più grande della sua dimensione effettiva grazie a caratteristiche sia intrinseche, specifiche ottiche del microscopio, che estrinseche, come l'interpolazione nella visualizzazione del dato (cfr. § *Approfondimenti*).
Appurato il vantaggio inziale dell'apparato proposto, il lavoro di ricerca è proseguito confrontando, inoltre, due nuovi microscopi della

Dino-Lite, differenti per dotazione di funzioni aggiuntive, anno di fabbricazione e fasce di prezzo: il primo del valore di circa 250 euro nel 2018 (l'AM 4113 ZT Universal, con 1,3 MP), il secondo, di più nuova fabbricazione, fornitoci in prova per l'occasione direttamente dai produttori, dal costo di 1000 euro (l'AM 73915 MZTL High Speed, con 5 MP). L'elemento che distingueva nettamente questi due microscopi era la Working Distance - WD, ovvero la distanza lineare tra l'estremità dell'ugello del microscopio e l'oggetto da rilevare, fattore che incide direttamente sull'ingrandimento (Magnification Factor - MF), sull'area inquadrabile (Field Of View - FOV) e sull'area nitida (Depth Of Field - DOF) dell'immagine acquisita.
Ulteriore discriminante è costituita dalle diverse modalità di funzionamento dei due apparecchi: per il modello "Universal" disponibile unicamente la modalità "Normal"; per il modello "High Speed" erano disponibili anche le modalità Extended Depth Of Field - EDOF (combinazione di più scatti su differenti piani di messa a fuoco per estendere l'area nitida), Extended Dynamic Range - EDR (sovrapposizione di immagini con differenti esposizioni per caratterizzare i dettagli di aree troppo scure o troppo luminose).
Le evidenze emerse da questa comparazione sono state pubblicate in *3Dino: configuration for a micro-photogrammetric survey. Applying Dino-Lite microscope for the digitalization of a cuneiform tablet*, contenuta negli Atti del convegno eCAADe 2021. Per il lavoro ci siamo avvalsi di una prima collaborazione con il Politecnico di Milano, sotto la forma di un tirocinio curriculare presso il locale Dipartimento di Architettura, Ingegneria delle Costruzioni e Ambiente costruito.
Quello che differenzia sostanzialmente le ricerche di questo nuovo lavoro è la volontà di ricostruire un'oggetto nella sua tridimensionalità, superando l'approccio quasi esclusivamente nadirale delle acquisizioni precedenti (con prese parallele). Fino a questo momento, il sistema "3Dino" non era ancora progettato per inclinare l'ottica del microscopio (ovvero, operare con prese convergenti) rispetto al piano di appoggio; ciò a causa delle iniziali perplessità sulle limitazioni dei microscopi USB nell'acquisire oggetti con una terza dimensione più accentuata rispetto a quella di una lamina o di una moneta. Difatti, i tempi di acquisizione erano già abbastanza lunghi, e le procedure onerose, limitandoci a sole due

superfici (fronte e retro, per così dire) del reperto: il dover aumentare necessariamente il numero di scatti, per tentare di restituire un modello veramente tridimensionale, costituiva sulla carta una vera e propria scommessa. Anche per tali ragioni, i primi test a prese convergenti sono stati condotti su una replica di una tavoletta cuneiforme spessa quasi 1 centimetro, complessa e dettagliata quanto l'originale. La necessità di acquisire le superfici laterali dei bordi ha richiesto l'implementazione di accessori ideati sulla base delle casistiche precedentemente affrontate, quali l'illuminazione anulare, un nuovo calibratore e la possibilità di inclinare l'ottica del microscopio rispetto al soggetto (con la gestione della profondità di campo ridotta che l'inclinazione comporta).
Per quanto concerne gli accessori: l'illuminazione è stata modificata e snellita, inoltre i suoi costi sono stati abbattuti, sostituendo la centralina flash fotografica con una illuminazione LED integrata a un cilindro diffondente; il calibratore è stato modificato nella profondità dei fori e nell'interasse, consentendo l'individuazione di più punti di coordinate note e quindi l'utilizzo di un numero più elevato di Control Points e di Check Points.
Per quanto riguarda la gestione della profondità di campo, si tenga presente che uno dei concetti fondamentali della fotografia riguarda la messa a fuoco del soggetto, considerando che questa avvenga rispetto a un unico – e solo – piano parallelo al sensore dell'apparecchio fotografico. Un esempio emblematico è quello della riproduzione dettagliata delle tavolette cuneiformi, la cui forma a cuscino determina una variazione di quota tra gli angoli e la zona centrale del manufatto; se la regolazione della messa a fuoco è effettuata in corrispondenza della superficie centrale, generalmente i quattro spicchi periferici della tavoletta risulteranno fuori fuoco (o sfocati) perché idealmente contenuti in un piano parallelo al sensore, ma arretrato di diversi millimetri rispetto a quello che contiene la porzione centrale. Tecnicamente, quindi, la regolazione avviene in un punto e si estende a quell'unico piano passante per il punto di taratura e parallelo al sensore. Solamente se gli oggetti fotografati sono assimilabili ad un unico piano (come nel caso della laminetta e delle monete), limitandosi ad acquisizioni parallele, il problema dell'area nitida diventa trascurabile.

Ma che cosa accade ai punti non contenuti nel piano di messa a fuoco? Il concetto di area nitida ruota attorno alla percezione che si ha dei punti fuori dal piano di messa a fuoco che, osservati a una certa distanza, saranno giudicati come sufficientemente nitidi (puntiformi piuttosto che circolari). Per cui è possibile definire non più solo un piano, ma uno spazio fra due piani paralleli a quello del sensore entro il quale i punti, quelli più vicini e quelli più lontani, appaiono accettabilmente nitidi. Questa regione, comunemente definita area nitida riferendosi al piano bidimensionale dell'immagine prodotta, prende il nome di profondità di campo.
Condurre delle acquisizioni inclinate per oggetti a prevalenza bidimensionale e/o, in generale, acquisire oggetti con dimensioni comparabili lungo i tre assi e quindi non assimilabili a un semplice piano, comporta il non trascurare la misura della profondità di campo, parametro complesso peraltro dipendente da altre grandezze quali lunghezza focale, distanza dal soggetto, distanza principale, apertura di diaframma e diametro del cerchio di confusione. Un calcolo e una progettazione della geometria di cattura sono diventati, a questo punto, necessari (cfr. § *Approfondimenti*).
Tali approfondimenti sono stati oggetto di studi sulle caratteristiche delle due apparecchiature implementate, una fotocamera digitale SRL full frame e il microscopio portatile USB. Nello specifico, la ricerca si è così focalizzata sull'individuazione del metodo e della geometria di acquisizione più adatti a gestire il problema della ridotta profondità di campo per ottenere una base[37] per la definizione di un gemello digitale, completo nel suo sviluppo tridimensionale.
I risultati sono stati poi confrontati con un set di dati di riferimento provenienti da un'acquisizione a sensore attivo per la necessaria validazione della procedura. Le operazioni sono state condotte senza l'ausilio di tecniche per l'elaborazione digitale delle immagini finalizzate all'estensione 'a posteriori' della profondità di campo, quale la procedura di focus stacking; ciò al fine di testare la bontà dei risultati mantenendo il processo snello anche nei tempi di acquisizione.

[37] Un gemello digitale si distingue dal modello digitale, poiché ne costituisce una successiva implementazione. Pertanto, il gemello digitale, sulla base della virtualizzazione, prevede successive implementazioni (inserimento di sensori sull'oggetto reale che comunicano col modello digitale) per compiere simulazioni.

Come accennato in precedenza, il focus stacking consiste nell'acquisire più immagini a diversi piani di messa a fuoco, successivamente fuse in un'unica immagine nitida nel suo complesso. Senza voler scendere nel dettaglio, tale operazione richiede, notoriamente, molto tempo per essere effettuata nel rispetto rigoroso delle procedure fotogrammetriche. Si è accennato a una sperimentazione in tal senso con la funzionalità aggiuntiva Extended Depth Of Field - EDOF di Dino-Lite, automatica e basata sulla fusione di immagini acquisite a messa a fuoco variabile, che tuttavia è risultata non migliorativa in termini di qualità delle immagini, ovvero poco risolutiva e di circa dieci volte superiore in termini di tempo speso per le acquisizioni. Ogni variazione della messa a fuoco, infatti, comporta una variazione della lunghezza focale, che modifica il campo visivo e la prospettiva[38], affliggendo il processo con un grado di incertezza non tracciabile e risultati poco affidabili. Per tale ragione è risultato preferibile spostare l'intero sistema ottico su una slitta micrometrica per mettere a fuoco i diversi piani senza variazioni di messa a fuoco; tuttavia tale metodo richiede un'automazione del sistema meccanico esterno al sistema ottico, che vada oltre un più semplice e meno costoso algoritmo software di "variable-focus-based" (tali circostanze rimangono uno spunto di approfondimento aperto che denota la necessità di risolvere il problema della profondità di campo con procedure ottimizzate). Queste tematiche sono affrontate nella pubblicazione *Optimized Configurations for micro-photogrammetric surveying adaptable to macro optics and digital microscope* sulla rivista "International Archives of the Photogrammetry, Remote Sensing and Spatial Information Sciences", con un'estensione dei contenuti nel più recente paper *Cuneiform tablets microsurveying in a photogrammetric optimized configuration* pubblicato sulla rivista "HERITAGE".
Le ricerche hanno restituito risultati positivi e ciò ci ha spinto a effettuare dei nuovi test su delle tavolette cuneiformi originali, conservate presso la Ghent University, in Belgio; in questa sede, inoltre, sono stati approfonditi alcuni aspetti teorici, garantendo un

[38] Clini, P., Frapiccini, N., Mengoni, M., Nespeca, R., Ruggeri, L. SfM technique and Focus Stacking for digital documentation of archaeological artifacts. *The International Archives of the Photogrammetry, Remote Sensing and Spatial Information Sciences* 2016, *XLI-B5,* 229-236.

flusso di lavoro più rigoroso, con l'arricchimento delle collaborazioni con la locale "Assyriology Unit of the Department of Languages and Cultures" e del "3D Survey Group" del Politecnico di Milano.
Nel dettaglio, l'attenzione è stata rivolta all'identificazione di un modello geometrico di camera in ambiente software SfM Agisoft Metashape compatibile con il microscopio USB utilizzato (AM 7013 MZT) e all'individuazione e verifica della distanza principale, operando ancora in mancanza di dati EXIF. Quindi, partendo dai valori noti dichiarati dal produttore e utilizzando un target di calibrazione, costituito da una scacchiera quadrata con passo di griglia di 1 mm, è stata validata la bontà del modello di camera computato dal software per i microscopi USB. Ciò ha consentito di conoscere a priori, per ciascun ingrandimento scelto, un valore prossimo a quello di distanza principale calcolato durante la fase di allineamento delle immagini: partendo da un valore input vicino a quello reale, la procedura di bundle-block adjustment convergerà più velocemente, ottimizzando i tempi di elaborazione.
Accanto a queste riflessioni sui parametri di orientamento, ulteriori implementazioni hanno visto un aumento del numero di riferimenti locali sul calibratore, grazie all'impiego di una stampante tridimensionale EOS M270 a produzione additiva di polvere d'acciaio. È stato così realizzato un pattern di 279 fori tronco-conici (rispetto ai 99 precedenti), con un angolo di svasatura di 60° e un diametro di base minore di 0,35 mm. Inoltre, la forma del piatto è stata modificata da rettangolare a circolare per meglio consentire la rotazione dell'oggetto rispetto al sistema ottico.
La geometria di acquisizione a prese prevalentemente parallele è stata poi confrontata con un secondo sistema a prese continue convergenti basato sul minimizzare l'area di contatto con il manufatto (limitare la presenza di punti ciechi) e sull'impiego di un semplice calibratore adesivo. Il confronto tra queste due geometrie di acquisizione (effettuato rispetto a un modello di riferimento ottenuto da luce strutturata in ambiente software CloudCompare), ha confermato che piccoli manufatti caratterizzati da una terza dimensione più accentuata rispetto a quella di una lamina o di una moneta richiedano più set di acquisizione con diverse inclinazioni del microscopio. Pertanto, se il sistema a prese parallele si è dimostrato performante

per i casi studio precedenti, nel caso delle tavolette cuneiformi – e, in generale, di oggetti dallo spessore non trascurabile – il sistema a prese convergenti consentiva di ottenere risultati più accurati, facilitando al contempo l'operatore nel realizzare più prese nel medesimo tempo, con una maggiore varietà di inclinazioni.
Nella successiva pubblicazione *Geometrical feature identification of cuneiform signs on micro survey reconstruction* è stato poi condotto uno studio caratterizzato da un più spinto livello di ingrandimento rispetto alle precedenti applicazioni; con l'impiego di microscopi Dino-Lite sono stati raggiunti valori di magnificazione di 40×, corrispondente ad un GSD di 3.8 μm/px (diversamente, in precedenza, era stata impiegata una magnificazione di 20×, pari a 7,6 μm/px di GSD).
Il nuovo livello di dettaglio ha permesso di esaltare – attraverso una rappresentazione particolareggiata – la complessità formale e materiale, spesso non percepibile ad occhio nudo, del patrimonio culturale di dimensioni ridotte; è così possibile attuare una metodologia in grado di enfatizzare il valore di beni difficilmente apprezzabili nella loro configurazione espositiva tradizionale, per una rinnovata fruizione pubblica. A tale proposito, il contributo *3D digital tools for the archaeological massive artifacts documentation*, pubblicato negli atti del "Convegno Internazionale dei Docenti delle Discipline della Rappresentazione" - UID 2022, sintetizza alcune esperienze di acquisizione su diversi manufatti afferenti alle collezioni del Museo Archeologico Nazionale di Crotone, applicando tecnologie integrate e illustrando un rigoroso processo metodologico di analisi e controllo. Lo studio è frutto della collaborazione con il "Dipartimento di Architettura" dell'Università degli Studi di Palermo e si inserisce, all'interno del Progetto "Kroton Lab", promosso da NAOS LAB, così come il contributo sulla laminetta orfica nell'ambito del Progetto "Visualizing Innovative and Social Artworks", finanziati con fondi POR Calabria per la promozione della ricerca e dell'innovazione, al fine di introdurre nuovi meccanismi di fruizione del patrimonio.
In questa nuova esperienza è di fatto aggiunta un'ulteriore variabile ai sei fattori introdotti e che finiscono col caratterizzare il livello di complessità: il tempo utile disponibile per le acquisizioni in situ, parametro di cui tener conto per un processo che, come accennato,

possa essere definito 'ottimizzato'. Inoltre, si affronta il trattamento dei dati collezionati relativamente alla gestione della mesh per la disseminazione dei modelli su piattaforme di condivisione aperta.
Altri due capitoli riguardano una riflessione metrologica per la determinazione dell'accuratezza di un modello fotogrammetrico in relazione alle sue caratteristiche geometriche: *Methodologies for assessing the quality of 3D models obtained using close-range photogrammetry* e *A statistical analysis for the assessment of close-range photogrammetry geometrical features*. In questi ultimi studi si pone l'accento sul problema della tracciabilità e della affidabilità delle proprietà di virtualizzazione, prendendo in considerazione, oltre alla fase di acquisizione, anche il processamento dei dati in ambiente software. L'intento è quello di scoprire il rovescio della medaglia: quali sono i rischi che si corrono al giorno d'oggi a causa della semplicità di generazione di geometrie tridimensionali; come la diffusione di hardware e software image-based completamente automatizzati possa essere controllata consapevolmente dall'operatore; a quali parametri prestare attenzione all'interno di processi sempre più automatizzati che per questo rendono incredibilmente più complesso il tracciamento della qualità dei risultati.
Il quadro presentato (Tabella 2) definisce in generale una linea di ricerca applicata alla rappresentazione digitale di dettaglio con tecniche image-based. L'idea è quella di raccontare attraverso dieci pubblicazioni scientifiche le esperienze che hanno caratterizzato un originale 'percorso a ostacoli' per il rilievo di piccoli oggetti.
Le procedure descritte attraverso le differenti esperienze per la raccolta delle informazioni – metodi – sono state riversate gradualmente nello sviluppo applicativo – metodologia – al fine di generare un protocollo interdisciplinare efficace, con i diversi casi studio che si sono configurati come episodi di verifica e allo stesso tempo di evoluzione della metodologia.
Uno degli obiettivi principali è stato quello di studiare la codifica di un flusso di lavoro, rigoroso, estendendo la tecnica anche a strumenti non prettamente pensati per l'utilizzo fotogrammetrico. In tal senso, l'impiego di microscopi portatili USB per modellazioni tridimensionali, che diventa concreto grazie all'ideazione di accessori originali e facilmente riproducibili, può essere letto come uno degli apporti più originali.

Tabella 2. Riepilogo dei casi studio.

Caso studio	Cap	Dimensioni	Sensore	Risoluzione
 **Lamina Orfica in oro**	1	49/59×32 mm	Dino-Lite AM4113ZT	0,002 mm
			Nikon D800E	0,030 mm
 **Epigrafe in marmo**	2	310×200 mm	Konica Minolta Vivid 910	0,150 mm
			Artec EVA	0,200 mm
			Artec LEO	0,200 mm
			Nikon D800E	0,070 mm
 **Moneta in bronzo**	3	ø 12 mm	Dino-Lite AM4113ZT	0,004 mm
			Dino-Lite AM73915 MZTL	0,005 mm
 **Tavoletta cuneiforme in geopolimero**	4, 5	20×22×8 mm	Dino-Lite AM4113ZT	0,010mm
			Dino-Lite AM73915 MZTL	0,005 mm
			Nikon D810	0,006 mm
			SCAN in a BOX Open Tech	0,080 mm
			Dino-Lite AM7013MZT	0,006 mm
 **Tavolette cuneiformi in argilla**	6, 7	Da 20×20x5 mm a 50x50x10 mm	Dino-Lite AM7013MZT	0,008 mm
			SCAN in a BOX Open Tech	0,080 mm
			Nikon D800E	0,005 mm

 **Stratere in argento**	8	Ø 21 mm	Dino-Lite AM7013MZT	0,007 mm
 **Stele di Horo egizia**	8	54×96×23 mm	Nikon D800E	0,020 mm
 **Scultura in terracotta**	8	96×27×60 mm	Artec EVA	0,200 mm
 **Rilievo figurato in marmo**	8	0,9×1,2×0,25 m	Artec LEO	0,200 mm

 **Vaso in ceramica**	9	130×240 mm	Nikon D3300 Artec EVA	0,400 mm 0,200 mm
 **Vaso per unguenti in bronzo**	10	187×84×153 mm	Nikon D800E	0,040 mm

Il lavoro non ha certo la pretesa di identificare, analizzare e risolvere tutti gli aspetti del tema, bensì tende a fornire delle soluzioni pratiche a problematiche reali, affrontate sulla base di approfondimenti teorici e in maniera originale sul campo.
Il confronto interdisciplinare con studiosi afferenti a diversi contesti tecnico-scientifici e l'internazionalizzazione della ricerca ha contribuito, inoltre, ad arricchire il ventaglio di esperienze e a generalizzare le soluzioni proposte.
Elemento mai trascurato è stato la riproducibilità delle operazioni condotte, degli strumenti sviluppati e delle metodologie applicate, con l'obiettivo di compiere un piccolo passo avanti ad ogni applicazione; con il Dipartimento di Ingegneria Industriale dell'Università di Salerno e con la "Unidad de Investigación, Desarrollo y Transferencia - Grupo de Ingeniería Gráfica Aplicada" della Universidad Nacional de La Plata in Argentina, si è delineata una vera e propria sistematizzazione della configurazione image-based con sensori low-cost che possa costituire il prossimo risvolto di questa ricerca.

Non siamo molto distanti dalla celebre opera "Reale e virtuale" di Tomás Maldonado[39]: oggi, è possibile aggiungere a quelle riflessioni un'ulteriore urgenza, quella di godere della rappresentazione digitale *hic et nunc*, averla a portata di mano e di condivisione (per formato, peso e leggibilità del dato), sia essa prefigurativa o descrittiva di una realtà esistente. In tal senso, assistere e partecipare all'uso estensivo di modelli tridimensionali trasforma l'approccio alla rappresentazione e agli strumenti che la governano, svelando nuove possibilità di sperimentazioni per la disciplina del disegno.

[39] Maldonado, T. *Reale e virtuale*. Feltrinelli Editore: Milano, Italia, 2005.

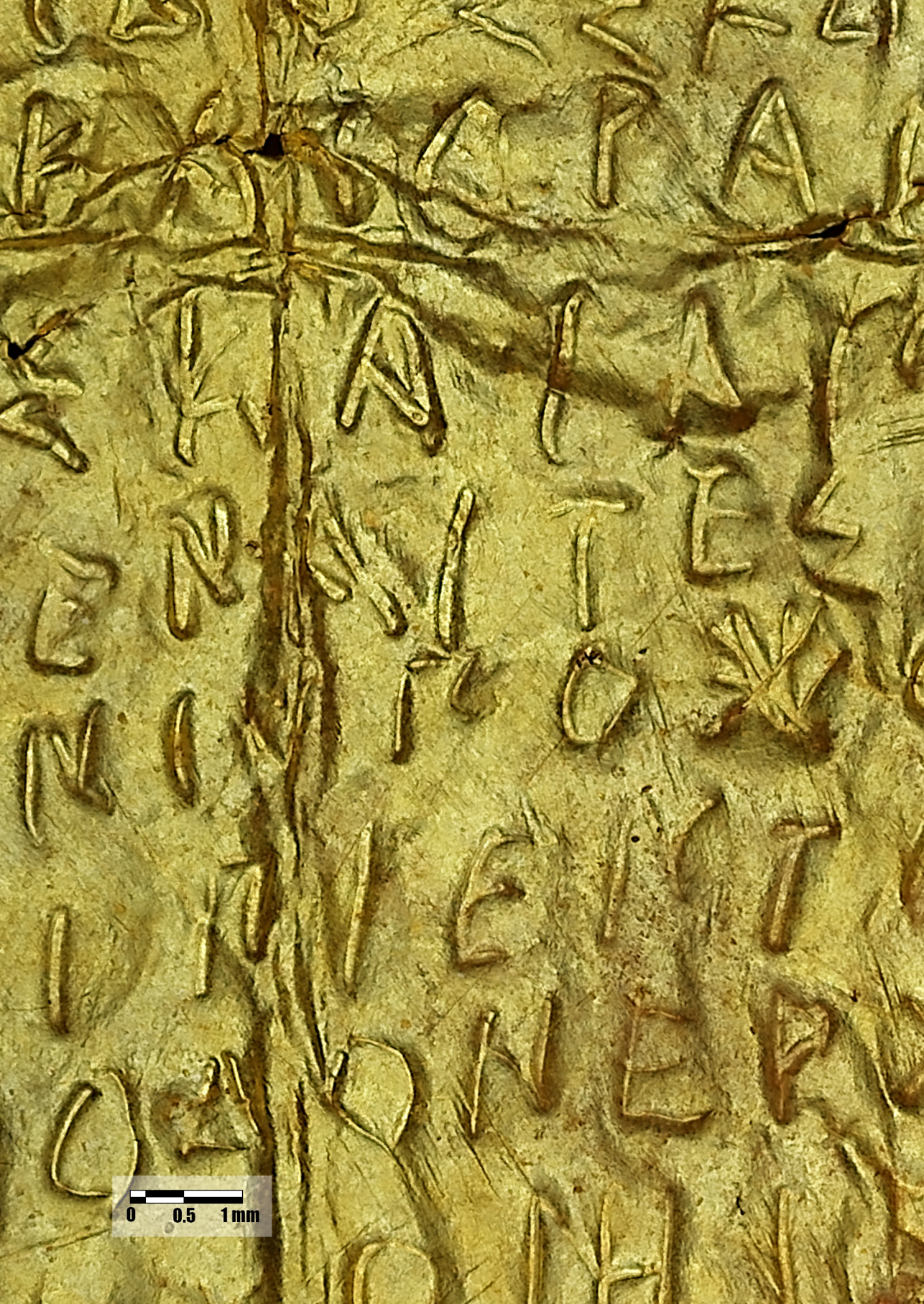
0 0.5 1mm

Capitolo 1
Macro and micro photogrammetry for the virtualization of the orphic foil (V-IV BC) of National Museum of Vibo Valentia

Abstract: Discussing photogrammetric surveying methods does not in itself constitute an innovative activity. However, modern application deserves an innovative and critic approach not only by a technological evolution of acquisition tools, but also for the challenge posed to us detectors and most commonly to the theory of measurement. The new opportunities for describing and representing reality are most commonly redirected to the historical built and the landscape, referring to consequent orders of magnitude and restitution scales. The codification and formalization of surveying techniques for small objects with high precision and accuracy, also in the case of "image-camera" and "range-camera" tools, is still little addressed. For this reason, is presented the case study of the photogrammetric acquisition of an orphic gold tablet, particularly challenging in order to discuss two problems at the same time: the size and the reflective material (gold with which the object is made). The acquisition is carried out with two different instrumentations: using a native "macro" photographic system, with dedicated photographic lens, in artificial light conditions obtained by developing a specific lighting technique (Ring Reflection Lighting - RRL) and using a "micro" system through digital microscope with polarized light. The results are compared in order to generate weaving relationships between of this foil within the "Visualizing Innovative and Social Artworks" project of Calabria region.

Keywords: Small Artefacts, Reflective Objects, Ring Reflection Lighting, Dino-Lite, Reality Capture.

1. Introduction

This paper focuses on challenges posed by photogrammetry approaching the survey of small objects in difficult light conditions. In detail, it is proposed to illustrate the procedural solutions identified to carry out the photogrammetric survey of an orphic gold tablet dating V-IV century BC, found[1] at *Hipponion* [1] e and now preserved in the National Museum of Vibo Valentia (Figure 1).

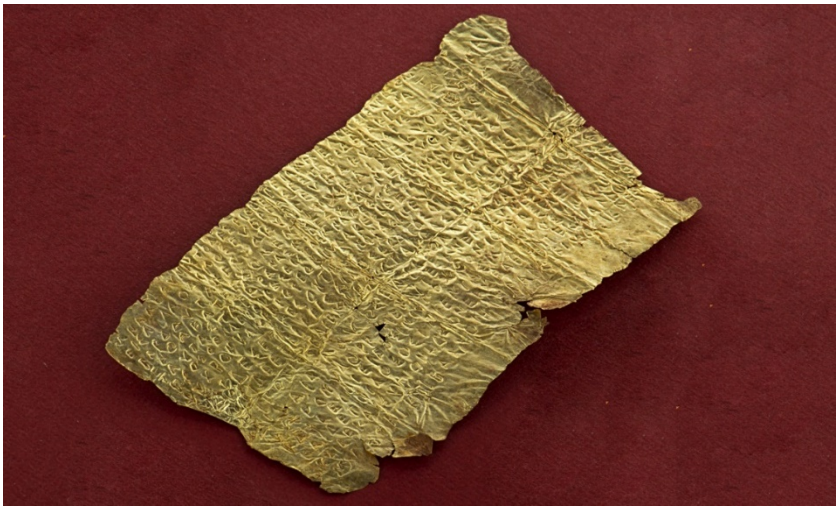

Figure 1. The Orphic lamina of *Hipponion* (today Vibo Valentia) found in 1969 inside a necropolis located in the lower part of the city.

The survey of this finding, in order to reach an adequate descriptive quality, required to solve three intrinsic and extrinsic conditions: its small size (maximum length: 59 mm, minimum length: 49 mm; height: 32 mm); the presence of a text made with micro-engravings that have a maximum relief of 2 mm; the highly reflective material (gold) of which it is made. These particular features make evident some critical aspects of the acquisition phase, critical issues that, in the first instance, result in the design and in the construction of an 'acquisition set' combined with a full frame camera and macro lens. The quality, speed, and cost-effectiveness of the first method were then compared with the data obtained from a portable digital microscope. What has been found in this experience is valid in order to propose a new pipeline for the documentation of small artefacts, up to about 5 cm, effective for a range of materials frequently present in museum collections.

2. Methodological premise

The 3D digital modelling based on digital photogrammetry has become one of the most important tools in solving actual needs for heritage analyses, procedural modelling and accuracy requirement [2], representing an extraordinary way to guarantee heritage conservation while maximizing their use. This is even more true for the considerable

number of finds stored in warehouses, whose use is often limited to study reasons only. In this operational context, photogrammetry is a surveying method which has the major advantages of being – usually – low-cost, portable, flexible, and able to deliver highly detailed geometries and textures at the same time [3]. Furthermore, the photogrammetric approach intrinsically involves the metric precision in the positioning of the single pixel on the surface and guaranties a metrically correct fusion between high detailed texture and normal maps [4]. These assumptions are true, given a solid knowledge of both photography and photogrammetric process [5], and ensuring that the acquisition campaign is preceded by a meticulous work of planning and controlling the boundary conditions of the subject (limited spaces, possibility or impossibility of moving the object, lighting conditions).

3. Equipment and acquisition procedures

3.1. VIVID 910 Scanner

A first attempt to acquire the object has been made with the VIVID 910 3D Scanner, a non-contact system by KONIKA-MINOLTA based on laser triangulation (Figure 2).

The instrument, equipped with three interchangeable optics according to needs, was used with the "telescopic" lens, specific for small, detailed surfaces, to which corresponds, with a measuring distance of 600 mm, a catching surface at 367×275 mm.

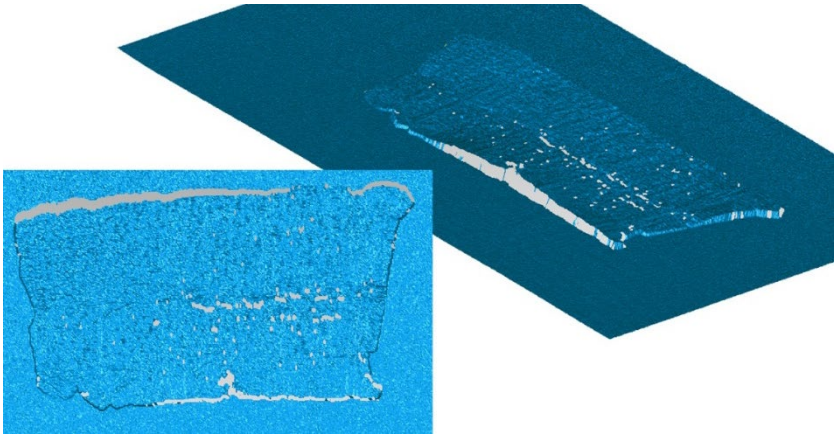

Figure 2. Polygonal mesh obtained with the VIVID 910 equipment.

The scan quality has been set to "fine," for a nominal resolution level of the order of tenth of a millimetre.

Because of gold's high superficial reflectance, making it react so differently to external solicitations, the answer of this surface to the laser scanner beam is difficultly predictable: consequentially some problems are noticed and mainly originated by surface characteristics and by particular combination of scanning angle and local macroscopic condition (causing by a loose of back signal).

The unsatisfactory results, especially as regards the detail of the micro incisions, have led to the search for more performing solutions.

3.2. Full-frame camera and macro lens

In the acquisition phase, as is well known, the data quality mainly depends on the external light, on the optical characteristics of the camera and on the instrumental resolution, in its dual declination of geometrical (GSD) and radiometric resolution [6].

In order to maximize the data quality, first consider the choice of the optical system: as it happens for the human eye, even photographic lenses are capable of focusing only up to a certain distance from the subject. Since in most lenses this distance is designed to fall within the meter order, taking very close shots can be problematic. The most suitable objectives for this case are called "macro" and, as well as allowing the close focus, they also represent, among the types of objectives, those optically less affected by distortions. In our case, an AF-S VR Micro-Nikkor 105 mm f/2.8G IF-ED was used, which allows a minimum focusing distance of 0.314 m.

Despite the advantages related to macro-optics, such as close-up shooting and the extremely high level of detail that can be reached, far superior to that of common optic systems, these are commonly considered suitable only for a narrow range of photogrammetric applications due to the very low depth of field. Even if multi-focused image stacking has been demonstrated as an effective countermeasure to restricted DOF with very small subjects, less than 2 cm across, however, it would significantly increase the number of photographs and unnecessarily burden the processing pipeline [7]. Consequentially we have chosen to manage the problem of blur starting from the concept that

the depth of field increases with the decrease of the aperture [8] increase in exposure times[2].
Depending on the digital camera used – Nikon D800E, characterized by a 35.9×24.0 mm and 36.3 MP CMOS sensor, for which a confusion circle of 0.0146 mm is assumed – a distance is imposed between the optical centre of the lens and the object equal to 70 cm, using an aperture of f/32. This way you can guarantee a depth of field of 35.4 mm, accepting a slight drop in sharpness caused by some shots not orthogonal to the plane of the object, but necessary for photogrammetric purposes. You put yourself in safety – during the ongoing campaign – by moving away from the foil of 10 cm and maintaining an aperture of f/32, extending the depth of field to 49.8 mm[3].

3.3. Ring Reflection Lighting

Let's focus on the choice of the acquisition system and the lighting conditions: since it is a small and movable object, it has been identified, as the most efficient way to acquire it, that of placing it on a rotating base with diffused light conditions that neutralize the shadow cones – without variations in the intensity of shadows, lights and colours – so as to have perfect lighting for each rotation. The sense is to have a lighting that is advantageous in terms of photographic shooting and that at the same time does not compromise – indeed possibly improve – the reconstruction of the geometry. For this purpose, it was necessary to use a type of light that did not directly affect the object. Then, the gold tablet, together with the opaque bottom's rotating base, was placed on a horizontal panel consisting of a diffusing material, a plexiglass panel backlit by a flashlight. The light coming from below is reflected on the object thanks to the use of a white forex cylinder, concentric to the rotating base, but built with a larger diameter, so that the difference between the diameters determines a ring of light that bounces on the cylindrical surface – acting then as a reflective panel (Figure 3) – uniformly illuminating the object. Note that the diaphragm is rather closed and if we were in continuous light conditions this would entail an exposure time of ten seconds at least. This is not a problem if you have a tripod, but some factors should not be underestimated such as the chrominance noise[4] , which increases as the exposure time increases and the incidence of the light from the scene on the object.

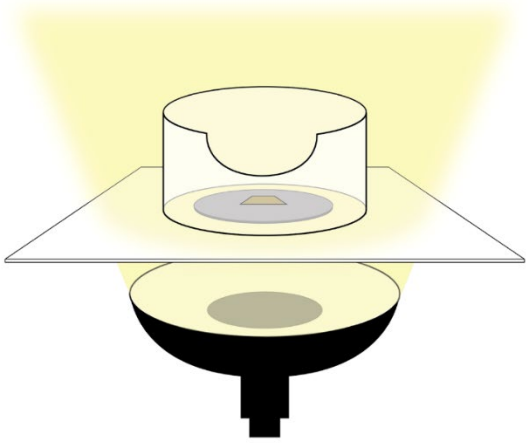

Figure 3. Scheme of the assembled RRL system for diffused acquisition lighting. Starting from the bottom: beauty dish (light source); plexiglass top (diffusing base); rotating table; forex cylinder (reflective panel).

The last factor grows with increasing exposure time, despite artificial light conditions imposed and the only chance to avoid this light influence is for the exposure to be short and, having a closed diaphragm, that it is balanced by a light power such as to guarantee the correct exposure (programmable on the flash unit).
Using this original system, named Ring Reflection Lighting - RRL, of the approximate assembly cost of € 5.000, 72 images were acquired (approximately one every 10 degrees base rotation with two different angles of tilting, 30°and 45°). The time required between setting up the system and acquiring (Figure 4a) is approximately 40 minutes.

3.4. Dino-Lite AM4113ZT

The urgency to verify the possibility of using cheaper and faster instrumentation than the one previously illustrated – as well as wanting to test its accuracy – prompted to compare the results obtained with macro photographic lens to those obtained with microscopic systems, in particular using a digital portable microscope, the Dino-Lite AM4113ZT. This instrument is part of the wide range of microscopes equipped with digital cameras used in recent years mainly for medical and industrial applications and applied to the field of cultural heritage [9]. Their lightness, ease of use and ability to move, allows to obtain easily images, ensuring adequate intersection angles respect to the object.

On the other hand, the narrow field and extremely limited depth of field represent obvious restrictions.

The instrument used is characterized by a 1.3 MP photographic sensor (1.280×1.024 px), polarized light, a magnification factor of up to 200× and a tool for measuring linear distances; the cost of this equipment is around € 500. Connecting the microscope to a portable station, through a dedicated procedure DinoCapture 2.0, 490 images were acquired at maximum resolution (3.75 MB Each), at an average operating distance of about 2 cm, with a 30× digital magnification factor. The images were acquired with a photogrammetric multi-image paradigm, thus ensuring an average overlap between the frames of about 70%, manually moving the support of the tablet under the microscope secured on a stand (Figure 4b). The operation lasted about 50 minutes, including the metric calibration operations for the chosen magnification factor. The need to acquire a large number of images for the object's documentation derives from the fact that the digital microscope used is characterized, at the operating distance chosen for the acquisition, by a FOV of 13.0×10.4 mm and a DOF of 1.9 mm.

4. Photogrammetric processing

The two sets of images were processed in a SfM (Structure from Motion) type software: RealityCapture. Both versions of the project were processed using the same PC equipped with Intel I9 9900k CPU, RTX2080ti GPU, 64 GB RAM.

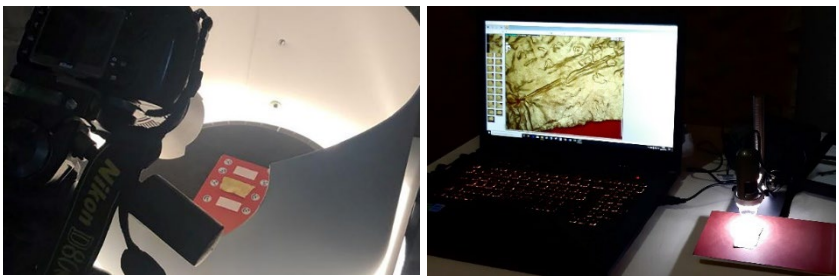

(**a**) (**b**)

Figure 4. (**a**) Foil acquisition with "macro" equipment; in the background: RRL lighting ring; (**b**) Foil acquisition with Dino-Lite AM4113ZT.

Both projects, with related temporary files, were placed on M.2 SSD. In RealityCapture the data processing is divided into three steps: Align Images (Max feature per image 70.000); Reconstruction (High detail); Texture. In the 'macro system' dataset case the time taken to process 1.12 GB of images was about 50 minutes; before the photogrammetric process, the exposure of the images was optimized in Camera Raw, and this process took around 15 minutes. In the 'micro system' dataset case the time taken to process 1.8 GB of images was about 60 minutes.
At the end of the elaboration process, a textured mesh and an orthophoto were exported for both models. In both cases, the generation and export of the orthophoto took about 10 minutes.
The mesh coming from the first system is made up of 6.7 million polygons, while the one made with Dino-Lite up of 19.8 (Figure 5).
As for orthophotos, an orthophoto (Figure 6) composed by 4315×2192 pixel was generated from the data obtained with photographic equipment, while from the data obtained with microscopic instrumentation, the orthophoto generated (Figure 7) is composed by 24808×40518 pixel.

5. Data validation

5.1. Data set up

The two models, using CloudCompare 2.10.2 open-source application, were brought into real world units (mm) through a direct scaling.

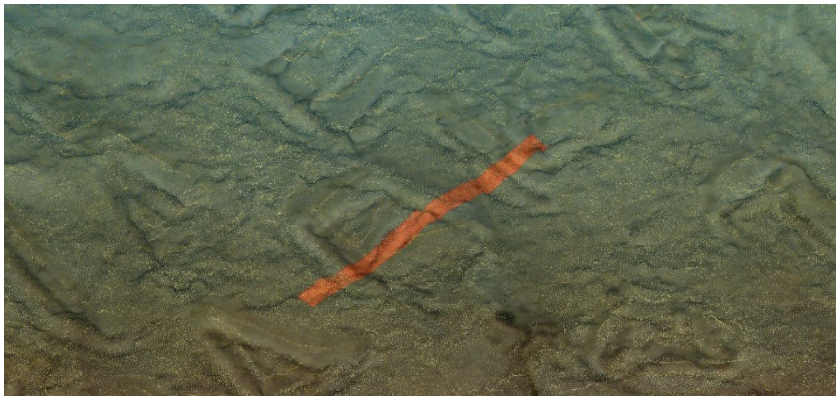

Figure 5. Photogrammetric cloud and resulting mesh (red one) generated by the 'micro system' (Dino-Lite).

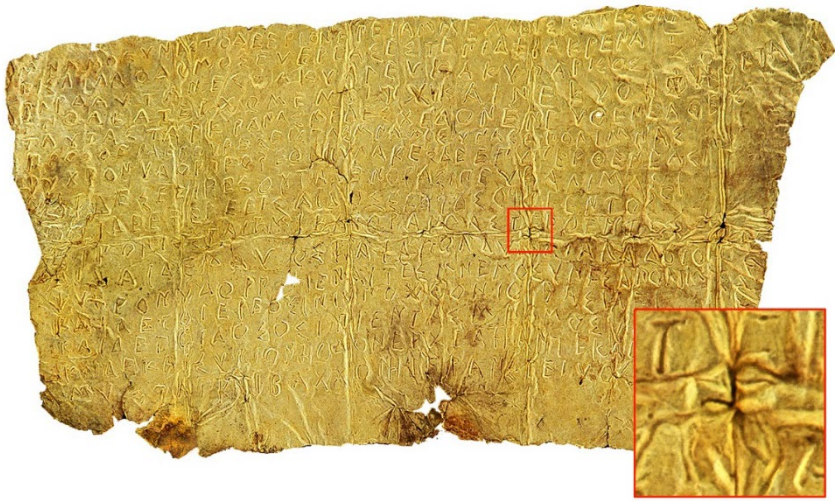

Figure 6. Orthophoto generated with the dataset from the photographic acquisition.

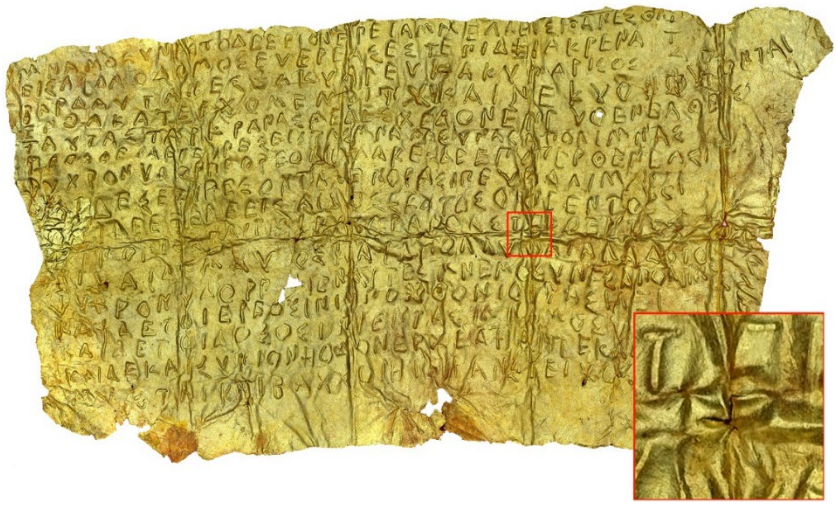

Figure 7. Orthophotos generated with the dataset from the microscopic acquisition.

In the 'macro system', this operation was carried out by positioning two scale bars in the scene (one for scaling and one for checking the accuracy of the operation). In the second case, considering the extremely modest FOV of the Dino-Lite, which would have required the acquisition of a few hundred additional images to be able to include in the scene the scale bars, it was made by using the measuring tool

present in DinoCapture 2.0. This tool, after generating a calibration profile for the magnification factor at the chosen distance, allows you to take sufficiently detailed flat measurements directly from the individual shots. After restoring the correct scale factor for the two surfaces obtained, in order to be able to compare their descriptive quality, they were aligned through homologous points and an automatic alignment was carried out by an ICP algorithm (Iterative Closest Point) to refine the overlap.

5.2. Dataset analysis

The evaluation phase of the surface's descriptive quality was carried out in open-source software environment CloudCompare, using the C2C tool, which searches, for each point of the cloud or triangle of the mesh in phase of comparing, the one closest to the reference entity, thus defining an offset value of the first compared to the second. Using the cloud generated with the Dino-Lite as a reference, it was compared with 'macro system' cloud, highlighting the deviations of the surfaces between -5 mm and 0 mm in false colours (Figure 8): the calculations show that the average deviations do not exceed 2 mm.

Note also that the major deviations (> 5mm) are mainly present on the sides of the scene.

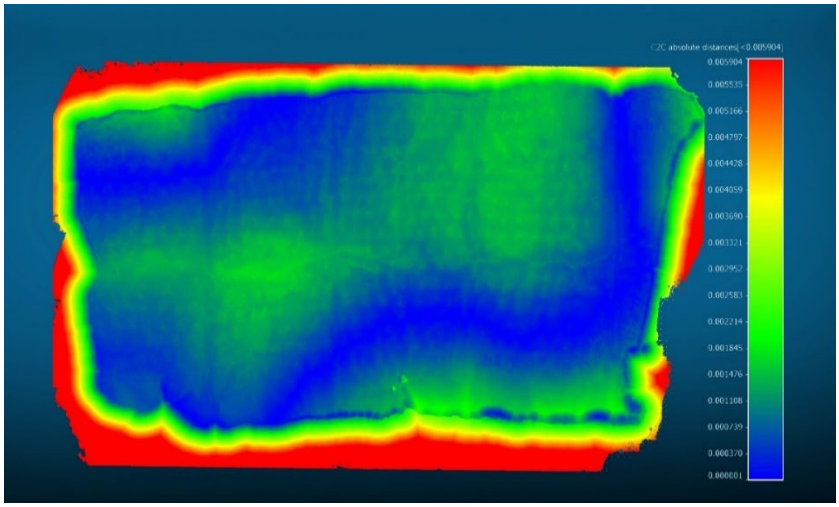

Figure 8. Cloud to cloud comparison in a Cloud Compare environment for the evaluation of cloud deviations obtained with two different acquisition techniques.

This difference is due to the distance of these areas from the point of interest of the relief, caused by the choice to use a rotating table in the macro photographic acquisition. In fact, it allowed to make a rapid succession of shots at a fixed distance from the subject, adjusting only the height of the camera and avoiding the repositioning of the tripod between each shot, but the need to frame the entire object for each shot has reduced the quality of the data significantly.
The difference between the two models in the marginal areas is furthermore accentuated by the extremely close orthogonal capture scheme followed by the Dino-Lite, whose input data are therefore not affected by any significant loss of detail.

6. First conclusions

Overall dimensions of the equipment and cost-effectiveness, with a price that is 90% lower and the overall quality of the data, especially the two-dimensional one, suggest that the Dino-Lite AM4113ZT should be used as a solution for predominantly thin objects (Figure 9).
As regards the three-dimensional description of the surface, there is a modest difference between the two systems, with a moderately better quality generated by the Dino-Lite AM4113ZT data compared to the 'macro system' data regarding to the description of the micro-incisions; on the contrary, the description of the general shape of the foil is definitely better in the survey obtained from the latter (Table 1).

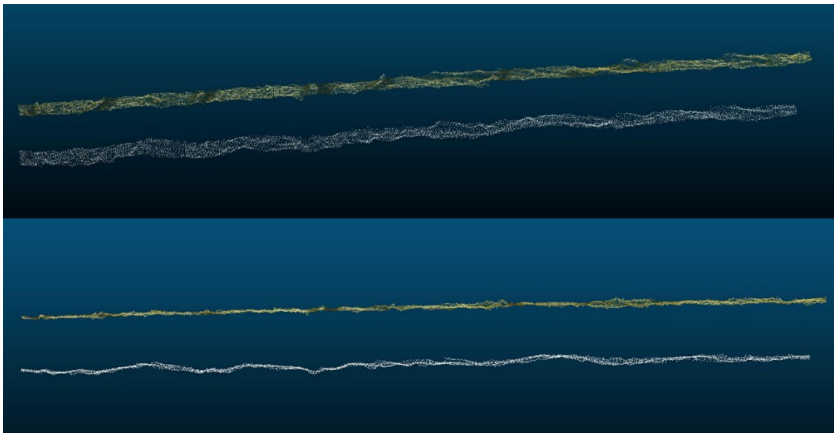

Figure 9. Comparison of a section's point cloud: colour per vertex effect to the data generated with the 'micro system', white coloured that generated with the 'macro system'.

Table 1. In brief the main characteristics of the two acquisition systems implemented.

	MICRO	**MACRO**
Equipment	Dino-Lite AM4113ZT	Nikon D800E + Micro Nikkor 105 mm f/2.8 + Bowens Flash Quad
Price	€ 500	€ 5000
Supply	Battery powered	Power supply
Acquisition running time	50 min no set up needed	40 min set up included
Number of acquisitions	490	72
Size of each	3.8 MB	73.8 MB
Total size	1.8 GB	2.5 GB
Magnification Ratio	0.28	0.17
DOF	1.9 mm	49.8 mm
GSD	0.0015 mm/px	0.014 mm/px
Orthophoto dimensions	40518×24808 px	4315×2192 px
Number of polygons	19.8×10^6	6.7×10^6

The result can be improved through the integration of the two techniques, which however would require long and cumbersome activities of recording the camera positions, in order to guarantee the goodness of the geometry obtained with the 'macro system' and costs and details of the 'micro' one.

Further experiments will be carried out by comparing the microscopic system with structured light equipment and photographic techniques aimed at obtaining a greater detail, by reducing the distance between the optical system and the object, using optical extension devices[5]. In this way, it will be possible to focus more closely on the subject, to have a greater magnification and to increase the detail of the acquisition, to knot the relationships and re-read the mystery history of this foil within the "Visualizing Innovative and Social Artworks" project of Calabria region.

Notes

1. The Orphic foil represents an important testimony of the cult of mystery religions in Calabria (perhaps already in use before the arrival of the Greeks). Placed, folded in four parts, on the chest of the deceased – who in the case was a girl of a noble family – it was intended to accompany her soul and guide her in the kingdom of Hades.
2. The increase in exposure time is defined here as "relative" because it depends not only on the aperture, but also on the amount of radiant energy available in the unit of time, or the light power supplied by the artificial source. It seems trivial to observe that, with the same diaphragm and in continuous light conditions (such as outdoors), the time will be univocally determined by the value of this quantity, fixed a priori; under conditions of artificial flash light, however, it happens that the time can be determined by the operator, setting the generator power upstream.
3. The explicit values derive from the mathematical formalization of the problem in the field of simplifying hypotheses introduced by geometric optics.
4. Noise consists of an undesirable by-product of image capture that obscures the desired information, overlapping with a 'perfect' signal, made up of two simultaneous components: the luminance noise and the chrominance noise. The former is proportional to the ISO value, the latter is a function of exposure time.
5. Optical system extension device positioned between the lens and the camera mount: by moving the lens away from the camera, the lens' front element will be closer to the subject, ensuring, despite this, the focus.

References

1. Pugliese Carratelli, G. *Le lamine d'oro orfiche. Istruzioni per il viaggio oltremondano degli iniziati greci.* Adelphi: Milano, Italia, 2001, p. 17.
2. García Fernández, J., Álvaro Tordesillas, A., e Barba S., An approach to 3D digital modeling of sur-faces with poor texture by range imaging techniques. 'Shape from stereo' vs. 'Shape from silhouette' in digitizing Jorge Oteiza's sculptures. *The International Archives of the Photogrammetry, Remote Sensing and Spatial Information Sciences* **2015**, *Volume XL-5/W4*, 25-29.
3. Nicolae, C., Nocerino, E., Menna, F., Remondino, F. Photogrammetry applied to problematic artefacts. *The International Archives of the Photogrammetry, Remote Sensing and Spatial Information Sciences* **2014**, *Volume XL-5*, 451-456.
4. Bolognesi, C. M., Fiorillo, F. Optimization of texture mapping process in the Reality-Based Modeling application. In *Rappresentazione/Materiale/Immateriale. 40° Convegno internazionale dei docenti delle discipline della Rappresentazione – Congresso della Unione Italiana per il Disegno*; Salerno Rossella (Ed); Gangemi Editore International: Roma, Italia 2018, pp. 337-342.
5. Marshall, M., Johnson, A., Summerskill, S., Baird, Q., Esteban, E. Automating photogrammetry for the 3d digitisation of small artefact collections. *The International Archives of the Photogrammetry, Remote Sensing and Spatial Information Sciences* **2019**, *Volume XLII-2/W15*, 751-757.
6. Russo, M. Fotomodellazione 2020: viaggio di sola andata? In *Riflessioni, l'arte del disegno/il disegno dell'arte. 41° Convegno internazionale dei docenti delle discipline della*

Rappresentazione – Congresso della Unione Italiana per il Disegno; Belardi Paolo (Ed); Gangemi Editore International: Roma, Italia 2019, pp. 425-430.
7. Sapirstein, P. A high-precision photogrammetric recording system for small artifacts. *Journal of Cultural Heritage* **2018**, *31*, 33-45.
8. Greenleaf Allen, R. *Photographic optics*. Macmillan: New York, USA 1950, p. 214.
9. Esmaeili, F.; Ebadi, H. Handy Microscopic Close-Range Videogrammetry. *The International Archives of the Photogrammetry, Remote Sensing and Spatial Information Sciences* **2017**, *XLII-4-W4*, 65-67.

In *UID, Congress of Unione Italiana per il Disegno, Volume: CONNETTERE un disegno per annodare e tessere, Reggio Calabria, Italy, 17-19 September 2021.*
http://dx.doi.org/10.3280/oa-548.86

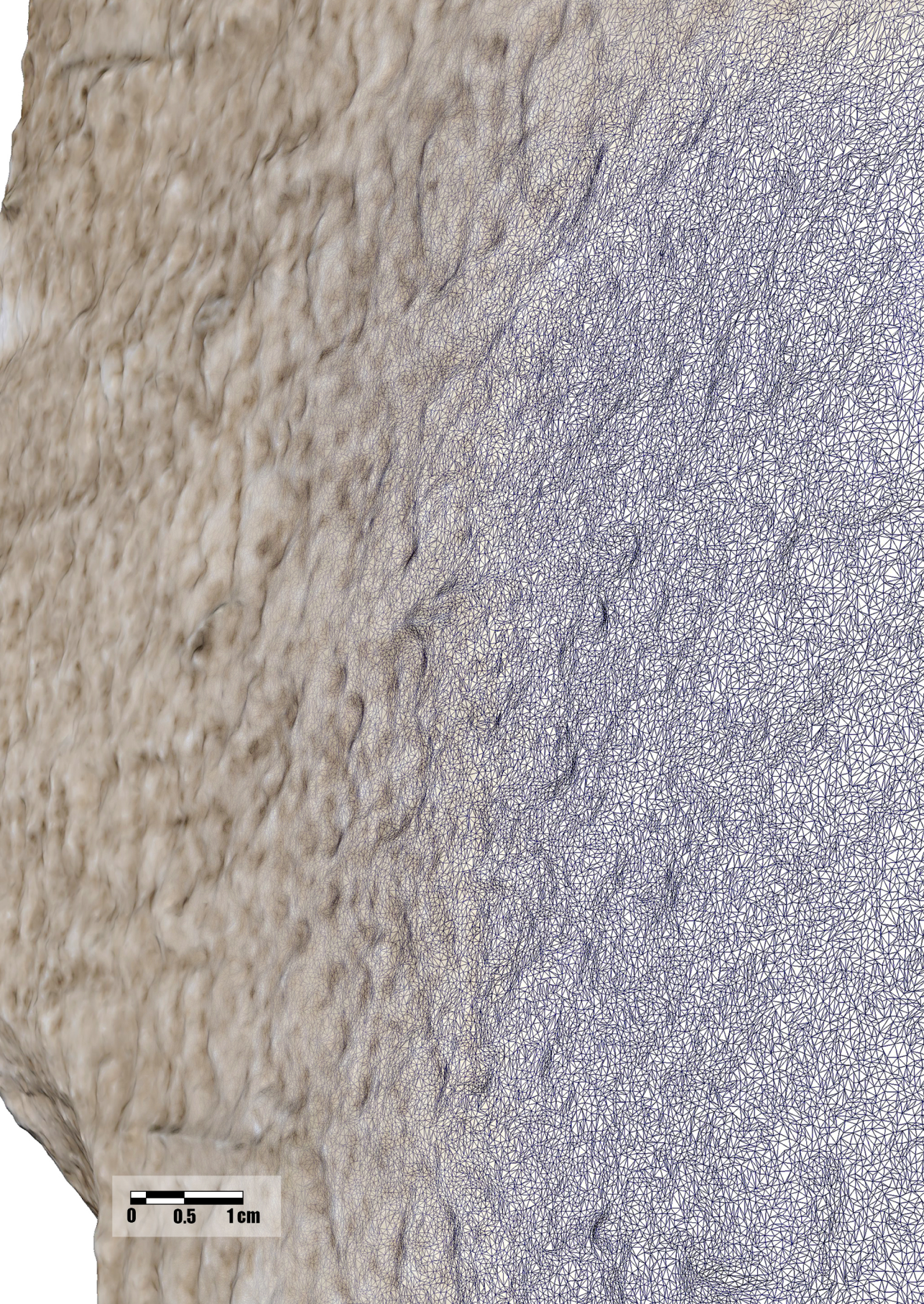
0
0.5
1cm

Capitolo 2
Digital survey and reconstruction for enhancing epigraphic readings with erode surface

Abstract: The contribution illustrates the applied procedure of the digital survey and documentation of a funerary epigraph written in Greek but dating back to the Roman period (dimensions of about 31×20 cm). It comes from Velia (Salerno), a Greek and then Roman city in southern Italy. It was found in 1967 and currently represents the only Greek funerary inscription of the Roman period coming, most probably, from the necropolis of Porta Marina Sud. The inscription presents many gaps and preserves only part of the upper right and lower margins. The surface is highly eroded, maybe due to the exposure to atmospheric agents, making the text interpretation extremely difficult. The implemented image-based and range-based techniques contributed to reading the inscriptions, letting to recover much information that was invisible to the naked eye. The 3D survey system choice has to be consistent with the work aims and the physical object characteristics. A high degree of geometric detail was essential for our case study. Therefore, a triangulation laser scanner performed the first digital capturing, subsequently integrated with a structured light system (Artec Eva and Leo) and finally, a close-range photogrammetric acquisition to produce a high-resolution orthophoto.

Keywords: Geometric detail, Laser Scanner, Structured Light Scanner, Macro photogrammetry, Epigraph.

1. Introduction

Thanks to the development of increasingly innovative and powerful systems in 3D surveying and graphic representation, we are witnessing a new and real need for digital cataloguing, preservation, and enhancement as a methodology for revitalizing Cultural Heritage. Archaeological disciplines are increasingly interested in using emerging digital technologies (often related to the geomatics field) that allows a rigorous geometric and radiometric description of archaeological remains and their contexts [1].

Besides, digitizing a cultural asset allows its remote sharing for interdisciplinary research (e.g., with physically distant experts). Furthermore, it offers the possibility of generating an extensive information storage system that can be modified, queried, and implemented over time and reached at any time. Finally, digital technology could also offer non-experts the possibility to enjoy cultural heritage through a virtual interaction experience [2], a very effective solution in the current pandemic situation.

Even though archaeometry investigations have been widely used, so much that this type of analysis can be considered consolidated, the same cannot be said about digital survey and graphic restitution technologies [3]. Although numerous cases of three-dimensional survey techniques have been applied, it is impossible to find in the literature a unitary and organic attempt to systematically deal with both the data acquisition procedures and the final documentation production. Indeed, techniques and methodologies change according to the object size and the results extracted from the digital model [4,5].

This contribution illustrates the applied procedure of the survey and digital restitution of a funerary epigraph written in Greek but dating back to the Roman period (Figure 1). Most of the stone surface is very damaged. It preserves only faint traces of letters, making the decipherment of the text complex even employing well-established techniques such as grazing light and/or UV fluorescence imaging. The implemented techniques, based on the integration of range-based and image-based systems, strongly contributed to reading the inscriptions, recovering much information that was invisible to the naked eye.

2. Case Study description

The epigraph comes from Velia (Salerno), a Greek and then Roman city on the Tyrrhenian coast of southern Italy.

Preserved in the deposits of the Archaeological Area, it is temporarily located, for needs of study and documentation, at the Department of Sciences of Cultural Heritage of the University of Salerno. The city original name was *Hyele*, becoming *Elea* in classical times and Velia in Roman times. It was founded around 540 BC by a group of Greeks from Focea (Asia Minor) that had abandoned their homeland after the Persian conquest.

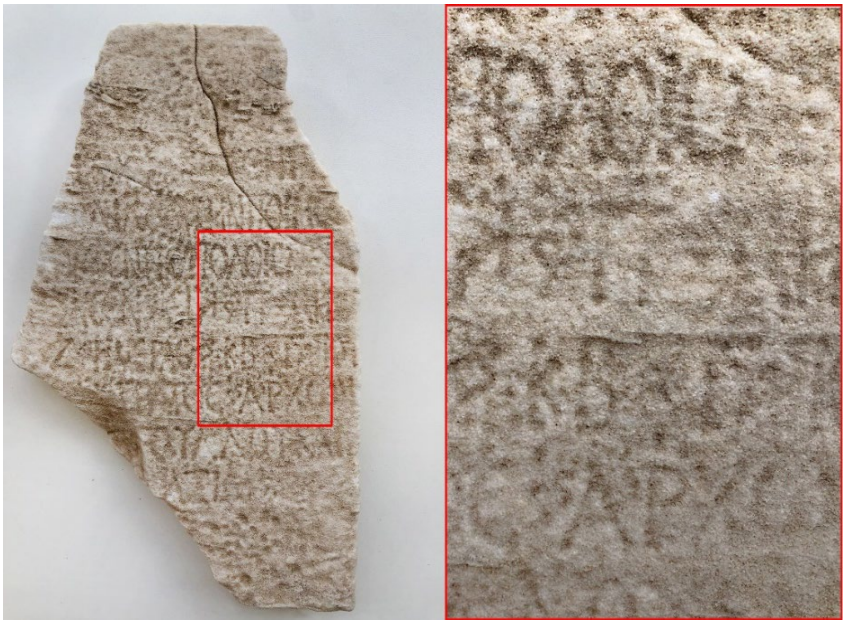

Figure 1. The funerary epigraph written in Greek but dating back to the Roman period.

It was the home of the philosophers Parmenides and Zeno, born and lived in the city in the fifth century BC, founders of an important philosophical school. In the Hellenistic period, Velia was particularly active in maritime trade, the source of its wealth, and soon became a faithful ally of Rome. In Roman times the city retained its cultural Greek character, as evidenced by the persistence of still using the Greek language in the imperial age.

The inscription under study belongs to this historical context, it is indeed written in Greek but can be traced back to the Roman period. It is possible to date it to the second century AD based on the presence of the ivy leaf (*hedera distinguens*) used as a sign of separation for the words. The epigraph, found in 1967 in the Porta Marina Sud area, is engraved on a sugar marble slab, probably of insular origin, and it unfortunately presents many gaps. It only partially preserves the upper right and lower margins (maximum height 31 cm, width 20 cm, thickness 3.5 cm).

The surface is highly corroded, maybe due to the prolonged exposure to atmospheric agents, making the interpretation of the text extremely difficult. Given the premises, it felt necessary to verify if digital survey techniques could improve the reading of the engravings.

The acquisitions were conducted by the "Laboratorio Modelli" of the Department of Civil Engineering (DICIV) of the University of Salerno.

3. Data Acquisition and Data Processing

The choice of 3D survey technique must always be consistent with the work aims and the physical object characteristics. For our case study, it was essential to obtain a high degree of geometric detail in the digital model generation.

For these reasons, as a first application, a triangulation laser scanner, the VIVID 910 Konica Minolta, was used. The device works in a range of distances from the object between 0.6 and 2.5 m and is equipped with a 640×480 pixel CCD sensor and three interchangeable lenses respectively corresponding to three different focal lengths: tele (f = 25.5 mm), middle (f = 14.5 mm) and wide (f = 8.0 mm). Working with the Tele lens at an average distance of about 50 cm, the model resolution corresponds to about 1.5 tenths of a millimetre. This estimated resolution allows reading most of the engravings on the marble slab.

The digital capturing of the entire epigraph, which surface area is less than 620 cm^2, involved 19 scans with an estimated overlapping of approximately 80%. The considerable overlap among the single range-maps ensures a robust alignment between the surfaces and a complete geometric model, in order to obtain a polygonal model free of data gaps or shadow zones [6]. Indeed, potential subsequent invasive editing actions on the mesh surface (e.g., filling holes or smoothing to reduce instrumental noise) could 'falsify' the model and interfere with the interpretation of the engraved text.

The software used to manage the data acquisition is the Polygon Editing Tool (PET), a Konica Minolta proprietary software. The main settings for the 3D measurements were the focus and the scanning quality, set to "fine" (in this way the laser beam strikes the object's surface three consecutive times with acquisition times of about 2.5 sec). PET also allows the processing of the acquired raw data.

However, it was conducted with Geomagic Wrap (3D Systems), a more versatile reverse engineering software characterized by many utilities for mesh processing.

The data elaboration workflow included the following steps: (i) Data filtering and noise reduction; (ii) Manual registration to align different

scans using homologous points; (iii) Global registration by automatic alignment optimization (Iterative Closest Point algorithm); (iv) Merging different scans into a single polygonal model; (v) Surface editing - manual and automatic - to correct possible errors and imperfections of the generated mesh (corrupted triangles, duplicate triangles, non-manifold edges, non-manifold vertices, etc.). Once the digital model was created, to further enhance the reading of the characters impressed on the surface, a best-fit plane was set at a 5 mm distance from the surface of the inscriptions. The best-fit plane was used as a reference to generate a DEM - Digital Elevation Model, which helped the reading and deciphering of part of the text.

Subsequent tests on the same epigraph were conducted with two structured light 3D measurement systems, the Artec Eva and Artec Leo scanners. The aim was to verify if the results could be integrated with the VIVID output to support and optimize the text interpretation.

The first one, the Artec EVA hand-held scanner, is ideal for making a quick, textured, and accurate 3D model of medium-sized objects: the linear field of view ranges from a minimum of 214×148 mm to a maximum of 536×371 mm. It scans quickly, capturing precise measurements in high resolution: the maximum resolution achievable is 0.5 mm, with an accuracy of 0.1 mm, acquiring up to 16 fps and the camera, available for the acquisition of colorimetric information, is 1.3 MP. EVA requires neither targets nor calibration to get started. The scanner uses a powerful hybrid geometry and texture tracking to reconstruct the 3D geometry. However, the data – collected by moving the instrumentation around the entire object with slow and uniform movements – can be monitored in real-time and displayed by the proprietary software on a computer or tablet only.

This drawback is solved by the more recent Artec Leo scanner, used for further acquisitions to compare the different instruments offered on the market and understand which best highlights the inscriptions on the epigraph. Leo is the first 3D scanner to provide automatic onboard processing, with a 512 GB SSD internal hard drive, providing a very intuitive workflow, making 3D scanning as easy as taking a video. As the user scans the object, he sees the 3D replica building in real-time on the Leo touch panel screen. Leo has higher technical specifications: first, it is faster, with a reconstruction rate up to 80 fps and higher resolution,

up to 0.2 mm; conversely, the accuracy remains at 0.1 mm. Its large field of view ranges from a minimum of 244×142 mm to a maximum of 838×488 mm.

The practical step of epigraph digital capturing with these hand-held scanners was not particularly difficult but still suffered from the homogeneity of the object's texture and 4 its predominantly two-dimensional shape. Artec 3D scanners, since they employ the structured-light method of 3D reconstruction and capture 3D frames using optical technology, are quite influenced by the surface optical characteristics of objects. In addition, the scanner has a defined depth range. If it's too close to the object, it may fail to capture all or part of the object. On the other hand, if the scanner is too far away, several types of 3D 'noise' will appear in the scene, complicating the postprocessing effort and affecting the results. Despite these challenging factors, the acquisitions phase kept few minutes with both instruments. The software used to manage the scans is Artec Studio 15 Professional, the Artec proprietary software.

The data elaboration workflow included the following steps: (i) Scans checking and editing; (ii) Alignment; (iii) Global Registration; (iv) Models generation (fusion); (v) Models editing; (vi) Texturing. During the revising step, the EVA scans were affected by misaligned frames, occurring because of the small size of the engravings and an insufficient number of geometrical features on the object. For that, some problematic scans were divided and edited or eliminated. In this way, the three EVA scan groups were successful aligned and registered, with an acceptable error that did not affect the outputs used. The 3D model, consisting of 363.619 polygons, has a resolution of 0.5 mm. For the four Leo scans, after checking if we had any scan result not well aligned (the on-board real-time processing allows the quality of the scans to be checked already during the scanning) with a maximum error equal to 0.1, a sharp fusion was carried out, obtaining 2.286.106 polygons with a resolution of 0.25 mm.

A final acquisition was conducted with a photogrammetric system [7] consisting of a DSLR Camera Nikon D800E, with a CMOS full-frame sensor (pixel size 4.87 micron) features an optical low pass filter with anti-aliasing properties removed. The camera was combined with an AF-S Micro NIKKOR 60mm f/2.8G ED, specific for sharp close-up and

macro images. The artefact, placed on a rotating table, was framed in its entirety. A total of 72 images were acquired, divided into three sets at different angles to the object of 24 shots each (one every 15 degrees of rotation). The GSD (Ground Sampling Distance) – considering 60 mm of focal length, the pixel size and the distance of the optic from the object – is equal to 0.069 mm/px. A closed diaphragm, f/32 specifically, combined with diffuse lighting, allowed a sharp depth of field that was quite large in relation to the size of the artefact.

The software used to manage the photogrammetric data is Agisoft Metashape, a stand-alone software product that allows, as well known, to process images into the high-value spatial information in the form of dense point clouds, textured polygonal models, georeferenced true orthomosaics. The data elaboration workflow included the following steps: i) Photos checking; ii) Alignment; iii) Build dense cloud; iv) Build mesh; v) Build texture; vi) Exporting. No problems occurred with the alignment phase, with an RMS reprojection error of 0.23 mm (1.55 px). A 3D model of 2.710.738 faces was generated and textured, allowing the generation of an orthophoto of the dimensions of 6232×6584 px.

The various 3D models obtained from the different sensors were aligned by identifying homologous points using the VIVID 910 as the master scan. Once aligned, other DEMs were generated with respect to the same best-fit plane generated at 5 mm from the surface of the inscriptions. Therefore, it was decided not to carry out a metric comparison between the models but to generate different maps to aid the reading of the inscriptions (Figure 2). On the other hand, the photogrammetric model was used to generate a high-resolution orthophoto to allow the letters identified on the image to be written. On this one, various filters were tested to optimize the text recognition: HDR toning filter to apply the full range of HDR contrast and exposure settings to the image and a threshold filter to convert the coloured image into a high-contrast, black-and-white image.

4. Result and conclusion

As a first result, it appears clear that the applications with range-based systems have facilitated the reading and interpretation of the engraving, bringing to light new and significant elements for the reconstruction of the text (results that will be discussed and presented elsewhere).

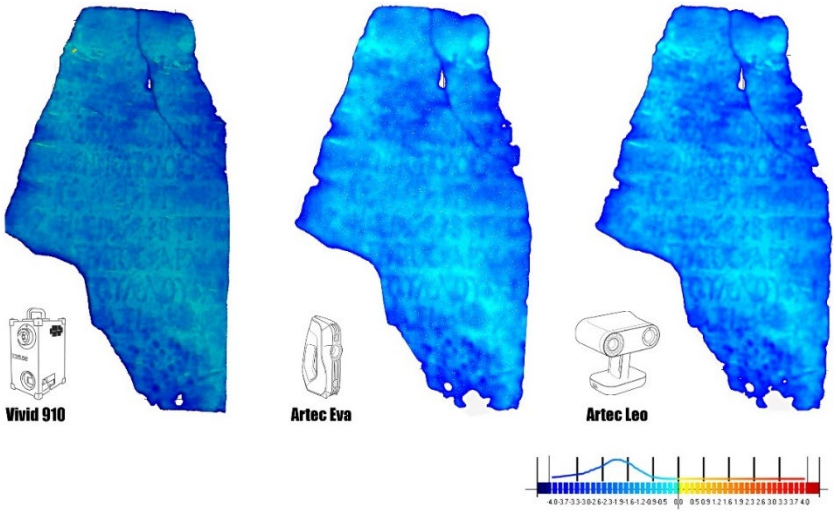

Figure 2. Different DEMs generated by range-based sensors, compared to the same best-fit plan.

The attempts of reading previously produced limited achievements and not very encouraging results. It is possible to recognize traces of at least 12 lines of text written in Greek. The excessive erosion of the surface makes the grooves of the letters often only barely perceptible to the naked eye.

Based on the elements that it was possible to acquire so far, we can say that this is a text of a funerary nature. The area of discovery (in front of Porta Marina Sud) was occupied by a Roman-age necropolis, with burials that date back to between the first and the third century AD, where a conspicuous group of funerary inscriptions was found, even though all of them were written in Latin. The name of the funerary dedication subject was probably contained in the first lines of text, which unfortunately are not well readable. In the central part of the text, we found the references to the age, expressed in years, months, and days, according to the typical form of Latin epigraphs. This aspect suggests that we are faced with a situation typical of a Romanized city that, on the other side, was still using the Greek language.

In particular, concerning the 12 lines of the writing of which traces remain, in the central part (lines 4-7) it is possible to recognize, with relative certainty, some expressions or key-words that are fundamental

to identify the type of inscription and guide the text reconstruction (Figure 3): (i) line 04 ΕΝ ΠΟΤΙΟΛΟΙC (ἐν Ποτιόλοις): state in place (in Puteoli), related to something that the personage to whom the inscription refers had done in Puteoli (Pozzuoli); (ii) line 05 [E]ZHCEN (ἔζησεν) = "lived", suggesting that this is a funerary inscription; (iii) line 06 Z HMEPAC (Ζ ἡμέρας) = 6 days: the previous part should contain the years and months indicating the duration of the life of the person to whom the inscription refers; (iv) line 07 ΑΡΧΩΝ (ἀρχῶν) = term relating to a magistrate's office probably held by the individual. The reference to a Greek-type role possibly held by the deceased is another distinctive aspect of Velia in the Roman age. Indeed, as for other Greek-origin cities of southern Italy, Romans were very often likely to hold, for matters of social prestige, Greek-type offices.

The text analysed, therefore, turns out to be of twofold importance, as it not only enriches the dossier of Greek inscriptions dating back to the Roman age found in Velia but also, above all, currently constitutes the only Greek funerary inscription coming, most probably, from the necropolis of Porta Marina Sud.

It also contributes to a better definition of the social and cultural context of the city in Roman times, especially as regards the use of the Greek language.

Figure 3. Lettering clearly distinguishable by DEM and RGB analysis overlayed on the orthoimage.

Aware of the preliminary aspect of this work, which would undoubtedly require the analysis of a more considerable number of digital survey scenarios and graphic restitution, the results achieved stimulate interest in other experiments to support the interpretation of the text contained in the epigraph.

References

1. Andreu, J., Serrano, P. Contributions of the digital photogrammetry and 3D modelling of Roman inscriptions to the reading of damaged tituli: An example from the Hispania Tarraconensis (Castiliscar, Saragossa). *Digital Applications in Archaeology and Cultural Heritage* **2019**, *12*, 1-7.
2. Orlandi., S., Santucci, R., Casarosa, V., Liuzzo, P. Information Technologies for Epigraphy and Cultural Heritage: In Proceedings of *The First EAGLE International Conference Collana Convegni 26*, Sapienza Università Editrice: Roma, Italia 2014, p. 532.
3. Bitelli, G., Borghi, B., Francolini, C., Galletti, F. New hypotheses and interpretations regarding the Longobard Basin in the "Jerusalem" of Bologna supported by 3D surveying methodologies. *Journal of Cultural Heritage* **2020**, *46*, 226-234.
4. Pires, H., Martínez Rubio, J., Arana, A. Techniques for revealing 3D hidden archeological features: morphological residual models as virtual-polynomial texture maps. *Int. Arch. Photogramm. Remote Sens. Spatial Inf. Sci.* **2015**, *XL-5/W4*, 415-421.
5. Morena, S., Barba, S., Álvaro-Tordesillas, A. Shining 3D Einscan-Pro, application and validation in the field of cultural heritage, from the Chillida-Leku Museum to the archaeological Museum of Sarno. *Int. Arch. Photogramm. Remote Sens. Spatial Inf. Sci.* **2019**, *XLII- 2/W18*, 135-142.
6. Ronchi, D., Fortunati, S., Limongiello, M. Roman fragmentary painting: surveying technologies and methodological approaches. *Metrology for Archaeology and Cultural Heritage* **2019**, 193-198.
7. Apollonio, F.I., Fantini, F., Garagnani, S., Gaiani. M. Photogrammetry-Based Workflow for the Accurate 3D Construction and Visualization of Museums Assets. *Remote Sensing* **2021**, *13*, 1-40.

In *METROARCHEO2021, 2021 IEEE International Conference on Metrology for Archaeology and Cultural Heritage, Milan, Italy, 20-22 October 2021.*
https://doi.org/10.1088/1742-6596/2204/1/012014


0
0.5
1mm

Capitolo 3
3DINO SYSTEM, shortening distances in precision surveys

Abstract: Rapid succession of technological innovations for cultural heritage digitization, as well as the uncertainty on the conditions and continuity of its fruition – with evident reference to asset's conservation, but also to the recent inaccessibility conditions – are imposing a deepening for structured procedures of three-dimensional survey and virtualization. These procedures, mainly addressed to orders of magnitude and scales of restitution for architecture, are however not oriented towards the codification and formalization of relevant practices for very small objects; this issue is made even more compelling by the need of acquiring highly uniform and/or reflective geometries and surfaces which, as known, make the recognition of homologous points more complex in Structure from Motion algorithms. The tests we conducted with Dino-Lite portable digital microscopes verified the potential of using 'micro' images also for Cultural Heritage documentation, highlighting, however, the need for some technological developments, especially related to depth of field and consequent acquisition geometry. This paper aims at solving some problems increasing the performance of microscopic photogrammetry by optimizing the acquisition procedures with the design of customized accessories for micro-photogrammetry. The results were pursued as part of a technology transfer agreement aimed at advancing a protocol for photogrammetric documentation of small artifacts.

Keywords: Dino-Lite Handheld Microscope, Cultural Heritage, Small artefacts, Ancient coinage, Macro photogrammetry.

1. Introduction

Sensors, acquisition techniques and computational systems continuous improvement constitutes the recording and visualizing data tools real strength [1]. This assumption facilitated the introduction of increasingly automated processes, with increasing accuracy, characterized by limited times and costs; circumstance that thickens the network of complementarity and interaction relationships among

various disciplines related to imaging and three-dimensional processing, including manufacturing industry, medical sciences, entertainment and, obviously, cultural heritage [2].
The increased need for three-dimensional measurements of objects with complex surfaces and sub-millimetre morphological characteristics generated various range-based solutions for micrometric applications [3]. However, not infrequently, both optical and mechanical limitations and non-negligible costs directed the interest towards precision photogrammetry, a rapid, accurate and cheaper paradigm, suitable for surveying both small and complex surfaces [4], although often to the detriment of the reconstruction of the entire sample's volume [5].
The advent of portable digital microscopes developed for inspection, documentation, and metrological digital analysis – already popular in the production and quality control industry, as well as in the medical field – revealed a not negligible potential for modelling small objects, reaching accuracies of the order of a tenth of a millimetre [6]. Within a few years, the possibility of using photographs taken by a microscope attracted the attention of sectors distant from the production-industrial one, such as that of cultural heritage. Among the most compelling reasons for this interest is the need to make accessible many finds, often very small, lying in the warehouses of our museums, also due to the limited exhibition spaces.
This need has recently been added to the unavailability of the visit in person at the exhibition site. In addition to the urgency of exhibiting and cataloguing these objects, the use of digital 3D representations would introduce significant improvements in the work of Cultural Heritage professionals, framing the asset in a global and holistic perspective, inserting it into a vast system of conservation of information, which can be modified and implemented at the same time [7].
Addressing small finds survey determines not only a change in the scale of representation, but also an acquisition operating system rethinking, also operating in situations that are often not easy [8].
The use of microscopes for photogrammetric purposes, difficult due to the narrow field of view and reduced depth of field characterizing the optical system, makes – in fact – an innovative challenge for adapting these instruments to the peculiarities of our scientific disciplinary

sector. Thus, as in other areas of close-range photogrammetry, the advantage of digital microscopic photogrammetric processing will lie, once obtained the full control of all system variables, on the one hand in encoding an automation of the acquisition process [9] and on the other hand in pursuing adequate and verifiable accuracy.
Currently on the market some range-based instruments are already available meeting the illustrated needs, but at not always low costs [10] and not so effective in re-positioning single pixels on the surface when compared to image-based systems [11], or integrated approaches still representing the most effective solution [12].
The contribution, therefore, will focus on the systematization of hardware tools, individually already available, to explore microscopic photogrammetry to define a standardized procedure for the acquisition of very small objects with complex details and textures.

2. Case study: surveying a 1st century BC bronze coin

The precision survey of a bronze coin from Velia, an ancient polis of Magna Graecia today belonging to the Archaeological Park of Paestum and Velia, represented a somewhat emblematic opportunity to experience the photogrammetric performance of some digital microscopes. The needs expressed by ancient numismatics studies, especially for coinage examination, lead not to rely solely on traditional documentation and analysis, consisting mainly of manual measurements and photographs; a type of documentation that can be limiting in terms of information acquisition and subsequent analytical approaches. More advanced methods for recording and examining the find are gradually establishing themselves in conservation practices and in the museum environment, becoming almost the norm today [13].
The object, selected to determine whether the proposed digital recording methods can support the research results, is a coin approximately 1.2 cm in diameter, weighing 2.93 g (inventory number 223964, suitable for size and surface's nature), which on the obverse has a helmeted Athena's head turned to the left and on the reverse a tripod with the letters "YELH", as reference to the Greek name of the city of Velia, from the nymph's name Yele. The find is part of a group of over a thousand similar specimens referable to the same production, currently the subject of studies[1] and datable to the second half of the 1st century BC.

To achieve an adequate descriptive quality, the survey was conducted with two different Dino-Lite (www.dino-lite.eu) portable digital microscopes, using a calibrated plate – designed by the authors and built for the occasion – to optimize alignment and scaling procedures for the three-dimensional model.
The intention, in fact, at this stage of the research, was to increase the descriptive potential of these microscopes.

3. Materials and methods: 3Dino Plate & Dino-Lite handheld digital microscopes

The research activity with the micro photogrammetric system we called "3Dino" was therefore based on the combined use of Dino-Lite portable polarized light microscopes and an original three-dimensional calibrator designed ad hoc. The latter, the "3Dino Plate", consists of a PLA plate obtained with a 3D filament printing, with dimensions of 18×15 cm and characterized by an orthogonal pattern of 99 truncated conical holes, with a flaring angle of 60° and diameter of the smaller base equal to 0.35 mm (Figure 1). Calibrator's accuracy, based on 3D printing settings[2] and relative errors evaluations, or the actual holes position conformity with respect to project file, has been estimated at 0.1 mm, which can be assumed as system's instrumental error value (i.e., markers accuracy).

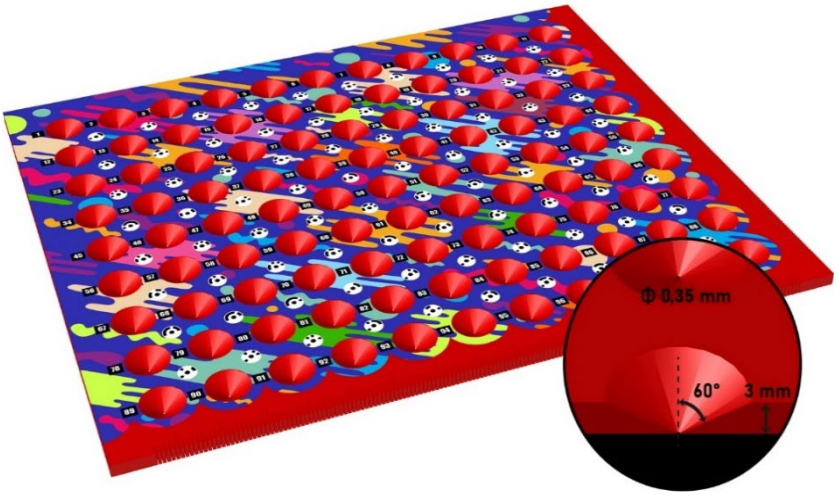

Figure 1. "3Dino Plate" 3D calibrator and a section detail of the truncated cone holes.

Each hole coordinate – with respect to a local reference system – is therefore known to the operator and can be imported into the photogrammetric project: this allows the perforated pattern to be used as a constraint point grid (GCP), homogeneously distributed on the area of interest for the optimization of the parameters governing orientation. In order to guarantee a more robust alignment an adhesive pattern, geometrically and chromatically non-repetitive, equipped with coded targets, was created, and applied to the calibrator's surface. The system also provided for the housing of the 3Dino Plate on a sliding track, allowing the calibration plate's manual translation with respect to the microscope (Figure 2).

Dino-Lite digital microscopes provide a powerful, portable, and functional solution for detail inspection. The models being tested, the AM4113ZT Universal[3] and the AM73915MZTL High Speed, belong to two different classes, both in terms of technical characteristics and special features (Table 1), and, consequently, with a quite different price range. The element that clearly distinguishes the two microscopes is the Working Distance - WD, or the linear distance between the tip of the microscope nozzle and the object to be detected (Figure 3).

Table 1. Technical specifications of the used Dino-Lite microscope.

	AM4113ZT	**AM73915MZTL**
Category	Universal	High Speed
Diffuser	Optional	Included
Magnification	10-70×, 200×	10-140×
Working Distance	Standard	Long
Resolution	1.3 MP (1280×1024)	5 MP (2592×1944)
Maximum Frame Rate	30 fps	45 fps
Interface	USB 2.0	USB 3.0
Housing material	Plastic housing	Metal housing
Special features	No	EDR, EDOF, FLC
Price	€ 200-350	€ 1000-1250

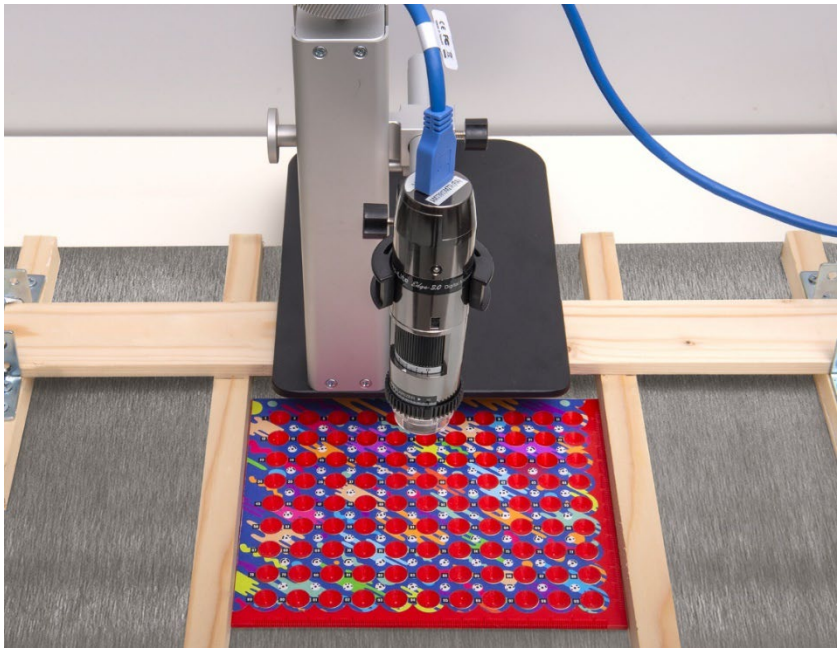

Figure 2. "3Dino Plate" combined with the "3Dino" slide system.

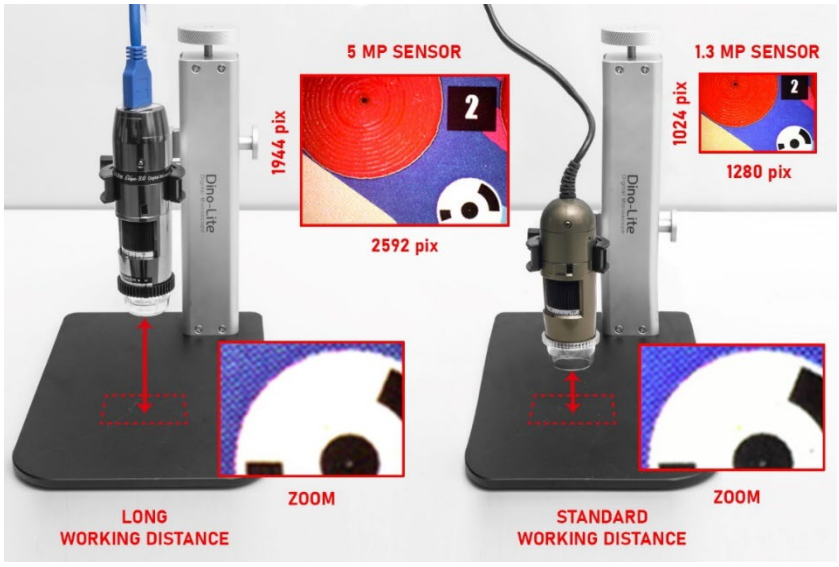

Figure 3. "Working Distance" of the "AM73915MZTL High-Speed" microscope (on the left, equal to 75.5 mm) and of the "AM4113ZT Universal" microscope (on the right, equal to 21.7 mm), housed on the "Dino-Lite RK-10-EX" and operating with the same magnification (30×). In detail, the acquisition of a portion of the calibrator and a detail of the pattern (ZOOM).

The Working Distance directly affects acquired image's magnification (Magnification Factor - MF), framed area (Field Of View - FOV) and the depth of field (DOF). It is trivial to observe that in photogrammetry it is important to establish a fair compromise among these factors.

Bear in mind that the further you are from the subject (high WD), the lower the magnification, with a wider field of view and greater depth of field; on the contrary, the closer you are to the subject (low WD), the greater the magnification, with a smaller field of view and less depth.

The Working Distance is therefore an extremely important parameter from a practical point of view and. depending on the different microscopes used (Table 2), inevitably binds the use of different magnifications[4] in the operational phase.

Table 2. Based on the magnification ("Magnification Factor"), the values of "Working Distance", Field Angle and Depth of Field have been reported for each model in millimetres; (*) the data does not consider the 15 mm frontal cap; (**) approximate estimate from linear interpolation.

	AM4113ZT			**AM73915MZTL**		
Magnification factor	**20×**	**40×**	**50×**	**20×**	**40×**	**90×**
Working Distance*	48.7	9.0	1.9	115.0	56.8	32.7
Field of View	19.8×14.9	9.9×7.4	7.9×5.9	39×29.2	9.8×7.3	4.3×3.2
Depth of Field	3.6	1.4*	0.9	12.0	1.8	0.4

Both models Universal and the High Speed one were combined with the calibrator, fixing the microscope in a special housing, the Dino-Lite RK-10-EX support, and connecting it to a portable workstation.

The acquisitions, therefore, were then carried out with the magnifications summarized in Table 2, operating with the dedicated DinoCapture 2.0 procedure (www.dino-lite.eu/index.php/it/software-dino-lite) using, for the occasion, also the Extended Dynamic Range - EDR and Extended Depth algorithms Of Field - EDOF, which we will deepen in the next paragraph.

The sets of images were thus processed in a SfM software type, Agisoft Metashape, according to the general photogrammetric workflow; the first acquisitions did not consider the variation in focal distance correlated to the different degrees of magnification (MF), exploiting the new possibilities offered by the SfM software to reconstruct accurate geometries also using less rigorous datasets.

4. Data Evaluation

The evaluations of the data generated with the microscopic instrumentation have, first of all, taken into consideration the software management procedures, using Agisoft Metashape, of the micro-photogrammetric images (Table 3).

Portable digital microscopes, unlike photographic cameras, reveal some specific problems for photogrammetric applications: among the most obvious, and limiting, the lack of Exif data.

Table 3. Agisoft Metashape survey data comparison: (*) the GSD shown in the table is affected by the variability of the images in terms of area covered by the acquisitions, "Working Distance" and focal distance, as well as the different sensors of the two models of microscope; (**) no analysis was carried out on the quality of the Tie Points; (***) the error was assessed using Control Points in the absence of sufficient Check Points due to the extension of acquired area; it will be necessary to reduce the size of the calibrator grid in order to thicken the targets and facilitate the use of Check Points. Further processing was carried out with Reality Capture, without any significant differences in the outputs, if not in the alignment times and models generations.

Model	Mode	Aligned Cameras	GSD*	TPs**	RMS error	CPs error***
AM4113 ZT Universal	Normal	110/111	4.0 µm/px	145.613	1.47 px	0.076 mm
AM73915 MZTL High Speed	EDOF	134/135	6.5 µm/px	104.520	1.01 px	0.094 mm
	EDR	100/103	3.5 µm/px	171.702	0.77 px	0.094 mm
	Normal	148/152	4.4 µm/px	169.503	1.77 px	0.089 mm

This information associated with the pixel matrix, as known, retains data relating to camera model, sensor size and focal length. These are essential variables, in the absence of a laboratory calibration, used by any software to process the appropriate calculations for distortion estimation and camera location. To this lack of information must be added the limited depth of field of these instruments: the possibility offered by the Extended Depth Of Field - EDOF to overcome this limit by acquiring and combining more shots on different focus planes, was not an improvement in terms of terms of image quality, but above all not very suitable and decisive for the case study (with this method it is also not possible to estimate a unique value of the focal distance for the image).
The other tested mode, Extended Dynamic Range - EDR, while not offering a solution to the reduced depth of field, by superimposing images with different exposures, proved to be useful for characterizing details of darker or brighter areas, highlighting a particular effectiveness for reflective surfaces, although the used microscopes already benefited from polarized light. It should be borne in mind that the two modes, Extended Depth Of Field - EDOF and Extended Dynamic Range - EDR, require a longer acquisition time (about 20 s for each single shot compared to Normal mode), due to the pre-processing of the data carried out directly in the proprietary application DinoCapture 2.0 (Table 4).

Table 4. Time comparison of DinoCapture 2.0 acquisition and Agisoft Metashape processing. The processing was performed with the same graphic workstation; (*) the total value includes the Marker Positioning phase and generation of DSM and Orthophoto.

Model	Mode	Acquis.	Align.	Dense cloud	Model	TOT*
AM4113 ZT Universal	**Normal**	15′	1h 08′	17′	30′	2h 41′
AM73915 MZTL High Speed	**EDOF**	45′	1h 56′	9′	40′	4h 02′
	EDR	45′	58′	11′	18′	2h 43′
	Normal	15′	2h 13′	11′	1h 02′	4h 12′

Table 5. Photogrammetric processing outputs comparison.

Model	Mode	Dense cloud (n. points)	Model (n. vertices)	DEM (elevation range)	Ortho (size)
AM4113 ZT Universal	**Normal**	32 148 558	3 222 831	3.0 mm	3850×3893 px
AM73915 MZTL High Speed	**EDOF**	49 018 983	4 949 755	7.5 mm	6026×5848 px
	EDR	24 577 548	2 465 745	2.8 mm	6043×5879 px
	Normal	48 697 228	4 911 372	6.0 mm	6265×6108 px

Right after a quick analysis it was possible to evaluate the results obtained by the Universal model as appreciable (Table 5), which guaranteed outputs comparable to the High Speed model, despite being considered entry-level. From our tests and graphs referred to in the previous tables and images, the study of a slice of a point cloud exported from the four homologous 3D models is particularly exemplary: although it is not possible to estimate the uncertainties in an absolute way (at the moment it has not yet been brought to term a range-based survey to be taken as reference model) the detail of the cloud produced with the data of the Universal model is however evident (Figures 4, 5, 6, 7).

Despite the confirmations about the performance of tested instrumentation, the data in possession do not allow, for now, more thorough, and analytical evaluations on the system's accuracy, which will make it necessary to carry out new studies to track back the parametric variables of its internal orientation.

Further investigations will be conducted by comparing the SfM procedures results with other survey technologies for the assumption of a reference surface to be used as an 'absolute' model of comparison. On the other hand, it must be specified that, in order to pursue the primary objective of each survey, namely the verifiability and reproducibility of the metric value, some key aspects still need to be better defined.

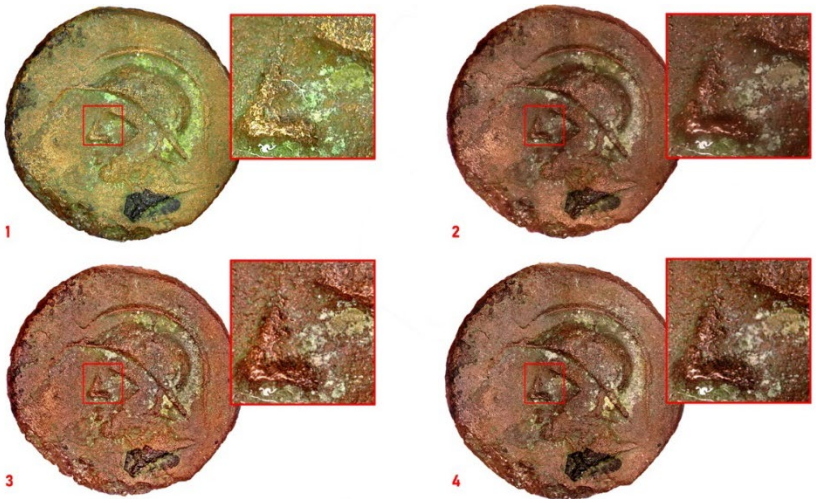

Figure 4. Comparison of models generated with different datasets: the first acquired with the "AM4113ZT Universal" microscope in Normal mode (i.e., in the absence of "special features"); the second, third and fourth models related to the acquisitions obtained with the "AM73915MZTL High Speed" microscope, respectively in EDOF, EDR and Normal mode. The "White Balance" has been set for an automatic colour analysis, without images post-corrections, resulting, however, a clear difference in the RGB data generated with the "AM4113ZT Universal" model (tending to green, top left), compared to those of the "AM73915MZTL High Speed" model (more chromatically accurate).

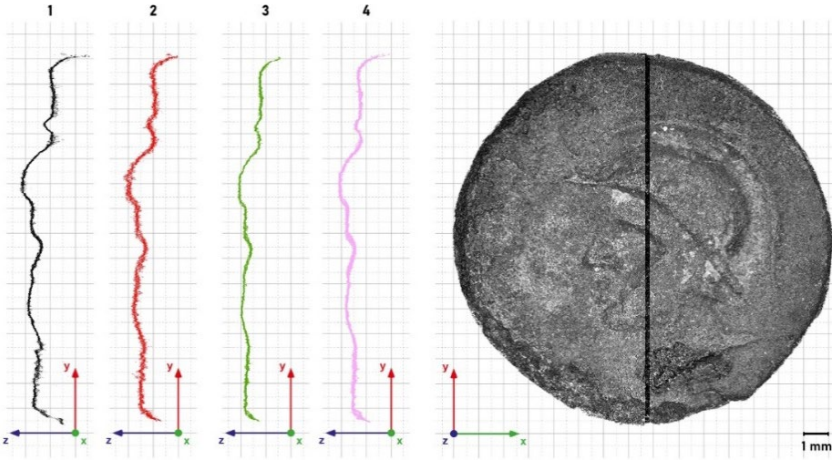

Figure 5. On the left, comparison among point clouds sections generated with different microscope models: the first with "AM4113ZT Universal" in Normal mode (i.e., in the absence of "special features"); the second, third and fourth with the "AM73915MZTL High Speed" microscope, respectively in EDOF, EDR and Normal mode. On the right, the point cloud obtained with the "Universal" microscope with the positioning of the slice chosen for the above comparison.

4. Considerations and future developments

The tests performed are suitable for defining the use of portable microscopes for photogrammetric purposes as valid.

The actual resolution of the data, the quality / price ratio, portability, and relative ease of use of these instruments, undoubtedly represent the strength of the method. In addition to software modifications, allowing Exif data to be saved, some modifications necessary to the calibrator in Figure 1 are now clear.

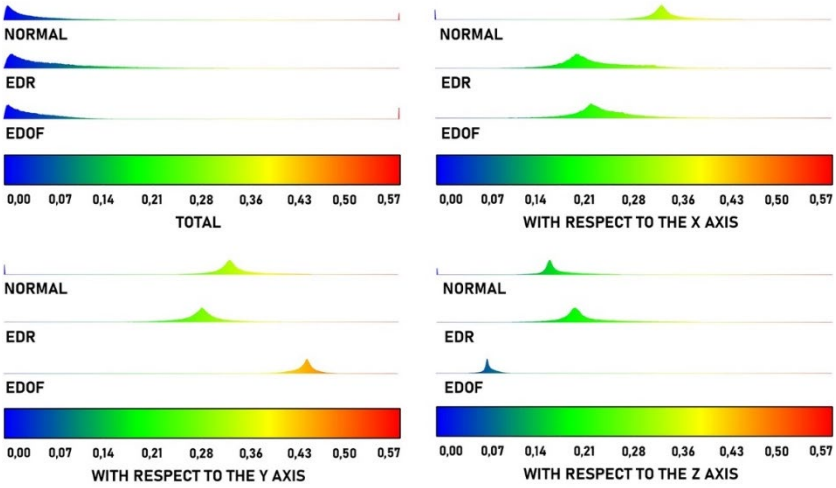

Figure 6. Global and relative deviations on the individual axes, expressed in millimetres. The data coming from the "Universal" microscope were taken as a reference in order to graph the deviations of the survey performed with the "High Speed" microscope (in Normal, EDOF or EDR mode).

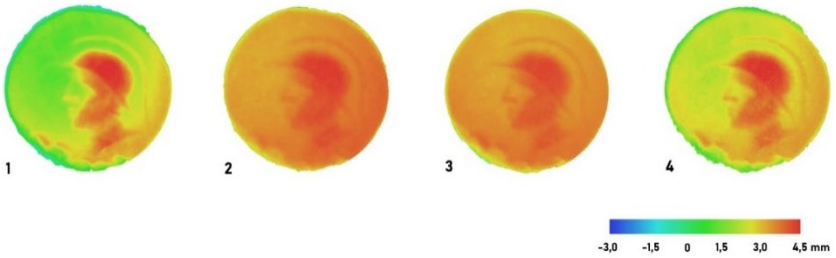

Figure 7. Comparison among Dense Surface Models generated with different datasets: the first with the "AM4113ZT Universal" microscope in Normal mode (i.e., in the absence of "special features"); the second, third and fourth models with the "AM73915MZTL High Speed" microscope, respectively in EDOF, EDR and Normal mode.

First, the thickness of the 3Dino Plate, which must be smaller than the one proposed.
This will allow the reduction of the distance between markers, allowing the identification of multiple points of known coordinates and therefore to have, in addition to Control Points, Check Points too.
Furthermore, it was observed the opportunity to modify plate's geometry, from rectangular to round, to adapt it to a motorized rotating plate, to facilitate possible acquisitions with an inclined axis, as well as providing it with protrusions on several levels, and to offer more planes of focus and a more rigorous tool for evaluating depths.
In addition, the acquisition procedure will have to be reconsidered in terms of magnification, blocking the microscope ring allowing to modify the Magnification Factor – keeping, therefore fixed the focal distance – and approaching and/or moving away from the object, or changing the relative Working Distance, always ensuring sufficient overlap (i.e., operating differently from combining shots with different MFs and WDs).
Despite the problems, within the framework of modern micro-technologies, more interesting ideas prevail from this work in progress for the three-dimensional documentation of very small artifacts that would otherwise be difficult to represent.

Notes

1. The issue of Velia "Atena/Tripode" is being studied by Federico Carbone, as part of the research project on monetary finds from Velia entitled "La moneta di basso conto a Elea/Velia: uso e produzione" (Directed by Renata Cantilena) and the Art Bonus project "Le monete di Elea/Velia - Un restauro per la conoscenza e la valorizzazione del patrimonio archeologico della città di Parmenide", carried out in collaboration with Soprintendenza Archeologia, Belle Arti e Paesaggio per le province di Salerno e Avellino and supported by the Fondazione Nazionale delle Comunicazioni (Rome).
2. Below are the settings of the 3D printer Creality CR-10 v 1.0 for the realization of the 3Dino Plate: bed temperature 50° C; nozzle temperature 200° C; nozzle diameter 0.3 mm; material used PLA 1.75 mm +/- 0.05 mm; layer height 0.12 mm; infill 20%; infill pattern cubic; printing speed 50 mm/s. The time taken was about 13 hours. The intrinsic characteristics of PLA make prints made with this material subject to relatively rapid deterioration due to moisture absorption and sensitivity to UV rays; this leads the authors to consider the choice of this material only valid for plate's prototyping phase. A steel prototype of the 3Dino Plate is being produced with the EOSINT M270 Xtended version printer.
3. The AM4113ZT Universal model was the subject of the previous publication, of which this contribution represents the natural continuation: Sara Antinozzi,

Diego Ronchi, Salvatore Barba (2020). Macro and Micro Photogrammetry for the Virtualization of the Orphic Foil (V-IV BC) of National Museum of Vibo Valentia / Macro e micro fotogrammetria per la virtualizzazione della laminetta orfica (V-IV a.C.) del Museo Nazionale di Vibo Valentia. In Arena A., Arena M., Brandolino R.G., Colistra D., Ginex G., Mediati D., Nucifora S., Raffa P. (a cura di). Connecting. Drawing for weaving relationships. Proceedings of the 42nd International Conference of Representation Disciplines Teachers / Connettere. Un disegno per annodare e tessere. Atti del 42° Convegno Internazionale dei Docenti delle Discipline della Rappresentazione. Milano: FrancoAngeli, pp. 1538-1555.

4. The aim of obtaining a greater detail leads to the use of high magnifications, but the different Working Distance of the two microscopes has not always allowed the use of the same magnification values. For example, magnification values close to 50x would have made contact of the AM4113ZT Universal microscope with the coin surface.

References

1. Adamopoulos, E., Rinaudo, F. An Updated Comparison on Contemporary Approaches for Digitization of Heritage Objects. In Proceedings of *2019 IMEKO TC-4 International Conference on Metrology for Archaeology and Cultural Heritage*; Catelani M., Daponte P. (Eds); Firenze, Italia, 4-6 Dicembre, 2019, pp. 1-6.
2. Pieraccini, M., Guidi, G., Atzeni, C. 3D digitizing of cultural heritage. *Journal of Cultural Heritage* **2001**, *2*, 63-70.
3. Hansen, H.N., Carneiro, K., Haitjema, H., De Chiffre, L. Dimensional Micro and Nano Metrology. *CIRP Annals* **2006**, *55*(2), 721-743.
4. Galantucci, L.M., Pesce, M., Lavecchia, F. A powerful scanning methodology for 3D measurements of small parts with complex surfaces and sub millimeter-sized features, based on close range photogrammetry. *Precision Engineering* **2016**, *43*, 211-219.
5. Gontard, L. C., Schierholz, R., Yu, S., Cintas, J., Dunin-Borkowski, R. E. Photogrammetry of the three-dimensional shape and texture of a nanoscale particle using scanning electron microscopy and free software. *Ultramicroscopy* **2016**, *169*, 80-88.
6. Esmaeili, F., Ebadi, H. Handy Microscopic Close-Range Videogrammetry. *The International Archives of the Photogrammetry, Remote Sensing and Spatial Information Sciences* **2017**, *XLII-4/W4*, 65-67.
7. Apollonio, F.I., Fantini, F., Garagnani, S., Gaiani, M. A. Photogrammetry-Based Workflow for the Accurate 3D Construction and Visualization of Museums Assets. *Remote Sensing* **2021**, *13(3),* 486-526.
8. Plisson, H., Zotkina, L. V. From 2D to 3D at macro- and microscopic scale in rock art studies. *Digital Applications in Archaeology and Cultural Heritage* **2015**, *2*(2-3), 102-119.
9. Mitchell, H. L., Kniest, H. T. Digital Photogrammetry and Microscope Photographs. In *Photogrammetric Record* **1999**, *16*, 695-704.
10. Tolksdorf, J. F., Elburg, R., Reuter, T. Can 3D scanning of countermarks on Roman coins help to reconstruct the movement of Varus and his legions. *Journal of Archaeological Science: Reports* **2017**, *11*, 400-410.
11. Bolognesi, C. M., Fiorillo, F. Optimization of texture mapping process in the Reality-Based Modeling application. In *Rappresentazione/Materiale/Immateriale. 40° Convegno internazionale dei docenti delle discipline della Rappresentazione – Congresso della Unione*

Italiana per il Disegno; Salerno Rossella (Ed); Gangemi Editore International: Roma, Italia 2018, pp. 337-342.

12. Morena, S., Barba, S., Álvaro-Tordesillas, A. Shining 3D Einscan-Pro, application and validation in the field of Cultural Heritage, from the Chillida-Leku Museum to the Archaeological Museum of Sarno. *The International Archives of the Photogrammetry, Remote Sensing and Spatial Information Sciences* **2019**, *XLII-2/W18*, 135-142.
13. Hess, M., MacDonald, L.W., Valach, J. Application of multi-modal 2D and 3D imaging and analytical techniques to document and examine coins on the example of two Roman silver denarii. *Heritage Science* **2018**, *6(5)*, 1-22.

In *UID, Congress of Unione Italiana per il Disegno, Volume: CONNETTERE un disegno per annodare e tessere, Reggio Calabria, Italy, 17-19 September 2021.*
http://dx.doi.org/10.3280/oa-693.108

0
0.5
1 mm

Capitolo 4
3Dino configuration for a micro-photogrammetric survey: applying Dino-Lite microscope for the digitalization of a cuneiform tablet

Abstract: Close-range photogrammetry, due to the possibilities offered by the technological evolution of acquisition tools and, above all, the relative original challenges posed to surveyors and the theory of measurements, deserve constant critical attention. The new opportunities to detect and represent reality are mostly focused on historical architecture, referring to consequent orders of magnitude and restitution scales. On the other hand, the formalization of relevant practices for very small objects is not frequently addressed. In recent tests carried out using two Dino-Lite handheld digital microscope models, polarized light digital microscopes generally used in medical and industrial fields, we proved the potential of using these imaging systems also for Cultural Heritage documentation, highlighting, however, some issues related to the depth of field and the consequent acquisition geometry. Therefore, this study aims to solve these problems, increasing the performance of microscopic photogrammetry by optimizing the acquisition procedures with the design of custom accessories for micro-photogrammetry (e.g., a calibrated plate). These developments will be carried out as part of a technology transfer agreement with the Dino-Lite company pointed to codify a protocol for high accuracy photogrammetric documentation of small artefacts.

Keywords: Digital Heritage, Small artefacts, Detailed 3D shape, Handheld microscope.

1. Introduction

The configuration of new survey approaches for Cultural Heritage's digitization in terms of conservation, management, and promotion is gradually asserting itself within the so-called "fourth industrial revolution". The possibilities offered by Industry 4.0 thicken the network of relationships of complementarity and interaction between

the different disciplines related to imaging and three-dimensional processing, including manufacturing industry, medical sciences, entertainment and, of course, Cultural Heritage [1].
In particular archaeological disciplines are greatly interested in using emerging and available digital techniques and technologies provided by Geomatics aiming at rigorous objects description [2] and preservation of human heritage, at least in digital format, by developing the concept of "preventive and planned conservation", for the restoration field, here declined in order to establish a "preventive digital memory" [3]. Furthermore, given the recent inaccessibility conditions, rethinking representation and visualization phases of the assets constitute a possibility for remote sharing, as well as the establishment of a vast system of information storage, editable and implementable at any time [4], as well as the representation of real-world heritage for interaction and virtual experience [5].
Usual procedures for documenting heritage objects are mainly addressed to orders of magnitude and architectural restitution scales, but still little oriented towards the coding and formalization of relevant practices for very small objects. In fact, interfacing with small finds represents a not easy challenge determining a change in the representation scale and a rethinking of the acquisition operating systems, not always in comfortable contexts [6]. In particular, applications for Cultural Heritage have stricter requirements on morphological details, whose correct reproduction necessarily refers to other factors such as object's size and shape and surface's reflective properties – whether it is opaque, glossy or translucent [7]. Several solutions for micrometric applications [8], including range-based ones [9], are increasingly succeeding in the field of Cultural Heritage study. However, not infrequently, certain optical or mechanical limitations, the need for specialized operators and the considerable costs direct the interest towards precision photogrammetry, which offers the possibility of obtaining the three-dimensional (3D) coordinates of an object from two-dimensional (2D) digital images in a rapid, accurate, reliable, flexible and economical way [10]. In detail, the possibility of using photographs taken by a digital microscope as a dataset for photogrammetric processing revealed a not negligible potential for small objects modelling, reaching about 0.1 mm accuracy [11].

A digital microscope is similar to a traditional optical microscope except that it is equipped with a CCD camera so that it can output a digital colour image to a monitor, and among the main types of a microscope are the most flexible and the least expensive [12].
Digital portable microscopes, born for inspection, documentation, and digital metrology analysis - already popular in the manufacturing and quality control industry, as well as used in the medical field - are easy to handle and versatile capturing systems. On the other hand, the images they provide do not have both: very high resolution (usually not exceeding 5 MP) and wide dynamic range. In addition to these problems, the narrow Field Of View (FOV) and shallow Depth Of Field (DOF), which could compromise close-range photogrammetry, should be mentioned. These limitations could, in fact, affect point matching, the number of conjugate points computed, and the resolution of the 3D model [13], also determining an increase in acquisition times because it makes necessary to move the microscope often to cover the object. In this case, the acquisition automation would make the entire process more advantageous [14].

2. Case Study

One of the current challenges is to configure a high performance micro-photogrammetric system using the now widely available on the market digital portable microscopes. The main aim is to test their validity on micro-scale survey, overcoming the obvious operational difficulties, especially in the acquisition phase. For this purpose, in this current work, the authors will focus on the systematization of individually available hardware tools to explore microscopic photogrammetry and define a standard procedure for the acquisition of very small objects. Therefore, it is proposed the procedural solutions identified to carry out the digital survey of a 3D printing replica[1] in geopolymer of a tablet with cuneiform writings. The text content concerns the administrative information for fish deliveries (a modern correspondent of a packing slip). Its dimensions are approximately 20×22×8 mm, and the characteristic wedge-shaped impressions have a depth of 1-3 mm (Figure 1). This paper focuses on studying the most suitable 3D measurement instrumentation and method to achieve a digital replica of this tiny, complex, and detailed object.

Figure 1. Recto and verso views of the 3D printed copy of the cuneiform tablet.

For the survey tests, it was used the 3D printing replica, as challenging as the original, with the intention of preserving the original spirit of multidisciplinary research that aims to use a physical (or digital) replica of the tablets for scientific purposes.
To achieve an adequate descriptive quality and evaluate results soundness, the survey was conducted with two different Dino-Lite portable digital microscopes (www.dino-lite.eu).
The quality, speed and cost-effectiveness of this first method were then compared with the data obtained from a Nikon full frame camera combined with macro optics. All photogrammetric results were compared with an active sensor, the SCAN in a BOX structured light 3D scanner, used as a reference.

3. Materials and Methods

2.1. 3Dino Plate

Digital close-range photogrammetry exploits several photographic captures taken from different viewpoints for accurately measuring objects and build a digital 3D model. Compared to the canonical close-range photogrammetry acquisition, a redesign of the acquisition hardware system at the dimensional scale is required to solve some critical issues strongly amplified at a sub-millimetre level. In detail, the innovative micro-photogrammetric scanning system proposed in this

study, called "3Dino System", is based on the combined use of a three-dimensional calibrator and Dino-Lite handheld digital microscopes.
One of the main problems is the need to include in the scene metric references or calibrated objects and, even by solving this difficulty, to be able to produce an adequate calibration pattern according to the magnitude of the object to be measured [15].
To address these issues, a calibrated plate – designed by the authors and built for the occasion – was used to optimize, align and for scaling procedures (Figure 2). This calibrator, called "3Dino Plate", consists of a PLA plate obtained with 3D filament printing, characterized by an orthogonal pattern of 99 truncated cone holes, with a countersink angle of 60° and a smaller base diameter of 0.35 mm.
The calibrator accuracy, based on the 3D printing settings[2] and the conformity of the actual position of the holes with respect to the project file, has been estimated at 0.1 mm, which can be assumed as an instrumental error value (i.e., markers accuracy).
The coordinates of each hole, in a local reference system, are therefore known to the operator and can be imported into the photogrammetric project and linked to acquisitions. This allows the use of the perforated pattern as a constraint points (GCP) grid – homogeneously distributed throughout all the area – to optimize cameras alignment.

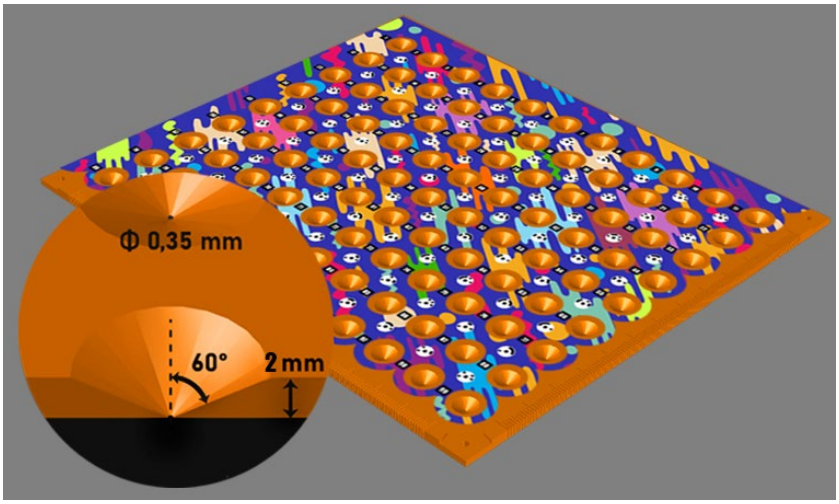

Figure 2. The three-dimensional calibrator "3Dino Plate" and detail of the section of one of the truncated cone holes.

To guarantee sufficiently robust results during the alignment phase, an adhesive geometrically and chromatically nonrepetitive pattern, equipped with coded targets, was printed and applied on the calibrator. The difficulty of manually conducting microscope acquisitions represents a further obstacle. To facilitate and speed up the acquisition phase, a portion of the calibrated plate was set on a plane allowing the object movement. Using the digital microscope housed on a vertical bracket at a fixed angle, a series of images with sufficient overlap can be taken just by sliding the calibrated plate manually once the magnification rate has been chosen (Figure 3).
The main problem encountered in microscopic optics is the short Depth Of Field (DOF), and it is emphasized when increasing magnification. This allows having in focus only a small portion of the artefact so that only a small portion of the image appears sharp enough to be used for 3D reconstruction [16]. In fact, the sharpness, joint with density and the resolution of the photoset, will determine the quality of the output point cloud data [17].
To overcome the problem of the short DOF, one possibility would obviously be to close the aperture of the optics as much as possible within the limits of the diffraction phenomena [18].

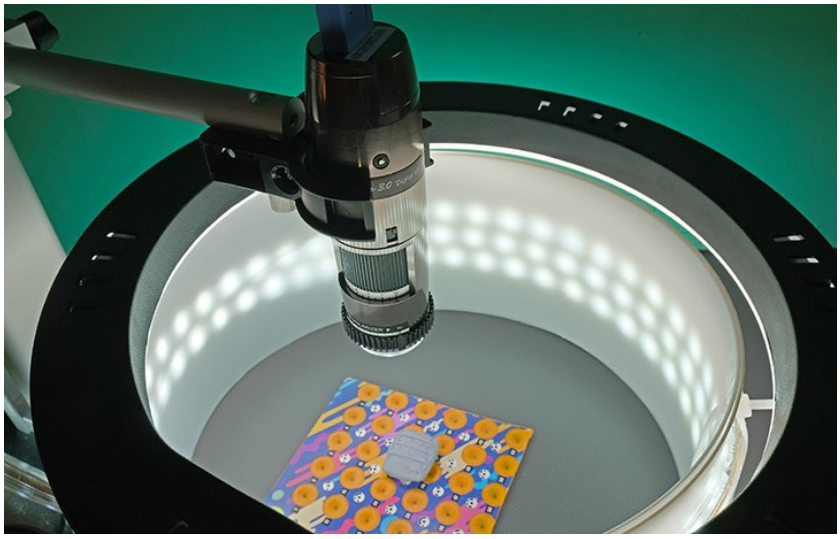

Figure 3. "3Dino Plate" here combined with the Dino-Lite microscope in the "3Dino System" configuration.

Since this possibility is not available on portable digital microscopes, where the diaphragm is fixed, it is necessary to use alternative solutions. For this purpose, the object is acquired from various focus planes by moving the microscope on a micrometric vertical rail to focus on different planes without changing the distance between the object and the optical centre.

2.2. Dino-Lite digital microscopes

Dino-Lite digital microscopes provide a powerful, portable, and functional solution for detail inspection. The models compared for this first experimentation, Universal (AM4113ZT) and High Speed, (AM73915MZTL) belong to two different categories, both in terms of technical characteristics and of special features, consequently falling into very different price ranges (Table 1).

The element that clearly distinguishes the two microscopes is the Working Distance (WD), i.e., the linear distance between the tip of the microscope nozzle and the subject (Figure 4).

This factor directly affects the Magnification Factor (MF), Field of View (FOV) and Depth Of Field (DOF).

Table 1. Dino-Lite microscopes technical specifications for the models used.

	AM4113ZT	**AM73915MZTL**
Category	Universal	High Speed
Diffuser	Optional	Included
Magnification	10-70×, 200×	10-140×
Working Distance	Standard	Long
Resolution	1.3 MP (1280×1024)	5 MP (2592×1944)
Maximum Frame Rate	30 fps	45 fps
Interface	USB 2.0	USB 3.0
Special features	No	EDR, EDOF, FLC
Price	€ 200-350	€ 1000-1250

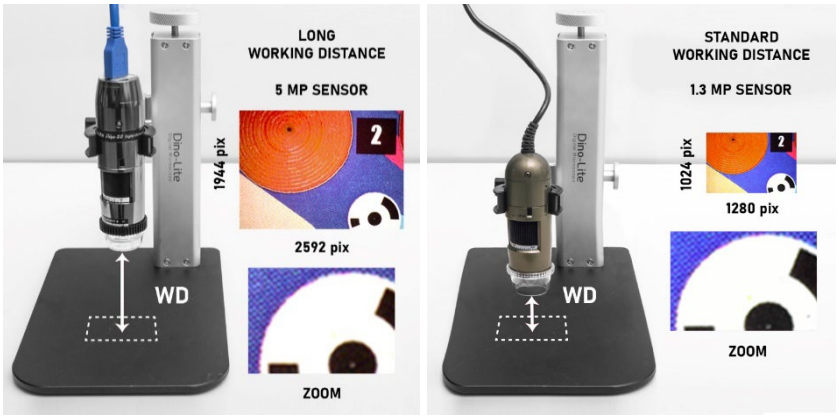

(**a**) (**b**)

Figure 4. Working Distance reached by the High Speed microscope (a, 75.5 mm) and by the Universal microscope (b, 21.7 mm), housed on the stand and operating at the same magnification (30×). Specifically, the acquisition of a relative portion of the calibrator and a detail of the pattern (ZOOM).

It is trivial to observe that a right compromise must be established between these factors, bearing in mind that the further you are from the subject (high WD), the lower the Magnification, with a wider Field Of View and more Depth Of Field; conversely, the closer you are to the subject (low WD), the greater the Magnification, with a smaller Field Of View and less Depth. Therefore, the WD is an extremely important parameter from a practical point of view and inevitably binds the use of different magnifications in the operational phase.

The lighting conditions, based on the polarized light of the microscopes, have been improved with the adoption of two LED illumination rings, one which is around the object and the other above it.

The light does not directly affect the object because of a cylindrical panel consisting of diffusing material, placed between the object and the light source: thus, diffused light conditions neutralize the shadow cones - without variations in the intensity of shadows, lights and colours.

Both Universal and High Speed models were combined with the 3Dino Plate System, fixing the microscope in the special Dino-Lite RK-10-EX stand and connecting it to a portable workstation (Figure 5a).

Hence, the acquisitions were carried out with the same magnifications, 30×, operating with the dedicated DinoCapture 2.0 procedure.

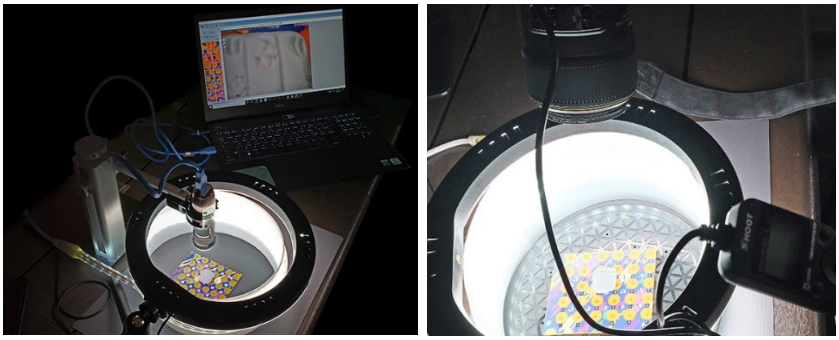

(**a**) (**b**)

Figure 5. (a) "3Dino System" with the special LED ring lighting set-up; (b) "3Dino Plate" and Nikon setup configuration for the photos acquisition. Take a look at the digital model here: https://skfb.ly/on67U.

2.3. Acquisition with Nikon camera

The validation of Dino-Lite digital microscopes results was supported by the photogrammetric survey with a Nikon D810 SRL and the calibrator 3Dino Plate, also suitable for digital cameras.

The best optical systems for small objects are the macro lens and, as well as allowing the close focus in order to maximize the data quality, they also represent, among the types of optics, those optically less affected by distortions. n our case, an AF-S VR Micro-Nikkor 105 mm f/2.8G IF-ED was used, which allows a minimum focusing distance of 0.314 m. In this case, it was possible to manage the shallow Depth Of Field and the related problem of blur. Starting from the concept that the Depth Of Field increases with the decrease of the aperture with the consequent reduction of the amount of light passing through and the relative increase in exposure times [19], an aperture of f/36 was used, shooting at about 35 cm, thus ensuring a DOF equal to about 2 cm.

A camera trigger system was used to remotely activate the shutter on the camera and reduce the vibrations, which are not negligible due to the relatively long exposure time (Figure 5b).

2.4. Tie points error reduction and optimization

The datasets obtained by Dino-Lite microscopes and by Nikon camera were thus processed in a SfM software, Agisoft Metashape, according to the general photogrammetric workflow (Table 2 and Table 3) and the

processing was completed with the same graphic workstation equipped with Intel I9 9900k CPU, RTX2080ti GPU, and 64GB of RAM. The sparse point cloud, made only by tie points (TPs), is the starting point for the realization of a complete 3D model. However, the removal of low quality TPs is appropriate because their presence affects the results of the next steps, which consist in the recomputation of the orientation parameters, and the creation of the final dense cloud [20]. The evaluation of image orientation quality within SfM methods can be performed using the Gradual Selection filter tool by Agisoft Metashape, which – like most photogrammetric software – allows you to filter the sparse point cloud based on some quality parameters. The parameters considered in this study were: Reconstruction uncertainty, Reprojection error and Projection accuracy.

Table 2. Recto Agisoft Metashape survey data comparison.

	Universal	**High Speed**	**D810**
Aligned cameras	501/502	507/591	167/167
Sparse Points	2.4×10^5	2.0×10^5	8.0×10^5
Dense Points	1.0×10^6	0.8×10^6	3.1×10^6
Ground Resolution	9.77 μm/px	4.82 μm/px	5.64 μm/px
RMS	0.324 px	0.797 px	0.829 px
Check Points error	0.076 mm	0.440 mm	0.089 mm

Table 3. Verso Agisoft Metashape survey data comparison.

	Universal	**High Speed**	**D810**
Aligned cameras	508/508	629/631	175/175
Sparse Points	2.4×10^5	1.9×10^5	8.0×10^5
Dense Points	1.0×10^6	0.9×10^6	3.0×10^6
Ground Resolution	9.24 μm/px	5.07 μm/px	5.59 μm/px
RMS	0.374 px	0.867 px	1.01 px
Check Points error	0.056 mm	0.47 mm	0.070 mm

4. Reference model equipment

The instrument employed – to have a reference model and check the overall geometrical dimensions of the photogrammetric reconstructions – is the SCAN in a BOX (@2015 Open Technologies SRL). The system is equipped with two high-resolution industrial USB cameras and a high definition light projector (ASUS S1).

All components are fixed on a thick aluminium rail, but the cameras can be moved in calibrated positions (base) to customize the work field (Figure 6). The main steps for the 3D measurements workflow are: (i) calibration of the optical setup, (ii) range maps acquisition, (iii) raw alignment, (iv) alignment optimization and (v) meshing.

Whenever the scanner is mounted or the camera setting on the support bar changes, the system needs to be configured and calibrated. The coded calibration master has three different patterns based on the working area selected. The optical setup provides for projector and cameras configuration (position, orientation, focus, exposition). The calibration allows calculating the optical parameters of the specific setting. According to the object dimension and the resolution required, it is to choose the scanning area more suitable, strictly connected to the working distance and the distance of the cameras on the plate.

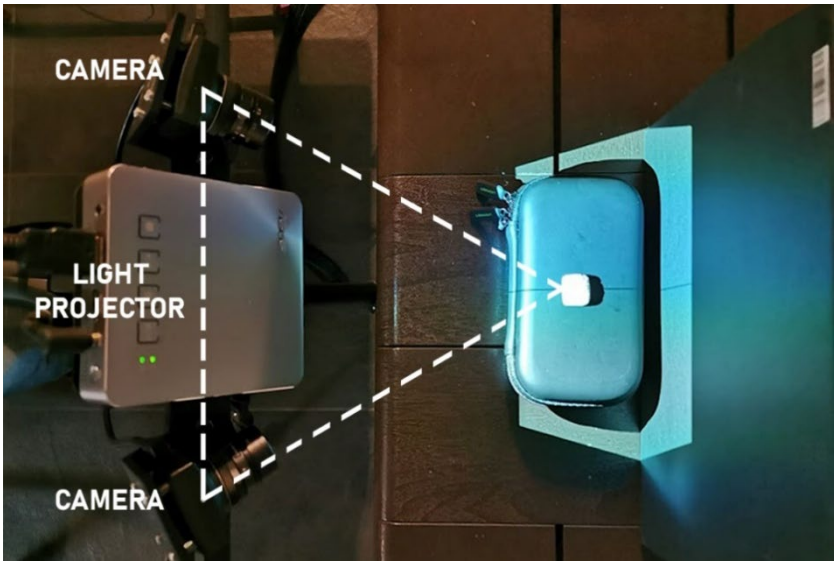

Figure 6. The "SCAN in a BOX" system.

For our case study, a Field Of View of 100×80 mm was set that implies the working distance scanner-object of about 200 mm, the minimum base between the two cameras and the minimum point spacing (resolution) on the surface 0.078 mm.
The digital reconstruction of the object surface and details was performed acquiring: 16 nadiral scans on both sides (8 for the verso and 8 for the recto), 16 tilted (8 for each side) and 8 nadiral to the four edges (totally of 40 range maps). The scanning time for each range map is less or equal to 4 seconds. The raw in progress alignment process was very useful to check real-time scan completeness. This initial registration is then optimized using an Iterative Closest Point (ICP) algorithm. The final mesh model (formed by about 400.000 polygons) have fewer details of the correspondent photogrammetric models but can be used to ensure a reference check of their global measures (Figure 7).

5. Data analysis

The aim of this analysis is to compare the procedures adopted to digitize of the cuneiform tablet with the various technologies.
The first consideration concerns the difficulty with the current 3Dino configuration and camera setting in acquiring the two sides of the object in a single set of photographs. This problem is related to the acquisition geometry and the calibrator shape. Two sets of images, one for recto and the other for verso side, do not have enough points in common to be merged into a single model.
It would have been necessary the acquisition of the very thin edge.
In this case, we would have had a depth of field problems that could have compromised the alignment of this possible set of additional images. A further consideration concerns the management procedures of the images in Agisoft Metashape for data and products obtainable with microscopes and camera. More specifically, among the most obvious and limiting digital microscopes problems, there is the absence of Exif data. This information associated with the pixel matrix, as well known, retains data relating to the camera model, sensor size and focal length, and are essential variables, in the absence of laboratory calibration, used by any software to perform adequate calculations for the internal and external camera calibration.

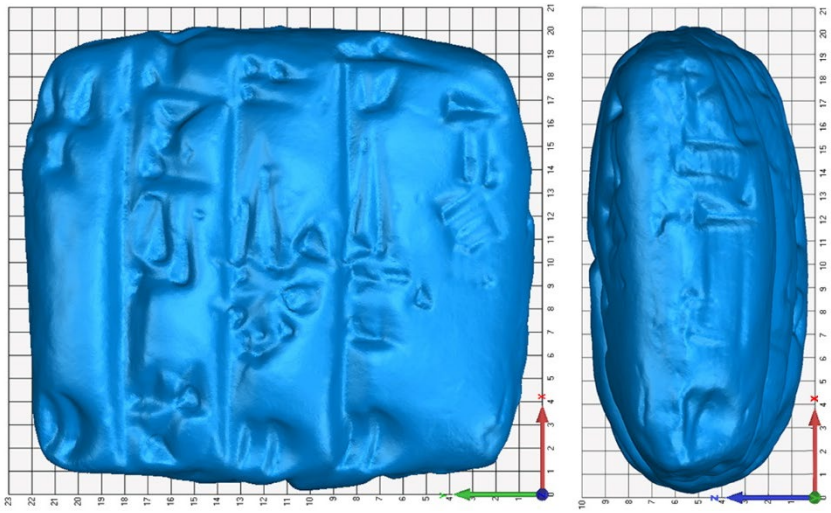

Figure 7. "SCAN in a BOX" polygonal model (1 mm grid background).

Therefore, the uncertainty generated by the absence of Exif data must be considered as a further detrimental parameter for the alignment processes. To provide a robust comparison[3] for the point clouds, a cloud to cloud registration has been performed using the data coming from the SCAN in a BOX as reference. The registration was carried out in two steps, providing: first, a manual registration using homologous points and then a global registration by automatic alignment algorithms (ICP[4]). The photogrammetric survey accuracy assessment was carried out using CloudCompare C2C (cloud to cloud) command. This tool searches, for each point being compared, the closer one in the reference entity, thus defining a shift value of the first with respect to the second. Using the cloud generated by the SCAN in a BOX as a reference, the clouds obtained from photogrammetry were compared.

The Figure 8 shows in false colours the deviations among the clouds. Through the calculations performed it is noted that the mean and standard deviations do not exceed the instrumental accuracy of the 3Dino Plate (0.3 mm). The comparison procedure showed a difference on the Z axis of the model compared with the reference one. This difference could have been determined by both the registration procedure and the higher resolution obtained from the photogrammetric survey performed with Nikon and Dino *Universal*.

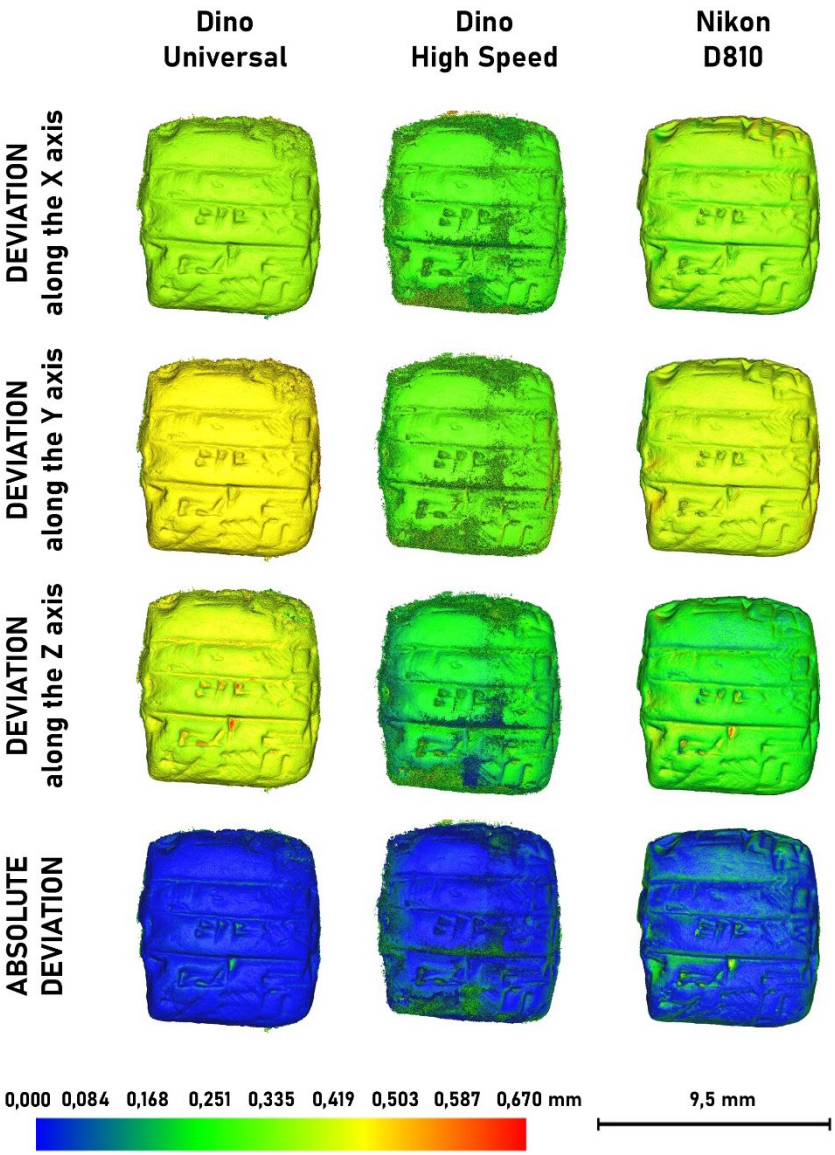

Figure 8. Global and relative deviations of micro photogrammetric dense clouds compared with the "SCAN in a BOX" used as reference model (verso side).

The noise, due to alignment problems, of the photogrammetric set acquired with Dino *High Speed* is evident. Absolutely comparable, and perhaps of slightly higher quality than the SCAN in a BOX, are the results coming from Dino *Universal* (Figure 10 and Figure 11).

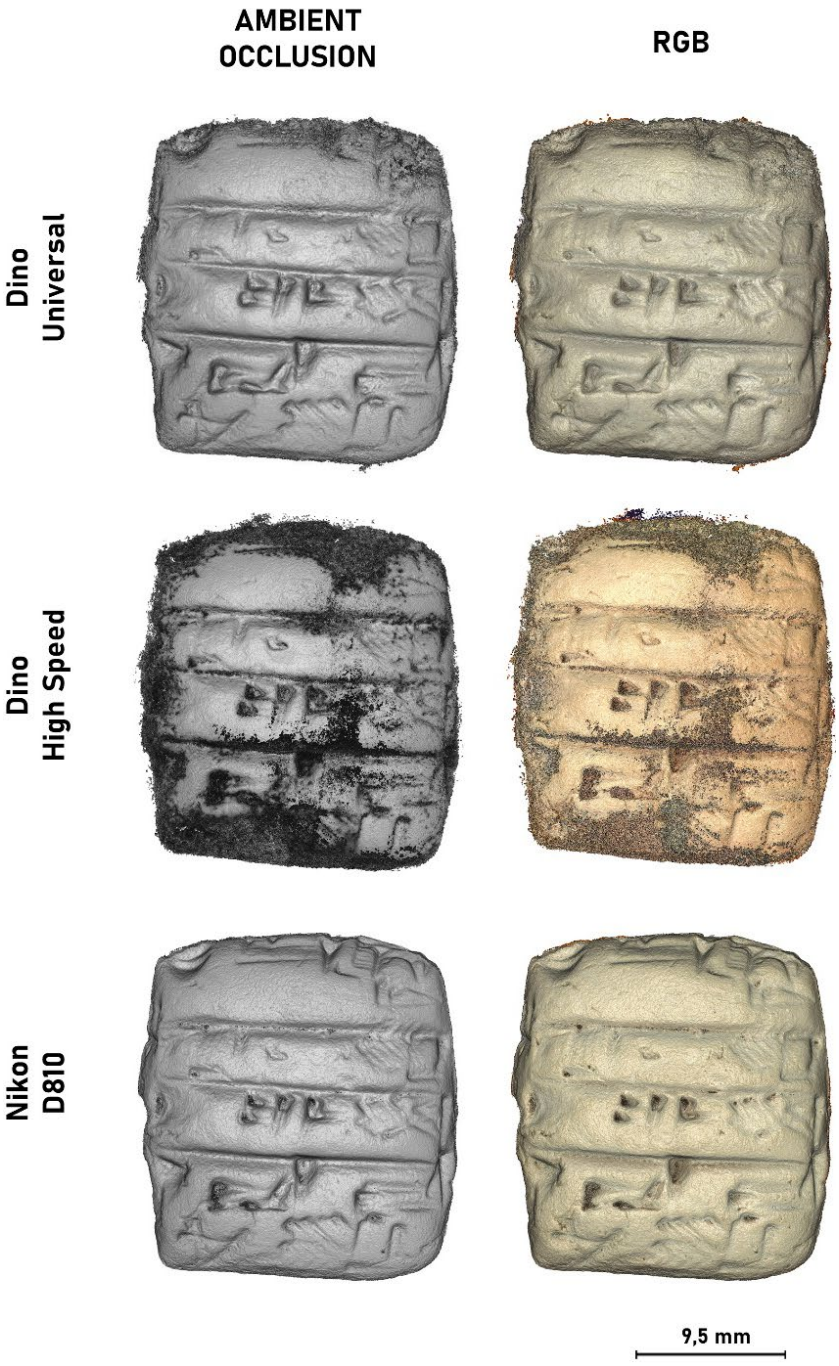

Figure 10. Colour per vertex of verso side acquired with the different passive sensors.

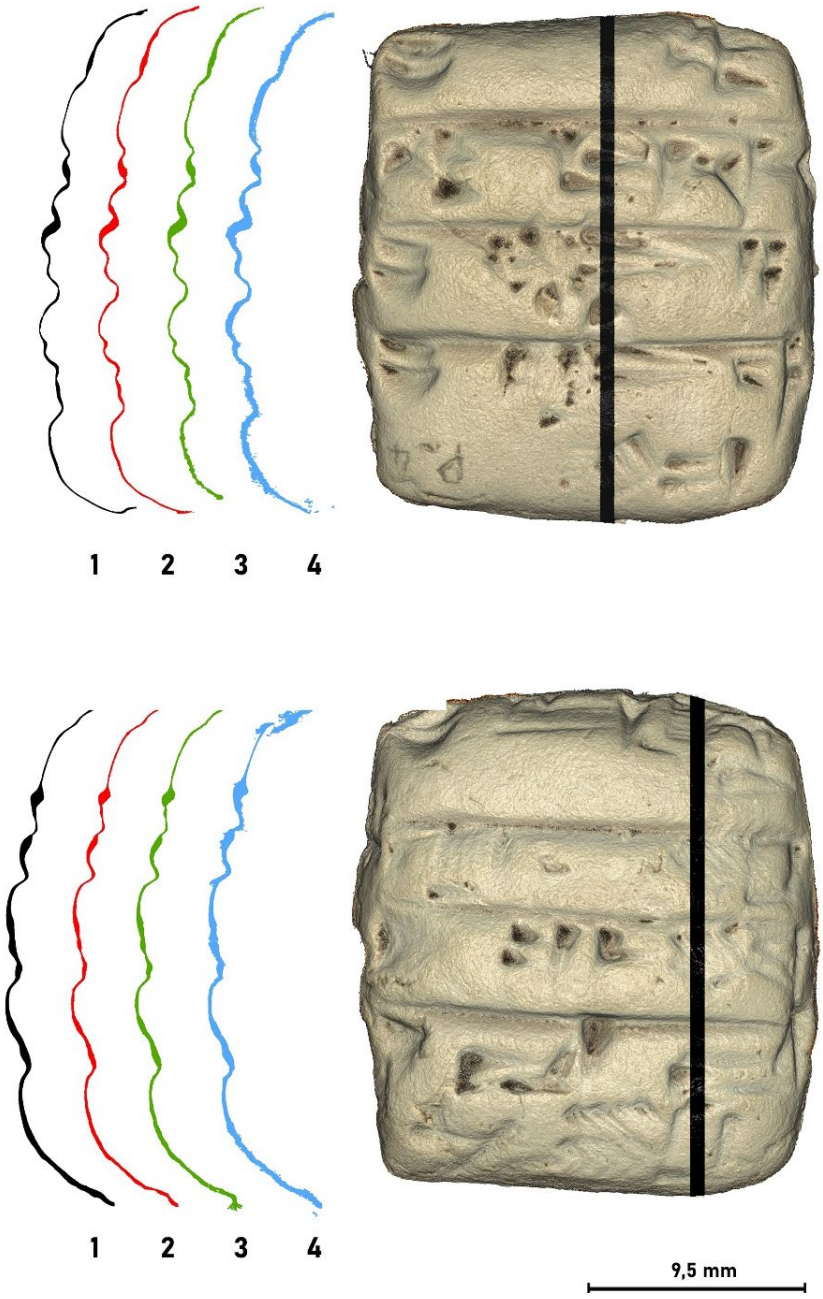

Figure 11. On the left, a comparison of point clouds sections generated with different datasets: 1) by "SCAN in a BOX", 2) by Nikon D810, 3) by microscope Dino Universal and 4) by microscope Dino High Speed. On the right, the point cloud obtained from the Nikon D810, with the positioning of the slice chosen for the comparison.

A final consideration concerns the parameters: cost, time and quality of output. In this regard, with a cost of a few hundred euros and a quality comparable to that obtained by Nikon and SCAN in a BOX, the Universal microscope is one of the most interesting instruments. The flaw concerns the acquisition time, still long (about 3-4 hours for 500-600 captures) that can be shorten with the design of an automatic capturing system.

6. Conclusions and future developments

The experimental tests conducted with Dino-Lite instrumentation are valid for defining a first approach to the photogrammetric use of portable USB microscopes.

The quality/price ratio of Dino-Lite microscopes, combined with the obtainable high resolution, undoubtedly represent the method strengths. Portability and ease of use are two additional and significant qualities. On the other hand, it is necessary to specify that, to pursue the survey primary objective, that is the verifiability of metric data, some key aspects are still to be more rigorously defined. In addition to software house changes to enable the Exif data to be saved, there are several changes required to the calibrator in Figure 2. Firstly, reducing the makers dimensions and spacing will allow more points of known coordinates to be identified. Moreover, the geometry of the plate could be modified to fit a motorized turntable to facilitate possible tilted-axis acquisitions. However, the 3Dino Plate is suitable for objects up to 2-3 mm thickness, i.e., mainly two-dimensional objects such as coins. In such cases, it would not be necessary to change the geometry of the plate. It should be borne in mind, however, that the use of the plate always requires two sets of acquisitions. The problem of shallow depth of field remains and can really be solved by reshaping the acquisition, e.g., with Focus Stacking techniques, using a micrometric slide to move the optical system. For these reasons, and in order to streamline the acquisition procedures and ensure a more rigorous workflow, the authors are designing a system that involves reformulating the plate geometry in order to adapt it to a rotary table system that makes the object rotate - and not translate - with respect to the sensor. Although still with limited architectural applications, this experiment showed that, verifying their great accuracy, it is possible to adopt this system for photogrammetric survey of tiny artifacts. Consequently, in further applications, this procedure could be

extended to different acquisition scales, such as architectural ornaments and friezes, possibly evaluating the integration of macro optics too.
Despite the problems within the framework of modern micro-technologies, more interesting ideas for the three-dimensional documentation of very small artefacts that would otherwise be difficult to represent prevail from this work in progress.

Notes

1. The cuneiform tablet used as a test is the 3D printing replica in geopolymer of the 724 tablet realized by the +LAB (www.piulab.it - Politecnico di Milano). The original 724 tablet was 3D measured by the 3D Survey Group (Politecnico di Milano). The interdisciplinary research aims to obtain a digital and physical clone of the cuneiform tables with high details and high accuracy for education and scientific purposes (e.g., shared analysis and studies among a team of archaeologists to decipher a text content).
2. The specific print settings for making the plate are listed below: print used: Creality CR-10 v 1.0; dimensions: bed 300×300 mm x height 400 mm; bed temperature: 50 °C; nozzle temperature: 200 °C; nozzle diameter: 0.3mm; material used: PLA 1.75 mm ± 0.05 mm; layer height: 0.12 mm; infill: 20%; infill pattern: cubic; printing speed: 50 mm/s; approximate time for printing: 13 hours.
3. To perform a homologous comparison for both active and passive techniques, the procedure was performed in CloudCompare 2.10.2.
4. The ICP (Iterative closest point) algorithm, because of its iterative nature, can only guarantee the convergence to a local minimum. The error in the final registration is expressed through RMSE, or RMS of the Euclidean distance between the match point pairs of the alignment process. For each ICP iteration the maximum number of matches was set to 50.000 and the number of iterations for the process equal to 60.

References

1. Pieraccini, M., Guidi, G., Atzeni, C. 3D digitizing of cultural heritage, *Journal of Cultural Heritage* **2001**, *2*, 63-70.
2. Bitelli, G., Girelli, V.A., Remondino, F., Vittuari, L. The potential of 3D techniques for Cultural Heritage object documentation, *Proc. SPIE 6491, Videometrics IX* **2007**, 244-253.
3. Carlucci, R. Dalla scomposizione della realtà alla memoria digitale preventiva. *Archeomatica – Tecnologie per i Beni Culturali* **2016**, *1*.
4. Apollonio, F.I., Fantini, F., Garagnani, S., Gaiani, M. A. Photogrammetry-Based Workflow for the Accurate 3D Construction and Visualization of Museums Assets. *Remote Sensing* **2021**, *13(3),* 486-526.
5. Djuric, I., Stojakovic, V., Misic, S., Kekeljevic, I., Vasiljevic, I., Obradovic, M., Obradovic, R. Church Heritage Multimedia Presentation: case study of the iconostasis as the characteristic art and architectural element of the Christian Orthodox churches. In Proceedings of *37 eCAADe and XXIII SIGraDi Joint Conference*, G. Castro Henriques, J.P. Sousa, P. Gomez-Zamora, H. Achten (Eds); Porto, Portugal, 11-13 September 2019; pp. 551-560.
6. Plisson, H., Zotkina, L. V. From 2D to 3D at macro- and microscopic scale in rock art studies. *Digital Applications in Archaeology and Cultural Heritage* **2015**, *2*(2-3), 102-119.

7. De Paolis, L.T., De Luca, V., Gatto, C., D'Errico, G., Paladini, G.I. Photogrammetric 3D Reconstruction of Small Objects for a Real-Time Fruition. In Proceedings of *Augmented Reality, Virtual Reality and Computer Graphics - AVR2020*, L.T. De Paolis, P. Bourdot (Eds); Springer International: Cham, Swizerland 2020, pp.375-394.
8. Hansen, H.N., Carneiro, K., Haitjema, H., De Chiffre, L. Dimensional Micro and Nano Metrology. *CIRP Annals* **2006**, *55*(2), 721-743.
9. Tolksdorf, J. F., Elburg, R., Reuter, T. Can 3D scanning of countermarks on Roman coins help to reconstruct the movement of Varus and his legions. *Journal of Archaeological Science: Reports* **2017**, *11*, 400-410.
10. Yilmaz, H.M., Yakar, M., Yildiz, F. Digital photogrammetry in obtaining of 3D model data of irregular small objects. *The International Archives of the Photogrammetry, Remote Sensing and Spatial Information Sciences* **2008**, *XXXVII*, 125-130.
11. Esmaeili, F., Ebadi, H. Handy Microscopic Close-Range Videogrammetry. *The International Archives of the Photogrammetry, Remote Sensing and Spatial Information Sciences* **2017**, *XLII-4/W4*, 65-67.
12. Atsushi, K.; Sueyasu, H.; Funayama, Y.; Maekawa, T. System for reconstruction of three-dimensional micro-objects from multiple photographic images. *Computer-Aided Design* **2011**, *43(8)*, 1045-1055.
13. Kontogianni, G.; Chliverou, R.; Koutsoudis, A.; Pavlidis, G.; Georgopoulos, A. Enhancing Close-Up image-based 3D Digitisation with Focus Stacking. *The International Archives of the Photogrammetry, Remote Sensing and Spatial Information Sciences* **2017**, *XLII-2-W5*, 421-425.
14. Mitchell, H.L., Kniest, H.T. Digital Photogrammetry and Microscope Photographs, *Photogrammetric Record* **1999**, *16*, 695-704.
15. Lavecchia, F.; Guerra, M.G.; Galantucci, L.M. Performance verification of a photogrammetric scanning system for micro-parts using a three-dimensional artifact: adjustment and calibration. *The International Journal of Advanced Manufacturing Technology* **2018**, *96*, 4267-4279.
16. Clini, P.; Frapiccini, N.; Mengoni, M.; Nespeca, R.; Ruggeri, L. SFM Technique and Focus Stacking for Digital Documentation of Archaeological Artifacts. *The International Archives of the Photogrammetry, Remote Sensing and Spatial Information Sciences* **2016**, *XLI-B5*, 229-236.
17. Westoby, M.J.; Brasington, J.; Glasser, N.F.; Hambrey, M.J.; Reynolds, J.M. 'Structure-from-Motion' photogrammetry: A low-cost, effective tool for geoscience applications. *Geomorphology* **2012**, *179*, 300-314.
18. Sapirstein, P. A high-precision photogrammetric recording system for small artifacts. *Journal of Cultural Heritage* **2018**, *31*, pp. 33-45.
19. Allen R. Greenleaf. *Photographic Optics*. The MacMillan Company: New York, 1950.
20. Barba, S., Barbarella, M., Di Benedetto, A., Fiani, M., Gujski, L., Limongiello, M. Accuracy Assessment of 3D Photogrammetric Models from an Unmanned Aerial Vehicle, *Drones* **2019**, *3*, 79-97.

In *Towards a new, configurable architecture - Proceedings of the 39th eCAADe Conference, Novi Sad, Serbia, 8-10 September 2021.*
https://doi.org/10.52842/conf.ecaade.2021.2.211

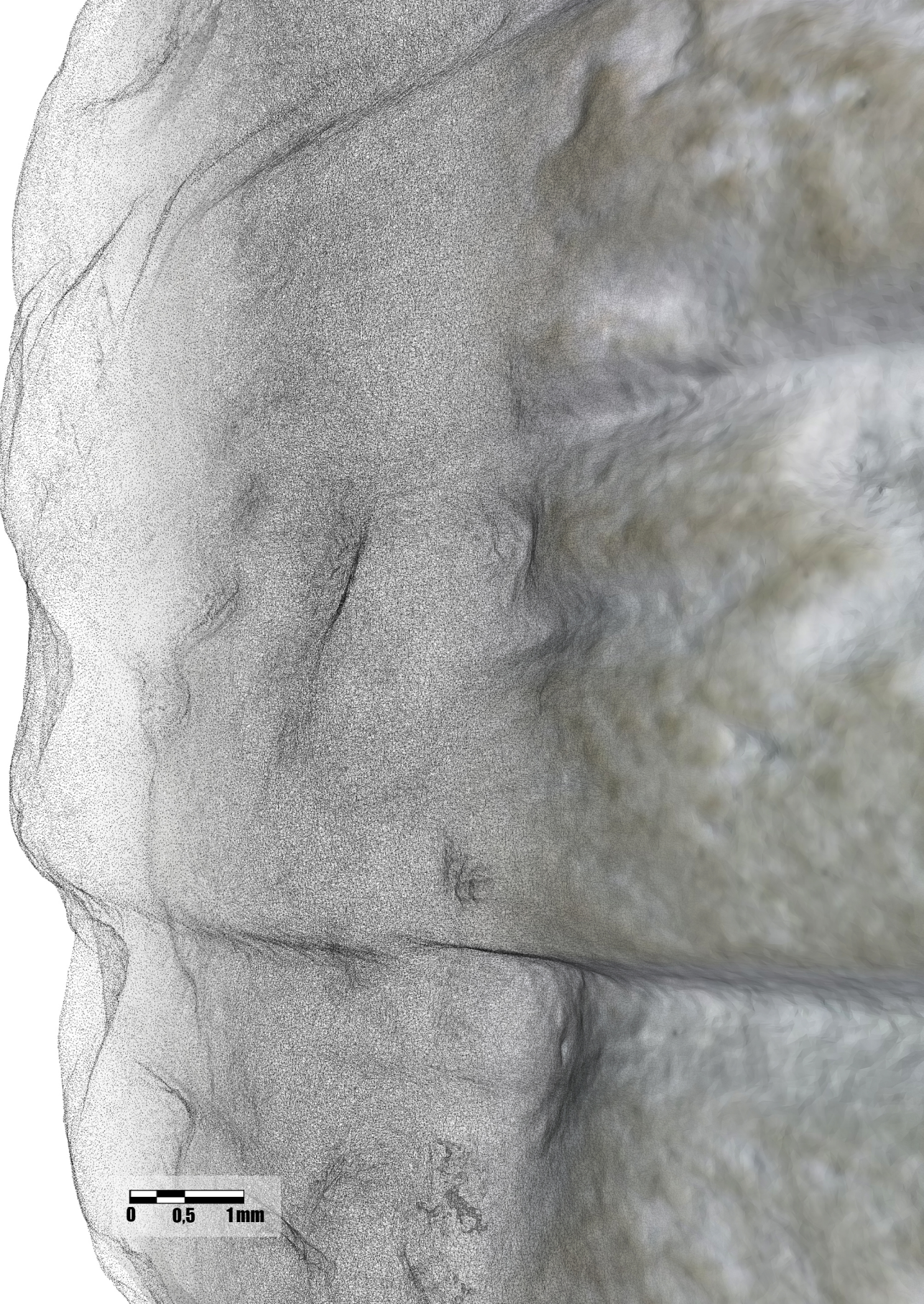
0
0,5
1mm

Capitolo 5
Optimized configurations for micro-photogrammetric surveying adaptable to macro-optics and digital microscope

Abstract: The configuration of new survey approaches for digitizing tiny artefacts is gradually emerging in favour of the related results sharing in new modalities such as 3D printing and or Cultural Heritage open-access datasets. Unfortunately, due to the still high cost of the instrumentations and the time required for specialized operators training, both the digital documentation of small artefacts and the dissemination of 3D data are still a long way from becoming truly mainstream practices. Alternative solutions, often at low cost, could be considered, involving the use of passive sensors for image-based modelling processes, relying on a widespread technology that is now within everyone's reach. Therefore, we intend to meet the demand for the three-dimensional representation of small objects with complex surfaces and sub-millimetre morphological characteristics by designing several custom accessories that optimize the photogrammetric workflow while maintaining very high metric rigour. In this current work, the authors will focus on researching the most suitable acquisition method and hardware setup to achieve a digital twin of a complex and detailed cuneiform tablet replica using the now widely available on the market digital portable microscopes, able to achieve high magnification. The results were compared with a reference dataset from an active sensor acquisition for the necessary procedure validations.

Keywords: Small Artefacts, Digital Heritage, Micro Survey, Detail Scale, Handheld Microscope, Image-based Modelling.

1. Introduction

The Cultural Heritage digital documentation techniques are well defined for dimensions and architectural graphic representation scales but still not conveniently formalized and codified for very tiny objects. Interfacing with small finds represents a complex challenge due to the

level of detail change and the need to update/re-think the measurements operating systems.

Nevertheless, the 3D reconstruction of small objects is becoming increasingly widespread in various fields, especially the manufacturing industry, mechanics, medical sciences, including also archaeological documentation, interested in using emerging and available digital methodologies and technologies provided by Geomatics, and aiming at rigorous objects description [1].

Several solutions for micrometric surveying applications [2], including range-based ones [3], or integrated approaches – still representing the most effective solution [4] – are increasingly succeeding in the task.

Unfortunately, most of these technologies are out of reach of most museums and cultural institutions due to the considerable hardware and software costs and the level of expertise required of the operators [5]. Today's market demand for practical, low-cost solutions directs the interest towards more affordable alternatives, such as micro-photogrammetry. This solution offers the possibility of obtaining three-dimensional coordinates of an object and, at the same time, the exact corresponding radiometric information from two-dimensional digital images in an accurate, reliable, flexible, and, often, money-saving way. The issue is even more interesting considering the demand for technologically advanced experiences we are currently used to when visiting museums, art galleries or archaeological sites.

All these factors open new frontiers to digital photogrammetry for renewing the use of Cultural Heritage [6]. In addition, such discipline is open to further technological developments and implementations, such as speeding up the acquisition phase. Today this first step represents its weak point because it is difficult, repetitive and time-consuming for operators.

Starting from this awareness, our current challenge is configuring a highly performative micro-photogrammetric system designed for both: (i) micro-photogrammetry most established solutions, based on digital camera combined with macro lenses; (ii) and also portable digital microscopes, whose validity has been tested for micro-scale survey also in our previous works.

Thus, this system aims to overcome some of the operational difficulties experienced in recent applications and to contain the problems that

affect very close-range photogrammetry, such as not very high resolution, lack of a wide dynamic range, narrow field of view and poor depth of field. Indeed, most of the problems that arise – despite the use of increasingly advanced software for photogrammetric processing – are actually generated by purely photographic errors or by a lack of knowledge of photographic tools [7].

Comparing two procedural solutions – simultaneously evaluating the development of the accurate and cost-effective micro-photogrammetric acquisition system – the authors propose to carry out the digital survey of a 3D printing replica in geopolymer of a tablet with cuneiform writings. This case study has approximately the dimensions of 20×22×8 mm, and the characteristic wedge-shaped impressions have a depth of 1-3 mm (Figure 1). Tablets inscribed with the cuneiform script were the 'portable information technology' of that time; in this case, the text content concerns the administrative information for fish deliveries (the modern correspondent of a packing slip).

The replica, used as a test, is a printed clone of the original 724 tablet (realized by the +LAB, www.piulab.it - POLIMI) surveyed using an active sensor system by the 3D Survey Group (POLIMI).

It should be noted that original tablets are easily susceptible to damage, and scholars have limited tools for accessing and recording these finds [8,9]. The success of the conducted tests on this copy can ensure that in the future, a digital clone with high accuracy of original cuneiform tablets – or even other similar artefacts with great tiny detail – can be quickly and lows cost obtained for educational and scientific purposes. The digital replica would allow the virtual manipulation of these delicate findings and facilitate their sharing among a team of archaeologists too, for example, to decipher the content of a text, thus favouring an interdisciplinary study among several experts.

2. Related works

Close-range photogrammetry involves many parameters that affect the acquisition process, and this is compounded by increasing difficulties as the scale of application reduces.

One of the main problems is the need to include metric references or calibrated objects in the scene, using adequate calibration patterns according to the magnitude of the object to be measured [10].

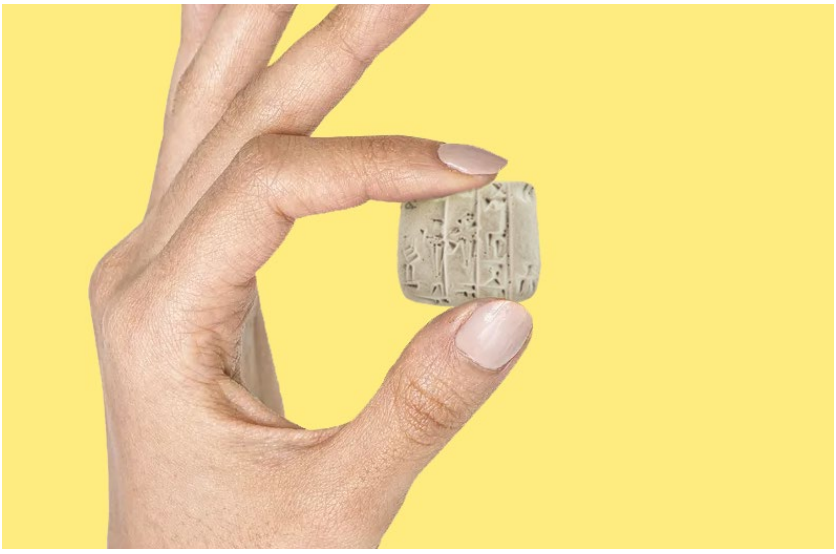

Figure 1. Recto of the 3D printed copy of the cuneiform tablet.

Another critical issue concerns the acquisition geometry, which must ensure sufficient overlap between the captured images to reconstruct the object surface and its feature continuity. Furthermore, while turntables facilitate and speed up the acquisition, there are very few possibilities of housing the object in an advantageous position to ensure the necessary base between the camera positions.
Finally, it should not be overlooked that the short depth of field issue is emphasized when increasing magnification. This aspect implies that only a tiny portion of the artefact is in focus on the photo, and so only a small portion of the image appears sharp enough to be used for 3D reconstruction [11]. Indeed, the sharpness, joint with photoset density and resolution, determines the output point cloud reliability, accuracy and quality [12]. These limitations could affect both the dataset acquisition and processing phases reciprocally. Indeed, to ensure the suitable number of point matching and conjugate points computed and the resolution of the 3D model [13], the survey times increase because it is necessary to move the camera often to cover the whole object surface. In order to overcome these difficulties, the authors conducted some experiments in previous studies to digital survey very tiny and problematic artefacts by optimizing the acquisition procedures with the design of custom accessories for micro-photogrammetry.

Using photographs taken by low-cost Dino-Lite (www.dino-lite.eu) digital microscopes (Figure 2) as a dataset for photogrammetric processing, a not negligible potential for small object modelling – compared with significantly more expensive instruments – was revealed [14].

As is well known, digital handheld microscopes are similar to traditional optical microscopes, except that they are equipped with a CCD camera to output a digital colour image to a monitor. Moreover, among the main types of microscopes, they are the most flexible, the easiest to use, and the least expensive [15]. Born for inspection, documentation, and digital metrology analysis – already widespread in the manufacturing and quality control industry and used in the medical field – digital microscopes can be used for micro-photogrammetric applications, reaching about 0.1 mm accuracy [16]. It may seem interesting, therefore, to insert these instruments within a systematized photogrammetric workflow.

Their main disadvantage is that they are not born purely for photogrammetric purposes and therefore need to be adapted, for example, through the design of a specific calibrator – to guarantee accurate results – and of an automatic system that speeds up the data acquisition.

Figure 2. Dino-Lite handheld digital microscope.

Furthermore, for the same reason, no technical calibration characteristics of the lens system are known.

3. Materials and methods

3.1. An original asset for the micro-photogrammetry

The previous tests conducted by the authors to achieve a digital twin of a complex and detailed 3D printing replica of a tablet with cuneiform writing, as challenging as the original, are valid for defining a first approach to the photogrammetric use of portable digital microscopes [17]. Nevertheless, on this occasion, some key aspects are still more rigorously investigated to streamline the acquisition procedures and ensure a more rigorous workflow.

A redesign of the acquisition hardware for this dimensional scale is required to allow you to have everything you would need in one single system for the photo modelling of tiny objects. It implies: calibrated stands to hold the object and at the same time ensure the metric accuracy, the rotating base to help you and speed up acquisitions, the lighting suitable for each situation. For this particular application, having already experimented with using a flat calibrated support, it was decided in a first step to implement the characteristics of the old, calibrated plate by designing a new one.

Subsequently, an alternative solution was tested, evaluating the possibility of using an adhesive pattern glued onto clamp support. Even in this second mode, therefore, it would have been possible to frame the metric references and the object at the same time, with the hope of further reducing surveying times. Hence, first, the authors designed a calibrated plate built for these tests (Figure 3) and used it for the standard photogrammetric procedure needs (images alignment, self-calibration optimization, and scale). This calibrator is obtained with an EOS M270, via additive manufacturing of steel powder and consists of a circular plate characterized by a pattern of 279 truncated cone holes, with a countersink angle of 60° and a smaller base diameter of 0.35 mm. The calibrator accuracy, based on the 3D printing settings and the conformity of the actual position of the holes with respect to the project file, has been estimated at 0.1 mm, which can be assumed as an instrumental error value (i.e., markers accuracy).

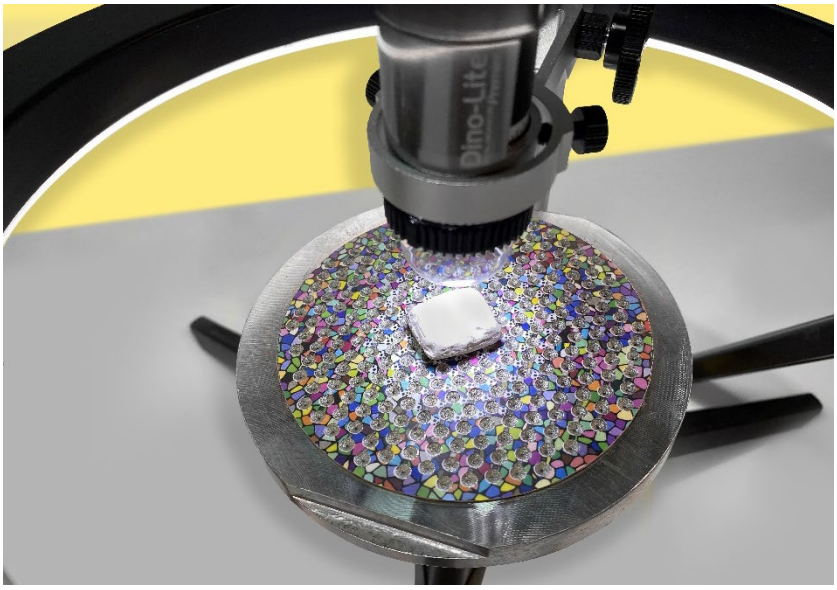

Figure 3. Three-dimensional calibrated plate combined with the digital microscope (updated prototype).

Therefore, each hole coordinates in a local reference system are known to the operator and can be imported into the project.

For this reason, the perforated pattern can be used as a constraint points (GCP) grid – homogeneously distributed throughout the whole area – to optimize the alignment of the cameras and scale the model.

The calibrated plate was set on a turning table to facilitate and speed up the acquisition phase. Once the magnification rate (optical zoom) has been chosen and placed the digital microscope on a fixed bracket at a fixed inclination, a set of images with sufficient overlap can be acquired by rotating the base. The angle of the plate to the camera is changed after each full rotation (Figure 4). The AM7013MZT Dino-Lite digital microscope was employed for this application. It is characterized by a 5-megapixel sensor for crystal clear images and a built-in adjustable polariser to reduce glare and reflection on shiny objects. This model offers a 'standard' working distance, as defined by the manufacturer, meaning a distance from the object that varies approximately from 50 to 2 mm: in our case, with a magnification rate of 20×, the focus is obtained at a working distance of 48.7 mm, with a depth of field equal to 3.6 mm.

(**a**) (**b**)

Figure 4. (a) Setup configuration for the first acquisition test, included calibrator, its support and lighting system; (b) Detail of the lighting ring coaxial to the rotating base, on which the calibrated plate is mounted.

In general, to overcome the problem of the short depth of field, one possibility would be to close the aperture of the optics as much as possible within the limits of the diffraction phenomena [18] and provide enough light to balance a correct exposure time. Since this possibility is not available on portable digital microscopes, where the diaphragm is fixed, and consequently, the sharp field range is also fixed, it is necessary to use alternative solutions. For this purpose, the object is acquired from various focus planes by moving the microscope on the micrometric vertical rail to focus on different planes.

The lighting conditions, based on the polarised light of the microscopes, have been improved with the adoption of a LED illumination ring (Figure 4b). The light does not directly affect the object because of the shape and the lens hood diffusing light source material; thus, diffused light conditions neutralize the shadow cones without variations in the intensity of shadows, lights, and colours.

With this system, two acquisition sets – one for the recto and the other for the verso of the tablet – averaging 250 captures each were required, for a total of about 1 hour of time needed.

One of the problems left open for the cuneiform tablet digital survey (and therefore for similar small objects with a not negligible thickness) is the impossibility to have the joined 3D model of the two faces (recto and verso) using the microscope dataset, although inclined acquisitions have been made. This particular and not trivial circumstance has forced us to take a further step forward.

Having selected an object that, for its size and complexity, allows to stress the acquisition system and bring out its weaknesses, we understood how to deal with this critical issue by maintaining a low-cost approach.
We have come, therefore, to conceive the possible modification of the object support (Figure 5), incorporating the calibrator in it. In this way, the surveyor has the possibility to use the same shooting system, choosing, if necessary, the support that is best suited to fix the object to be detected. The plate would, thus, be mainly suited only when it can be brought into sharp focus, even with objects of significant 3D shape (in the case of cameras where adjustment of the diaphragm of the optical apparatus allows the depth of field to be increased). Conversely, such as in our case, a screw clamp (Figure 5 and Figure 6), commonly used in model making, would be more convenient to acquire objects to be placed at knife-edge in reference to the microscope camera. This acquisition mode enables the calibrated pattern to be positioned approximately coplanar to the plane of the object's focus (Figure 7a).
Easily available, the clamp was coated with an adhesive pattern on which automatically recognized targets of known coordinates were printed.

Figure 5. Three-dimensional calibrated plate combined with the digital microscope (updated prototype).

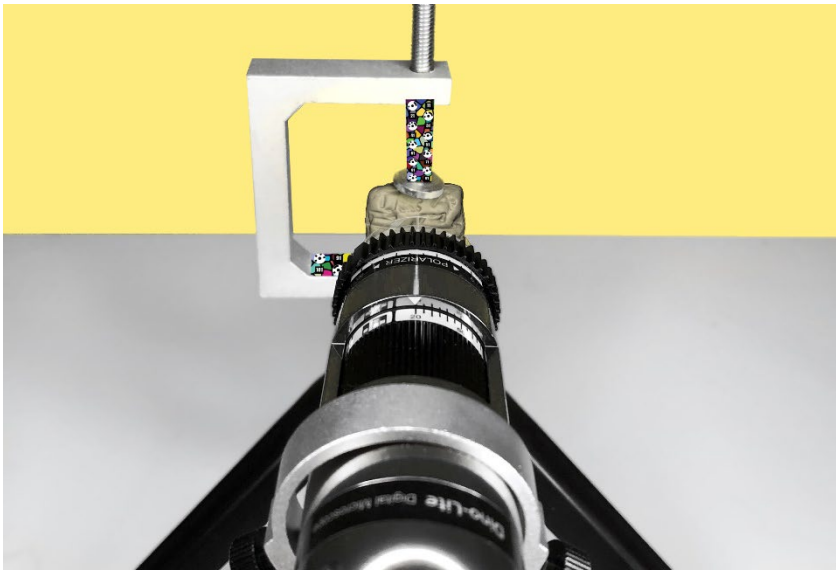

Figure 6. Detail of the positioning of the tablet in the clamp for the second acquisition test.

Similarly, to the calibrated plate, the clamp was also placed on a rotating base, taking care to align the rotation centre with the mounting axis of the object. Other photogrammetric accessories remain almost unchanged when compared to the previous setup.

A set of about 700 captures was required with this system, and a supplement set for the small parts hidden by the clamp (about 100 captures), for a total of about 1 hour required.

For both mounting systems used, the acquisitions were carried out with the same magnifications, 20×, operating with the dedicated DinoCapture 2.0 software procedure. The datasets obtained were thus processed in a SfM software, Agisoft Metashape, according to the general photogrammetric workflow (Table 1) and the processing was completed with the same graphic workstation equipped with AMD Ryzen 9 5900HX CPU and 32GB of RAM.

During the processing of the first test, there is a significant difficulty in aligning tilted photos due to the shallow depth of field and the homogeneous texture of the tablet. This problem was not encountered in the second test because the capture geometry forced (and facilitated) the operator to take more photos due to the particular location of the object with respect to the camera (Figure 7b).

Table 1. Survey data comparison.

	Calibrated Plate Set	Screw Clamp Set
Aligned Cameras	506/518	718/718
Sparse Cloud	4.3×10^5 points	4.1×10^5 points
Dense Cloud	10.4×10^5 points	8.3×10^5 points
Ground Resolution	6.3 μm/px	7.1 μm/px
RMS	0.87 mm	0.027 mm
Processing Time	4 h	2 h

The sparse point cloud, made only by tie points (TPs), is the starting point for the realization of a complete 3D model. However, removing low-quality TPs is appropriate because their presence affects the following step results, which consist of the re-computation of the orientation parameters and the creation of the final dense cloud [19]. The evaluation of image orientation quality within SfM methods can be performed using the Gradual Selection filter, a tool by Agisoft Metashape that, like most photogrammetric software, allows you to filter the sparse point cloud based on some quality parameters. The parameters considered in this study were: Reconstruction uncertainty, Reprojection error and Projection accuracy.

(**a**) (**b**)

Figure 7. (a) Different ability to focus on target and object at the same time using the calibrated plate (left) or the clamp (right); (b) Camera spatial positions during the calibrated plate (left) and screw clamp acquisition test (same time taken: 1h).

3.2. Reference model equipment

The quality, speed, and cost-effectiveness of the two surveys conducted with the portable Dino-Lite digital microscope were compared to data obtained from the SCAN in a BOX structured light 3D scanner to have a reference model and check the overall geometrical dimensions of the photogrammetric reconstructions.

The SCAN in a BOX (@2015 Open Technologies SRL) is equipped with two high-resolution industrial USB cameras and a high definition light projector (ASUS S1). All components are fixed on a thick aluminium rail, but the cameras can be moved in calibrated positions (base) to customize the work field (Figure 8).

The main steps for the 3D measurements workflow are the following: (i) calibration of the optical setup; (ii) range maps acquisition; (iii) raw alignment; (iv) alignment optimization; (v) meshing. The system needs to be configured and calibrated whenever the scanner is mounted, or the camera setting on the support bar changes. The coded calibration master has three patterns based on the selected working area. The optical setup provides the configuration of the projector and cameras (position, orientation, focus, exposition).

Figure 8. "SCAN in a BOX" system and polygonal model of the tablet acquired (1mm grid background).

The calibration allows calculating the optical parameters of the specific setting. According to the object dimension and the resolution required, choosing the scanning area is more suitable, strictly connected to the working distance and the distance of the cameras on the plate.
For our case study, a Field Of View of 100×80 mm was set, implying the working distance scanner-object of about 200 mm, the minimum base between the two cameras, and the minimum point spacing (resolution) on the surface, i.e., 0.078 mm.
The digital reconstruction of the object surface and details was performed, acquiring 16 nadiral scans on both sides (8 for the verso and 8 for the recto), 16 tilted (8 for each side) and 8 nadiral to the four edges (totally of 40 range maps). The scanning time for each range map is less or equal to 4 seconds. The raw in progress alignment process helped check real-time scan completeness. This initial registration is then optimized using an Iterative Closest Point (ICP) algorithm.
The final mesh model (formed by about 400.000 polygons) have fewer details of the correspondent photogrammetric models but can be used to ensure a reference check of their global measures.

4. Evaluation of the results

This analysis aims to evaluate the photogrammetric models obtained from the two different procedures illustrated: the first based on the use of a calibrated plate on which to place the object being surveyed, the second on the use of a clamp in which to secure the object and a portion of which is covered by a calibration pattern. This is to draw some first conclusions on the efficiency and accuracy capabilities of the two different acquisition methods. A cloud to mesh registration has been performed using the data from the SCAN in a BOX as a reference to provide a robust comparison of the results. The registration was carried out in two steps, providing: first, a manual registration using homologous points and then a global registration by automatic alignment algorithms (ICP). The photogrammetric survey accuracy assessment was carried out using CloudCompare C2M cloud to mesh) command. This tool searches, for each point being compared, the closer reference entity, thus defining a shift value of the first with respect to the second. The clouds obtained from photogrammetry were compared using the SCAN in a BOX model as a reference.

Figure 9 shows the deviations among the clouds in false colours. Through the calculations performed it is noted that the mean and standard deviations from the reference do not exceed 0.3 mm for both photogrammetric models. This difference could have been determined by both the registration procedure and the higher resolution obtained from the photogrammetric survey.
Indeed, the SCAN in a BOX mesh model is smoother and has less resolution (about 0.08mm).
The results obtained using the calibrated plate are noticeably affected by greater deviations, due on the one hand to image alignment problems, which have also significantly increased the noise of the dense cloud, and on the other hand to the difficulty of joining the two sides of the tablet. This comparison suggests that the shape of our object requires different capture sets, with different inclinations of the microscope, probably much more than those made by rotating the object placed in the clamp.
Therefore, the manual acquisition will be more challenging to consider a corresponding increase in processing time due to the need to perform the same photogrammetric workflow for each acquisition set and merge the different blocks.
Therefore, we consider the result of the first test satisfactory both metrically and for an overall reading of the artefact, but the three-dimensional model, excessively noisy and needing interventions a posteriori, is not excellent for a complete user experience. However, it is believed that the calibrated plate remains a valuable tool when used for mostly flat objects and/or combined with SLR cameras and macro lenses, allowing for greater depth of field and wider angle of view. As acknowledged, in fact, a generally applicable geometric configuration for photogrammetric measurement cannot be defined [20] as this depends on the specific object to be detected. Nevertheless, having several alternative supports available allows the capture geometry to be quickly modified. Although also in the second test, it was necessary to turn the piece over and partially repeat the capture process for the occluded part, in order to achieve full digitization of the tablet, the results obtained using the clamp are very satisfactory.
In the post-processing phase, it was expeditious to align the partial scans and create a single 3D mesh of the complete object.

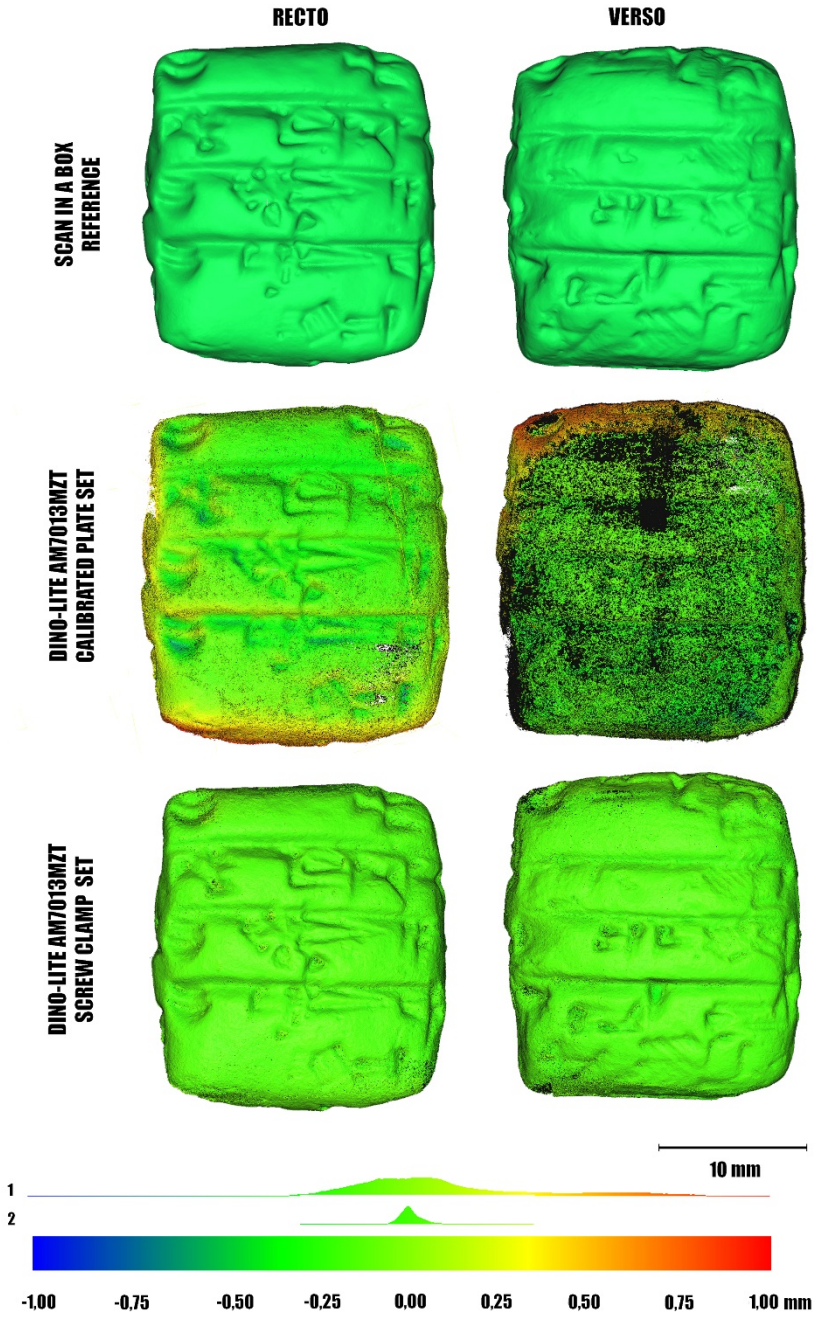

Figure 9. Global deviations of the photogrammetric dense clouds obtained using the calibrated plate and the screw clamp as support, compared with the reference model of the SCAN in a BOX (recto and verso side view).

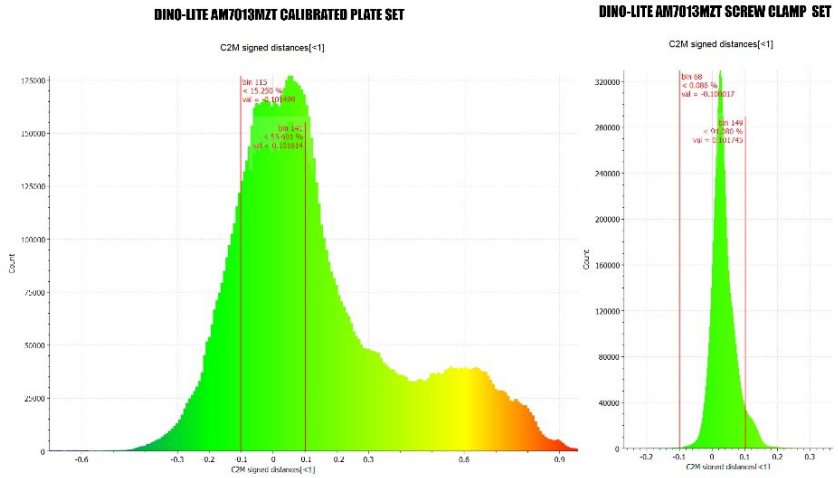

Figure 10. Global distribution detailed chart of photogrammetric cloud deviations from the reference model: in the central portion of the graphic, approximately 40% (left) and 94% (right) of the points are included in a difference of +/- 0.1mm.

For this second model, approximately 94% of the points are included in a smaller difference than +/- 0.1mm, versus around 40% of the previous (Figure 10). Noise is very low, limited only to certain portions of the object, and the final model is readable and complete, lending itself to wide dissemination: https://skfb.ly/o8GSr

The two models' comparison (Figure 13) highlights in detail that the model generated with the calibrated plate setup has problems both along the edges and in some parts of the main faces, with unnatural bulbs on the surface due to excessive noise. Indeed, in this case, the sparse cloud filtering – performed to detect and remove outliers and mismatches affecting the image orientation results – would have caused excessive data loss, returning equally noisy but severely incomplete three-dimensional reconstructions. In addition, in both cases, the uncertainty generated by the absence of Exif data must be considered as a further detrimental parameter for the alignment processes and the resulting issues.

Despite the problems within the framework of modern micro-technologies, the results from Dino-Lite are absolutely comparable in shape and size to the SCAN in a BOX, ensuring a slightly higher resolution and thus demonstrating that digital microscopes combined with an optimized setup can be effective and interesting tools for micro-photogrammetry.

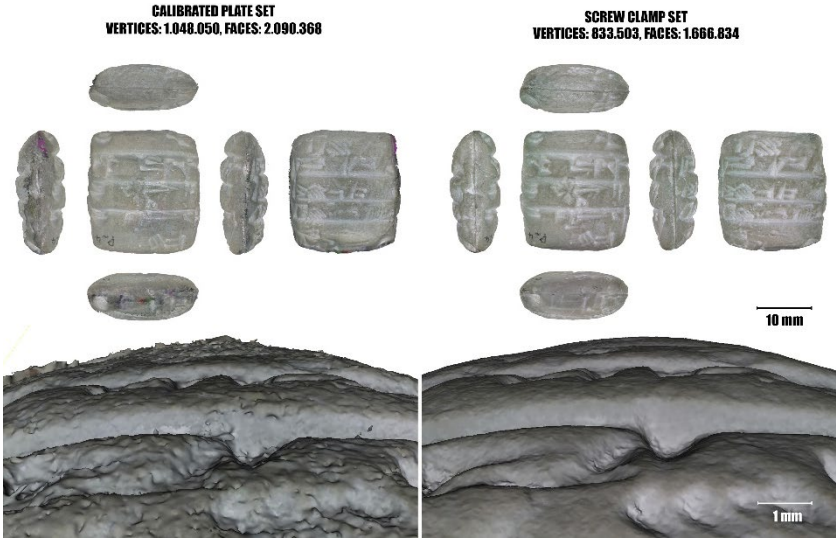

Figure 10. Qualitative comparison of the models obtained using the calibrated plate (left) and the screw clamp as support (right).

5. Future developments

Having access to a low-cost system based on the principles of close-range photogrammetry, at the same time efficient and affordable, is, therefore, a still unmet need for those who want to share and circulate digital models of objects with particular reference to the scale of detail. In this sense, in order to meet this demand, there are still several key issues to be resolved not as mere executors but as proponents of new tools and technologies. Indeed, each object represents a uniqueness for which it is necessary to design a custom survey plan. Nevertheless, today it is possible to realize, at quite low costs, different interchangeable supports, equipped with calibrated patterns, in order to fix the object in the best way, to neutralize the shadow cones at the most and to guarantee the metric accuracy, which is the primary aim of the survey.

Therefore, the main purpose of this research in the future will focus on implementing the design of three-dimensional calibrators to support the 3D reconstruction of tiny objects with a not negligible thickness. This will be followed by the characterization of the other necessary components, including, for example, the diffuse annular illumination, the support for the optical system and the rotating base, which at this stage have been combined in a still 'rudimentary' way.

These latest experimental tests conducted with the Dino-Lite instruments are valid to take a further step forward in an attempt to combine the various elements and solutions that make up a complete photogrammetric system, optimized for acquisition and ensuring the control of the subsequent management of the measurement data.
Furthermore, there are interesting ideas for the three-dimensional documentation of very small artefacts that would otherwise be difficult to represent from this work in progress. Indeed, additional tests are already planned to use more resolute and accurate active sensors to verify further the results achieved. In this way, it would be possible to replicate at low cost and with adequate accuracy the work of instrumentation that exceeds the cost of these microscopes with a relatively low effort.

References

1. Bitelli, G., Girelli, V.A., Remondino, F., Vittuari, L. The potential of 3D techniques for Cultural Heritage object documentation, *Proc. SPIE 6491, Videometrics IX* **2007**, *64910S*, 244-253.
2. Hansen, H.N., Carneiro, K., Haitjema, H., De Chiffre, L. Dimensional Micro and Nano Metrology. *CIRP Annals* **2006**, *55*(2), 721-743.
3. Tolksdorf, J. F., Elburg, R., Reuter, T. Can 3D scanning of countermarks on Roman coins help to reconstruct the movement of Varus and his legions. *Journal of Archaeological Science: Reports* **2017**, *11*, 400-410.
4. Morena, S., Barba, S., Álvaro-Tordesillas, A. Shining 3D Einscan-Pro, application and validation in the field of Cultural Heritage, from the Chillida-Leku Museum to the Archaeological Museum of Sarno. *ISPRS International Archives of the Photogrammetry, Remote Sensing and Spatial Information Sciences* **2019**, *XLII-2/W18*, 135-142.
5. Caine, M., Maggen, M. Low Cost Heritage Imaging Techniques Compared. In Proceedings of *The Conference on Electronic Visualisation and the Arts,* London, UK, 11-13 July 2017, pp. 430-437.
6. Mancuso, A. Pasquali A. Digital Micro-Photogrammetry. New ways to dialogue with future researchers. In Proceedings of The *20th International Conference on Cultural Heritage and New Technologies,* Vienna, Austria, 10-12 November 2015, 1-16.
7. Verdiani, G., Formaglini, P., Giansanti, F., Giraudeau, S. Close-Up, Macro and Micro-photogrammetry and Image Perspective: A Comparative Studio on Different Lenses at Work with Small and Medium Size Objects. *Computer Reviews Journal* **2018**, *2*, 235-248.
8. Surdi, M. Dalla tavoletta al tablet: metodi classici e nuove tecnologie a confronto per l'Assiriologia. *Archeomatica* **2017**, *7(4)*, 40-46.
9. Lewis, A., Ch'ng, E. A Photogrammetric Analysis of Cuneiform Tablets for the purpose of Digital Reconstruction. *International Journal of Cultural Heritage in the Digital Era* **2012**, *1*, 49-54.

10. Lavecchia, F., Guerra, M.G., Galatucci, L.M. Performance verification of a photogrammetric scanning system. *The International Journal of Advanced Manufacturing Technology* **2017**, *96*, 4267-4279.
11. Clini, P.; Frapiccini, N.; Mengoni, M.; Nespeca, R.; Ruggeri, L. SFM Technique And Focus Stacking For Digital Documentation Of Archaeological Artifacts. *The International Archives of the Photogrammetry, Remote Sensing and Spatial Information Sciences* **2016**, *XLI-B5*, 229-236.
12. Westoby, M.J.; Brasington, J.; Glasser, N.F.; Hambrey, M.J.; Reynolds, J.M. 'Structure-from-Motion' photogrammetry: A low-cost, effective tool for geoscience applications. *Geomorphology* **2012**, *179*, 300-314.
13. Kontogianni, G.; Chliverou, R.; Koutsoudis, A.; Pavlidis, G.; Georgopoulos, A. Enhancing Close-Up image based 3D Digitisation with Focus Stacking. *The International Archives of the Photogrammetry, Remote Sensing and Spatial Information Sciences* **2017**, *XLII-2-W5*, 421-425.
14. Antinozzi, S., Ronchi, D., Barba, S. 3Dino System, Shortening Distances in Precision Surveys. In A. Arena, M. Arena, D. Mediati and P. Raffa (eds.), *Connecting. Drawing for weaving relationship. Languages Distance.* FrancoAngeli, Milano, Italy, 2021, 1922-1941.
15. Atsushi, K.; Sueyasu, H.; Funayama, Y.; Maekawa, T. System for reconstruction of three-dimensional micro objects from multiple photographic images. *Computer-Aided Design* **2011**, *43(8)*, 1045-1055.
16. Esmaeili, F., Ebadi, H. Handy Microscopic Close-Range Videogrammetry. The International Archives of the Photogrammetry, Remote Sensing and Spatial Information Sciences **2017**, XLII-4/W4, 65-67.
17. Antinozzi, S., Ronchi, D., Fiorillo, F., Barba, S. 3Dino: configuration for a micro-photogrammetric survey. Applying Dino-Lite microscope for the digitalization of a cuneiform tablet. In Proceedings of *the 39th eCAADe Conference - Towards a new, configurable architecture.* Novi Sad, Serbia, 8-10 September 2021, 2, pp. 211-222.
18. Sapirstein, P. A high-precision photogrammetric recording system for small artifacts. *Journal of Cultural Heritage* **2018**, *31*, pp. 33-45.
19. Barba, S., Barbarella, M., Di Benedetto, A., Fiani, M., Limongiello, M. Comparison of uavs performance for a roman amphitheatre survey: The case of Avella (Italy). *ISPRS International Archives of the Photogrammetry, Remote Sensing and Spatial Information Sciences* **2019**, *3XLII-2/W11*, 179-186.
20. Luhmann, T., Robson, S., Kyle, S., Harley, I. *Close Range Photogrammetry. Principles, techniques and applications*. Whittles Publishing, Dunbeath, Scotland, UK, 2011, p. 443.

In *The 9th International Workshop 3D-ARCH "3D Virtual Reconstruction and Visualization of Complex Architectures", Mantua, Italy, 2-4 March 2022.*
https://doi.org/10.5194/isprs-archives-XLVI-2-W1-2022-25-2022

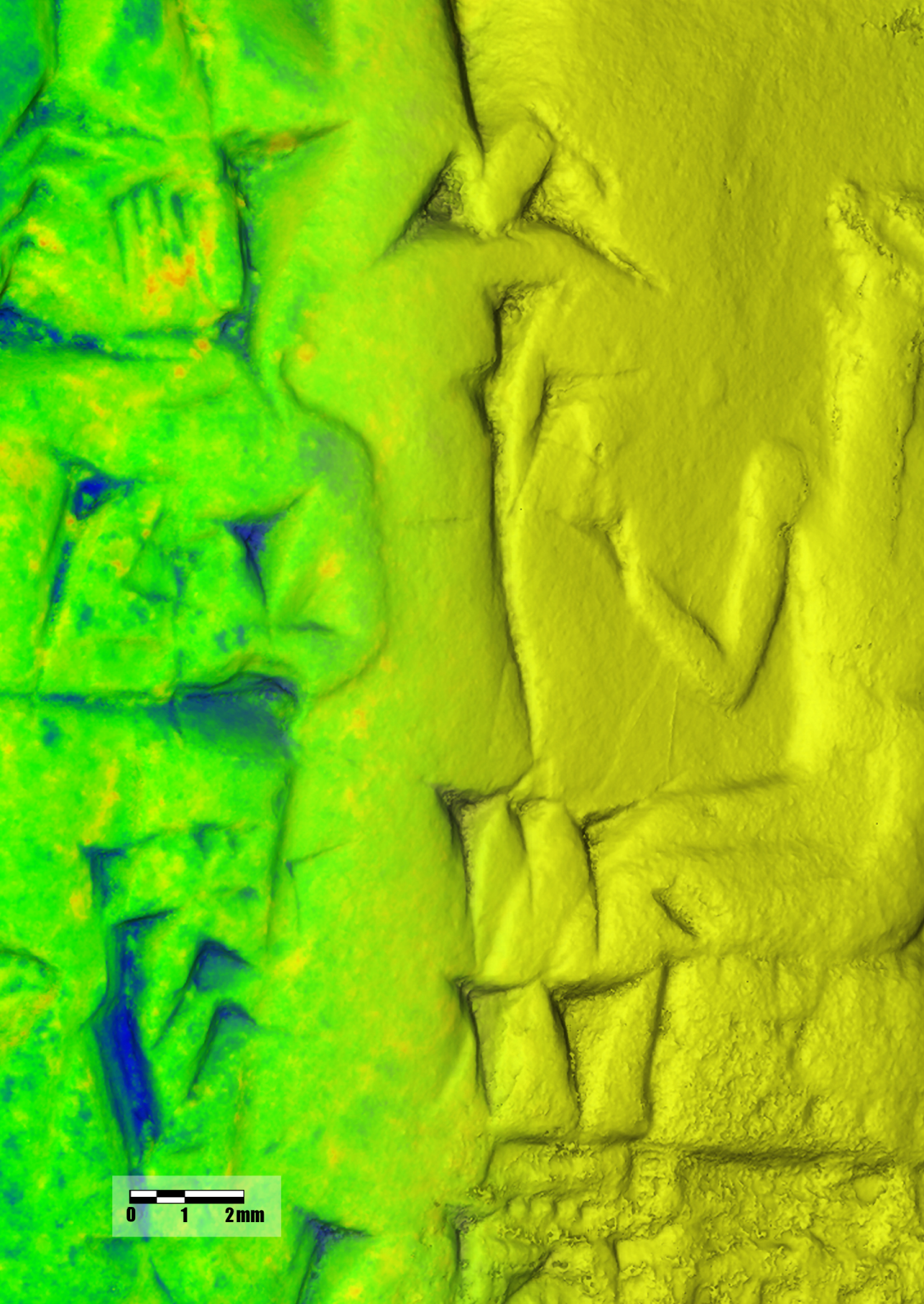
0
1
2 mm

Capitolo 6
Cuneiform tablets Micro-Surveying in an Optimized Photogrammetric Configuration

Abstract: In the 3D digital documentation current panorama, the survey of tiny artifacts with micrometric details is strongly influenced by two factors: firstly, the still high cost of the instruments and technologies (active sensors) required to achieve the necessary level of accuracy and resolution; secondly, the needed professional skills for the macro-photogrammetric approach. In this context, this research aims to meet the demand for a digital survey and 3D representation of small objects with complex surfaces and sub-millimetre morphological characteristics, using a low-cost configuration (passive sensors) for an image-based approach. The experiments concerned cuneiform tablets, which are challenging due to their morphological and geometrical characteristics. The digital replica of these unique artefacts can be helpful for their study and interpretation and many innovative applications: access and sharing, a collaborative interdisciplinary study among several experts, experiment with machine learning for automatic character recognition, and linguistic studies. The micrometric surveying system described proves to be an efficient and reliable solution for the cuneiform tablets digitization and documentation.

Keywords: Tiny Artifacts; Digitized Heritage; Micrometric Details; Handheld Microscope; Macro-Photogrammetry; Cuneiform Tablet.

1. Introduction

Digital documentation techniques for Cultural Heritage (CH) are nowadays well established and well defined for detailed drawing sizes and scales, but still not conveniently formalized and codified for tiny objects. In fact, small artifacts represent a complex challenge due to the level of detail and accuracy required.

The tiny object 3D reconstruction is widely used in many fields, such as mechanics or medical sciences [1], thanks to technologies that perform very well in terms of the specific size and representation scale

requirements. Advanced research in micro- and nano-metrology now challenges its limits even as the critical dimensions shrink, and the geometric complexity of objects increases [2].
However, several examples of micrometric survey applications using high-resolution 3D scanning can also be found in the CH field [3]. Unfortunately, these technologies are often beyond the reach of most museums and cultural institutions due to the considerable hardware and software costs[1] and the level of expertise required by operators [4]. Consequently, the current market demand for practical and low-cost solutions directs interest towards cheaper alternatives, such as macro-photogrammetry. Actually, image-based approaches for detailed digital documentation of even tiny artifacts have become widespread in CH applications [5-8]. Such image-based approaches have the great advantage of offering the possibility of obtaining the three-dimensional coordinates of an object and, at the same time, the exact corresponding radiometric information from two-dimensional digital images in an accurate, reliable, flexible and, often, inexpensive way. In the current panorama of 3D digital documentation systems, two factors strongly influence the survey of tiny artifacts with micrometric detail. The first is the still very high cost of the instruments and technologies (active sensors) required in function of the level of accuracy and resolution[2]. The second is the specialized skills needed in macro-photography and micro-photogrammetry, characterized by certainly lower costs (but still not low due to the cost of macro-optics and some indispensable accessories). In addition, acquiring the photographic dataset for tiny objects currently represents a repetitive and time-consuming process [9].
The presented research focuses on configuring an optimized acquisition system for small items based on low-cost passive sensors with high magnification requirements, such as USB portable microscopes (whose price starts at a few hundred euros). The recent use of photographs taken with digital microscopes as a dataset for photogrammetric processing has revealed a non-negligible potential for modelling small objects, especially when compared to significantly more expensive tools [10].
Therefore, the authors have previously tested the photogrammetric capability of a USB portable microscope [11,12] and have now applied it to larger data samples to confirm its effectiveness.

Although the effort is to employ more affordable hardware for micro-scale surveys, the research also aims to find an optimal geometry to suit the unusual photogrammetric instrumentation and facilitate operator work. Indeed, some of the operational difficulties experienced by the authors recently [12] show that instrumentation that was not born in the purely photogrammetric field can be effective, but needs to be adapted, also to deal with problems naturally related to macro-photogrammetry [13,14], such as lack of wide dynamic range, narrow field of view, and poor depth of field.

The choice of cuneiform tablets, a particularly complex case study in terms of both geometry and texture, allows stressing the proposed acquisition system precisely with the problems just mentioned and validating the methodology.

The success of the tests on this type of artifact with great tiny details can allow us to ensure that an accurate digital clone of original cuneiform tablets can be quickly and low-costly obtained.

The digital replica can be helpful for many reasons and many innovative applications: (i) allows the virtual manipulation of these delicate findings; (ii) allows the access and the sharing of artifact documentary information; (iii) facilitates a collaborative interdisciplinary study among several experts; (iv) allows to experiment with machine learning for automatic character recognition, and linguistic studies [15-17]. The digitization of cuneiform tablets in 3D has many positive implications for both research and 'edutainment' [18]. For example, the 3D models can also be utilized to establish digital libraries [19,20] for educational and scientific reasons, thereby facilitating an interdisciplinary study among various experts and providing new information and new representations of the tablets that were not available with traditional documentary methodologies.

The present article is organized as follows. In section 2, various methods for documenting and representing cuneiform tablets have been described and compared in order to provide a better understanding of the methodologies already in use and their advantages and disadvantages from an assyriological perspective. Section 3 contains the test on the use of a digital microscope for accurate micro-photogrammetric reconstructions, research to design an optimized data acquisition set, and method validation using a benchmark.

Section 4 describes the calibration procedure for the optical system, which enabled rigorous results to be obtained. Finally, section 5 reports the digitization campaign of some cuneiform tablets belonging to the collection of Ghent University and the resulting models.

2. Cuneiform Tablets digital documentation: aims and purposes

2.1. Overall characterization

Cuneiform tablets are among the oldest written documents of human history, dating back to 3300 BC. For over three millennia, clay tablets were by far the most common media for conveying information in the ancient Near East. Among many shapes of the extant clay documents [21], the most frequent are square or rectangular pillow-shaped clay artifacts, generally covered with cuneiform signs impressed on the wet clay with a stylus. The dimensions of the tablets can vary according to the genre, chronology, and provenance of the texts. Cuneiform tablets range from ca. 1.5×1.5 cm to 36×33 cm in size [22], but most usually fit comfortably in one's hand (Figure 1).

According to an estimate by the assyriologist M.P. Streck [23], more than 530.000 cuneiform objects (including cuneiform tablets) have been unearthed and are currently stored in different collections worldwide. Unfortunately, less than one-quarter of them are published.

Figure 1. Some fragments of cuneiform tablets belonging to Ghent University.

However, more tablets are being unearthed yearly by legal and illegal excavations. Therefore, despite our access to a wealth of written sources of ancient history, we do not have an accurate survey of what is actually available, what is buried in museums, and what is still resting in the mounds of the Middle East. The enormous number of administrative texts so far survived can be accounted for by the simple yet essential fact that clay tablets can survive fire and other agents of deterioration much better than other materials used elsewhere or later (such as papyrus, parchment, and paper). Furthermore, over the course of thousands of years, thanks to its versatility, the cuneiform script has been used for nearly fifteen different languages in the ancient Near East area: from Iran to the Mediterranean, from Anatolia to Egypt [24].
In summary, cuneiform tablets: (i) are three-dimensional artifacts in clay; (ii) exhibit a three-dimensional script, characterized by wedges measuring even a few millimeters; (iii) have different sizes, but most commonly, they fit in one's hand; (iv) are available in hundreds of thousands of exemplars; (v) are nowadays scattered in collections all over the world and more exemplars are unearthed every year all over the Middle East. Documenting and publishing these precious clay artifacts have always been challenging due to the above characteristics. Based on the technologies available at the time, assyriologists attempted to document cuneiform tablets in the most convenient and accurate manner possible.

2.2. Acquisition and publication: limits of the standard methodologies

For the acquisition and publication of cuneiform tablets, the most common methods are hand tracing copies, photographs, flatbed scans, and, more recently, 2D+ height maps based on Polynomial Texture Map (PTM) technology and 3D modeling by photogrammetry and structured-light scanning.
The salient features of the procedures for the study and visualization of these complex surfaces are briefly illustrated below. Furthermore, special attention is paid to the advantages and disadvantages of each methodology from an assyriological perspective. By doing so, we seek to (i) contextualize the technique proposed in this article within the group of methodologies already in use; (ii) evaluate the effectiveness of micro-photogrammetry for cuneiform tablets compared to the other techniques.

2.2.1. Hand tracing: ink on paper and vector-based techniques

Hand copies and photographs represent the two very first and oldest methods used for publication in the early days of Assyriology, both still used today. In order to best read a cuneiform tablet, that is, to identify the signs correctly, it is necessary to vary the light source. Thus, the tablet is usually held in one's hand and rotated in different directions and angles to find the optimal illumination that will reveal the signs. Consequently, it is easy to understand why, even in the presence of the original artifact, many difficulties exist in reading the text, possibly due to the tablet morphology and their current state of preservation.

Despite these difficulties, the assyriologists have made many cuneiform texts available to the scientific community. Traditionally, cuneiform tablets are copied using pencils, calipers, and graph paper. The skills of the person who is copying the tablet, as well as the amount of time available in museums, collections, and archaeological sites determine the quality and accuracy of hand copies. In some cases, the hand copies may appear sketchy and represent only the cuneiform signs preserved without any other detail (Figure 2a). In the best cases, assyriologists have attempted to reproduce every detail of the tablet on paper, including the cuneiform signs and any fractures or abrasions that may have rendered the original text unreadable (Figure 2b). Even though this method may seem outdated today, autographed copies of tablets are still used for specialized scientific publications. Despite the best efforts of the copyist, errors can occur: in fact, it is essential that the assyriologist first reads the sign, then interprets it, and finally copies it on paper. Every step in this chain of actions can be affected by human error, e.g., misreading the original sign on the tablet, misinterpreting and/or confusing it with another similar sign, and finally miscopying the sign on the paper. Due to the aforementioned reasons, it is not uncommon for scholars to collate the tablet, i.e., verify the accuracy of the hand copy through an autoptic inspection of the original tablet. Hand copies have numerous advantages since they require, at the very least, a pencil and some paper, which means that they can be produced anywhere at any time. Once the hand copy is ready, it is usually scanned and reproduced in the publication. In contrast, the disadvantages are multiple, such as the time required for copying, the time available for execution, the copyist skills, and the non-objectivity of the copy.

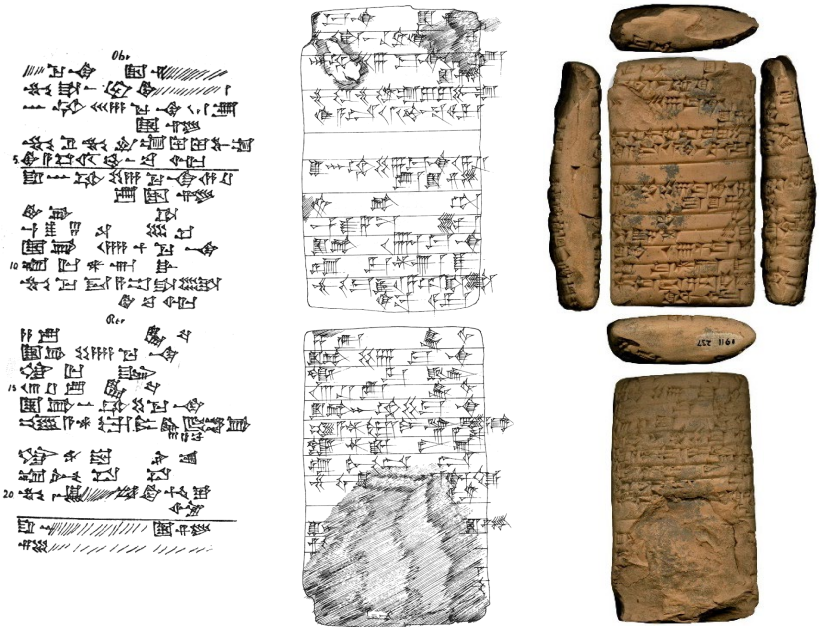

Figure 2. Tablet Ashm. 1911-237a-b from Umma (mod. Tell Jokha), datable to the Ur III period (2112-2004 BC): (a) copy adapted with permission from [25]. 1912, Langdon, S.H.; (**b**) copy adapted with permission from [26]. 1996, Grégoire, J.-P.; (c) flatbed scan from http://cdli.ucla.edu/ CDLI no. P142747 (accessed on 07/10/2022).

Nowadays, digital tracings of cuneiform tablets are a more accurate and efficient method of copying cuneiform texts. The chain of action is identical to the ink on paper hand copies (see above), but now cuneiform signs, fractures, and abrasions are traced on graphic devices using vector-based graphic software (such as Adobe Illustrator, Inkscape, etc.). Born-digital hand copies can be modified and processed multiple times. One of the greatest advantages of born-digital tracing is the possibility to create autographs on a layer overlapped with the photo of a cuneiform text. As with ink and paper hand copies, this method has the same disadvantages: its time-consuming nature and lack of objectivity. In addition, graphic tablets can be expensive and are not readily available everywhere at any time, unlike ink and paper.

2.2.2. Digital photography

Photography can overcome the drawbacks of hand copies, namely their potential non-objectivity.

Unfortunately, it is challenging to capture, with two-dimensional images, an irregular three-dimensional tablet with three-dimensional wedges (Figure 3). Other factors may affect the reading of a cuneiform tablet on a photograph: (i) different shades of colors on the surface as a result of (accidental) firings; (ii) stains (such as iron oxides black spots); (iii) brighter areas of salt efflorescence [27].

Since the 1970s, the technique of covering cuneiform tablets with a thin layer of ammonium chloride (NH_4Cl) to enhance the contrast in photographs and make uniform the areas of discoloration has become increasingly popular [28,29]. Despite the use of ammonium chloride, it is still difficult to accurately represent 3D objects with a photograph (Figure 4). With the introduction of digital photography, photographs can be digitally modified to improve the readability of cuneiform tablets [30,31].

Unfortunately, digital photography still suffers from the same limitations as analog photography, namely the inability to represent a complex three-dimensional object in its totality in two dimensions. In addition to the costs of the devices and, potentially, of the service, one should also consider taking the photos in a controlled environment, which is not always possible.

Cameras, however, can be easily transported anywhere. In the case of tablets coated with a thin layer of ammonium chloride, good results also rely on an additional operator who should work carefully to handle the toxic substance.

(a) **(b)**

Figure 3. The same tablet (LW21.CUN.133) belonging to Ghent University required two different pictures with two different lighting sources to make all signs readable: (**a**) very grazing light that accentuates the contrasts but darkens the lower part; (**b**) slightly grazing light that leaves the wedges at the bottom legible.

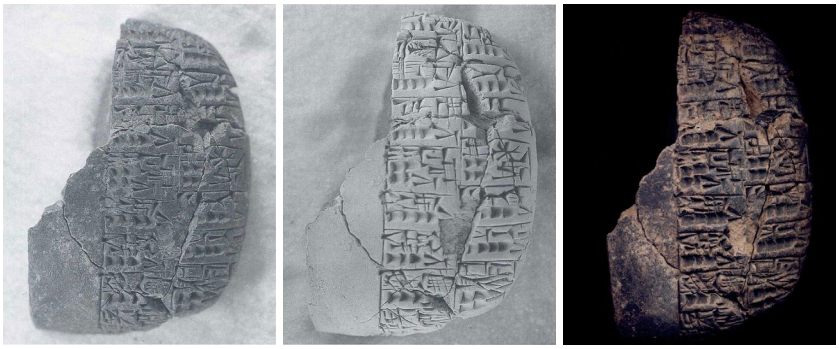

(a) (b) (c)

Figure 4. Cuneiform tablet from Tell Beydar (NMSDeZ Bey 95-001: verso): (**a**) photograph of the untreated tablet; (**b**) photograph of the tablet treated with ammonium chloride, reprinted with permission from [29]. 1997, Vandecasteele, C.; (**c**) tablet captured with a flatbed scanner, from https://cdli.ucla.edu/ CDLI no. P227324 (accessed on 07/10/2022).

2.2.3. Flatbed scanning

Flatbed scanners proved to be an effective, easy-to-use, and cheap alternative to photography. The Cuneiform Digital Library Initiative (CDLI) (http://cdli.ucla.edu/, accessed on 07/10/2022) has developed clear guidelines for scanning a cuneiform tablet: each side of the tablet is scanned and then edited and assembled into a single file [32]. The images, just as in photography, offer a clear, objective view of the artifact, but again, the convex, irregular surface of the tablet causes difficulty in illuminating each of the cuneiform wedges and some areas can be completely blurred or without the necessary contrast (Figure 2c).

2.2.4. RTI/PTM and Portable Light Dome

PTM (Polynomial Texture Map) or RTI (Reflectance Transformation Imaging) models are generated from multiple photographs of an object taken from a stationary camera. The light that is projected into each photograph comes from different known directions [33-37]. Based on the lighting information in the images, a mathematical model of the surface is produced, which enables the user to inspect the object by re-lighting it interactively. Additional effects and filters can be applied in order to improve the readability of cuneiform writing. The advantages of the RTI technique are many: good results can be obtained even with technical equipment suitable for conventional digital photography. Post-production and data processing have times that are also compatible with the study of archaeological artifacts in the field. Furthermore, thanks to the model size, the files can be easily uploaded and downloaded and viewed with relative ease by an average user.

The elaboration phase can produce models with different qualitative degrees of definition according to the needs.
However, the RTI mapping does not produce an integrable three-dimensional model; therefore, an acquisition must be performed for each side of the tablet. The 2D+ model produced is excellent for a detailed study of artifacts in a poor state of conservation but less suitable for a museum exposition of the tablet. Although 2D+ models are among the best methodologies for studying cuneiform tablets, some problems may arise as a result of their morphology (Figure 5).

2.2.4. 3D modeling: Photogrammetry and Structured Light Scanning
Thanks to active or passive sensor technologies, it is currently possible to obtain a faithful and 3D copy of the physical model at a resolution of a tenth millimeter or even a micron. One of the significant advantages of photogrammetry is the possibility of simultaneously detecting geometry and color with photographic quality. Compared to the active sensors and the other previously illustrated techniques, it generally requires higher data acquisition and processing times. Among the technologies based on active sensors, structured light scanners (SLS) ensure an excellent compromise between data resolution and survey speed. Often a lacking aspect is the poor texture quality so that it can be less attractive for museum exhibitions. The costs of these instruments increase as the accuracy and resolution required increase. The comparison between the active and passive sensors shows that the SLS

Figure 5. 2D+ models from PDL of tablet LW21.CUN.166 (Ghent University): (a) colour visualization; (b) shaded visualization; (c) "Sketch 1" visualization. Neither the verso nor the bottom edge of the 2D+ model clearly exhibit the cuneiform text highlighted in red.

benefits are faster data acquisition and processing times and the cleaning of the mesh surface. However, the expenses are significantly higher, and the texture quality is not always on par with the geometry quality. Photogrammetry, on the other hand, has the advantage of high-quality texture and a lower cost. But it is characterized by much longer times both for the acquisition of data and for their processing. In this framework, photogrammetry with a digital microscope (the solution described in the present research) represents a cost-effective approach because the microscope and related equipment can be significantly less expensive than a professional camera and photographic kit. However, the texture has good quality but not at the level of a professional photographic camera.
Table 1 collects and compares the main characteristics of all the systems analyzed. In this context, the digital survey, in general, and the resulting textured 3D models are the best option from an assyriological perspective. First, the 3D tablets can be objectively analyzed, i.e., they are not filtered by human work like in hand copies. Edges and marginal areas that are often not clearly visible in photographs can be visualized by rotating the model. A light simulator on the models can be used to simulate different directions of illumination so that the signs on the tablets can be read more clearly. Post-processing software can also be used to enhance the visibility of morphological details on the 3D model. For example, an effect similar to the ammonium chloride photographs can be achieved by applying specific filters (such as MeshLab's "Radiance Scaling" shader) to the 3D models to make the discoloration uniform and the wedges more prominent and thus improving their legibility (Figure 6).

(a) **(b)** **(c)**

Figure 6. Tablet LW21.CUN.159 belonging to Ghent University: (**a**) model textured; (**b**) mesh model; (**c**) mesh model with Radiance Scaling plugin by Meshlab. Mesh model from DSLR Camera Nikon D800E combined with AF-S Micro NIKKOR 60mm f/2.8G ED.

Table 1. Gathering and comparison of the key attributes of all the systems examined. For clarification purposes: (1) Exactness: how closely the final model is a true representation of the item; (2) Acquisition time: the average time required to create a high-quality copy of small-medium size tablets (such as those ones illustrated in the present article); (3) Lightning: the possibility to change/manage lighting effects at will on the result interactively; (4) Accessibility of technology: how widespread and popular is the instrumentation indicated.

	2D				2D+	3D		
	Hand Tracing		Raster		PTM	Photogrammetry		SLS
	Ink on paper	Vector based	Flatbed Scanner	Photo-graphy	Portable Light Dome	Reflex Macro Lens	USB Micro-scope	Scan in a Box
Objectivity	no	no	yes	yes	yes	yes	yes	yes
Exactness[1]	low-med	low-med	high	high	high	high	high	high
Acquisition[2]	± 24 h	± 24 h	± 10 '	≤ 10 '	± 30 '	± 1 h	± 3 h	± 30 '
Elaboration	± 1 '	0	± 5 '	± 5 '	≤ 20 '	± 3 h	± 3 h	± 5 '
Required skills	med-high	med-high	low-med	med-high	med-high	high	high	med-high
Level of Detail	low	low	med-high	med-high	high	high	high	high
Accuracy	low-med	low-med	high	high	high	high	high	very high
Text readability	high	high	low-med	med	high	high	high	high
Lightning[3]	no	no	no	no	yes	yes	yes	yes
Texture data	no	no	no	no	yes	yes	yes	yes
Accessibility of tech[4]	high	med.	med	high	med-high	med	low-med	low
Dissemination	high	high	high	high	med	low	low	low
Data size Manageability	high	high	high	med	med-high	low	low	low
Equipment cost	very low	med-high	med	med-high	med-high	high	med	high

Furthermore, there are two other advantages to using 3D models: the possibility of sharing online digital content and eventually the possibility of joining virtually one or more fragments of the same tablet together, not necessarily belonging to the same collection and in the same place [38]. In the case of the 3D models, two fragments can be joined together virtually without moving the real fragments from the original collection (Figure 7).

3. Towards the identification of an optimized acquisition system

3.1. USB microscopes as a new micro-photogrammetric tool

A digital microscope (Figure 8) is essentially the same as a conventional optical microscope without the eyepiece but with a CCD camera instead [39]. Therefore, USB handheld digital microscopes are more flexible, easy to use, and less expensive than traditional models.
Born for the inspection, documentation, and digital metrology analysis and already widespread in the manufacturing industry for quality control and in the medical field, digital microscopes have also been used for some applications of a micro-photogrammetric survey reaching even precision of about a tenth of a millimeter [40].
Therefore, integrating these tools into a structured photogrammetric workflow seemed promising.

Figure 7. Tablet LW21.CUN.159 (verso, bottom piece) and LW21.CUN.160 (verso, upper piece) belonging to the Ghent University and digitally joined. Mesh model from DSLR Camera Nikon D800E combined with AF-S Micro NIKKOR 60mm f/2.8G ED.

Therefore, integrating these tools into a structured photogrammetric workflow seemed promising. Their main drawback is that they were not designed from the start for photogrammetric applications and have therefore been adapted to increase the accuracy of the results, for instance, through the design of a particular calibrator and of an automatic system that accelerates the data acquisition.
Furthermore, for the same reason, no technical calibration characteristics of the lens system are widespread so far.

3.2 Initial experiments

The authors used a physical replica of a cuneiform tablet with wedges, which were as detailed, challenging, and complex as the original (Figure 9), to perform the first tests to evaluate the photogrammetric use of a digital microscope. The clone is a physical 3D printing of the original tablet no. 724 realized by the +LAB (www.piulab.it) and digitally surveyed by the 3D Survey Group - Politecnico di Milano[3].
The text concerns the administrative information for fish deliveries (the modern correspondent of a packing slip). This case study was chosen as a test case for the micro-survey system because it was the smallest and most complex. Indeed, the tablet is about 20×22×8 mm in size, and its distinctive wedge-shaped impressions have a depth of 1-3 mm.
The early research has yielded positive and promising results [11]. The next step was to deepen some theoretical aspects and streamline the acquisition (MO procedures, ensuring a more rigorous workflow [12].
The first aspect on which our research focused was to design an ad hoc acquisition setup for this micro-scale of size and detail. Therefore, during several acquisition campaigns, the following were studied and tested: calibrated support to arrange the object and simultaneously provide a metric reference; rotating base to simplify and speed up acquisitions; specific lighting setting.

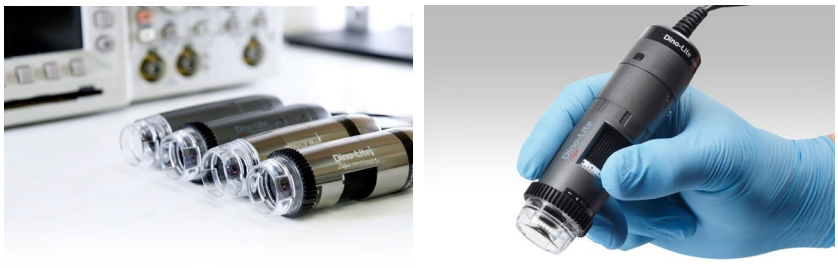

(a) **(b)**

Figure 8. Dino-Lite USB digital microscopes: (**a**) different models; (**b**) microscope handheld configuration.

Figure 9. Scale comparison of the original tablet no. 724 from the private collection Durac-Donner (Genève). Mesh model from Scan in a Box 3D scanner.

The first configuration used (Figure 10) for data acquisition with the microscope consisted of a calibrated plate, two LED illumination rings (one around the object and the other above it) and the Dino-Lite RK-06A stand [41] to house the microscope with a vertical axis (standard configuration).

The plate, printed with PLA filament, was designed with an orthogonal pattern of 99 truncated conical holes, with a countersink angle of 60° and a base diameter of less than 0.35 mm. Calibrator accuracy was estimated to be 0.1 mm (marker accuracy) based on 3D print settings and compliance of physical hole locations with the design file.

In this configuration, the digital microscope is stationary, housed on the vertical bracket at a fixed angle. Instead, the calibrated plate is manually slid for image acquisition of the tablet surface. Several problems were encountered: long acquisition times also due to the difficulty in keeping the plate integral with the object during sliding; overestimated target size on the plate; the impossibility of rigorously aligning the two faces of the tablet.

Indeed, the two sets of images, one for the *recto* and the other for the *verso*, do not have enough common points to be merged into a single model. It would have been necessary to survey the thin edge with a severe depth of field problems.

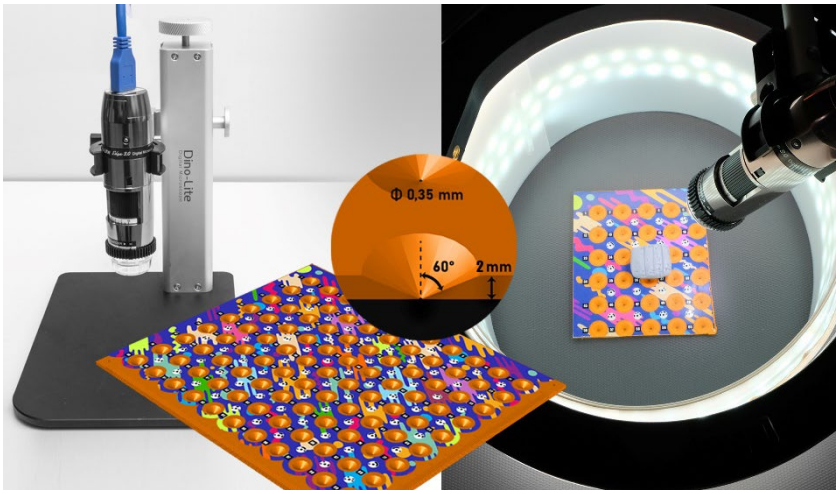

Figure 10. The raw configuration components: on the left, the standard stand to house the microscope with a vertical axis; in the middle, the plate calibrator with a section detail of a truncated cone hole; on the right, two illumination rings combined with the microscope asset and the cuneiform tablet on the calibrated plate.

To solve the problems encountered during the first test, two configurations were designed for the acquisitions. The first setup improved the previously described with the microscope vertical axis on a customized tripod and the horizontal support plate for the cuneiform tablet (Figure 11).

A new alternative solution consists of a clamp to house the tablet with a vertical axis and a tripod to position the microscope with a horizontal axis (Figure 12). On the clamp support, a pattern with the marker is glued; therefore, even in this second mode, it is possible to frame the metric references and the object simultaneously.

The Dino-Lite AM7013MZT was used for the tests and also in the next campaign to digitize the original cuneiform tablets. It was chosen to work with a 20× magnification, at which the working distance is 48.7 mm, and the depth of field is 3.6 mm with this model.

The model has a built-in adjustable polarizer to reduce reflections on shiny objects. However, lighting conditions have been improved with the adoption of an LED illumination ring. The light does not directly hit the object due to the shape and diffusing material of the lens hood. Therefore, diffused light conditions neutralize shadow cones without changes in the intensity of shadows, light and colors.

(a) **(b)**

Figure 11. The first acquisition configuration with the turntable calibrated plate: (**a**) three-dimensional calibrated plate (updated prototype) detail; (**b**) complete setup configuration.

For the first configuration (vertical microscope axis), a calibrated circular plate was designed, obtained with an EOS M270, by additive manufacturing of steel powder and characterized by a pattern of 279 truncated conical holes, with a countersink angle of 60° at all times and a base diameter of 0.35 mm. Therefore, the coordinates of each hole in a local reference system are known, and the perforated plate can be used as a grid of constraint points (GCP) evenly distributed over the entire area to optimize camera orientation and scale the model.

The calibrated plate was placed on a rotating table to facilitate and speed up the acquisition phase.

Once the magnification rate (optical zoom) was chosen and the digital microscope was placed on the fixed bracket at a fixed angle, a series of images with sufficient overlap could be acquired by rotating the base. Thanks to the customized tripod, the inclination of the microscope related to the plate changes after each complete rotation.

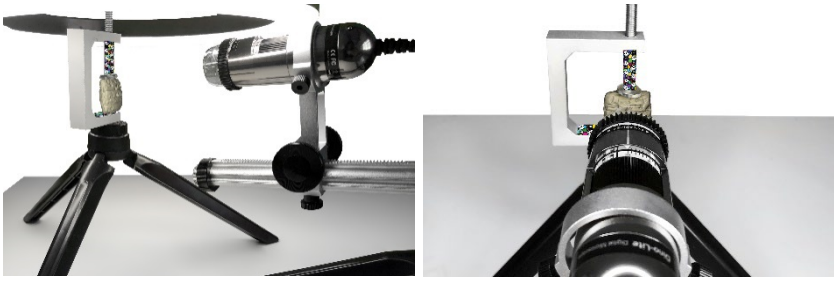

(a) **(b)**

Figure 12. The second acquisition configuration with the screw clamp: (**a**) the screw clamp coaxial to the rotating base; (**b**) detail of the positioning of the tablet in the clamp.

In general, to overcome the problem of a shallow depth of field, one possibility would be to close the aperture of the optics as much as possible within the limits of diffraction phenomena [42] and provide enough light to balance a correct exposure time. This option is not available on digital microscopes, which have a fixed diaphragm and, as a result, a fixed sharp field. Therefore, the object is captured from different focusing planes by moving the microscope on the vertical micrometric rail to focus on different planes.
With this first updated configuration, two acquisition sets were required, one for the *recto* and the other for the *verso* of the tablet, with an average of 250 shots each and approximately 1 hour of data acquisition work.
One of the problems that remained open for the digital survey of the cuneiform tablet (and thus for similar objects of small size and non-negligible thickness) was the impossibility of having a merged 3D model of the two faces using only the microscope dataset, even though inclined acquisitions were also carried out to frame the sides.
The second data acquisition setup was designed with a low-cost strategy in mind to address this specific gap. Indeed, the wedge-shaped tablet turned out to be a real challenge which, due to its size and complexity, allowed us to stress the acquisition system and bring out its weak points.
The second configuration involves a screw clamp commonly used in model making to position the object knife-edge related to the microscope camera. The clamp was covered with an adhesive pattern with printed coded markers. As for the calibrated plate, the clamp was also placed on a rotating base, taking care to align the center of rotation with the mounting axis of the object. The other photogrammetric accessories remained virtually unchanged from the previous configuration.
This setup took roughly an hour to acquire 700 photographs, plus an additional set for the tiny parts concealed by the clamp (around 100 shots). By positioning the model in this second acquisition mode, we were able to lessen the issues brought on by the shallow depth of field by ensuring that the pattern of encoded markers was always coplanar to the plane of focus on the surface of the object.
In the first configuration, we had numerous problems connected with the impossibility of focusing the markers and the surface of the wedge-shaped tablet simultaneously. With this configuration, however, this problem has been completely resolved.

Figure 13 displays the different performance abilities to simultaneously focus markers and the object surface using the calibrated plate (a) or clamp (b). The two datasets generated from the two acquisition settings were then processed using Structure from Motion (SfM) software (Agisoft Metashape Professional v.1.8.3), following the conventional photogrammetric workflow and using the same workstation (AMD Ryzen 9 5900HX CPU and 32 GB RAM). Due to the short depth of field and uniform texture of the tablet, aligning the tilted photographs during the processing of the first set of acquisitions proved to be very challenging.
This issue was not present while using the second configuration with the clamp because it gave us a more straightforward, more regular (with a higher number of shots for the edges) and, consequently, more efficient capture geometry (Figure 14). The GSD for the two photogrammetric projects is 6.3 μm for the calibrated plate acquisition and 7.14 μm for the screw clamp acquisition, respectively. Table 2 contains the key details.

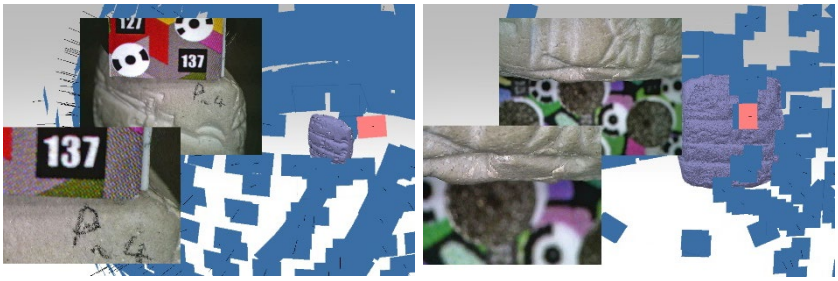

(a) **(b)**

Figure 13. The different performance abilities to simultaneously focus markers and object surface is compared using: (**a**) the calibrated plate; (**b**) or the clamp.

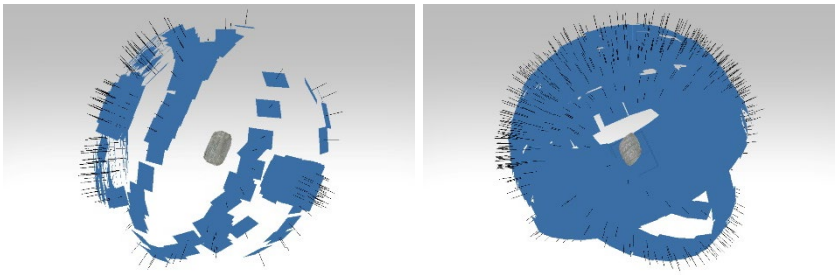

(a) **(b)**

Figure 14. The capture geometry network corresponds to the use of: (**a**) the calibrated plate; (**b**) the screw clamp. The acquisition time is the same (1h) even if the second configuration has more photos.

Table 2. Photogrammetric project properties.

Acquisition Network Geometry	Calibrated Plate Set	Screw Clamp Set
Aligned Cameras	506/518	718/718
Sparse Cloud	4.3×10^5 points	4.1×10^5 points
Sparse Cloud Filtered	3.8×10^5 points	2.1×10^5 points
Dense Cloud	10.4×10^5 points	8.3×10^5 points
GSD	6.3 μm/px	7.14 μm/px
RMS Error	0.87 mm	0.027 mm
Processing Time	4h	2h

3.3 Benchmark and evaluation comparisons

The tablet 724 replica was also digitally surveyed with a structured light scanner (Scan in a Box @2015 Open Technologies SRL) in order to have a digital reference model against which to check the overall geometric dimensions of the photogrammetric reconstructions generated from the previous tests.

The final mesh model (Figure 15), which has an average resolution of 0.08 mm and is made up of around 400.000 polygons, has fewer details than the corresponding photogrammetric models but can still be utilized to ensure a reference check of their overall measurements.

The scanner mesh model was used as a reference to align the photogrammetric clouds in the same coordinate system and to provide a comparison of the results obtained. In this analysis, the photogrammetric models obtained with the two configurations described in Figures 11 and 12 were evaluated: the first based on the use of a calibrated plate on which to place the object, the second on the use of a clamp in which to fix the object, covered by a calibration pattern.

The results of the first basic setup acquisition, shown in Figure 10 [11] – were excluded, and only the optimized configurations were considered to choose the better one for this case study.

Cloud-to-mesh registration (CloudCompare v. 2.12 alpha, open-source software) was performed in two stages: a manual registration using homologous points and a global registration using automatic alignment algorithms (Iterative Closest Point). Figure 16 displays the false-color deviations between the photogrammetric clouds and the laser mesh reference.

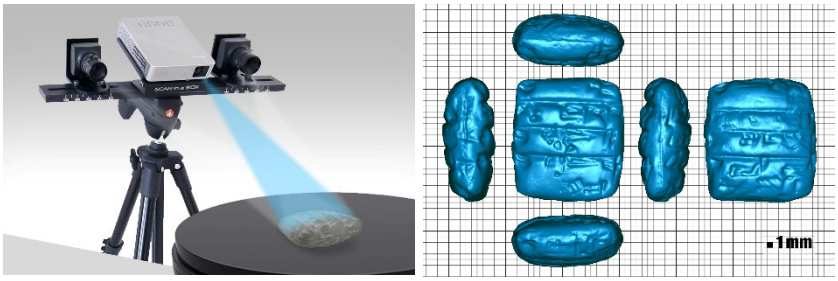

(a) (b)

Figure 15. The benchmark survey: (**a**) the Scan in a Box system; (**b**) the polygonal model of the cuneiform tablet replica (1 mm grid background).

It should be observed that for both photogrammetric models, the mean and standard deviations from the reference do not exceed 0.3 mm.
Moreover, it can be seen from the image that many deviations are punctual and are mainly localized in some deeper incisions. Therefore, there are probably no differences in the overall dimensions of the tablet nor deformations in the morphology. Most of these deviations seem related to the higher resolution obtained from the photogrammetric survey.
The scanner mesh is smoother and has a lower resolution: 0.08 mm against 0.007 mm GSD. These considerations allow us to conclude that the microscope acquisitions have been correctly processed within the photogrammetric workflow and that the digital models are satisfactory both from the metric point of view and for the subsequent interpretation of the data. Concentrating instead on the comparison between the model generated by two network geometries, Figure 17 illustrates that for the screw clamp setup, 94% of the points are included in a difference of +/- 0.1mm, while about 40% for the calibrated plate configuration are included in a difference of +/- 0.1mm.
In-depth, the results produced using the calibrated plate show more considerable deviations. This is because of problems with photo alignment, which have made the cloud noise worse (in the lower right corner of the *recto* and on the whole face of the *verso*) and difficulty merging the two sides (Figure 18). In conclusion, the calibrated plate remains a valuable tool for predominantly flat objects and/or combined with reflex cameras and macro lenses, allowing for greater depth of field and a wider angle of view. However, as known, it is not possible to define a photogrammetric survey configuration appropriate to all scales, sizes, and morphologies [43]. The availability of different supports and accessories (tripods, light setup, calibrators) allows us to quickly change the acquisition geometry or even the acquisition tool (camera, cell phone, microscope).

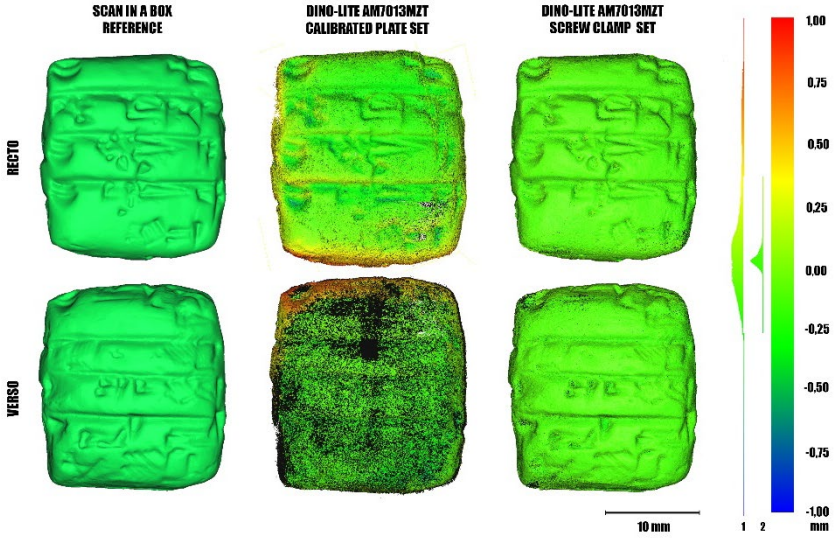

Figure 16. False-colour deviations from the Scan in a Box reference model of the photogrammetric dense clouds obtained with the calibrated plate and screw clamp as support (recto and verso side).

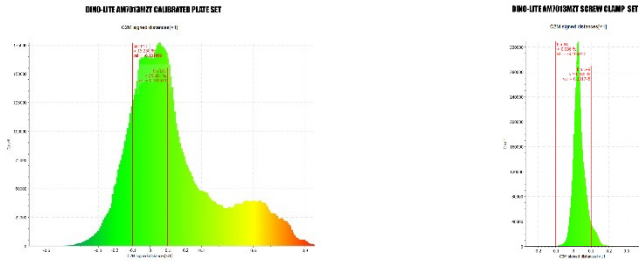

(a) **(b)**

Figure 17. Deviations of the photogrammetric clouds from the reference model: (**a**) in the calibrated plate setup, 40% of the points are within +/- 0.1mm; (**b**) in the screw clamp setup, 94% of the points are within +/- 0.1mm.

Concentrating instead on the comparison between the model generated by two network geometries, Figure 17 illustrates that for the screw clamp setup, 94% of the points are included in a difference of +/- 0.1mm, while about 40% for the calibrated plate configuration are included in a difference of +/- 0.1mm.

In-depth, the results produced using the calibrated plate show more considerable deviations.

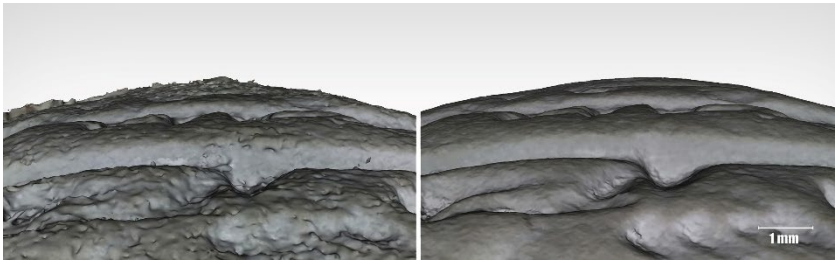

Figure 18. Comparison between the surface of the models; the reconstruction related to the first setup acquisition with the calibrated plate presents more noise.

This is because of problems with photo alignment, which have made the cloud noise worse (in the lower right corner of the *recto* and on the whole face of the *verso*) and difficulty merging the two sides (Figure 18). In conclusion, the calibrated plate remains a valuable tool for predominantly flat objects and/or combined with reflex cameras and macro lenses, allowing for greater depth of field and a wider angle of view. However, as known, it is not possible to define a photogrammetric survey configuration appropriate to all scales, sizes, and morphologies [43]. The availability of different supports and accessories (tripods, light setup, calibrators) allows us to quickly change the acquisition geometry or even the acquisition tool (camera, cell phone, microscope). Therefore, the system has been built to be flexible such that alternative network geometries are conceivable using the same equipment for data collecting (in this case, the microscope) by selecting the most appropriate support based on the shape and features of the object.

4. USB microscope optical calibration

4.1. Premise

The 'so-called' USB microscopes constitute an optical inspection system designed to obtain as output the image on a monitor, possibly by means of dedicated software [44]. As shown, the magnifying capacity and the ability to be tilted, given the shape and small size, enable images with appropriate intersection angles to the object to be obtained for the generation of three-dimensional models [40] according to known SfM procedures. One of the main problems in SfM concerns the identification of two essential items: (i) the position and orientation of the camera in space (the external parameters of the camera); (ii) how the camera maps the perspective projection points of space onto its

image plane (the internal parameters). The determination of these parameters is significant for the accuracy of the 3D reconstructions, as well as for reducing the number of unknowns in the collinearity equations and thus speeding up the bundle-block adjustment procedure. While the software available on the market today has made enormous strides and allows for fairly accurate three-dimensional models, even for uncalibrated cameras within a self-calibrating bundle adjustment [45], the effectiveness of the reconstruction obtained requires validation.
The question then arises as to whether it is possible to define the optical parameters of the Dino-Lite microscope (in detail with reference to the AM7013MZT model used for this research activity), operating in the lack of EXIF data and thus just starting from the known values stated by the manufacturer. In detail, the focus is on the identification of a geometric model compatible with the USB microscope used and the estimation and verification of the main distance. It should be noted that the only a priori known data relating to the optical system are the sensor size in pixels (5.0 MP, 2592×1944 px), and depending on the Magnification rate (M)[4], the Field Of View (FOV) and Working Distance (WD)[5] [48], look at Table 3.

Table 3. Working Distance (WD), Field of View dimensions (FOV) among x and y directions as a function of Magnification rate (M) for AM7013MZT Dino-Lite microscope expressed in millimeters.

M	WD	X_{FOV}	Y_{FOV}
20	48.7	19.8	14.9
30	21.7	13.2	9.9
40	9.0	9.9	7.4
50	1.9	7.9	5.9
60	-2.3	6.6	5.0
220	-0.1	1.8	1.4
230	1.0	1.7	1.3
240	2.1	1.7	1.2

To develop a method for estimating the unknown parameters of an optical system for photogrammetric purposes, a model that acceptably synthesizes the geometry of the system must be assumed.
The type of model used performs according to the same laws as the pinhole camera model (Perspective Projection) and follows the Gaussian Lens (Thin Lens) Law.

4.2. Optical model

Following the geometrical optics, the image formation using a lens provides a relationship between the object in real space and its image on the sensor plane.
In general, the distance of the object from the lens called *H*, and the distance of the sensor from the lens, called *f*[6], are in a conjugate proportion (similar triangles). Observing this general law, then it is possible to admit that the field framed at a given magnification, i.e. for a given position of the optical unit[7], is related to the image framed totally by the sensor (Figure 19).
In other words, if a graduated bar is photographed at a given magnification, the framed – and thus visible – field of the image corresponds to a specific, quantifiable length, called Field of View, along the horizontal (XFOV) and the vertical direction (YFOV) of the sensor.
This is a very important piece of information, easily verifiable experimentally, allowing the field framed at each magnification to be related to the size of the sensor, as follows.

$$|X_{FOV}/X_S| = |H/f| \quad (1)$$

$$|Y_{FOV}/Y_S| = |H/f| \quad (2)$$

Unfortunately, Equations (1) and (2) require the dimensions in millimeters of the sensor to be known. For now, the discussion on this is postponed to the next paragraph. The first thing one can do, however, is to calculate the so-called GSD, "Ground Sample Distance" from the ratio $|X_{FOV}/X_S|$, expressed in millimeters divided by pixels, choosing a magnification from the microscope dial, setting up at the correct working distance and photographing a graduated bar, as previously indicated. For instance, the values for 20× magnification are considered as follows:

$$GSD = X_{FOV}/X_S = 19.8/2592 = 0.00764 \text{ mm/px} \quad (3)$$

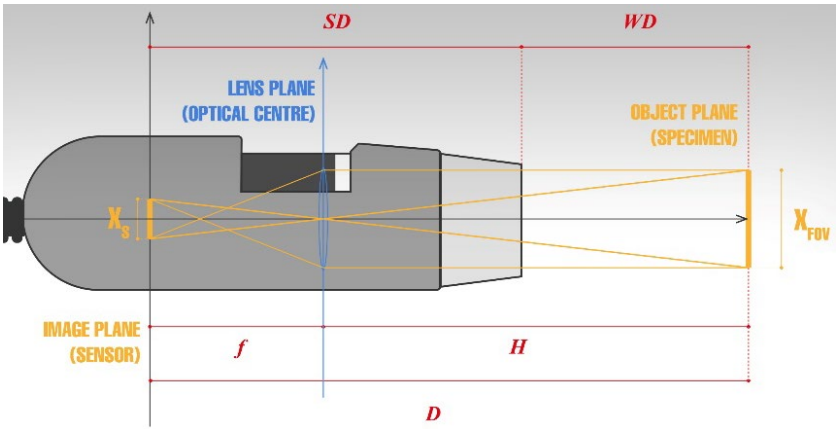

Figure 19. Comparison between the surface of the models; the reconstruction related to the first setup acquisition with the calibrated plate presents more noise.

At this point, proceeding experimentally in the Agisoft Metashape software environment, it is possible to derive the missing data of the (1) via the "calibrate lens" function, using a printed calibration target accepted by the software consisting of a square chessboard with a 1 mm grid step. Ensuring that the magnification, i.e., framed field of view, is 19.8 mm among the x direction, the chessboard is then framed and photographed from different angles, trying to acquire a number of images greater than ten.

The lens calibration procedure supports the full camera calibration matrix estimation, including non-linear distortion coefficients [49].

The estimated parameters pertain to Brown's model: f – main distance measured in pixels; c_x, c_y – principal point coordinates; k_1, k_2, k_3 – radial distortion coefficients; p_1, p_2 – tangential distortion coefficients. Following the process of the lens calibration steps, image orientation and scaling and referencing in a local coordinate system according to the grid, the calibration parameters of the camera were extrapolated. Both the known a priori parameters and those obtained from the calibration process for the 20× magnification are then summarized below (Table 4).

Note that at this stage, f is relevant regarding internal orientation and H and GSD regarding data derived from external orientation.

It is clear that the lens calibration output parameters may fluctuate, albeit slightly, as experimentally obtained data from the procedure described above.

Table 4. Declared data and computed data after calibration (besides distortions and coordinates of the principal point) for 20× magnification.

Declared parameters					Calibration output parameters		
WD	**X_S**	**Y_S**	**X_{FOV}**	**Y_{FOV}**	**GSD**	***f***	**H**
48.7 mm	2592 px	1944 px	19.8 mm	14.9 mm	0.0076 mm/px	13413 px	102.46 mm

The additional difficulty of manually setting the magnification to perfectly match the 20× value indicated on the control ring also can influence variations in the results. From the table, it can be seen that the GSD value calculated by the software is coincident with that calculated a priori both from the declared value in Equation (3). Having the main distance calculated by the software in pixels – the size of the main distance in millimeters remains unknown because the pixel pitch value is unknown – the value of H for the assumed camera model can be verified from Equation (1) as follows:

$$H = f \cdot (X_{FOV}/X_S) = f \cdot GSD = 102.48 \text{ mm} \quad (4)$$

It can be seen that the two values of H, the first in Table 2 and the second obtained from Equation (4), are very close.

So, it is possible to accept about H = 102.5 mm as an exact value.

4.3. Sensor Size

At this point, the issue of sensor size needs to be clarified. In the absence of information on the size in millimeters of the entire sensor and thus the pixel pitch, nor on its geometric location in the model, it is not possible to identify it with certainty.

Even if one wanted to proceed iteratively, any sensor among those on the market and compatible with the geometry of the microscope would have an acceptable solution: this is because, in the absence of a metric reference of the sensor, it is understood that 2592 px along the x sensor direction can be accommodated by any sensor that physically fits into the microscope: [50] (Table 5).

Table 5. Different sensor sizes potential suitable for the model assumed and the derived *f* in pixel for 20× magnification. For each sensor, the value of *f* in millimeters was derived by multiplying *f* shown in Table 2 per the pixel pitch. It is not a surprise that *f* in millimeters changes since (1) shows the direct proportionality between Xs and *f*.

Sensor	Xs		Ys		pixel pitch	*f*	
1/9″	2592 px	1.60 mm	1944 px	1.20 mm	0.0006 mm/px	13413 px	8.28 mm
1/6″	2592 px	2.40 mm	1944 px	1.80 mm	0.0009 mm/px	13413 px	12.42 mm
1/4″	2592 px	3.60 mm	1944 px	2.70 mm	0.0014 mm/px	13413 px	18.63 mm
1/3″	2592 px	2.80 mm	1944 px	3.60 mm	0.0019 mm/px	13413 px	24.84 mm
1/2.5″	2592 px	5.76 mm	1944 px	4.32 mm	0.0022 mm/px	13413 px	29.81 mm

Consequently, it was necessary to contact the manufacturer to know the sensor size: the sensor of the AM7013MZT measures 3.67×2.74 mm, resulting in a pixel pitch of 0.0014 mm, values compatible with a 1/4″ sensor. Let a further quantity be introduced: this is a constant quantity called SD, which defines the position of the sensor with respect to a known point on the model, a point which can be assumed for convenience to coincide with the tip of the front cap. SD is defined as:

$$SD + WD = f + H = D \tag{5}$$

It is therefore trivial to calculate the value for the given sensor deriving that the position of the sensor is approximately 72 mm anterior to the end of the microscope, a value further confirmed by the manufacturer (Table 6):

Table 6. Values of characteristic quantities for the sensor used in the USB microscope from calibration test.

Sensor	WD	*f*	H	D	SD
1/4″	48.70 mm	18.6 mm	102.5 mm	121.1 mm	72.4 mm

4.4 Result validation

With the aim of performing a final cross-check with the initial calibration, parameter estimation will then be repeated, assuming that the sensor is known from the beginning. Indeed, it should be recalled that the initial lens calibration was performed without EXIF data, i.e., the software only estimated the quantities from the features recognized on the calibration grid and the grid step size. Therefore, the sensor input data can be used to verify the validity of the estimation made by the lens calibration tool.

Then the ratio of the framed field to the corresponding sensor size in millimeters for the two magnifications considered previously is computed as follows:

$$X_{FOV} / X_S = 19.8/3.67 = 5.4 \tag{5}$$

By noting that the WD for each magnification is known and experimentally verifiable and that SD is declared by the manufacturer equal to 72 mm, the sum of SD and WD is known, so the (4) can be applied. Then, the following systems can be formulated and solved for the unknowns f and H:

$$f + H = 121.1 \tag{6}$$

$$H/f = 5.4 \tag{7}$$

Then, the values obtained from this verification are compared with those of the calibration (Table 7):

Table 7. Values of characteristic quantities for 1/4" sensor at 20x magnification in the Dino-Lite AM7013MZT USB microscope.

Values	f		**H**	**GSD**
calibrated	13413 px	18.6 mm	102.5 mm	0.00764 mm/px
calculated	13481 px	18.9 mm	101.8 mm	0.00764 mm px

The differences related to the software calibration can be considered negligible, considering the result obtained by the software as acceptable, as well as the model used.

5. Massive cuneiform tablets digitization

The tests described in the preceding paragraphs (3 and 4) highlighted the problems faced when surveying small objects by USB microscopes, which have driven the evolution of the solutions adopted to streamline procedures, paying attention to optical calibration. It then emerged that the network geometry obtained with the screw clamp setup was much more effective than the nadiral one. Indeed, despite the tablet shape and morphology, it ensures sufficient overlap between the pairs of stereoscopic images, improving the camera orientation, allowing a complete and continuous reconstruction of the surface, and facilitating and speeding up the acquisition.

Therefore, it was possible to carry out expeditious digitization of the original tablets at the University of Ghent by the screw clamp setup, including the microscope Dino-Lite AM7013MZT, a LED illumination ring and a turntable (Figure 20).

Figure 20. Acquisition system based on the turntable and clamp with ring illumination to support the microscope-integrated LED illumination. Magnification related to working distance: 20×.

Table 8. Cuneiform tablet digitized at Ghent University with the USB microscope Dino-Lite AM7013MZT.

Tablet LW21.CUN.	Recto	Verso
160 959 captures GSD: 0.00752 mm/px		
159 930 captures GSD: 0.00781 mm/px		
133 949 captures GSD: 0.00766 mm/px		
126 1343 captures GSD: 0.00766 mm/px		

The resulting less noisy models solved two critical issues: (i) there were no severe problems focusing the tablet surface and the markers (fixed to the stand) at the same time, despite the small depth of field; (ii) the front and back of the tablet could both be simultaneously captured. Although it was necessary to turn the piece upside down and partially repeat the capture process for the occluded part, the alignment of this second set of photos is not problematic, guaranteeing legible and complete final models.

In a first survey campaign, four cuneiform tablets were digitized in two full days of work, with an average of two complete tablets per day (Table 8). The images of each dataset were then imported into the Agisoft Metashape software for SfM processing. The internal and external orientation parameters are calculated during the image alignment step with the bundle block adjustment process based on collinearity equations [51].

The computer vision SfM algorithm converges faster to a solution if it starts from input data about the optical calibration close to the real ones. Unfortunately, this information cannot be automatically deducted from the EXIF data as they are absent. Therefore, the initial approximation of the interior orientation parameters is specified before starting the process according to the calibration results (see paragraph 4).

Subsequently, it is possible to identify encoded targets in each capture automatically. To perform this function, it is necessary to design a pattern of software-generated targets to be introduced into the scene based on the object size [52]. However, the need to include metric references or calibration tools in the captured scene, using appropriate patterns in the function of the object dimension, still represents a critical issue: indeed, it is not trivial to estimate the accuracy of the print and ensure the flatness of the reference surface, as well as to position the targets themselves simultaneously close to the object and within the sharp area.

A first orientation optimization is then based on the markers automatically generated by the recognition of these encoded targets. This operation simultaneously refines the external and internal camera orientation parameters and the coordinates of the triangulated constraint points. At this stage, the local coordinates for each marker are not specified, although known by design, in order not to stiffen the model geometry with the introduction of errors related to the marker printing accuracy.

A second optimization is performed after filtering the sparse cloud points (tie points) based on specific criteria. The parameters considered are: (i) Reconstruction uncertainty; (ii) Reprojection error; (iii) Projection accuracy. The typical consequence of points generated from nearby photographs with a thin baseline is a great amount of Reconstruction uncertainty. These points may create a noise noticeably on the surface with variable density. Even though removing such points does not affect optimization accuracy, it may be advantageous to improve the clearness and correctness of the reconstruction geometry.

High Reprojection error typically indicates poor localization accuracy of the corresponding point projections during the point matching step. False matches are also common. Eliminating these spots can increase the accuracy of the next optimization stage. The Projection accuracy criterion enables the removal of points whose localization of projections was substantially poorer due to their larger size.

Therefore, the point cloud filtering tools allowed us to distinguish and remove the points that substantially impact the reconstruction quality.

After the filtering-based optimization, the coordinates of the markers were entered for the sole purpose of scaling the model (absolute orientation). The accuracy given by RMSE (Root-Mean-Square Error)[8] of measured image coordinates is always less than 0.5 pixels in all 8 chunks of the tested cases, with the most significant total displacement error between 1 and 2 tenths of a millimeter.

Next, following the canonical steps of photogrammetric reconstruction, the dense cloud, mesh, and model texturing were generated.

Two chunks were created for each tablet because it is necessary to integrate the first complete round of acquisitions with another set of photos of the area occluded by the support and the pattern. The two groups are then aligned using homologous natural features (marker-based) to obtain a complete reconstruction of each tablet. It should be emphasized that the joining chunks may sometimes be imperfect, invalidating the final result, with merging errors that must subsequently be post-produced (Figure 21). For this reason, the study of overlapping areas should be carefully planned upstream of the acquisition. In this regard, safe and complete overlap work is still laborious due to minimal movement difficulty, which is controlled without the aid of micrometric slides, which should therefore be included in the system soon.

Additionally, the shallow depth of field (due to the magnification increasing) implies that only a tiny portion of the artifact is in focus on the photo, so only a small part of the image appears sharp enough to be used for 3D reconstruction [53]. The photo sharpness is one of the parameters determining output point cloud reliability, accuracy, and quality [54]. So, computational photography techniques to extend the sharp field, such as the well-known Focus Stacking, allow less noisy results with more incisive surface detail [55]. Unfortunately, this is undoubtedly time-consuming and does not lead to time optimization. In all 4 cases examined, however, it was possible to achieve the completeness of the model without severe criticalities, thus ensuring optimal three-dimensional legibility of the tablets (Figure 22, 23, 24).

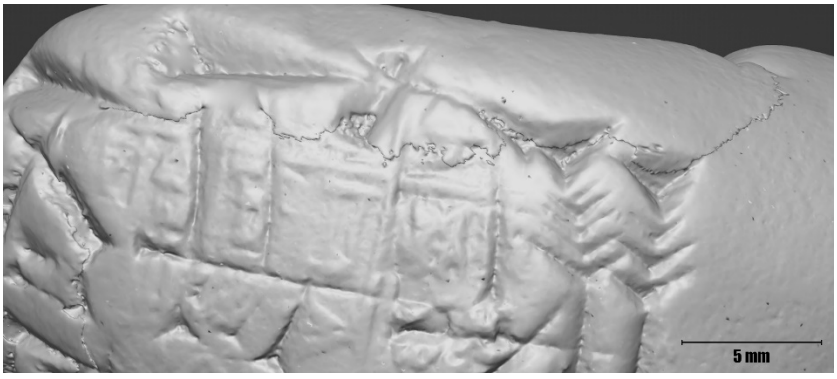

Figure 21. Detail of the mesh obtained by joining two partial models: evident is the stitching of the two pieces, which can be smoothened in post-processing.

Figure 22. Complete mesh model of the Tablet LW21.CUN.133, obtained by photogrammetric survey with the Dino-Lite AM7013MZT microscope.

Figure 23. Complete mesh model of Tablet LW21.CUN.126, obtained by photogrammetric survey with the Dino-Lite AM7013MZT microscope, under different light conditions: diffuse light on mesh only; semi-grazing light on mesh and texture; very grazing light on mesh and texture.

Figure 24. Complete mesh model of Tablet LW21.CUN.160 (left) and Tablet LW21.CUN.159 (right), obtained by photogrammetric survey with the Dino-Lite AM7013MZT.

As already done for the preliminary tests (section 3), comparing the outputs of different instruments used during the massive acquisition phase was helpful for the following reflections.

Photogrammetry emerges as an excellent alternative to structured light scanning and can be conducted with valid results not only using consumer cameras (suitably equipped to achieve high magnifications) but also with USB microscopes of a few hundred euros.
However, the comparison of digital models of the same find (Figure 25) shows that, despite the accuracy achieved by the different instruments in metric terms for the reconstruction, the size of the sensor and the quality of the optics used still have a clear impact on the rendering of details (the camera model has sharper details than the others). Therefore, high magnifications are not synonymous with higher quality [56], especially if the depth of field, an essential photogrammetric requirement, is sacrificed.

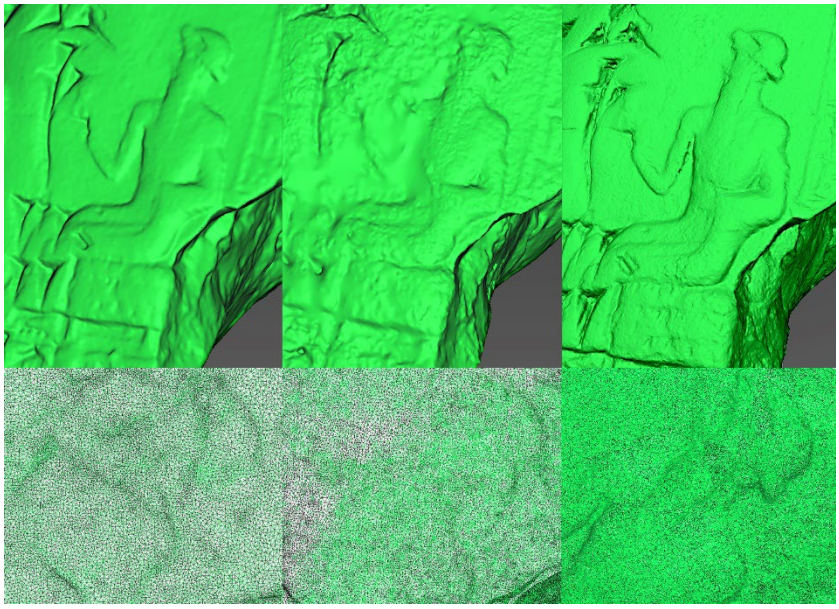

Figure 25. Detail and wireframe zoom of Tablet LW21.CUN.159 (verso), obtained by surveying with Scan in a Box 3D Scanner (left), Dino-Lite AM7013MZT microscope (centre), DSLR Camera Nikon D800E combined with AF-S Micro NIKKOR 60mm f/2.8G ED (right).

6. Conclusions

The initial examination of the various conventional and innovative techniques for the documentation of the wedges present on the cuneiform tablets has allowed us to focus on the specific needs of this type of study.

In general, the digital micro-survey and the related polygonal model can be considered an optimal solution for the reading and interpretation of the text, as well as for the possible sharing with other researchers and researches.

The solution proposed for the photogrammetric detail survey based on a customized configuration for a digital microscope was very effective. The various experimental survey campaigns made it possible to define the "screw clam" as the most suitable and fastest digital microscope acquisition setup in the function of the object shape and the required detail (see paragraphs 3 and 5). Figures 23 and 24 show a complete textured reconstruction obtained. The resulting accuracy and the geometrical model correctness were validated using a reference benchmark (section 3). In conclusion, the presented micro-photogrammetric configuration allows for meeting various needs: a low cost of equipment, high resolution (7-8 microns), and the color of the mesh as additional information to the geometry.

Notes

1. The most common and most expensive micro-survey solution is the structured light scanner, which can cost upwards of 30.000 euros at the highest standards (without taking into account the costs of licenses for data management software). In general, it allows reaching accuracies of 0.01 mm and resolutions down to 0.03 mm [artec3d.com/it/portable-3d-scanners/artec-micro; einscan.com/handheld-3d-scanner/einscan-pro-hd/; creaform3d.com/en/portable-3d-scanner-handyscan-3d; hexagonmi.com/products/structured-light-scanners; lmi3d.com/family/line-profile-sensors/]. However, today, various low-cost 3D scanners (from 500 euros) are also available, which are naturally designed for non-professional applications, with correspondingly much poorer accuracy and resolution, and for mostly amateur use [www.xyzprinting.com/en/product/3d-scanner-2-0; it.shop.revopoint3d.com/; matterandform.net/store; creality3d.shop/products/creality-cr-scan01-portable-3d-scanner?logged_in_customer_id=&lang=it; scandimension.com/products/sol-3d-scanner].
2. As a rough estimate, the price of a Dino-Lite microscope begins at a few hundred euros and varies based on the technical specs (resolution, magnification, LEDs, polarize, etc.). A mid-range costs approximately 500 euros. In contrast, the price of a set for micro-photogrammetry varies widely based on the technical data (sensor size, resolution, lens quality, accessories for macro photography, etc.). However, the price of a high-level reflex camera+macro lens typically exceeds 3000 euros (the cost estimation is refereed to Europe).
3. The digital survey took place in Geneva (Switzerland) from 21/01/2018 to 24/01/2018 with the collaboration of Mirko Surdi (Ghent University), Francesco Fassi and Fausta Fiorillo (3D Survey Group, Politecnico di Milano), and Catherine Mittermayer (University of Geneva). The survey documented with high-definition 3D models (photogrammetry and structured-light scanner) a small lot of cuneiform

tables, foundation cones, and votive plaques of Mesopotamian origin from the Durac-Donner private collection.

4. It is important to note that with regard to Dino-Lite USB microscopes, the reported magnification incorporates digital magnification forms [46,47]. Thus, as suggested by the manufacturer, in this case it is often more useful to compare field of view rather than magnification, i.e., to compare the physical dimensions of the original item being magnified to the resulting size of the item on the display.
5. The reference zero for the WD value is the outer end of the plastic nozzle, so negative WD values are motivated by the need to make the specimen compenetrate the nozzle (assuming the specimen size allows this).
6. Also known as photogrammetric principal distance.
7. For this optical system, adjusting the magnification is equivalent to moving the lens plane backwards or forwards between the object and the sensor. In this mechanism, therefore, it is not possible to define for all magnifications a single value of f (main distance), nor of H (flight height), nor of their sum $D=f+H$, since the distance to the object will vary, as will the position of the center of the optical unit.
8. Root Mean Square Error (RMSE) is the standard deviation of the residuals (prediction errors). In other words, it is a measure of accuracy that allows for measuring the difference between predicted and observed values. From a mathematical point of view, it is the square root of average squared errors. Larger errors have a disproportionately large effect on RMSD; consequently, outliers affect RMSD. It is always non-negative, and a value of 0 (almost never achieved in practice) would indicate a perfect fit to the data.

References

1. Gallo, A.; Mazzupappa, M.; Bruno, F. 3D reconstruction of small sized objects from a sequence of multi-focused images. *Journal of Cultural Heritage* **2014**, *15(2)*, 173-182.
2. Hansen, H.N.; Carneiro, K.; Haitjema, H.; De Chiffre, L. Dimensional Micro and Nano Metrology. *CIRP Annals* **2006**, *55(2)*, 721-743.
3. Tolksdorf, F.J.; Elburg, R.; Reuter, T. Can 3D scanning of countermarks on Roman coins help to reconstruct the movement of Varus and his legions. *Journal of Archaeological Science: Reports* **2017**, *11*, 400-410.
4. Caine, M.; Magen, M. Low-Cost Heritage Imaging Techniques Compared. In Proceedings of *Electronic Visualisation and the Arts*, London, United Kingdom, 11-13 July 2017.
5. Bitelli, G.; Girelli, V.A.; Remondino, F.; Vittuari, L. The potential of 3D techniques for cultural heritage object documentation. In Proceedings of *Videometric IX*, 6491, San Jose, CA, United States, 29 January 2007.
6. Douglass, M.; Lin, S.; Chodoronek, M. The application of 3D photogrammetry for in-field documentation of archaeological features. *Advances in Archaeological Practice* **2015**, *3(2)*, 136-152.
7. Porter, S.T.; Roussel, M.; Soressi, M. A simple photogrammetry rig for the reliable creation of 3D artifact models in the field *Advances in Archaeological Practice* **2016**, *4(1)*, 71-86.
8. Marziali, S.; Dionisio, G. Photogrammetry and Macro Photography. The Experience of the MUSINT II Project in the 3D Digitization of Small Archaeological Artifacts. *Studies in Digital Heritage* **2017**, *1(2)*, 298-309
9. Lastilla, L.; Ravanelli, R.; Ferrara, S. 3D high-quality modeling of small and complex archaeological inscribed objects: relevant issues and proposed methodology. *The International Journal of Advanced Manufacturing Technology* **2019**, *XLII-2/W11*, 699-706.

10. Antinozzi, S.; Ronchi, D.; Barba, S. Macro and micro photogrammetry for the virtualization of the Orphic Foil (V-IV B.C.) of National Museum of Vibo Valentia. In *CONNETTERE un disegno per annodare e tessere – UID, Congress of Unione Italiana per il Disegno*; Arena, A., Arena, M., Brandolino, R.G., Colistra, D., Ginex, G., Mediati, D., Nucifora, S., Raffa, P., Eds.; Franco Angeli: Milano, Italy, 2020; 1538-1555.
11. Antinozzi, S.; Ronchi, D.; Fiorillo, F.; Barba, S. 3Dino: configuration for a micro-photogrammetric survey. Applying Dino-Lite microscope for the digitalization of a cuneiform tablet. In *Towards a new, configurable architecture - Proceedings of the 39th eCAADe Conference;* Stojaković, V., Tepavčević, B., Eds.; GRID, Faculty of Technical Sciences: Novi Sad, Serbia, 2021; Volume 2, 211-222.
12. Antinozzi, S.; Fiorillo, F. Optimized Configurations for Micro-Photogrammetric Surveying Adaptable to Macro Optics and Digital Microscope. *The International Archives of the Photogrammetry, Remote Sensing and Spatial Information Sciences* **2022**, *XLVI-2/W1*, 25-32.
13. Verdiani, G.; Formaglini, P.; Giansanti, F.; Giraudeau, S. Close-Up, Macro and Micro Photogrammetry and Image Perspective: A Comparative Studio on Different Lenses at Work with Small and Medium Size Objects. *Computer Reviews Journal* **2018**, *2*, 235-248.
14. Gajski, D.; Solter, A.; Gasparovic, M. Applications of macro photogrammetry in archaeology. *The International Archives of the Photogrammetry, Remote Sensing and Spatial Information Sciences* **2016**, *XLI-B5*, 263-266.
15. Solter, A; Gajski, D. Project "Towards the Virtual Museum" – Exploring Tools and Methods for 3D Digitalization and Visualization. *Opvscvla archaeologica* **2018**, *39/40 (1)*, 117-124.
16. Homburg, T.; Zwick, R.; Mara, H.; Bruhn, K.-C. Annotated 3D-Models of Cuneiform Tablets. *Journal of Open Archaeology Data* **2022**, *10*, 1-8.
17. Bogacz, B.; Mara, H. Digital Assyriology—Advances in Visual Cuneiform Analysis. *Journal on Computing and Cultural Heritage* (JOCCH) **2022**, *15(2)*, 1-22.
18. Rey-López, M., Vilas, A., Díaz Redondo, R. A Model for Personalized Learning Through IDTV. In Proceedings of *Adaptive Hypermedia and Adaptive Web-Based Systems*. Dublin, Ireland, 21-23 June 2006.
19. Mara, H. HeiCuBeDa Hilprecht - Heidelberg Cuneiform Benchmark Dataset for the Hilprecht Collection. *IWR Computer Graphics* **2019**, *2*,
20. H. Mara, Bogacz, B. Breaking the Code on Broken Tablets: The Learning Challenge for Annotated Cuneiform Script in Normalized 2D and 3D Datasets. In Proceedings of *International Conference on Document Analysis and Recognition.* Sydney, Australia, 20-25 September 2019.
21. Taylor, J.H. Tablets as Artefacts, Scribes as Artisans. In *The Oxford Handbook of Cuneiform Culture*; Radner, K., Robson, E., Eds.; Oxford University Press: Oxford, United Kingdom, 2012; 4-31.
22. Charpin, D. *Reading and Writing in Babylon*. Harvard University Press: Cambridge, United Kingdom, 2010; 75.
23. Streck, M.P. Großes Fach Altorientalistik. Der Umfang des keilschriftlichen Textkorpus. In *Altorientalistik im 21. Jahrhundert: Selbstverständnis, Herausforderungen, Ziele,* Mitteilungen der Deutschen Orient-Gesellschaft 142; Hilgert, M., Ed.; Druckerei Benedict Press: Schwarzach am Main, Germany, 2010; 35-58.
24. Walker, C.B.F. *Cuneiform*. British Museum: London, United Kingdom, 1987; 40.
25. Langdon, S.H. The Sumerian expression 'si-ni-tum' capital, balance carried forward. *Babyloniaca* **1912**, *6*, 41-53.
26. Grégoire, J.-P. *Contribution à l'Histoire Sociale, Économique, Politique et Culturelle du Proche-Orient Ancien. Archives Ad'istratives et Inscriptions Cunéiformes de l'Ashmolean Museum et de la Bodleian Collection d'Oxford (AAICAB). I*. Les Sources: Paris, France, 1996.

27. Reade, J.E. The manufacture, evaluation and conservation of clay tablets inscribed in cuneiform: traditional problems and solutions. *Iraq* **2017**, *79*, 163-202.
28. Owen, D.I. *The John Frederick Lewis collection*. Multigrafica: Rome, Italy, 1975; pp. 14, 32 fn. 21.
29. Vandecasteele, *C.* Deposition of Ammonium chloride on Cuneiform Tablets. In *Subartu II, Ad'istrative Documents from Tell Beydar (Seasons 1993-1995)*; Ismail, F., Sallaberger, W., Talon, P., Van Lerberghe, K., Lebeau, M., Eds.; Brepols: Turhout, Belgium, 1997, 193-194.
30. Vandecasteele, C.; Van Gool, L.; Van Lerberghe, K.; Van Rompay, J.; Wambacq, P. Digitising Cuneiform Tablets. In *Images and Artefacts of the Ancient World*; Bowman, A.K., Brady, M., Eds.; British Academy: London, United Kingdom, 2005, 31-34.
31. Wambacq, P.; Mariën, D. Enhancement of the Quality of Photographs of Tablets Using Digital Techniques. In *Subartu II, Ad'istrative Documents from Tell Beydar (Seasons 1993-1995)*; Ismail, F., Sallaberger, W., Talon, P., Van Lerberghe, K., Lebeau, M., Eds.; Brepols: Turhout, Belgium, 1997, 195-198.
32. CDLI: wiki. Available online: https://cdli.ox.ac.uk/wiki/doku.php?id=start (accessed on 08 August 2022).
33. Malzbender, T.; Gelb, D.; Wolters, H.; Zuckerman, B. Enhancement of Shape Perception by Surface Reflectance Transformation. *Hewlett-Packard Laboratories Technical Report* **2000**, 38, 1-3.
34. Malzbender, T.; Gelb, D.; Wolters, H. Polynomial texture maps. In Proceedings of the 28th Annual Conference on Computer Graphics and Interactive Techniques - SIGGRAPH 2001, Los Angeles, California, United States, 12-17 August 2001.
35. Mudge, M.; Malzbender, T.; Schroer, C.; Lum, M. New Reflection Transformation Imaging Methods for Rock Art and Multiple-Viewpoint Display. In *Proceedings of the 7th International Symposium on Virtual Reality, Archaeology and Cultural Heritage - VAST2006*, Nicosia, Cyprus, 30 October - 4 November 2006.
36. Luxman, R.; Castro, Y.E.; Chatoux, H.; Nurit, M.; Siatou, A.; Le Goïc, G.; Brambilla, L.; Degrigny, C.; Marzani, F.; Mansouri, A. LightBot: A Multi-Light Position Robotic Acquisition System for Adaptive Capturing of Cultural Heritage Surfaces. *Journal of Imaging* **2022**, *8(5)*, 134, 1-11.
37. Hameeuw, H.; Willems, G. New visualization techniques for cuneiform texts and sealings. *Akkadica* **2011**, 132(2), 163-178.
38. George, A.R. *The Babylonian Gilgamesh Epic: Introduction, Critical Edition and Cuneiform Texts*. Oxford University Press: Oxford, United Kingdom, 2003, 272-273.
39. Atsushi, K.; Sueyasu, H.; Funayama, Y.; Maekawa, T. System for reconstruction of three-dimensional micro-objects from multiple photographic images. *Computer-Aided Design* **2011**, *43(8)*, 1045-1055.
40. Esmaeili, F.; Ebadi, H. Handy Microscopic Close-Range Videogrammetry. *The International Archives of the Photogrammetry, Remote Sensing and Spatial Information Sciences* **2017**, *XLII-4-W4*, 65-67.
41. Dino-Lite RK-06A stand technical data sheet. Available online: https://www.distrelec.it/Web/Downloads/s3/6b/RK-06A_eng_tds.pdf (accessed on 12 June 2022).
42. Sapirstein, P. A high-precision photogrammetric recording system for small artifacts. *Journal of Cultural Heritage* **2018**, *31*, pp. 33-45.
43. Luhmann, T.; Robson, S.; Kyle, S.; Harley, I.; *Close Range Photogrammetry. Principles, techniques and applications*. Whittles Publishing: Dunbeath, Scotland, United Kingdom, 443.
44. Digital Microscope. Available online: https://www.academia.edu/42195781/Digital_Microscope (accessed on 12 June 2022).

45. Peipe, J.; Tecklenburg, W. Photogrammetric Camera Calibration Software - A Comparison. *The International Archives of the Photogrammetry, Remote Sensing and Spatial Information Sciences* **2006**, *XXXVI-5*, 1255-1258.
46. What Does 30,000:1 Magnification Really Mean? Available online: leica-microsystems.com/science-lab/what-does-300001-magnification-really-mean/ (accessed on 11 October 2022).
47. Traditional vs digital microscope magnification. Available online : dinolite.us/support/how-does-magnification-differ-between-traditional-and-digital-microscopes/ (accessed on 11 October 2022).
48. The Dino-Lite Premier AM7013MZT. Available online : https://www.dino-lite.com/products_detail.php?index_m1_id=9&index_m2_id=0&index_id=48 (accessed on 12 June 2022).
49. Lens Calibration (using chessboard pattern) in Metashape. Available online : https://agisoft.freshdesk.com/support/solutions/articles/31000160059-lens-calibration-using-chessboard-pattern-in-metashape (accessed on 13 June 2022).
50. A CMOS Sensor Size Comparison and Format Type. Available online: https://commonlands.com/blogs/technical/cmos-sensor-size (accessed on 15 July 2022).
51. Agisoft Metashape User Manual. Available online: https://www.agisoft.com/pdf/metashape-pro_1_8_en.pdf (accessed on 15 July 2022).
52. Lavecchia, F.; Guerra, M.G.; Galantucci, L.M. Performance verification of a photogrammetric scanning system for micro-parts using a three-dimensional artifact: adjustment and calibration. *The International Journal of Advanced Manufacturing Technology* **2018**, *96*, 4267-4279.
53. Clini, P.; Frapiccini, N.; Mengoni, M.; Nespeca, R.; Ruggeri, L. SFM Technique and Focus Stacking for Digital Documentation of Archaeological Artifacts. *The International Archives of the Photogrammetry, Remote Sensing and Spatial Information Sciences* **2016**, *XLI-B5*, 229-236.
54. Westoby, M.J.; Brasington, J.; Glasser, N.F.; Hambrey, M.J.; Reynolds, J.M. 'Structure-from-Motion' photogrammetry: A low-cost, effective tool for geoscience applications. *Geomorphology* **2012**, *179*, 300-314.
55. Kontogianni, G.; Chliverou, R.; Koutsoudis, A.; Pavlidis, G.; Georgopoulos, A. Enhancing Close-Up image-based 3D Digitisation with Focus Stacking. *The International Archives of the Photogrammetry, Remote Sensing and Spatial Information Sciences* **2017**, *XLII-2-W5*, 421-425.
56. Plisson, H.; Zotkina, L.V. From 2D to 3D at macro- and microscopic scale in rock art studies. *Digital Applications in Archaeology and Cultural Heritage* **2015**, *2*, 102-119.

In *Heritage* **2022**, *5(4), 3133-3164,* an Open Access Journal edited by MDPI.
https://doi.org/10.3390/heritage5040162


0
0.5
1 mm

Chapter 7
Geometrical feature identification of cuneiform signs on micro survey reconstruction

Abstract: According to the increasing possibilities offered by technological innovation, new ways of visualizing and exploring data are now accessible in the context of 3D digital documentation. Surveying small artifacts and accurately representing their geometry, however, remains challenging. It can be ascribed to the still high cost of the most popular equipment for that purpose (active sensors) as well as the requirement for professional expertise when employing less expensive methods (passive sensors). This project aims to provide a low-cost configuration for an image-based approach to the demand for a digital survey and 3D representation of sub-millimeter morphological features. A portable USB microscope was used as equipment. The subject of the experiments is a cuneiform tablet belonging to the collection of Ghent University (Belgium) and datable to the end of the third millennium B.C. More specifically, the study seeks to examine the geometry of the wedge-shaped impressions on the artefacts. Going beyond the traditional practices of text analysis, an accurate representation of the cuneiform signs can be helpful for researchers in conducting comparative geometric studies. This goal can be enriched by recognizing from the analysis the type of stylus used to validate a manufacturing identity and the chronological classification. It is desirable that the data collected can then be shared, on the one hand, by enabling descriptive assessments even between different collections around the world and, on the other hand, by improving the promotion and interaction with the contents of a future exhibition.

Keywords: Cuneiform Tablet, Geometric Feature, Detail Scale, USB Microscope, Digital Legacy.

1. Introduction

Although digital documentation techniques are well-defined for architectural sizes, small-scale items provide a complex challenge owing to the level of detail and accuracy required. Only some research fields specialized in high-precision metrological applications, such as

mechanical and medical [1], are nowadays achieving highly performing results [2] in the three-dimensional reconstruction of very small objects, usually under 5 cm and with sub-millimetric characteristics. Unfortunately, due to the prices, generally high, of hardware and software as well as the level of expertise expected by operators [3], these techniques for very accurate micrometric surveys usually are out of the price range of the majority of museums and cultural organizations[1]. As a result, the current market's need for affordable and effective solutions drives attention toward less expensive alternatives, such as image-based technologies for accurately digitizing even the smallest artefacts.

Without the support of mechanical automation, photogrammetric solutions could be repetitive and time-consuming [4]. In addition, photogrammetry still requires in-depth knowledge of photography along with issues specific to macro photography, most notably the narrow depth of field. Although there is a benefit to digital micro surveying procedures based on passive sensors: they are flexible and open to novel technology experimentations and applications. Therefore, based on previous experiments conducted by the authors [5,6], an attempt was made to implement the photogrammetric acquisition workflow by employing the images obtained with Dino-Lite USB digital microscopes as a data set for photogrammetric processing. The results have shown a non-negligible potential for modelling small objects, especially when compared to much more expensive instruments, highlighting greater flexibility due to the small size and weight of the hardware and its ease of use due to simplified photo controls. It consequently appeared promising to incorporate these tools into a structured photogrammetric workflow, keeping in mind that their principal disadvantage is that they were not initially intended for photogrammetric applications.

The authors chose a highly complex case study, i.e., a cuneiform tablet (LW21.CUN.126) ascribable to the Third Dynasty of Ur (2112-2004 B.C.), coming from ancient Mesopotamia (modern Iraq), and nowadays belonging to the collection of Ghent University (Belgium) (Figure 1). Cuneiform tablets are among the oldest written artifacts of humankind (the very first exemplars date back to 3300 B.C.). Ancient scribes realized the tablets in clay and conveyed information on them by

impressing with a stylus wedge-shaped signs, giving rise to the so-called cuneiform script, a writing system that lasted for more than three millennia. The current study focuses on tablet LW21.CUN.126 but intends to establish a standard methodology repeatable for this type of artefact, capable of satisfying the aims and requirements of the related assyrological research. In this direction, a low-cost setup based on a USB microscope and customized for macro-photogrammetric acquisitions (Figure 2 and deep descriptions in section 2) is used for the cuneiform tablet digitalization.

Special requirements that limit common problems associated with an uneven form, degradation from environmental causes, low-contrast areas, and discoloration are needed to ensure acceptable readability of every portion of the artefact despite the high reproduction ratio. After fully reconstructing the individual tablet geometry, the focus was directed on studying some particularly significant wedges engraved on them, using higher magnifications of the digital microscope. Indeed, the three-dimensional modelling of the single wedge geometry makes it possible to identify certain characteristic features for defining the specific shape of the signs.

The objective is to generate a digital replica that is always consultable, 3D explorable and geometrically accurate. The possible applications of the digital reconstructions of the cuneiform tablet are truly manifold.

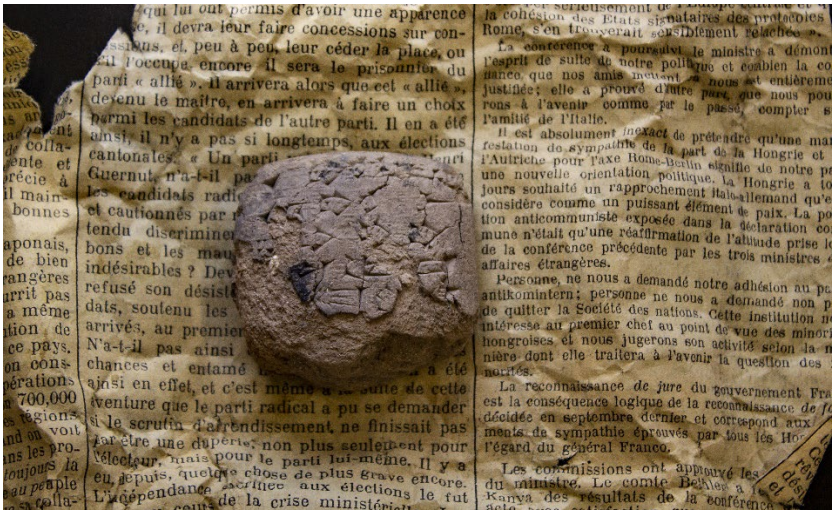

Figure 1. Clay cuneiform tablet LW21.CUN.126, recto.

Figure 2. A turntable- and clamp-based acquisition system with ring illumination that supports integrated LED lighting of microscope. The USB microscope is fixed on a plastic micro-phone holder customized to be set to a plate with flexible hooks.

Digital visualization aims to provide experts with a way to read tablets without actually holding one in their hands, enabling virtual manipulation of these delicate artefacts and offering additional details on artefacts that conventional documentary methods did not allow [7]. Furthermore, digital models can be used to experiment with machine learning and artificial intelligence applications for the automatic recognition of characters and wedges imprinted on the clay [8,9]. In addition, a precise digital model facilitates communication for further examination and comparison, enabling interdisciplinary research among various experts. For example, the creation of digital libraries also would provide a unique opportunity for the multitude of artefacts buried in museum warehouses or simply un-published for some reason. A potential installation, distribution, and promotion of 3D models of cuneiform tablets would be of significant interest and facilitate the display and exhibition of these artefacts, particularly remotely in the form of virtual museums.

It is intended to implement virtual communication with the public and the visualization of archaeological artefacts, which are among the main objectives of several European projects that have been launched in recent years in the field of cultural heritage management [10].

Finally, from a broader perspective, the representations carried out in this study can be an inspiration for exhibition designers and artists who

work with scales of detail and who, for an investment of a few hundred euros, can capture, show, share and promote details of their works that would be difficult to observe with the naked eye.

2. Materials and methods

USB digital microscopes were initially developed for inspection, documentation, and digital metrology analysis. They are already widely used in the medical field and in the manufacturing industry for quality control. Nevertheless, employing these instruments for the photogrammetric surveys makes it possible to obtain 3D models even a tenth of a millimeter in precision [11]. In fact, due to their tiny size and form, they can tilt, allowing pictures to be taken with the proper intersection angles to the object for the creation of three-dimensional models by established SfM processes. These instruments can be considered optical inspection devices [12] that are made to obtain an image and display it on a screen, optionally using specialized software. The USB microscope used for this research activity is the Dino-Lite AM7013MZT model, characterized by a 5.0 MP CMOS sensor (2592×1944 pixel). The following Table 1 summarizes the technical specifications of the employed microscope in the function of the declared magnification achievable [13].

Table 1. Working Distance (WD), Field Of View (FOV) dimensions related to the Magnification rate (M) expressed in millimetres for Dino-Lite AM7013MZT.

M	WD	X_{FOV}	Y_{FOV}
20	48.7	19.8	14.9
30	21.7	13.2	9.9
40	9.0	9.9	7.4
50	1.9	7.9	5.9
60	-2.3	6.6	5.0
220	-0.1	1.8	1.4
230	1.0	1.7	1.3
240	2.1	1.7	1.2

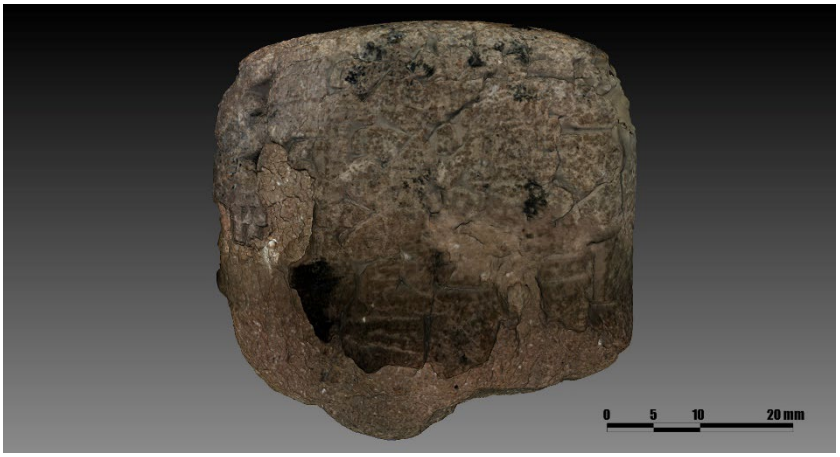

Figure 3. Clay cuneiform tablet LW21.CUN.126, recto of the texturized digital model.

Digital magnification[2] values of 20× were used for reconstructing the entire geometry of the tablets Figure 3). In contrast, values of 40× were used for individual wedges. The relative spatial resolution in order to quantify the less visible details, i.e., Ground Sampling Distance (GSD), measures respectively 7.64 μm/px and 3.82 μm/px. Before beginning the photogrammetric image processing, the first estimation of the interior orientation parameters is supplied (data configured based on the calibration results), because this information cannot be automatically inferred from the EXIF, as metadata are not present in the raster data file for these microscopes.

Due to the minimal Field of View, the requirement to incorporate metric references or calibrated items in the scene to scale the model is one of the key issues at high magnification. Even after overcoming this obstacle, it is still challenging to build a calibration pattern appropriate for the size of the measured item [14]. The problem was overcome by designing an adhesive pattern of coded targets introduced into the scene, ensuring it was fixed on a flat rigid support and could be correctly focused. Each target pattern has a diameter proportional to the area framed related to a chosen magnification so that it can be photographed in several contiguous images and subsequently automatically recognized by the photogrammetric software. Optimized camera calibration is achieved by using the pattern as a grid of constraint points (GCPs) spread uniformly over the framed region. In order to avoid invalidating the process with

unquantifiable uncertainties associated with the pattern printing process, the operator might import the coordinates of each target into the photogrammetric project just to scale the model.

The problem of the shallow Depth of Field was addressed by focusing the object on different planes, similar to the well-known manual Focus Stacking technique [15]. The dense point cloud generated by SFM is subjected to the following specific criteria filtering of the sparse cloud points noise generated by the blurred areas: (i) Re-construction uncertainty; (ii) Reprojection error; (iii) Projection accuracy.

The microscope incorporates an integrated adjustable polarizer to lessen reflections at very close-range acquisition distances.

However, installing an illumination ring [16] has improved the lighting condition at the image borders, avoiding the typical light decrease at the edges of the frame.

In order to orient the object knife-edge relative to the microscope camera, the acquisition geometry included a screw clamp frequently used in model-making. The clamp is mounted on a rotating base, taking care to align the center of rotation with the mounting axis of the object. Despite the limited Depth of Field, this arrangement enables adequate sharpness of the tablet surface and the markers, as well as simultaneous capturing of the tablet front and back.

With this configuration, an average of 1.000 photos are taken per tablet to acquire the whole volume, taking about two hours for each artefact. Data processing took an average of 3-4 hours, often motivated by the tablet's very homogeneous texture, which makes recognizing homologous points between images more difficult. Acquiring the individual wedges was a much faster operation, considering 10-15 shots per wedge and a processing time of 10 min for each.

At the end of the acquisition campaign, both complete and detailed models for each tablet are obtained.

3. Experimental results and discussion

The model of the entire tablet volume was entirely reconstructed with high definition (Figure 4), i.e., a GSD equal to 0.0076 mm/px. The resulting mesh can be oriented and zoomed as well as subjected to grazing lighting to highlight the wedges in a more contrasted manner.

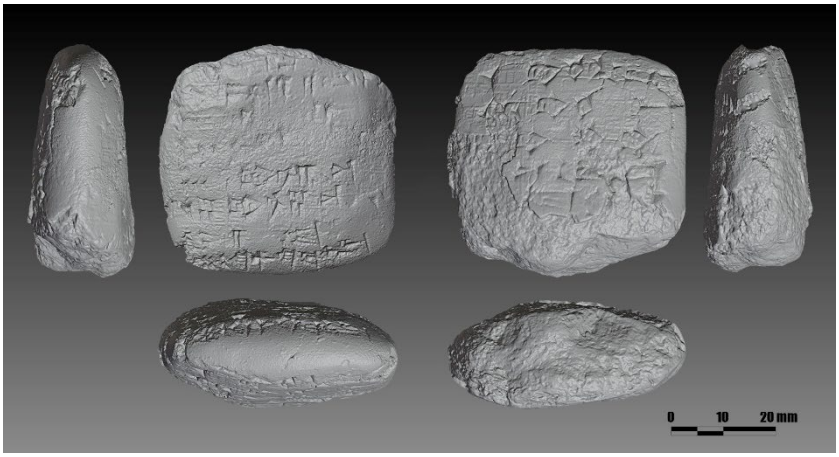

Figure 4. Clay cuneiform tablet LW21.CUN.126, digital model mesh surface.

In order to extract key features for the single imprints of the stylus, the wedge was considered to be formed by the union of three triangular surfaces sharing a vertex, generating three impluvium (grooves) that match the stylus footprint (Figure 5).

Two approaches were followed for the identification of the geometrical features: the first involved identifying the faces of the wedge by employing a plane that maps the mesh surface; the second involved identifying the edges of the wedge imprint by automatic contour recognition of the mesh ridges.

Concerning the first approach, the triangular mesh of the area over which each wedge insists was imported into the Artec Studio 16 software environment. As a first step, a manual selection was necessary in order to define the surface of the wedge of interest only in the larger region imported. A plane is formed for each wedge face by a primitive construction based on a fitting on the polygonal mesh selected. The planes were then imported into the CAD environment for angle measurements between planes (Figure 6). This process was repeated five times for each wedge to strengthen the estimation; the average results are reported in Table 3. It can be observed that mean of the measurements for each angle (α=90°, β=95° and γ=96°) shows that the stylus is characterized by dihedral angles tending to be right angles. The deviation is, on average, 9 degrees. These wedge features are consistent with the shape of the reed stylus proposed by Messerschmidt [17].

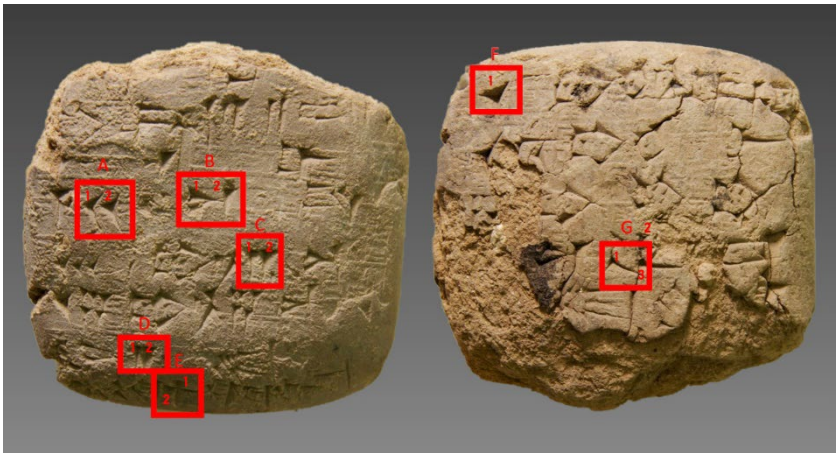

Figure 5. Identification of the wedge locations on the recto (left) and verso (right) of the tablet LW21.CUN.126.

Indeed, reed fibrous impressions can be observed on the left-hand face of the wedges both on the original tablet and on the 3D models.

The second detection method was performed in the Geomagic software environment. After noise reduction filtering, the software automatically allows the recognition and contours of the region of maximum curvature extraction.

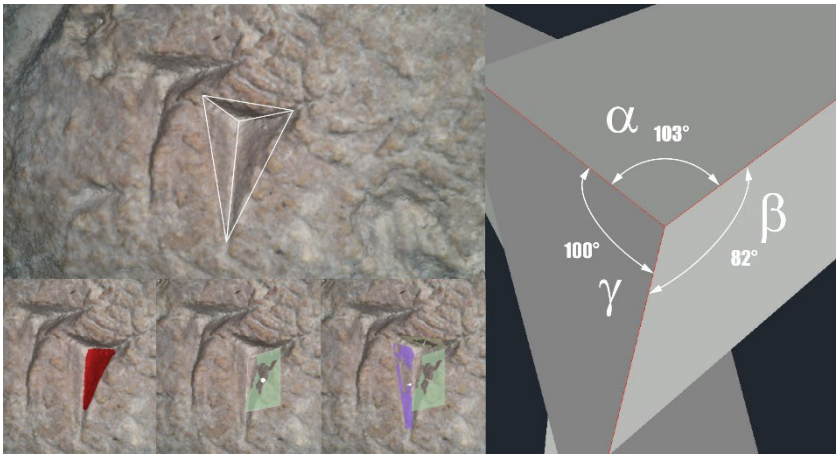

Figure 6. Wedge identification faces selection and planes of the modelling (on the left). Subsequent export for the measurement of dihedral angles (on the right). A2 wedge is represented.

Table 2. The estimated average value of the angles between the wedge planes obtained by Artec Studio 16 fitting algorithm for 14 wedges of tablet LW21.CUN.126.

	α	β	γ
A1	97°	104°	96°
A2	105°	83°	96°
B1	79°	105°	105°
B2	73°	101°	101°
C1	106°	85°	104°
C2	98°	93°	98°
D1	93°	96°	101°
D2	103°	98°	95°
E1	90°	102°	96°
E2	93°	97°	106°
F1	89°	87°	94°
G1	83°	101°	79°
G2	63°	94°	93°
G3	82°	86°	83°

A contour recognition check was performed on the automatic line generation to optimize inconsistencies. Then a model is produced (i.e., a template model) to define the line of the primary wedge geometry. The template is exported as an IGES model and imported into the CAD environment for edge line generation (Figure 7). The observations from this latest analysis show slightly larger angles.

Unfortunately, comparing the two methods does not deliver sufficient consistency in the results. Nevertheless, the former method seems more accurate than the latter because the irregularity of the impluvium does not allow an exact reference for the precise measurement of angles.

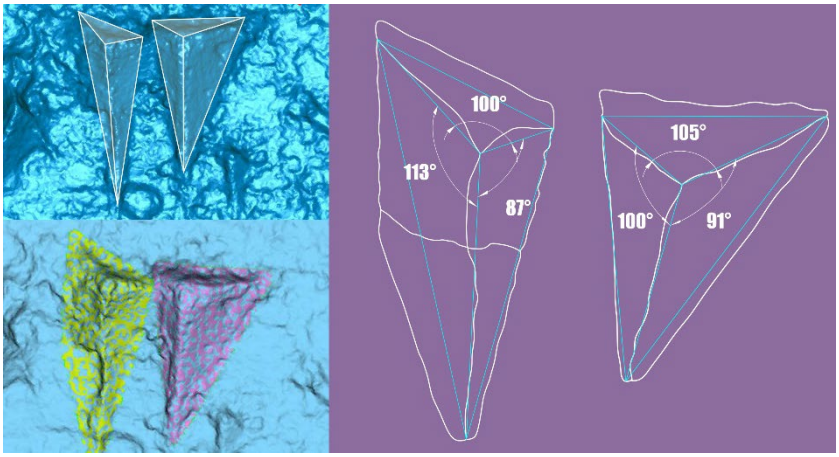

Figure 7. Wedge identification and contour extraction of the main geometry from the mesh model (on the left). Subsequent measurements of dihedral angles (on the right). C1 and C2 wedges are represented.

The limited number of observations and several factors, such as model noise due to instrumental limitations and deformations due to the proximity of other wedges, are among the most uncertainty-generating factors [18].

In addition, possible variations of the stylus writing trajectory [19] can lead to a wedge with angles that do not correspond to those of the stylus, with non-negligible geometric consequences between wedge and wedge that further complicate the re-construction and recognition of a given stylus. These variables will be taken into account for future analyses, which will include a larger sample, different tablets, and other software (e.g., Cuneiform Analyzer) for the extraction and analysis of the cuneiform wedges [20-22].

However, what becomes evident is that contemporary digitizing and computing systems provide the basis for a novel method for studying the cuneiform script, enabling structured investigations and wedge layouts in relation to specific quantities for the development of more accurate paradigms.

4. Conclusions

The study proposes a method for identifying key features on cuneiform tablets from three-dimensional models generated with low-cost USB

microscopes. The aim is both to reconstruct the complete geometry of a complicated micro-engraved object and to propose a classification not only on the legibility of the entire volume but also on the individual signs, possibly including the exact shape of the impression tools used for the wedges. It is shown that the question remains open as to whether the level of accuracy achieved does not allow experts to distinguish the distinctive handwriting of the scribe or the shape of a particular stylus. Anyway, this first approach reveals the need to conduct the survey with more accurate instrumentation for wedge analysis and a comparison between different tablets. In this sense, future research will be oriented to analyze a larger sample and extrapolate data with smaller uncertainties.

An expeditious approach nevertheless proves satisfactory for a reconstruction of the general geometry of the tablets and a formulation of an applicative methodology. An aim that starts from archaeological necessity, but which has repercussions on the artistic value of these artefacts and emphasizes their complexity, making their representation clearer and more attractive to an audience not only of technicians. Presenting artefacts to the public through the display of three-dimensional models is a challenge for many.

However, improving the documentation of artefacts preserved and displayed to visitors is possible even for complex objects. Digitalization constitutes the prerequisite for Virtual Reality and Augmented Reality applications, video animations, games and generally all activities that benefit from the digital reproduction of detailed artifact for both technical and artistic filed.

Notes

1. The most expensive systems, direct competitors of micro-photogrammetry nowadays, are structured light scanners. Among the best-performing ones currently available on the market, there are desktop scanners that achieve accuracies of 0.01 mm, resolution down to 0.03 mm, color acquisition, and marker-less registration. The cost is around €30,000 (e.g., artec3d.com/it/portable-3d-scanners/artec-micro). Whereas with slightly lower performance, the average cost can be around €10,000 (e.g., einscan.com/handheld-3d-scanner/einscan-pro-hd/). However, one also comes across low-cost scanners, i.e., from €500, which are naturally designed for non-professional applications, with correspondingly much lower accuracy and resolution and mostly for educational and/or amateur use, and which do not perform well enough for micro-metrological applications (e.g., it.shop.revopoint3d).

2. It is noteworthy to point out that the reported magnification for Dino-Lite USB microscopes includes digital magnification forms. As the manufacturer advises, it is frequently more beneficial to compare the field of view in this instance rather than the magnification, that is, to compare the actual dimensions of the original object being enlarged to the final size of the object on the display.

References

1. Gallo, A., Muzzupappa, M., Bruno, F. 3D reconstruction of small sized objects from a sequence of multi-focused images. *Journal of Cultural Heritage* **2014**, *15(2)*, 173-182.
2. Hansen. H.N., Carneiro, K., Haitjemac, H., De Chiffrea, L. Dimensional Micro and Nano Metrology. *CIRP Annals* **2006**, *55(2)*, 721-743.
3. Caine, M., Magen, M. Low-Cost Heritage Imaging Techniques Compared. In Proceedings of *EVA-Electronic Visualisation and the Arts*; BCS Learning and Development Ltd.: London, United Kingdom, 11-13 July 2017, pp. 430-743.
4. Collins, T., Woolley, S.I. Gehlken, E. Ch'ng, E. Automated Low-Cost Photogrammetric Acquisition of 3D Models from Small Form-Factor Artefacts. *Electronics* **2019**, *8(12)*, 1441-1458.
5. Antinozzi, S.; Fiorillo, F. Optimized Configurations for micro-photogrammetric surveying adaptable to macro-optics and digital microscope. *ISPRS International Archives of the Photogrammetry, Remote Sensing and Spatial Information Sciences* **2022**, *XLVI-2/W1-2022*, 25–32.
6. Antinozzi, S., Fiorillo, F., Surdi, M. Cuneiform tablets micro-surveying in an optimized photogrammetric configuration. *Heritage* **2022**, *5(4),* 3133-3164.
7. Cohen J., Duncan, D., Snyder, D., Cooper, J., Kumar, S., Hahn, D., Chen, Y., Purnomo, B., Graettinger, J. iClay: Digitizing Cuneiform. In Proceedings of *The 5th International Symposium on Virtual Reality, Archaeology and Cultural Heritage - VAST*; Y. Chrysanthou, K. Cain, N. Silberman, F. Niccolucci (Eds); The Eurographics Association: Eindhoven, Netherlands, 6-10 December 2004, pp. 135-14.
8. Bogacz B., Mara H. Digital Assyriology—Advances in Visual Cuneiform Analysis. *J. Comput. Cult. Herit.* **2022**, *15*, 1-22.
9. Homburg T., Zwick R, Mara H., Bruhn K.-C. Annotated 3D-Models of Cuneiform Tablets. *J. Open Archaeol. Data* **2022**, *10*, 1-8.
10. Official website of the European Union. Available online: https://culture.ec.europa.eu/it/cultural-heritage/cultural-heritage-in-eu-policies/european-digital-heritage
11. Esmaeli, F., Ebadi, H. Handy microscopic close-range videogrammetry. *ISPRS - International Archives of the Photogrammetry, Remote Sensing and Spatial Information Sciences* **2017**, *XLII-4/W4*, 65-67.
12. Mokobi, F. Digital Microscope. Available online: https://www.academia.edu/42195781/Digital_Microscope
13. Dino-Lite Products. Available online : https://www.dino-lite.eu/it/component/eshop/am7013mzt?Itemid=0
14. Lavecchia, F., Guerra, M.G., Galatucci, L.M. Performance verification of a photogrammetric scanning system. *The International Journal of Advanced Manufacturing Technology* **2018**, *96(9)*, 4267-4279.
15. Clini, P., Frapiccini, N., Mengoni, M., Nespeca, R., Ruggeri, L. SfM technique and focus stacking for digital documentation of archaeological artifacts. *ISPRS - International*

Archives of the Photogrammetry, Remote Sensing and Spatial Information Sciences **2016**, XLI-B5, 229-236.
16. Antinozzi, S., Fiorillo, F. Optimized configurations for micro-photogrammetric surveying adaptable to macro-optics and digital microscope. *ISPRS International Archives of the Photogrammetry, Remote Sensing and Spatial Information Sciences* **2022**, *XLVI-2/W1*, 25-32.
17. Messerschmidt, L. Zur Technik des Tontafel-Schreibens. *Orientalistische Literaturzeitung* **1906**, *9*, 185-380.
18. Richardson, A., Smilansky, U. Geometrical Feature Extraction for Cuneiforms. In Proceedings of *ECAI 2014 - 21st European Conference on Artificial Intelligence*; T. Schaub et al. (Eds); IOS Press: Amsterdam, Netherlands, 18-22 August 2014, pp. 1173-1178.
19. Cammarosano, M. The Cuneiform Stylus. *Mesopotamia* **2014**, *XLIX*, 53-90.
20. Fisseler, D., Weichert, F., Müller, G. G.W., Cammarosano, M. Towards an interactive and automated script feature Analysis of 3D scanned cuneiform tablets. *Scientific Computing and Cultural Heritage* **2013**, 1-10.
21. Cammarosano, M., Müller, G. G.W., Fisseler, D., Weichert, F. Schriftmetrologie des Keils: Dreidimensionale Analyse von Keileindrücken und Handschriften. *Die Welt des Orients* **2014**, 2-36.
22. Cuneiform Analyser. Available online: http://www.cuneiform.de.

In *11th EAI International Conference: ArtsIT, Interactivity & Game Creation - Special Track on Dialogues between Geometry, Computer Graphics and the Visual Arts, Faro, Portugal, 21-22 November 2022.*

in press: https://link.springer.com/conference/artsit


0 0.5 1 mm

Capitolo 8
3D Digital tools for the archaeological massive artifacts' documentation

Abstract: This study focuses on 3D acquisition and documentation procedures, innovating and implementing traditional survey methods to promote and increase the efficacy of the historical and archaeological heritage fruition. Especially within museum itineraries, modern digital technologies, if consistently applied, can promote a better interpretative reading, implementing the knowledge of scholars. Moreover, in coherence with the Horizon Europe "Cultural Heritage" area of intervention, for a new future inextricably linked to the history of Cultural Heritage, it is essential to experiment approaches that favour innovative mechanisms of fruition and promotion of works of art, based on the idea that the user is an active part of the experiential path. The study presents some acquisition experiences on different archaeological artifacts collected at the National Archaeological Museum of Crotone, applying integrated technologies and defining a rigorous methodological process of analysis and control.

Keywords: CH survey, Digital heritage, Semantic description, 3D modelling, Texture correction.

1. Introduction

In recent years, the Cultural Heritage (CH) field has experienced a rapid increase in the use of new technologies for more fluid and advanced knowledge, supporting, often, the creation of a heterogeneous integrated database, accessible to scholars and visitors, sharable and, implementable over time [1]. In this process, non-invasive technologies for the generation of digital heritage models have produced an exponential quality growth of the acquired data [2]. However, there are still several issues in identifying a single approach that meets high levels of accuracy at the morphological, topological and texture mapping levels. This is even more relevant when interfacing with museum collections, for which an operational strategy has to be identified in order to optimize the process, often in a not ideal environment [3].

Photogrammetry is one of the most portable, effective and flexible tool, guaranteeing efficient workflows also under difficult conditions [4] or in presence of objects with special material characteristics.
Nevertheless, in relation to the object, the photogrammetric acquisition and processing times could be quite long and, in same case, as for small objects with complex surfaces and sub-millimetre morphological characteristics, a high level of expertise and experience is required [5]. Indeed, the operational challenges are compounded by increasing difficulties as the scale of application is reduced [6].
Another significant contribution to the generation of increasingly metrically correct models has come from the great development of handheld structured light scanners [7]. These techniques provide rapid data acquisitions, a non-contact process, and ensure precise and accurate measurements, returning scaled digital 3D object copies. However, generally these scanners are specifically designed to capture a precise size range of the object and have a defined depth range in which to operate. In addition, as known, they are also quite influenced by the surface optical features of objects [8] and often have cameras with limited resolution, influencing the result of the final texture. As can be inferred, therefore, in case of reduced timeframes and high-performance demands, a fair compromise between different acquisition equipment should be found.

Figure 1. Finds from the National Archaeological Museum of Crotone: (i) The strater; (ii) The stele; (iii) The sculpture; (iv) The figurative relief.

Then, once the data has been obtained, it is necessary to work on the weak acquisition points, according to the mesh management and texture mapping process.

The study presents an operational pipeline that outlines the relevance and challenges of the acquisition phase and discusses how to implement and optimize digital data for obtaining complex and semantic 3D models with high information density.

The process has been tested on heterogeneous finds preserved in the National Archaeological Museum of Crotone (Figure 1), each characterized by its own dimension, shape and material:

(i) the silver strater from the mint of Crotone (about 400-350 BC), showing on the recto the head of Hera Lakinia with diadem and on the verso Heracles seated on a rock with a bow, holding a cup in his right hand;

(ii) the stele known as the 'Cippus of Horo on the crocodiles', a charm made of engraved basalt from the Late Egyptian period (378 BC), which has engravings on the front, back and sides, although the façade is composed almost exclusively of bas-reliefs;

(iii) the female terracotta sculpture of a nude figure leaning on a column (first half of the 3rd century BC)

(iv) the figurative relief of a votive character of the end of the 5th century BC, depicting two female divinities in conversation.

Closely linked to the characteristic of the case studies is the choice to use several instruments that differ in type and specifications.

The different parameters taken in consideration are: (i) the size of the object and its surface details, which forces evaluations on the achievable resolution by the instrument; (ii) the shape and the position of the artifact in the museum environment, which leads to specific projects for the acquisition set; (iii) the material and consequently the texture, for which, besides understanding which is the most suitable technology, it is necessary to guarantee coherence and uniformity in lighting; (iv) the available time, which forces to choose, besides the method that guarantees the best results, also the most efficient one in saving time and energy, bearing in mind first of all the final purpose of digitization. Based on these considerations, two parallel approaches were followed, illustrated below.

2. Materials and methods

2.1. Detailed, reflective and dark artifacts: photogrammetric approach

An efficient photogrammetric system for tiny object detection is based on the multi-viewpoint acquisition [9], in which the camera is fixed on a tripod and the object is rotated by a turntable. Starting from this configuration, different sensors were employed to survey two detailed findings (Table 1): (i) a Dino-Lite USB digital microscope for the silver Croton strater; (ii) a full-frame Nikon camera, with a 105 mm macro lens, for the basalt Egyptian stele.

Table 1. Technical specifications of micro and macro photogrammetry instruments used for strater and stele survey.

	Dino-Lite AM7013MZT	**Nikon D800E**
Supply	battery powered	power supply
Magnification Ratio	up to 200:1	up to 1:1
Sensor	CMOS 3.7× 2.6 mm	CMOS 35.9 × 24 mm
Sensor pixel size	$1.4 \cdot 10^{-3}$ mm	$4.8 \cdot 10^{-3}$ mm
Resolution	5 MP	36.3 MP

Digital USB microscopes are portable devices, configured as a webcam with a high-powered macro lens that connects to a computer, showing images directly on the display; they are the most user-friendly and the least expensive [10]. Widely implemented in several fields, these instruments can be used for micro-photogrammetric applications (Figure 2), reaching about 0.1 mm accuracy [11].

Meanwhile, not very high resolution, lack of a wide dynamic range, narrow field of view, and poor depth of field are the weaknesses of this device. The AM7013MZT microscope, in our case, was implemented for the coin survey, working with a total magnification rate of 20×, the focus at distance of 48.7 mm and with a depth of field to 3.6 mm.

The difficulty of carrying out a complete survey with a USB microscope of an object that is small, but not negligible in thickness compared to the coin, led to the use of a more 'conventional' camera for the survey of the stele (Figure 3). In fact, full frame cameras combined with macro lenses

are widely used for micro-photogrammetry [12]. The Nikon D800E SRL camera, equipped with the AF-S VR Micro-Nikkor 105 mm f/2.8G IF-ED, was adopted to achieve high quality and close focusing with limited optical distortion. At a focusing distance of 700 mm, assuming a tabulated circle of confusion value of 0.29 mm, the depth of field is approximately 115 mm. However, each artifact was placed on a turning table, then camera inclination and rotational step angle were chosen in relation to the objects. The survey has been designed with calibrated plates built for both photogrammetric systems: calibration patterns which can be used as a constraint points (GCP) grid for the standard photogrammetric procedure needs. The lighting conditions, based on the polarized light of the microscopes and/or on the artificial lighting of the museum, have been improved with the adoption of a LED illumination ring. As regards the silver Croton strater, two acquisition sets – for the recto and for the verso of the coin, averaging 80 captures each – were required, for a total of about 30 minutes of time. In the case of the stele, however, a single set of about 100 captures was sufficient, for about 20 minutes of work. The datasets obtained were thus processed in a SfM software, Agisoft Metashape, according to the general photogrammetric workflow. The sparse point cloud was checked before proceeding with the reconstruction of the model, removing low-quality TPs via the Gradual Selection filter, a tool by Agisoft Metashape.

Figure 2. Zoom-in view and 3D model with texture mapping applied of the silver Croton strater acquired with Dino-Lite microscope.

Figure 3. Zoom-in view and 3D model with texture mapping applied of the basalt Egyptian stele acquired with Nikon.

2.2. Opaque medium-size artifacts with simple textures: structured light scanner approach

Structured light techniques, in the last years, have benefited from recent advances in digital technology; the necessary hardware is increasingly available as well as better performance of data management software [13]. Such progress, moreover, has made the instruments more practical, easily transportable and, therefore, implementable also in several fields as well as in the CH [14].

In case study, the museum finds were surveyed with the use of two different handheld scanners (Table 2): i) Artec Leo for the figurative relief, ii) Artec Eva for the female terracotta sculpture.

The operating technology of structured light scanners is like stereoscopic vision systems in which depth information are based on the principle of triangulation; however, the instrument, in this case, projects on the surface of the object a particular pattern to ensure greater accuracy in the measurement as well as a higher acquisition speed [15].

Artec Eva is a structured light scanner produced by the Artec 3D and ideal for prompt acquisition of medium-sized objects (Figure 4). Acquisitions were made rotating around the object by setting geometry and texture tracking modes and enabling HD data density with a value of 4× (time required: about 40 minutes). However, with this instrument, the collected data must be monitored in real time on the notebook and

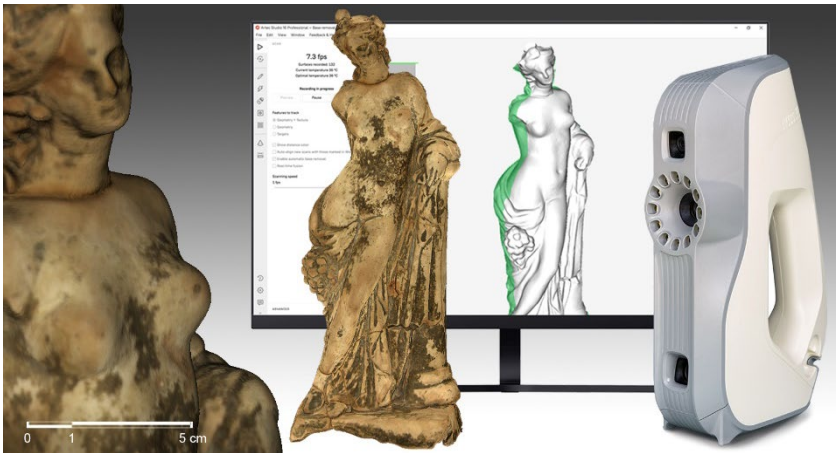

Figure 4. Zoom-in view and 3D model with texture mapping applied of the female terracotta sculpture acquired with Artec Eva scanner.

visualized by the proprietary software with the aim to control any lost tracking. This drawback is overcome with Artec Leo (Figure 5), which is also a portable structured light scanner, but which allows the 3D replica of the object to be displayed directly in real time on its touch panel screen. Therefore, given the larger size and limited space around the figurative relief, this device was used for the survey of the second find. The hardware features, in fact, allow on-board real time processing without notebook support as well as a fast and intuitive workflow.

The acquisitions were carried out with the previous modes; but, due to the improved performance of the Artec Leo, data control and waiting time for registration of scans in HD mode was faster, about 30 minutes.

Table 2. Technical specifications of structured light system instruments used for sculpture and figurative relief survey.

	Artec Eva	**Artec Leo**
Supply	battery powered	power supply
Field of View	214×148-536×371 mm	244×142-838×488 mm
3D Resolution	up to 0.2 mm	up to 0.2 mm
Acquisition speed	18 mln points/s	35 mln points/s
Texture Resolution	1.3 MP	2.3 MP

Figure 5. Zoom-in view and 3D model with texture mapping applied of the figurative relief acquired with Artec Leo scanner.

The software used to manage the data is Artec Studio 15 Professional, a proprietary software, operating according to the typical steps foreseen by the program. Longer acquisition and post-processing times were found mainly with the surveys carried out with Artec Eva.

The scans of the female terracotta sculpture, following the global registration, presented a max error of 0.3; the fusion of the scans was set with a resolution of 0.5 mm of and with the texturization in atlas mode (8192×8192 px). For the model of the figured relief, realized with the Artec Leo, being able to control the quality of the scans already during the acquisition phase, the max error reached was of 0.1, and the final model was obtained setting a resolution of 0.6 mm and an atlas texture of 8192×8192 px.

3. Data Optimization

The set of collected data required a reasoned management process due to the heterogeneity of the information associated with them. Each case study acquired presents different parameters in relation to: density and structure of the processed mesh surfaces; quality of the applied textures; size and complexity of the resulting geometric model.

The methodology used defines a path aimed at the optimization of digital 3D mesh models that have a high quality of both the geometric surface and the applied texture.

As known, in the texture mapping phase the most common problems, due to the often not ideal gripping conditions, are: low texture resolution; gaps and undercuts; photographic inconsistencies (variation of light and reflections) and topological errors due to the formal geometric complexity.

The mesh management and texture mapping process proposed consist of the following steps: mesh parameterization, mesh partitioning, mesh segmentation unwraps, UV map and island projection, UV layout optimization, mesh packing and baking.

The quality of the result ensures effective consultation in the subsequent phases of investigation and an easy fruition to the public.

The procedure follows a reasoned path that elaborates the topological structure of the geometric model, analysing and resolving computational and colour errors, areas the under-squares and gaps, segmenting and reorganizing the collected data according to criteria defined in synergy with the Museum's scholars and experts [16].

4. Results and discussion

Before proceeding, therefore, to mesh segmentation, it was necessary to check the topological errors generated during post-processing.

For each of the 3D models, the following steps were developed: removal of double vertices from the mesh and closure of the seam, and review of the edge connections. Particular attention was paid to the control of the polygonal loading of the surfaces with the aim of not losing the quality of the detail, but at the same time, to ensure easy management on a dedicated digital platform, to support the digitized version of the case studies, adding to the semantic models, through the creation of specific tags: notes, historical information, metric data or comments of scholars and experts.

Since the models will be displayed online on web dissemination platforms, re-meshing and re-topology processes were initiated on the polygonal models. The algorithm employed replaces the original mesh with a new one that preserves some formal characteristics (vertex position and edge geometry). The reconstructed mesh with a reduced number of polygonal faces (low poly) must maintain the geometric-formal structure of the original mesh (high poly).

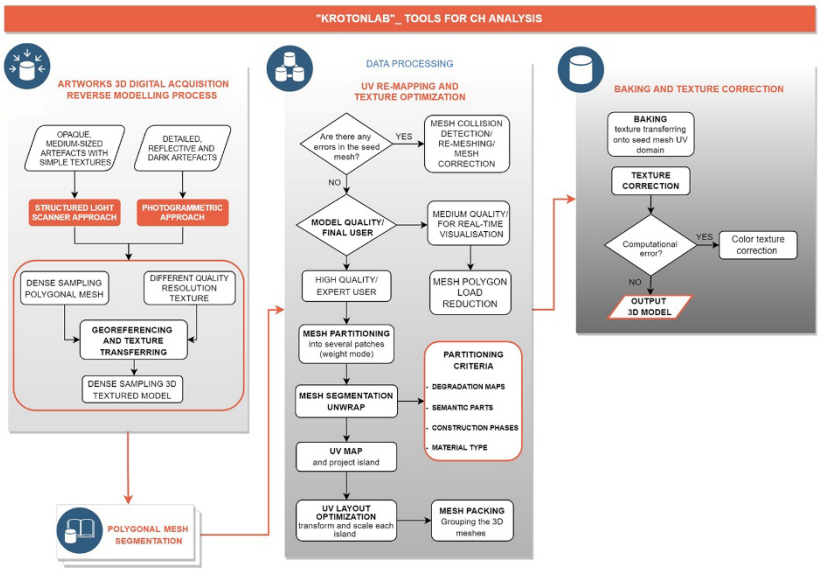

Figure 6. The flowchart for developing high accuracy 3D shape measurement in relation to the object characteristics and to optimize the mesh and texture mapping process.

The pipeline described below can be replicated on a variety of commercially available software.

We preferred to develop the process (Figure 6) within the open source working environment Blender (stable version 2.93 and beta version 3.0). For each artefact, the same methodological procedure was applied allowing, at the end of the process, to obtain 3D models with a good sampling in terms of geometric-formal definition and quality of the applied texture. The goal is to create digital products that meet the requirements of the CH dissemination standards.

The phase involving texture mapping includes multiple preliminary processing, such as mesh partitioning, mesh parameterization, and texture transfer, which are interrelated and affect the result [17].

Newer software technology uses dedicated UV vertex map generation tools to assign the texture to a numerical model with a complex geometric shape. Because the texture is a planar 2D figure, UV vertex maps establish a bidirectional correspondence between the vertices of the 3D polygon mesh and the pixels in the image. The libraries available within Blender software use an automated procedure to create UV maps. The tool is called the "Smart UV Project".

Before assigning texture to the edited surface (Baking), a new material component was created through procedural techniques within Blender's "Node Editor". New information encoded in 2D maps, shaders (Displacement map, Lightmap, Cavity map, etc.) was associated with the component properties. In the final step, after Baking, some areas of interest have been selected with the Texture Painting mode tool and emphasized (by creating masks) editing some parameters such as: saturation, contrast and brightness (Figures 7-10).

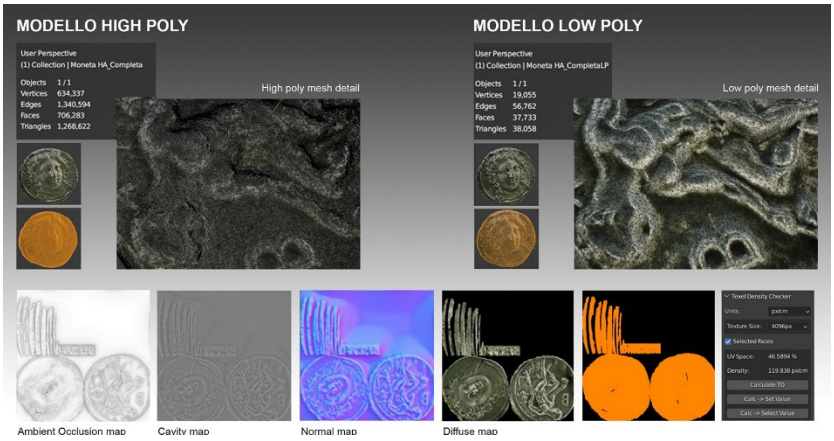

Figure 7. Optimization process of polygonal load and of the UV-Map of the silver Croton strater for online content dissemination.

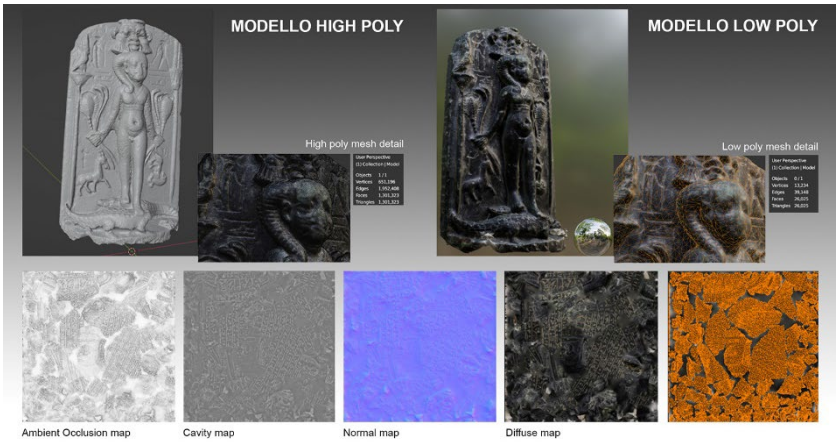

Figure 8. Optimization process of polygonal load and of the UV-Map of the basalt Egyptian stele for online content dissemination.

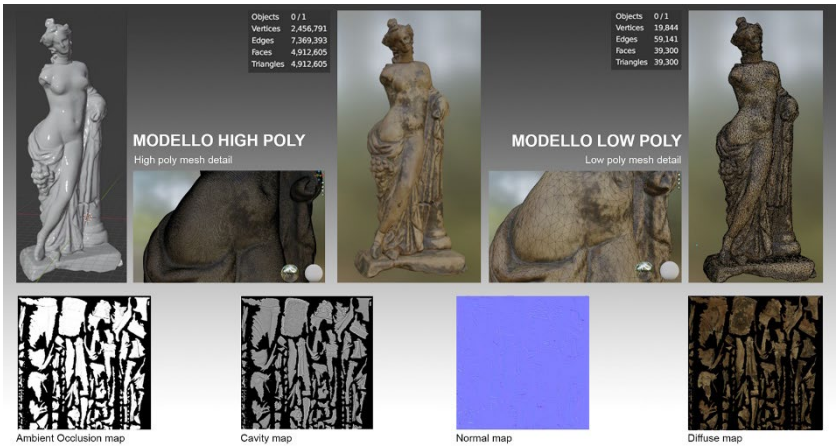

Figure 9. Optimization process of polygonal load and of the UV-Map of the female terracotta sculpture for online content dissemination.

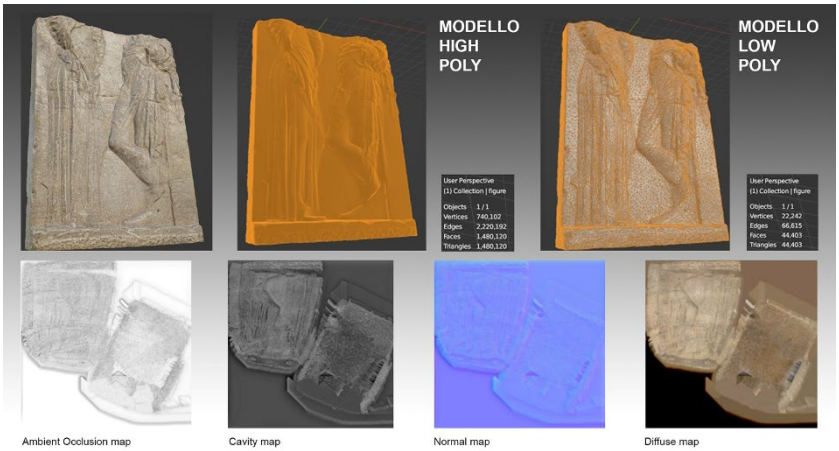

Figure 10. Optimization process of polygonal load and of the UV-Map of the figurative relief for online content dissemination.

The analysis and optimization process applied to the case studies generated digital models with a polygonal loading about 1/100 less than the original one (Blender modifier unsubdivision: collapse vertices). The polygonal mesh density computation was calculated having as target the preservation of the geometric peculiar features of the case studies. Regarding, instead, the surface texture mapping, the original texture was edited trying to maintain the highest possible resolution for the final baking phase.

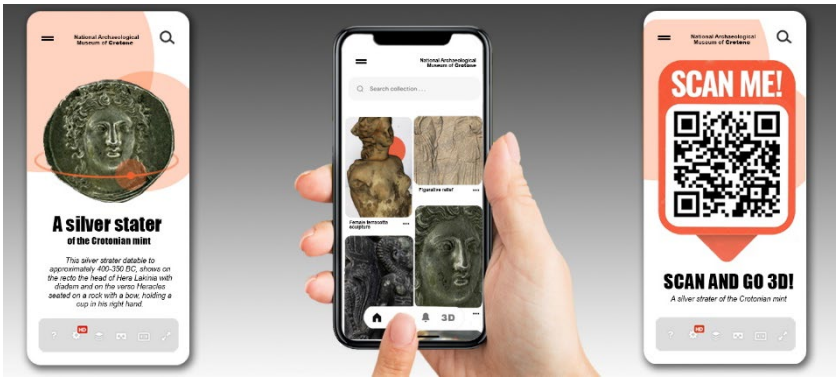

Figure 11. Data acquisition and optimization process results for the digitization of cultural assets and their sharing on digital platform.

Strategically, the analysis workflow has been experimented on different case studies for geometric-formal typologies, for materials and for logistic difficulties of capture.

The results confirm that the methodology can be applied to several heterogeneous contexts with digital results expendable and manageable for other disciplinary studies, without losing the necessary information that distinguishes the artworks analysed.

5. Conclusions

The Horizon Europe "Cultural Heritage" area of intervention is one of the research policies recognized at European level, because it represents an opportunity for the entire multidisciplinary community to develop specific methods that keep in consideration the specificity and complexity of CH. In the field of "Digital Heritage", technological innovation and specific training are able to return meaning and vitality to the CH, through renewed interpretations and according to functional criteria of conservation, diagnosis, restoration and fruition (Figure 11). The study describes the path of data acquisition and elaboration of different historical-archaeological artifacts.

The use of appropriate devices in relation to the object and environmental characteristics and the data optimization will allow the creation of 3D models, digital twins, rich in information and useful for appropriate future restoration interventions. It is a priority to systematize the potentialities of the new digital procedures, to create

platforms of open sharing that really bring to the future generations an added value in terms of knowledge, dissemination of the carried out research results.

References

1. Apollonio F. I., Basilissi V., Callieri M., Dellepiane M., Gaiani M., Ponchio F., Rizzo F., Rubino A. R., Scopigno R., Sobra' G. A 3D-centered information system for the documentation of a complex restoration intervention. In *Journal of Cultural Heritage* **2018**, *29*, 89-99.
2. Inzerillo, L., Di Paola, F., Alogna, Y. High quality texture mapping process aimed at the optimization of 3D structured light models. *The International Archives of the Photogrammetry, Remote Sensing and Spatial Information Science* **2019**, *XLII-2/W9*, 389-396.
3. Plisson, H., Zotkina, L. V. From 2D to 3D at macro- and microscopic scale in rock art studies. *Digital Applications in Archaeology and Cultural Heritage* **2015**, *2*(2-3), 102-119.
4. Nicolae, C., Nocerino, E., Menna, F., Remondino, F. Photogrammetry Applied to Problematic Artefacts. *The International Archives of the Photogrammetry, Remote Sensing and Spatial Information Science* **2014**, *XL-5*, 451-456.
5. Apollonio, F.I., Fantini, F., Garagnani, S., Gaiani, M. A. Photogrammetry-Based Workflow for the Accurate 3D Construction and Visualization of Museums Assets. *Remote Sensing* **2021**, *13(3)*, 486-526.
6. Antinozzi, S., Ronchi, D., Barba, S. Macro and Micro Photogrammetry for the Virtualization of the Orphic Foil (V-IV BC) of National Museum of Vibo Valentia. In Arena A., Arena M., Brandolino R.G., Colistra D., Ginex G., Mediati D., Nucifora S., Raffa P. (eds). *Connecting. Drawing for weaving relationships. Proceedings of the 42nd International Conference of Representation Disciplines Teachers*, Reggio Calabria, Italy, 16-18 September 2021, Franco Angeli: Milan, Italy, pp. 1538-1555.
7. Morena, S., Barba, S., Álvaro-Tordesillas, A. Shining 3D Einscan-Pro, application and validation in the field of Cultural Heritage, from the Chillida-Leku Museum to the Archaeological Museum of Sarno. *The International Archives of the Photogrammetry, Remote Sensing and Spatial Information Sciences* **2019**, *XLII-2/W18*, 135-142.
8. Georgopoulos, A., Ioannidis, C., Valanis, A. Assessing the performance of a structured light scanner. *The International Archives of the Photogrammetry, Remote Sensing and Spatial Information Sciences* **2010**, *XXXVIII-5*, 250-255.
9. Collins, T., Woolley, S.I., Gehlken, E., Ch'ng, E. Automated Low-Cost Photogrammetric Acquisition of 3D Models from Small Form-Factor Artefacts. In *Electronics* **2019**, *8*, 1441-1458.
10. Atsushi, K.; Sueyasu, H.; Funayama, Y.; Maekawa, T. System for reconstruction of three-dimensional micro objects from multiple photographic images. *Computer-Aided Design* **2011**, *43(8)*, 1045-1055.
11. Esmaeili, F., Ebadi, H. Handy Microscopic Close-Range Videogrammetry. The International Archives of the Photogrammetry, Remote Sensing and Spatial Information Sciences **2017**, XLII-4/W4, 65-67.
12. Verdiani, G., Formaglini, P., Giansanti, F., Giraudeau, S. Close-Up, Macro and Micro-photogrammetry and Image Perspective: A Comparative Studio on Different Lenses at Work with Small and Medium Size Objects. *Computer Reviews Journal* **2018**, *2*, 235-248.

13. Zhang S. High-speed 3D shape measurement with structured light methods: A review. *Optics and Lasers in Engineering* **2018**, *106*, 119-131.
14. Limongiello, M., Antinozzi, S., Vecchio, L., Fiorillo, F. Digital survey and reconstruction for enhancing epigraphic readings with erode surface. *Journal of Physics Conference Series, 2204(1)* **2022**, 1-6.
15. Bell, T., Li B., Zhang, S. Structured Light Techniques and Applications. In *Wiley Encyclopaedia of Electrical and Electronics Engineering*, Webster J. G. (Ed); John Wiley & Sons: Hoboken, New Jersey, USA, pp. 1-24.
16. Niang, C., Marinica, C., Markhoff, B., Leboucher, E., Malavergne, O., Bouiller, L., Darrieumerlou, C., Laissus, F. Supporting Semantic Interoperability in Conservation-Restoration Domain: The Parcours Project. *Journal on Computing and Cultural Heritage* **2017**, *10(3)*, 1-20.
17. Lai, J.Y., Wu, T.C., Phothong, W., Wang D.W., Liao C.Y., Lee J.Y. A High-Resolution Texture Mapping Technique for 3D Textured Model. *Applied Sciences* **2018**, *8(11)*, 1-22.
18. Mitchell, H.L., Kniest, H.T. Digital Photogrammetry and Microscope Photographs. In *Photogrammetric Record* **1999**, *16*, 695-704.
19. Valinasab, B., Rukosuyev, M., Lee J., Jun, M.B.G. Atomization-based Spray Coating for Improved 3D Scanning. *Journal of the Korean Society of Manufacturing Technology Engineers* **2015**, *24* (1), 23-30.

In UID, Congress of Unione Italiana per il Disegno, Volume*: Dialoghi. Visioni e visualità. Testimoniare Comunicare Sperimentare*, Genova, Italy, 15-17 September 2022.
https://doi.org/10.3280/oa-832-c148


0
0.5
1cm

Capitolo 9
Methodologies for assessing the quality of 3D models obtained using close-range photogrammetry

Abstract: Although reality-based models are widely used to describe the geometric surfaces of an entity in a digital space, a systematic and universally recognized treatment of issues such as accuracy is lacking. The topic is certainly complex as this analysis should involve not only shape approximation but also other attributes (e.g., colour). Limiting itself to geometry alone, this work proposes solutions for assessing the quality of photogrammetric models, differentiating them according to possible scenarios: sometimes, homologous models obtained using several techniques and technologies are accessible. In these cases, a matching between digital reconstructions can serve to effectively quantify accuracy; more often, no terms of comparison are available, and we are forced to derive indicators from the same photogrammetric process to describe quality. For this last scenario, we suggest a statistical analysis on the covariance matrix of the estimated coordinates for the Tie Points. The main goal is to provide a range of possible approaches to the conscious management of survey data.

Keywords: Tolerance intervals, Coordinate covariance matrix, Hausdorff distance, Accuracy assessment.

1. Introduction

The use of reality-based models, derived from techniques such as laser scanning or photogrammetry, is widely used in fields ranging from heritage documentation to reverse engineering on mechanical components [1, 2]. The need for realism and detail has produced, over time, a continuous increase in the complexity and size of virtual descriptions, challenging the storage, transmission, and processing capacity of hardware. Given these assumptions, it seems clear that the properties of a digital outputs must be calibrated, both in terms of

richness of detail and accuracy, in relation to the specific goals. Despite intensive use of models, whether in the form of point clouds or polygonal meshes [3], there is no agreement on the most appropriate method for defining their quality, and a common criterion for formalizing error is lacking. This is because computing processes, and in particular algorithms for handling raw data, can differ widely [4].
The main goal of this paper is to provide effective solutions for quantifying the reliability of a photogrammetric description in relation to geometric attributes. We limit ourselves to close-range applications [5], investigating two opposite scenarios: (i) in the former case we have, in addition to the photogrammetric model, a homologous digital object obtained by more reliable and accurate processes or tools. It is then possible to use the latter as a reference and perform a comparison to analyse the distribution of distances between the two entities. The steps to be followed must obviously be detailed according to the features of the investigated items; (ii) in the second one, there are no supporting digital descriptions and therefore quality indicators must be derived directly from the photogrammetric process, which requires strict control of all parameters governing it.
The proposed approaches provide maximum flexibility and are applicable to both point clouds and meshes, regardless of the algorithms used to produce them.
In the following paragraphs they will be duly elaborated and tested with reference to a vase of ceramic material, surveyed by both photogrammetric technique and structured light scanner. The two scenarios outlined before will be treated appropriately, highlighting the possible critical issues, and differentiating the procedures according to the specifics of the case.

2. Background

2.1. Comparing homologous models

It often happens that, in processes of digitizing an object, it is detected and returned (totally or partially) using multiple techniques. There can be many reasons for this redundancy of information, ranging from data integration (at any level) to the production of multi-resolution outputs [6]. Regardless of the purpose, it is possible to exploit this content to

quantify the accuracy of geometric attributes. Among the homologous models, there will be one that is more reliable both in terms of how the data is acquired and how it is processed, depending on the employed technique. This description can be used as a reference, calculating the distances of the other models from it and studying the discrepancy distributions with appropriate statistical tools.
However, the intuitiveness of the process hides a complexity that depends largely on the way the different products are obtained, which is why we do not have a one-size-fits-all solution in the literature to perform a comparison. For clarity, it is appropriate to report the questions that underlie many disagreements on the procedure to be followed:

- How should we choose the reference entity? (i)
- How should models be registered? (ii)
- What characteristics should digital descriptions possess? (iii)
- What is the most appropriate algorithm for quantifying distances? (iv)

Starting with the first question (i), the most reliable model should be used as a reference, but its determination is not unambiguous and depends on many factors. The foremost is the resolution, i.e., the level of recognition of the smallest variation in magnitude on the surface of the digitized object. This is followed by the accuracy of the campaign, related to acquisition and processing techniques. For example, the proposed applications include a comparison between a model obtained from a single scan with a structured light instrument and a resolution of 0.2 mm, used as a reference, and a photogrammetric one with a Ground Sample Distance (GSD) of 0.4 mm/pixel. In general, active optical sensors are more reliable from a purely geometric perspective. This depends not only on the inherent features of the instrumentation but also on the fact that the operator, in both the detection and handling phases of the raw data, must control a very limited number of factors, internal and environmental, compared with a process involving passive sensors. Furthermore, photogrammetric acquisition is clearly separated from the data management step, the variables of which can greatly affect the final product according to subjective choices by technicians. A model generated with manufacturer-declared specifications with almost no

influence by personal preferences would therefore provide a reliable basis for comparison. For the definition of a common reference system (ii), we prefer a punctual approach using the coordinates of appropriate targets positioned in the surveyed scene. Solutions that involve entire digital objects, such as ICP-derived algorithms [7], are certainly more robust but, as they do not rely on homological relationships between points, they attempt to reduce distances by searching for the configuration that ensures the best overlap, running the risk of localized anomalies not being duly revealed.

About the features of the compared models (iii), it is preferable that they have a similar resolution or surface density, or at least a higher one for the reference entity, since almost all algorithms available to quantify discrepancies are based on the calculation of normals or local modelling applied to the latter, which is fundamental to the success of the analysis.

Linked to the previous argument is the choice of the algorithm (iv). If you have a reference in the form of a polygonal mesh, you can use the Cloud-to-Model (C2M) distance [8, 9]. This approach is the most common technique in inspection. Surface change is calculated by the distance between a point cloud and a reference 3D mesh or theoretical model. It works well on flat surfaces, as a mesh corresponding to the average reference point cloud position can be constructed [10].

This approach is not always convenient. Creating a surface mesh is complex for point clouds with significant roughness at all scales or missing data due to occlusion. The process of creating a surface could smooth out some details that may be important to assess local roughness properties. In other cases, the interpolation over missing data introduces uncertainties that are difficult to quantify, requiring time-consuming manual inspection.

Therefore, it is preferable to use the Multiscale Model-to-Model Cloud Comparison (M3C2) algorithm, which, with its parameters, allows better control of sources of uncertainty. This algorithm combines three crucial elements: it performs directly on point clouds without meshing; it calculates the local distance between two point clouds along the surface normal direction (i.e. considering 3D variations in surface orientation); it estimates for each distance measurement a confidence interval that depends on the roughness of the point cloud and the registration error [11].

The M3C2 algorithm calculates a local average cloud-to-cloud distance for a point in the reference cloud, termed the core point, through the use of a search cylinder projected along a locally oriented normal vector [11]. Then, the distance is assigned as an attribute of the core point. The entire reference cloud can be defined as core points, or a subsampled set of the reference cloud. The original resolution of both point clouds is used in the M3C2 computations, regardless of whether the data is subsampled in the process. The core point's normal vector is estimated from its surrounding neighbourhood, which should be of a scale such that it captures the surface geometry without being sensitive to local surface roughness [11]. Points encompassed by the search cylinder are used to compute the average position of the compared clouds. The distance between the average positions (along the normal vector) is the M3C2 distance. The projection diameter size and the maximum search length are chosen based on the application, point spacing, and surface complexity [12].
The analysis of distance distributions requires additional statistical tools. Very effective are the tolerance intervals [13], which allow the nature of the distributions and the size of the samples to be properly considered. The above considerations provide good coverage of the possible scenarios that arise during operations.
Before proceeding further, it is worth mentioning that a more reliable reference object cannot always be found. In this case, it is preferable to derive, from the distance distributions, the mutual surpluses, and then calculate the Hausdorff distance [14, 15] between the two entities. However, this approach requires prior filtering to remove outliers, which can be performed, for example, with a box plot [16, 17].

2.2. Direct accuracy assessment of photogrammetric models

The evaluation of a photogrammetric model accuracy is more difficult without a reference object for a comparison since quality indicators must be derived directly from the data processing. In the structure estimation and optimization steps, which include the internal and external (relative and absolute) orientation of the frames, it is essential to know the coordinates or dimensions of certain elements arranged in the object space (the scene to be digitized). In applications of very close-range photogrammetry, it is common practice to add to the scene

punctual objects with known coordinates (targets). Although simply natural image features or textures can be used for this stage, the employment of artificial targets is encouraged by faster computation times and higher accuracy in the recognition. Their purpose, therefore, would be to define a local coordinate system, to scale of the model and highlight real matches to improve the photo alignment procedure.
However, targets – in the form of Ground Control Points (GCPs) or Check Points (CPs) – are often used as the basis for analysing the accuracy of the model. Despite a good distribution across the scene, this is not a robust strategy, as their number cannot be compared with the multitude of points from which the final product is composed.
There are then additional critical issues. Let's start with CPs, whose coordinates are not directly used to optimize the model structure, but only to perform an a posteriori check on the output. We could think of combining the error associated to the CPs – expressed through the discrepancy between input target coordinates and those estimated by the photogrammetric process – and the error that characterizes the definition of target coordinates in object space (e.g., the tolerance on the production of a scale bar). Unfortunately, there is correlation among the two sources of uncertainty, and we cannot apply a simple propagation law. One would then have to go into the nature of this correlation to resolve the problem rigorously, which is far from straightforward. These considerations can be extended to GCPs, with the aggravation that their 3D coordinates are used to solve the Bundle Block Adjustment. It is therefore expected that the error associated with them will be less than that of any other constituent point in the model, since the geometric structure is built and optimized precisely around their coordinates.
Robust solutions should consider more points. Certainly, one solution would be to consider the TPs obtained from the orientation phase. However, such an approach requires a very strict control of the parameters governing the photogrammetric process.
First, the accuracy of target coordinates in object space (how the 3D coordinates are measured or estimated) and in image space (how the targets are identified in the photos).
Then follows the accuracy of TPs also in image space, which is mainly related to the quality of the acquisition campaign. Such an approach will be detailed in the next section.

3. Materials and Methods

As anticipated, our analysis is conducted on a close-range photogrammetric process applied to a ceramic material vase.

The average GSD of the dataset is 0.4 mm, and the project consists of 96 images with 6000×4000 pixels, acquired with entry-level Nikon D3300 SLR camera. The lens is an 18-55 zoom set at 30 mm throughout the campaign, adjusting the focus beforehand to preserve the acquisition main distance. We can then proceed with the orientation.

Agisoft Metashape, the software used in our applications, detects points in the source photos which are stable under viewpoint and lighting variations and generates a descriptor for each point based on its local neighbourhood. These entities are used later to identify correspondences across the photos. This is like the well-known Scale-Invariant Feature Transform (SIFT) approach but uses different algorithms for a higher alignment quality (feature detection). The software then applies a greedy procedure to find approximate camera locations (feature matching) and refines them later using a Self-Calibration Bundle Block Adjustment (structure estimation) [18, 19]. The latter solves the problem of internal and relative external orientation at the same time.

The next step is to import outward references to optimize the frame installation and to solve the problem of absolute external orientation. We use bars whose extremes consist of uncoded targets, which are also easily identifiable as reference elements, called "Markers". Metashape can locate them automatically, simply by choosing the type of artificial object placed in the scene (in this case uncoded cross-shaped targets). After recognition, we proceed with a visual check and eventual optimization. At this stage, we select the appropriate local reference system.

We can then optimize the alignment (structure optimization). The goal is to obtain only high-quality tie points and repeatedly improve the camera model. This is the most subjective section of the workflow and testing how many points can be removed at each stage may be necessary to create a successful product.

The error reduction phase relies on robust tie point and marker accuracy estimates, referred to the image coordinates quality (and, of course, on the accuracy of the reference elements in the object space). The

proportion between these two parameters distributes the weight given to markers and tie points in the whole process [20]. Correct reference settings inputs prevent misleading statistics while an incorrect estimate of them generate a not representative error models, with lens coefficients that are very sensitive to these parameters. Parallel to photogrammetric processing, a homologous model of the vessel is made with a structured light scanner capable of 0.2 mm resolution, which is essential for the development of the section for comparison.

3.1. Comparison-based workflow

For tests on the proposed methodology (Figure 1), we use two homologous models. The reference is a polygonal mesh obtained from a single scan with a structured light instrument. The model compared is instead a dense point cloud obtained through the photogrammetric process. The vertices of the bar scales (9 points) distributed in the digitized scene are used to register the models, avoiding approaches derived from the ICP for the reasons explained in the section 2.1. Since the scanner directly returns a mesh, in this case we can employ the C2M algorithm to quantify the distances between the two entities. The same procedure is applicable if the object being compared is also a mesh.

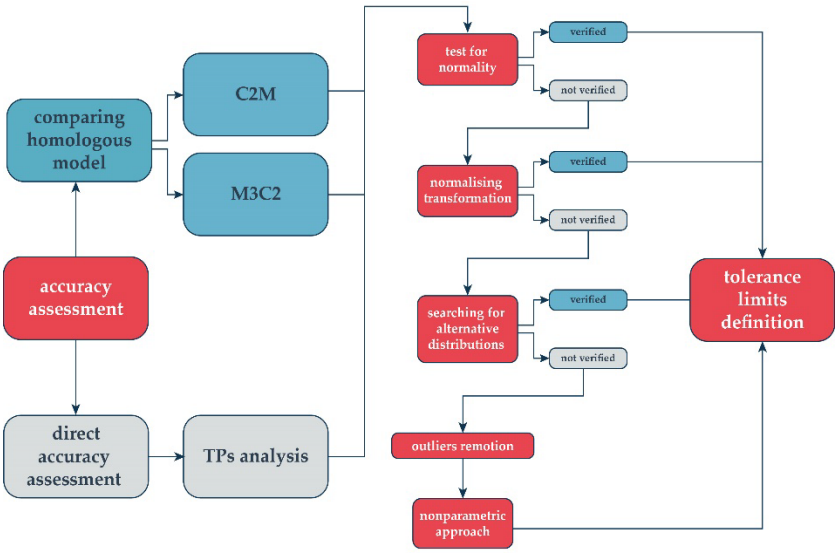

Figure 1. Diagram summarizing the two proposed methodological approaches.

In this case, only the vertices are considered. If the vertices of this mesh are too scattered, it may be convenient to subsample the model with a surface density approaching that of the reference.
In all other cases, it is preferable to use the M3C2, which is much more refined and can isolate distances between objects more effectively, purifying them of the registration-dependent component.
In the case of distances between digital entities, it is worth mentioning that we work with signed quantities. To summarise the distance distributions, we use tolerance intervals, according to a procedure detailed in the section 3.2.
A similar approach can be followed even in the absence of a superordinate reference, considering the two entities as equally reliable and deriving the distributions of each other's distances. From these, we can derive tolerance intervals or, alternatively, the Hausdorff distance as a punctual indicator. The latter provides an interesting measure of the proximity between two digital objects, indicating the maximum distance of each point of the first one from the other: therefore, it can be more effective than the minimum distance, which completely neglects their spatial configuration, to which, instead, the Hausdorff distance is sensitive. In this case, it is necessary to perform a prior treatment of the distance distributions to eliminate any outliers, such as by constructing a box-plot diagram.

3.2. Direct assessment procedure

On the assumption that the control of the accuracy of all input data (relative to object space and image space) is of fundamental importance for a rigorous photogrammetric process, we have prepared a special Python script, with which we are able to export, after the orientation optimization phase, the covariance matrices associated with the coordinates estimated for the TPs in the object space.
Many commercial software implements a similar tool that returns an uncertainty vector obtained by composing the semi-axis lengths of the error ellipsoid with k = 1. This solution is not very cautious since the probability that the theoretical mean value of the Tie Point coordinates falls in this region is 19.95%. Instead, we consider the ellipsoid with k = 3, with probability greater than 95%, and study the length distribution of its major semi-axis to derive an accuracy indicator.

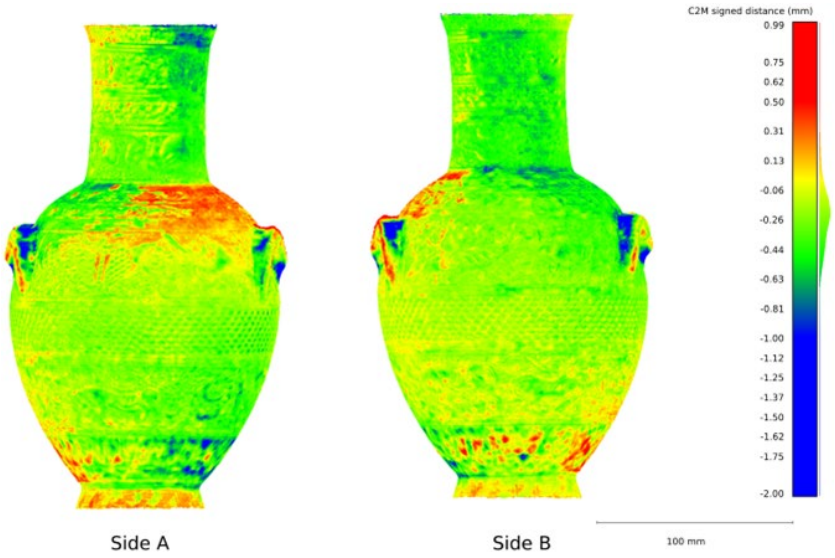

Figure 2. C2M distance between photogrammetric (compared) and scanner model (reference).

The statistical tools used for this analysis are tolerance intervals. They allow us estimating, from a sample, the extremes that contain a certain percentage of a population with a specific level of confidence. In this case the quantities involved are defined as positive, so we construct one-sided gaps. The procedure can be outlined in the following steps: (i) test for normality; (ii) search for normalising transformation (when the distribution is not normal); (iii) alternative distributions (when transformation approach fails); (iv) if all approaches fail, we calculate nonparametric tolerance limits (removal of outliers).
In general, we construct tolerance intervals with 95% confidence and 95% population. Only one parameter between the population percentage and confidence value can be defined in the case of non-parametric tolerance limit computations, with the other being determined later in the process. In that case, preventive treatment of the distributions may be necessary to eliminate possible outliers, e.g., by constructing a box-plot diagram. The approach therefore seems reasonable, considering that the TPs will constitute only a part of the final photogrammetric cloud. To be fair, the dense image matching phase and its algorithms should also be involved, but this would become too complicated. We will therefore limit ourselves to using the results of the Structure from Motion step here.

4. Results

4.1. Comparison

After registering the mesh model obtained from the scanner (reference) and the photogrammetric dense cloud (comparison) using the extremes of the bar scales, we used the C2M algorithm to obtain a distribution of distances between the two digital objects (Figure 2). This distribution has a normal pattern, as verified by a special test. Considering then that the algorithm returns oriented distances, we constructed a two-sided tolerance interval with a confidence level of 95% and a population percentage of 95%, obtaining the value of -0.78 mm as the lower limit and +0.35 mm as the upper limit. Wanting to reason in absolute terms, we can take the value 0.78 mm as a synthetic indicator.

4.2. Direct assessment

Figure 3 shows step by step the results of the direct assessment procedure. The test for normality is not satisfied for the distribution of major semi-axes relative to ellipsoids with k = 3, as can be quickly seen from the Q-Q Plot and as verified rigorously through the Shapiro-Wilk test; this leads to the attempt to normalise the distribution. Unfortunately, a suitable power transformation could not be found; the same applies to fitting a different distribution. Non-parametric tolerance limits approach is finally performed, after removing the outliers from the distribution by constructing a box-plot diagram. Precisely this latter approach is applied to the case study fixing a confidence level of 95%, and step 4 of Figure 3 shows the results. Since the semi-axis length is a positive definite quantity, we employ a one-sided interval, obtaining an upper tolerance limit of 2.22 mm, which can be used as an indicator of the accuracy of the entire photogrammetric process.

4. Discussion and conclusions

The issue of traceability of data from photogrammetric surveying is as timely as ever. Given the numerous parameters that govern the processing process, there is still a lack of systematic treatment of the topic and no agreement on how to quantify error.

The main objective of this study is to provide a response to this need,

capable of ensuring maximum flexibility and adaptability to the needs of the specific case study.

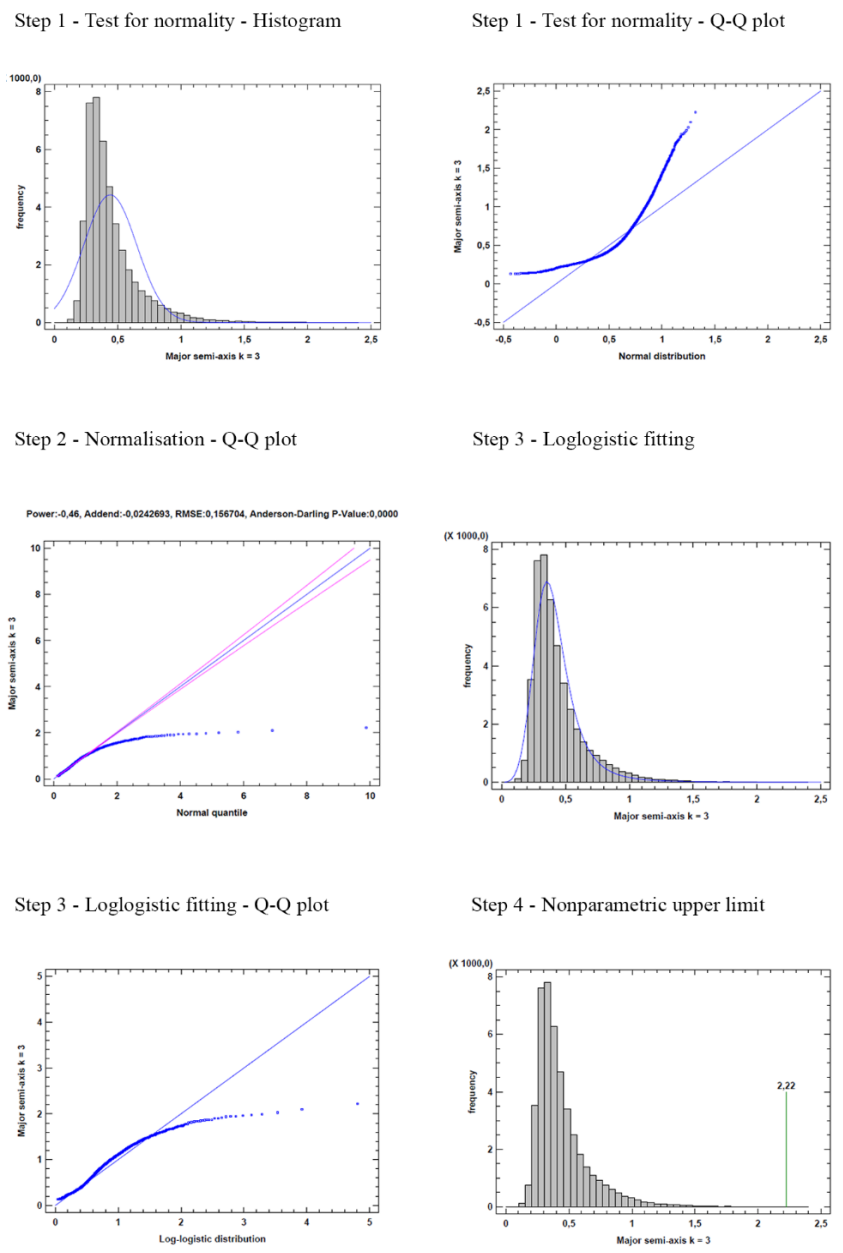

Figure 4. Direct verification procedure on photogrammetry. distribution of major semi-axes for ellipsoids with k = 3.

The proposal is differentiated and follows two possible scenarios. On the one hand, the possibility of having a more reliable homologous model, obtained, for example, by laser scanning techniques. In this case, the assessment on accuracy is based on a comparison.
In procedures of this kind, it is of paramount importance to consider aspects such as the topology of the models, their nature, how they are aligned, and how they are compared, to obtain robust results that can be compared effectively. Tolerance intervals are the statistical tools primarily used to describe distributions of distances because they are not bound by assumptions about their type and are sensitive to the sample size analysed. Of course, different approaches involving metrics such as Hausdorff distance can also be used, a sign of the great flexibility of the procedure. The second scenario excludes the presence of superordinate models for accuracy and focuses directly on the photogrammetric process. By appropriately calibrating the weights of all input data, we derive the covariance matrices associated with the estimated coordinates for the TPs to construct appropriate error ellipsoids, studying the distributions of their major semi-axes and extending the results to the entire model through the tolerance intervals. The two procedures described can be used regardless of the nature of the outputs, whether point clouds or meshes. Moreover, they are not limited to the photogrammetric technique but can also be extended to laser scans or otherwise exploiting active optical sensors. Future developments will focus precisely on the applicability of the methodology to scenarios not yet investigated with the case study, proposing appropriate implementations for adaptation to the specificity of the case.

References

1. Guidi, G., Russo, M., Angheleddu, D. 3D survey and virtual reconstruction of archeological sites. *Dig.Appl. in Archaeology and Cultural Heritage* **2014**, *1(2)*, 55-69.
2. Grilli, E., Remondino, F. Classification of 3D Digital Heritage. *Remote Sensing* **2019**, *11(7)*, 847.
3. Denning, J.D., Kerr, W.B., Pellacini, F. MeshFlow: interactive visualization of mesh construction sequences, in *ACM SIGGRAPH 2011 papers*. 2011, Association for Computing Machinery: Vancouver, British Columbia, Canada.
4. Morena, S., Barba, S., Álvaro-Tordesillas, A. SHINING 3D EINSCAN-PRO, APPLICATION AND VALIDATION IN THE FIELD OF CULTURAL HERITAGE,

FROM THE CHILLIDA-LEKU MUSEUM TO THE ARCHAEOLOGICAL MUSEUM OF SARNO. *Int. Arch. Photogramm. Remote Sens. Spatial Inf. Sci.* **2019**, ***XLII-2/W18***, 135-142.

5. Luhmann, T., Robson, S., Kyle, S., Boehm, J. *Close-Range Photogrammetry and 3D Imaging*. De Gruyter: Berlin, Germany, 2013.
6. Ramos, M.M., Remondino, F. Data fusion in cultural heritage-A review. *Int. Arch. Photogramm. Remote Sens. Spatial Inf. Sci.* **2015,** *40(5)*, 359.
7. Chetverikov, D., Svirko, D., Stepanov, D., Krsek, P. The Trimmed Iterative Closest Point algorithm. *2002 International Conference on Pattern Recognition*, **2002**, 3, 545-548.
8. Guerin, A., Hants, D., Rossetti, J.P., Jaboyedoff, M. *Brief communication "Estimating rockfall frequency in a mountain limestone cliff using terrestrial laser scanner". Nat. Hazards Earth Syst. Sci. Discuss.* **2014**, *2*, 123-135.
9. Kromer, R.A., et al. Identifying rock slope failure precursors using LiDAR for transportation corridor hazard management. *Engineering Geology*, **2015**, *195*, 93-103.
10. D'Amato, J., et al. Influence of meteorological factors on rockfall occurrence in a middle mountain limestone cliff. *Nat. Hazards Earth Syst. Sci.*, **2016**, *16(3)*, 719-735.
11. Lague, D., Brodu, N. J. Leroux, Accurate 3D comparison of complex topography with terrestrial laser scanner: Application to the Rangitikei canyon (N-Z). *ISPRS Journal of Photogrammetry and Remote Sensing* **2013**, *82*, 10-26.
12. Nourbakhshbeidokhti, S., et al. A Workflow to Estimate Topographic and Volumetric Changes and Errors in Channel Sedimentation after Disturbance. *Remote Sensing* **2019**, *11*.
13. Natrella, M.G., *Experimental statistics*. Dover Publications: Mineola, NY, USA, 2005.
14. Gregoire, N., Bouillot, M. *Hausdorff distance between convex polygons. Web project for the course CS 507 Computational Geometry*, McGill University, 1998.
15. Mezhenin, A., Zhigalova, A. Similarity analysis using Hausdorff metrics. In *10th Majorov International Conference on Software Engineering and Computer Systems,* D. Mouromtsev, S. Bykovskii (eds); Saint Petersburg, Russia, December 20-21, 2018.
16. Williamson, D.F., Parker, R.A., Kendrick, J.S. The box plot: a simple visual method to interpret data. *Ann Intern Med* **1989**, *110(11)*, 916-21.
17. Potter, K.C. Methods for Presenting Statistical Information: The Box Plot. In *Visualization of Large and Unstructured Data Sets, GI-Edition Lecture Notes in Informatics (LNI),* H. Hagen, A. Kerren, P. Dannenmann (eds), pp. 97-106, 2006.
18. Nex, F., Remondino, F. UAV for 3D mapping applications: a review. *Applied Geomatics* **2014**, *6(1)*, 1-15.
19. Remondino, F., Fraser, C. Digital camera calibration methods. Considerations and comparisons. In *ISPRS Commission V Symposium 'Image Engineering and Vision Metrology'*, H.-G. Maas, D. Schneider (eds); Dresden, Germany, September 25-27, 2006.
20. Tang, R. *Mathematical Methods for Camera Self-Calibration in Photogrammetry and Computer Vision*. Institute of Photogrammetry University of Stuttgart: Munchen, Germany, 2013.

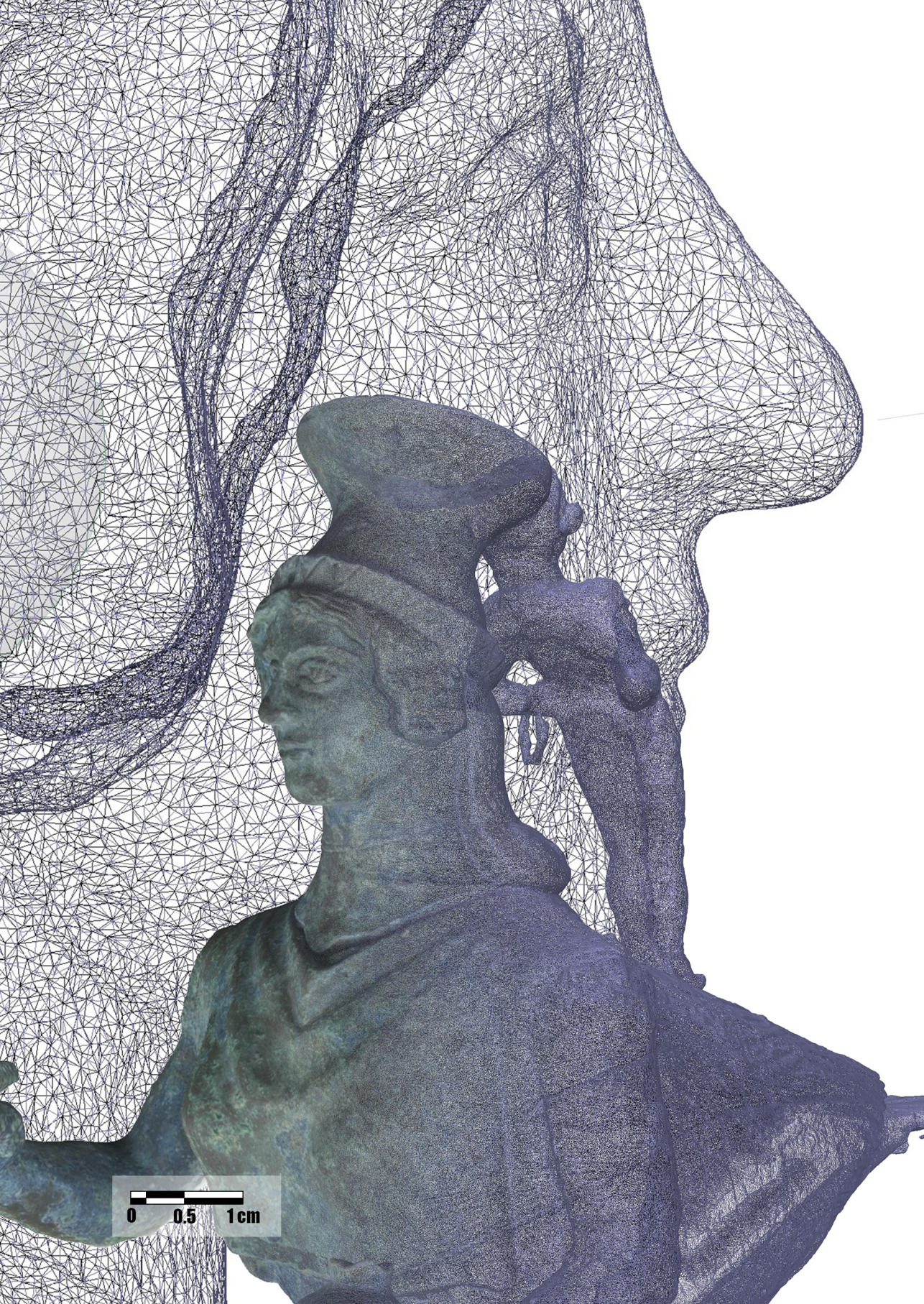
0
0.5
1cm

Capitolo 10
A statistical analysis for the Assessment of Close-Range Photogrammetry geometrical features

Abstract: An examination of the traceability and dependability of the virtualisation properties is prompted by the widespread use of three-dimensional models. The challenge of obtaining accuracy indicators directly from the photogrammetric method when a reference model is missing is widely acknowledged. In this study, a robust method based on a statistical analysis of the uncertainty associated with Tie Points (TPs) is presented to provide a strict framework for the informed processing of photogrammetric survey data. In the phases of Structure estimation, Structure optimisation, and Dense Cloud generation, the key steps and variables affecting data processing are described. The workflow is then applied to a specific bronze museum finding smaller than 20 cm in size. All tie points that overcome the filtering phase are included in the procedure and for their coordinates the covariance matrix is examined. The error ellipsoid is calculated and the distribution of the lengths of the major semi-axes is analysed to calculate an appropriate tolerance interval which can be used as an indicator of the accuracy of the entire photogrammetric process. Indeed, using the tolerance intervals tool allows for the derivation of a representative indicator that can be compared with the outcomes of other photogrammetric processes while overcoming the ambiguity of statistical indicators that are not representative in the case of a non-normal distribution.

Keywords: Photogrammetric processing, Accuracy evaluation, Agisoft Metashape, Tie Points Filtering, Covariance Matrix.

1. Introduction

The demand for 3D reality-based models is growing in popularity and ambition due to the level of realism and detail expected today. Although hardware and software solutions are getting increasingly innovative and outstanding, somehow fulfilling the challenging task, a question arises regarding the traceability and reliability of virtualisation properties [1].

Particularly nowadays, the simplicity of generating 3D geometries due to the spread of completely automated image-based technologies makes it incredibly more complex to trace the quality of outcomes. Thus, leading to the false belief that these 3D models are accurate. This assumption is most likely a result of the common idea that the widespread use of image-based computer programmes automatically guarantees consistency and reproducibility [2]. It is therefore expected that modelling processes, and in particular algorithms for handling raw data, can improve significantly [3]. Hence, despite the extensive use of three-dimensional models, automation and innovation have otherwise made it more challenging to come up with effective approaches for determining the accuracy of a photogrammetric model in relation to its geometric features, resulting in the absence of a common criterion for formalising errors [4].

Moreover, a systematic method to describe the quality of virtualisation has not yet been well developed, despite the extensive research in the literature on evaluating the accuracy of photogrammetry in relation to the acquisition phase's best practices, with a specific focus on systematic errors due to: (i) camera factors (i.e., type, principal point, principal distance, and camera lens distortion coefficients); (ii) imaging settings (i.e., shooting distances, baselines, percentage of photo overlaps, number of overlapping photos, camera intersection angles, and angles of incidence) [5].

The widespread way of dealing with the quality task is based on assessing the accuracy of geometric descriptions of an object by comparing homologous models produced through different techniques. The model considered most reliable can be adopted as a reference, calculating the deviations of other digital descriptions from it.

The need for data integration and/or for producing multi-resolution models results in the redundancy of data useful for such distance-based comparative analyses. However, several issues do not make the choice of reference entity trivial: (i) how to unambiguously define the accuracy and reliability of processes and tools that make the reference appropriate; (ii) how to register the models before comparison; (iii) which algorithm is most suitable for quantifying distances. The instrumental resolution, followed by the rigour of the acquisition campaign and the technology employed, are the factors that mainly

contribute to making the reference model unambiguous. For the definition of a common reference system, two main types of approaches can be employed: the former based on the identification of specific points, such as targets distributed over the survey scene, and the latter involving the entire object, such as ICP-derived algorithms [6]. Regarding the choice of algorithm, it seems appropriate to adopt the cloud-to-model (C2M) distance in the case of a polygonal mesh reference model; while for other scenarios, the multiscale model-to-model cloud comparison (M3C2) technique is preferable because it employs parameters that allow for better control over the sources of uncertainty [7]. When a reference model is not available, the evaluation of the accuracy of the final model is more challenging, as accuracy indicators need to be derived directly from the photogrammetric process. Even when Ground Control Points (GCPs) or Check Points (CPs) are evenly distributed in the scene, basing the entire analysis on a limited number of points is not a robust approach [8]. Thus, the direct accuracy assessment of the photogrammetric model should be performed by studying the uncertainties related to the Tie Points (TPs). Nevertheless, it must also be taken into account that the quality of the orientation process and associated reconstruction outputs is inevitably affected by the feature extraction and matching techniques [9], for which not only the number of TP must be considered representative, but also their correctness [10].

Under these assumptions, a statistical analysis of the covariance matrix associated with the estimated TP coordinates is proposed in this study. The primary objective is to present a potential strategy for the conscious treatment of survey data.

The experimentation is conducted on the close-range photogrammetric process [11] applied to a bronze ointment vase (Askòs) called "La Sirena di Murgie" (Figure 1). The finding, dated 5th century BC, is preserved at the National Archaeological Museum of Crotone, Calabria Region, and depicts a Mermaid: the hybrid mythological being that, according to Greek iconographic tradition, is a half-human and half-bird [12]. The total height of the vessel is 15.3 cm, while the length and width measure 18.7 cm and 8.4 cm.

Although generating models of small objects in the field of Cultural Heritage is often only aimed at AR or Web visualisation applications,

in this case, it seemed appropriate to test the validity of the acquisitions that were conducted in a difficult context, such as the museum environment, thus lacking controlled settings such as a well-equipped laboratory [13]. The objective was to guarantee high accuracy with portable and affordable equipment, even in extreme conditions.

2. Materials and Methods

The influence of factors governing the orientation process on the quality of a three-dimensional model obtained from photogrammetry is well-known. The essential steps and parameters governing data processing are outlined below. As explained in the following section, they were employed in a specific workflow, highlighting the necessity for a case-by-case approach to the procedures (section 3).

2.1. Structure estimation

During the orientation phase, within the piece of software used – Agisoft Metashape Professional v.1.8.3 (AM) – the pixels in the input photos that are stable under changes in lighting and viewpoint are identified. Then each is assigned a descriptor that places it on the basis of its immediate neighbours. Similar to the well-known scale-invariant feature transform (SIFT) algorithm, these entities will be later utilised to locate correspondences between the images (feature detection).

Figure 1. "La Sirena di Murgie", National Archaeological Museum of Crotone.

After approximately identifying the camera locations (feature matching), the calculation is refined via Self-Calibration Bundle Block Adjustment (structure estimation), solving both the problem of internal and relative external orientation [14]. The parameters involved in this process are presented below:

- Accuracy, which adjusts the downsampling of the input data according to the original pixel size.
- The key Points limit concerns the maximum number of feature points searched for in each image. The value 0 corresponds to "no limit"; 40,000 is the recommended default value (more points would be obtained by setting higher values, but their reliability would gradually decrease). However, an upper limit still ensures reliable points if high-quality images are employed in the procedure.
- The TPs limit concerns the maximum number of matching points found in each image. The value 0 corresponds "no limit"; 4,000 is a recommended default value. It would be preferable not to limit TPs if one intends to reduce them after alignment.

The recently added option in the software, called Adaptive Camera Model Fitting, if selected, introduces unpredictable solutions in order to find the combination of camera model coefficients that best fits the minimum error model. Allowing AM control over the decision-making process may lead to lesser error, but it also causes overfitting of the data or the generation of a complex camera model that doesn't exactly reflect the equipment utilised.

2.2. Structure optimisation

The subsequent filtering phase is aimed at obtaining only high-quality TPs and, although subjective in terms of the number of points to be eliminated, is governed by the following parameters:

- Reconstruction Uncertainty, which reflects poor geometric relations between cameras. It is calculated as follows:

$$\sqrt{\lambda_1/\lambda_3} \tag{1}$$

Where λ_1 is the largest eigenvalue of the tie-point covariance matrix, and λ_3 is the smallest. Basically, it is the ratio between the largest and the smallest semi-axis of the error ellipsoid for 3D point coordinates (k = 1). The latter region corresponds to the uncertainty of the point triangulation alone, without considering the propagation of ambiguities arising from interior and exterior orientation parameters.

- Projection Accuracy, which identifies low match accuracy internally assigned by the software, is defined as the average image scale at which picture coordinates of the TP are measured, computed as:

$$\sum_i {}^{s_i}/_{n} \tag{2}$$

Where s_i is the image scale at which corresponding, projections are identified on the i^{th} image, and n is the number of photos where the TP is detected. This criterion enables the removal of points whose larger size causes their projections to be relatively poorly localised. Projection Accuracy is essentially a representation of the fidelity in the identification of the TP location, given the size of the key points that intersect to create it.

- Reprojection Error, which highlights false correspondences and is defined as the distance between the point on the image where a 3D point can be projected, and the original projection of that 3D point detected on the photo and used as a basis for the 3D point reconstruction procedure. The filter evaluates the maximum Reprojection Error in normalised units across all pictures where TP is identified:

$$Max_i \, {}^{|x_i' - x_i|}/_{s_i} \tag{3}$$

Where x_i' is the point projection according to adjusted orientation parameters on the i^{th} image in pixels, x_i represents the measured point projection coordinates on the i^{th} image in pixels, and s_i is the image scale at which corresponding projection is evaluated on the i^{th} image.

Iterative selection and removal procedures are used in the application, as specifically described in the next paragraph.

The aim is to improve the estimated internal and external orientation parameters by removing poor TPs. However, each time TPs are deleted, the accuracy of the remaining TPs changes, requiring re-optimisation of the project before going on.

Alongside these considerations on the robustness of TPs, there are those relating to marker accuracy (regarding the image space) and measured control data accuracy (regarding the object space). Precisely, the proportion between these two parameters – the quality of the coordinates identified in the image and the quality of the coordinates measured in the scene – allocates the weight assigned to the markers and TPs throughout the process. In this regard, in AM, the Reference Settings panel allows the inputs of Images Coordinates Accuracy and Measurement Accuracy to be correctly balanced. This setting prevents misleading statistics, as their incorrect estimation generates unrepresentative error models since lens coefficients are very sensitive to these parameters [15].

The section Measurement Accuracy, which refers to external real world (m), deals with capturing geotags and calculating the accuracy of targets used as CGPs and the overall surveying methods.

Focusing on the Image Coordinates Accuracy (pixel) section, the two parameters to be refined are:

- TPs Accuracy, which corresponds to the normalised accuracy of TPs projections detected at the scale equal to 1, considering a pyramid built applying Gaussian blur. TPs identified on other scales will have accuracy proportional to their ranks.
- Marker Accuracy, which depends to a large extent on how they are positioned in the frames when pinning a marker on a feature, typically on a target, with an indirect correlation with the capture resolution.

In both cases, establishing a priori the proper values is difficult. Therefore, the default values (1 pixel for the TPs Accuracy and 0.5 pixels for the Marker Accuracy) can be used for the first optimisation step and then gradually adjusted during the optimisation iterations. It is worth mentioning that an indicator of the goodness of the realistic estimation related to these metrics is the discrepancy between the error

(m) and accuracy (m) values for GCPs and CPs. In the case of a correct estimate, they will converge. For monitoring the refinement of the camera model, several strategies can be implemented:

- Checking the generated reports in the Console Panel during the optimisation process. The number of iterations required to calculate the lens coefficients will be displayed via a sequence of "x". If the string is long and does not get shorter during the procedure, the solution might be divergent, or the modelled coefficients may not be sufficient to reach the internal trigger that would otherwise put an end to the optimisation process. In these scenarios, starting from the post-alignment phase is preferable to overfitting the solutions.

  The reports also show the values of Sigma0, the AM equivalent of the photogrammetric adjustment quality indicator sigma naught (σ_0), which is the Standard Error of Unit Weight (SEUW). The farther the SEUW is from 1, the poorer the estimated TP accuracy.

  It corresponds to the degree of deviation from an assumed quality or how closely the RMS Reprojection Errors match the predefined error values. However, since the weighting it is based on is not fully documented, using it as the main indication for process monitoring is impractical. Instead, its convergence towards unity becomes valuable in the advanced optimisation stages.
- Observing the number of projections for each image, defined as the number of valid TPs found on a given capture. A specific image will not be used to generate the final outputs if the number of projections for that image is less than 100. To achieve a robust orientation, it would be better to adopt a cautious limit of projections.
- Monitoring the Root Mean Square (RMS) Reprojection Errors in the chunk point cloud property. To increase the robustness of the process, especially when there are blurry photographs or photos with few distinguishing features or textures, the TPs are placed at several map scales.

  Then, the map scale information is used to weigh the TPs Reprojection Errors by the software. Unfortunately, since the

scaling parameters and weighting procedures are not disclosed in AM, the meaning of the mentioned metric becomes convoluted: of the two reported RMS Reprojection Errors related to orientation, the weighted value is the first one in the units of key point scale, and the unweighted one, written in pixels, is the second one.
The optimal unweighted value is generally less than 0.3 pixels. If too many TPs are deleted during the subsequent filtering steps, the camera model may deviate from a particular solution, increasing the unweighted RMS Reprojection Error.

Estimating the TPs covariance matrix, which is related to the execution of the Bundle Block Adjustment, is a way to visualise the uncertainty in the camera models after each optimisation cycle. The evaluation outcomes can be examined by switching the TPs cloud display mode to a specific one (Figure 2).
The vector associated with each TP indicates the direction and magnitude of the error for the TP estimated position (its three components correspond to the semi-axes of the error ellipsoid with k = 1 determined by the covariance matrix).

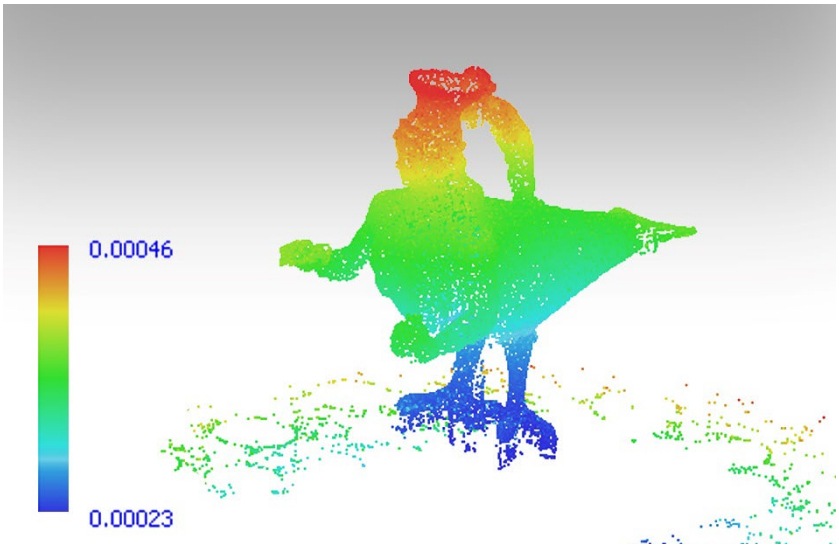

Figure 2. TPs covariance view mode, after Gradual Selection filtering, in Agisoft Metashape SfM software.

2.3. Dense Cloud generation

Dense Clouds are reconstructed from depth maps computed through pairs of overlapping images, identified by their internal and relative external orientation parameters, which are estimated using Bundle Block Adjustment.

Multiple pairwise depth maps generated for each camera are merged into a combined depth map, employing excessive information in the overlapping regions to discard wrong depth measurements. The products are transformed into partial dense point clouds, which are subsequently merged into a final model, thanks to an additional noise filtering step applied in the overlapping regions. The normals in the partial dense point clouds are calculated using plane fitting to the pixel neighbourhood in the combined depth maps, and the colours are sampled from the images.

The number of contributing maps is recorded and stored as a confidence value for every point in the final dense point cloud. This number will be used later to perform additional filtering. A list of parameters governing the procedure is explored below:

- Quality, which affects the detail and accuracy of the reconstructed geometries as well as the processing time, depending on the number of depth maps calculated.
- Depth filtering, which removes outliers from the cloud due to aspects such as noisy or badly focused images by checking them within the raw depth maps. This step is performed using a connected component filter that operates on segmented depth maps based on the pixel values.
- Whether and how the process associates the RGB information to the individual points.
- Point confidence calculation, which enumerates how many depth maps are generated for each point so that further filtering can be performed.

Once the Dense Cloud has been reconstructed, noise removal can be performed. In addition to the interactive intervention, which is useful for deleting badly located elements, a filter can be applied according to the number of depth maps per point. The results of this operation

depend primarily on the pattern chosen to capture the frames. The algorithm is based on a non-linear selection scale ranging from 0 to 255, where lower values indicate fewer depth maps involved in the reconstruction of the 3D position of the point (Figure 3).
This last operation ends the photogrammetric process.

2.4. Uncertainty assessment

To provide a rigorous framework for the informed handling of photogrammetric survey data in the absence of a reference model, a statistical analysis of the uncertainty associated with Tie Points (TPs) in object space can be performed.
Sources of uncertainty related to instrumentation, techniques, their integration, and the statistical description of their distributions can be identified. In this way, their propagation law and a dispersion indicator or an interval that effectively summarises the accuracy of the survey can be obtained. However, finding sources of uncertainty and combining them is not easy. There is no single unambiguous solution, which depends heavily on the detection methods and the transformation of the raw data into a reality-based model.

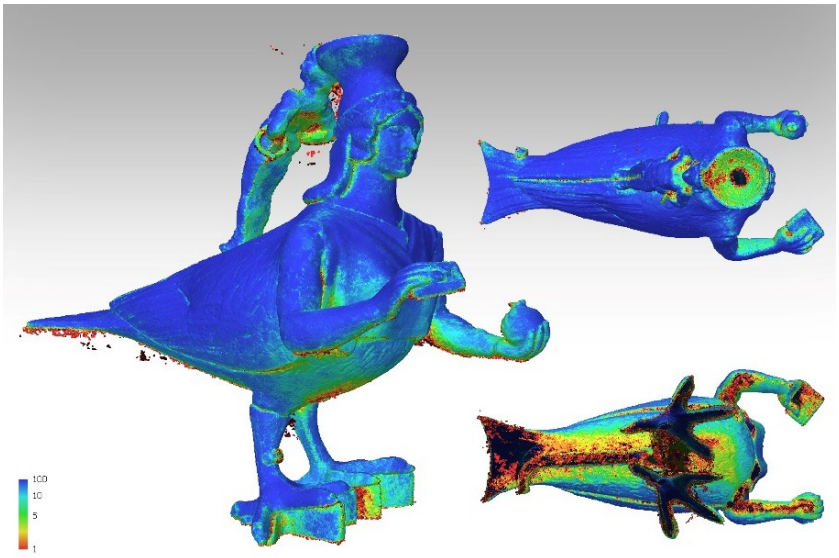

Figure 3. Point Confidence view mode, before Dense Cloud filtering, in Agisoft Metashape SfM software.

Given that it is impossible to list and describe every possible combination, an inductive approach is preferable, starting from a practical case and highlighting the distinctive aspects that affect the decisions. Nonetheless, evaluating the sources of uncertainty in photogrammetric operations cannot rely just on the coordinates of the codified targets. In fact, as a hypothetical solution, the uncertainty related to the Check Points (CPs), expressed by the difference between input and output data, and the uncertainty connected to the support survey may be combined. However, the two sources of uncertainty have a correlation, which would need further elaboration to be adequately described. Albeit the points are evenly distributed around the picture, basing the entire analysis on a small number of points is unquestionably not a robust strategy. The same reasoning may be extended to GCPs, with the aggravating factor that their coordinates, utilised to resolve the structure optimisation phase, generate a reduction in the error associated with them, making them inappropriate for this kind of evaluation.

The previous paragraphs clarified how crucial it is for a rigorous photogrammetric procedure to trace the accuracy of all input data (related to both the object space and the picture space).

After the orientation optimisation phase, the covariance matrix connected to the predicted coordinates for the TPs in the object space is exported using an ad-hoc Python script we developed. From the matrix, the standard error ellipsoid and the configuration corresponding to a probability of containing the theoretical mean value of the coordinates of 97.75% (k =3) are derived. Of this last ellipsoid, the major semi-axis is considered, and an appropriate tolerance interval is calculated by studying its distribution for all the Tie Points. This tool allows estimating, from a sample, the extremes that contain a certain percentage of a population associated with a specific level of confidence. The approach is therefore considered reasonable, noting that the TPs will constitute only a part of the final photogrammetric cloud. To be fair, the dense image-matching phase and its algorithms should also be involved, but this would become too complicated according to the current state-of-the-art. We will then merely employ the results of the Structure from Motion step here. Section 3.2 elaborates on the procedure for determining these ranges.

3. Applicative workflow and Results

3.1. The SfM process

The workflow is applied to data from Nikon D800E SRL camera, equipped with the AF-S Micro NIKKOR 60mm f/2.8G ED, mounted on a tripod in landscape orientation and operated by remote control.

The frames captured have a size of 7360 × 4912 pixels. Considering the focused distance from the object to be 0.6 m, in order to frame the object entirely in a single shot and limit the time and number of acquisitions, a GSD of about 0.04 mm/px was determined. In addition, a Depth Of Field of 12 cm was achieved with an f/32 aperture, using a Circle Of Confusion of 0.015 mm (about half the conventional values for such equipment, to be on the safe side).

The ISO sensitivity values were kept low (100) to avoid digital noise. The shutter speed was estimated to obtain the correct exposure, requiring a remote trigger to avoid vibration. Manual focusing was employed since the main distance would not change during the acquisition campaign, as the focus would only be adjusted just once before starting to capture the photos. The object, placed on a turntable, was rotated in front of the camera approximately every 15 degrees at three different camera angles. The complete dataset consists of about 73 images, ready to be oriented.

Files imported into AM for processing were converted from the proprietary .NEF format to lossy JPG sRGB 24-bit type, which is a good compromise between file size and quality. An initial estimate of the quality of such data was based on sharpness. The method consists of comparing the contrast gradients in the most peculiar regions of the source images, taking into account both the originals and the images with the Gaussian blur filter applied. All frames with a rate below 0.5 were excluded from the process.

Then, the calibration table was examined. The software produces a single calibration group since the loaded photos for each project are identical in terms of size, focal length, and other factors derived from the exchangeable image file (EXIF). Therefore, the camera type (frame), pixel size, and focal length were checked. No pre-calibration data were available for the camera. No position data were known, and therefore a local system was set for the cameras.

The orientation phase was governed by the parameters shown in Table 1, so as to use a higher limit for Key Points due to the high image quality and not limiting the number of TPs as they will be reduced after alignment (section 2.1). The import of external references is the subsequent operation to optimise the configuration and address the issue of absolute external orientation.
A metric reference – that employs a non-repetitive pattern and 56 targets whose coordinates are known by design – was placed on the rotary table and used as an external reference.

Table 1. Orientation parameters.

Parameter	**Setting**
Accuracy	Highest
Generic preselection	Yes
Reference preselection	Sequential
Key point limit	100.000
TP limit	0
Exclude stationary TPs	No
Guided image matching	No
Adaptive camera model fitting	No
Matching time	6 minutes 12 seconds
Alignment time	55 seconds

The targets were visible in the photos, so AM could locate them automatically by simply choosing the type of artificial object placed in the scene (16-bit circular encoded targets). After the recognition, a visual check was performed, followed by an eventual optimisation. Not all markers were used as GCPs to solve the absolute external orientation; some would indeed be discarded from this process, to be later employed as CPs to validate the optimisation results, ensuring a homogeneous distribution of the two groups in the detected scene. The optimisation phase started here (section 2.2).
At this stage, activating every coefficient might reduce error.

Still, it also could cause overfitting of the data or the generation of an overly complex camera model that does not accurately reflect the equipment used, leading to underestimating or increasing actual error. Therefore, the affinity and nonorthogonality, also known as skew coefficients (B1 and B2), should be initially suppressed and only included in case of an inflated RMS Reprojection Error value indicating the possible presence of distortion related to these phenomena. The same applies to the radial distortion coefficient K4.

After duplicating the chunk containing the data processed so far to store a backup copy and checking the correctness of the input reference data, the first optimisation cycle was performed by selecting the appropriate coefficients and estimating the covariance of the TPs. Along the procedure, the number of projections per frame and the unweighted RMS Reprojection Error were monitored.

For calibrating the accuracy of the image coordinate, the latter is helpful mainly when associated with RMS Reprojection Error on markers and mean Key Point size.

The error reduction procedure first consists in removing points resulting from poor camera geometry through the Reconstruction Uncertainty filter. High Reconstruction Uncertainty is typical for points identified through nearby photos with a small baseline. They can noticeably deviate from the object's surface, causing noise in the cloud. While removing such elements should not affect the optimisation accuracy, it may be useful to delete them to improve the visual appearance of the reality-based model. A Reconstruction Uncertainty of 10 is roughly equivalent to a good base-to-height (or base-to-distance) ratio of 1:2.3 (parallax angle of about 23°), whereas 15 is almost equal to a marginally acceptable ratio of 1:5.5 (about 10°) [16]. Our workflow reiterated the filtering of TPs with this parameter twice, taking care not to remove more than 50 per cent of the TPs. The optimisation process used the same lens coefficients as the preliminary stage. After removing the TPs, a single iteration is sufficient if a Reconstruction Uncertainty of 10 is achieved in the first attempt and less than 50% of the TPs are selected. Repeated filtrations have diminishing returns and may overfit the camera model before more poor-quality TPs can be removed. Once again, we monitored the status indicators used during the first cycle.

The second part of the error reduction procedure aims to remove points based on Projection Accuracy. AM saves an internal accuracy and scale value for each TP as part of the correlation process. The highest reliability points are assigned to level 1 and are weighted based on the relative size of the pixels. A TP allocated to level 2 has twice as much inaccuracy as level 1. Not all projects can tolerate removing points at a level of 2 to 3, particularly if the images have been compressed or their quality is compromised due to noise or blur. A gradual selection level of 5 or 6 may be the best that can be obtained. The threshold limit can be defined by remembering that this filtering phase should not eliminate more than 50 per cent of the TPs inherited from the previous one, targeting two cycles. Lens coefficients used in the process are the same as in the second step. Repeated applications show reduced returns and may overfit the camera model. If the project can support an initial filtering of level 3 without selecting more than 50 per cent of the TPs, a single optimisation after deleting the points is sufficient. In our applications, the threshold value was 2. Once again, we monitored the process quality indicators before going any further.

The third step of the error reduction procedure concerns the Reprojection Error, which, unlike the previous ones, is directly related to the parameters governing internal and external orientation. It is, therefore, necessary to correctly define the accuracies for the measurements and image coordinates before proceeding.

As far as measurements are concerned, these are known by design, so their accuracy is only related to the printing process for their physical realisation. Printer accuracy, linked to critical dot size, shape and position accuracy, is not evaluated here. However, for inkjet printers, the error is 10 μm on average [17], then this value can be taken as a lower limit for the marker accuracy parameter (m) in the measurement accuracy section. Concerning the image coordinates parameters, the marker accuracy can assume values below 0.5 pixels if the identification procedure is rigorous, as in our case, and supported by automatic extraction algorithms. Considering the high resolution and the quality of the captures, we assumed the marker accuracy value equal to 0.05 pixels, verifying that the discrepancy between the error (m) and the accuracy (m) associated with the GCPs

and CPs does not grow uncontrollably during the next optimisation phase. As for the accuracy of TPs we gradually reduced it by checking the convergence of Sigma0 to 1. As a rule, we always give markers more weight than tie points.

After the calibration of these parameters, we performed a new optimisation cycle and tested if the value of Sigma0 tended towards 1. If this did not happen, it was necessary to pay attention and, eventually, repeat the previous phases. Finally, we achieved a value of 0.1 pixels for the accuracy of TPs.

High reprojection error usually indicates poor localisation accuracy of the corresponding projections at the point matching step. It is also typical of false correlations. The threshold set for filtering in our applications is 0.3 pixels, not reached directly but by operating in successive cycles and selecting only 10 per cent of the tie points at a time. After the first cycle of this phase, we checked that the error of the markers (m) did not exceed the accuracy (m). In this case, it is convenient to stop the process, revaluate, and correct the a priori reliability of the image coordinates in light of new data, such as the RMS reprojection error. We then checked whether Sigma0 converged to 1. The selected lens coefficients were again those chosen for the previous steps. If confluence does not occur, it is possible to consider involving other coefficients and use additional corrections. At the end of all the cycles of the task, we check the number of projections for each frame, the effective reduction of the iterations within the succession of the cycles, the survival of at least 15-20% of the original tie points and the possible overfitting of the camera model.

If no inconsistencies or anomalies emerge, the orientation process (so-called Structure from Motion - SfM) can be considered concluded (Table 2).

In order to be thorough, the relationship between the calibration coefficients of the camera was examined [18]. This is an effective approach to check for overfitting and may show that some of these parameters are really not relevant to represent the equipment. The set used for the application is an 8-term set derived from the one originally formulated by Brown (1971), including internal orientation parameters of main distance and principal point offset, as well as the three coefficients of radial and two of tangential distortion.

Table 2. Error reduction and reference system parameters consistent with input data.

Parameter	Setting
Reconstruction Uncertainty filter	10
Projection Accuracy filter	6
Marker Accuracy (m)	0.0005
Marker Accuracy (px)	0.05
Tie Points Accuracy (px)	0.1
Reprojection Error filter	0.3
Control Points error (m)	0.0003
Check Points error (m)	0.0004
Sigma0	0.97

The correlation between the radial coefficients (Figure 4) is physiological and depends on the structure of the model itself; for this reason, we can neglect it. The decentring distortion is also strongly projectively coupled with the principal point offset, and, in general, this relationship increases with focal length or when a poor convergence of the image axes occurs.

	Value	Error	F	Cx	Cy	K1	K2	K3	P1	P2
F	12598.7	0.672439	1.00	0.04	-0.22	-0.16	0.22	-0.18	0.03	-0.06
Cx	90.3494	0.986818		1.00	-0.03	-0.07	0.06	-0.08	0.97	-0.06
Cy	-19.782	1.30691			1.00	-0.28	0.37	-0.28	-0.02	0.55
K1	-0.0405119	0.000623855				1.00	-0.92	0.83	-0.09	-0.11
K2	0.731	0.0138645					1.00	-0.97	0.08	0.08
K3	-1.60927	0.0861545						1.00	-0.09	-0.07
P1	0.00267437	2.95114e-05							1.00	-0.05
P2	-0.000827401	2.39623e-05								1.00

Figure 4. Correlation analysis between camera calibration coefficients.

These reasons confirm that the correlation is negligible.

Based on the exterior and interior orientation parameters, the dense image matching phase (section 2.3) was then performed. A list of the parameters governing the procedure is summarised in Table 3.

Table 3. Error reduction and reference system parameters consistent with input data.

Parameter	Setting
Quality	High
Depth filtering	Moderate
RGB data	Yes
Points Confidence	Yes

The high-quality setting used in our applications implies preliminary image size downscaling by a factor of 4 (2 by each side), a good compromise between model density and computational load. The moderate depth filter was selected to preserve the small, discernible details in the scene to be reconstructed. The noise remotion was carried out after the generation of the Dense Cloud. Unfortunately, the confidence-based filter working process is blinded, therefore we rely on the indications provided by the developers, according to which the relevant part of the noise belongs to the range 1-5. After filtering, the SfM process can be considered terminated.

3.2. Towards tolerance limit formation

After deriving the error ellipsoid with k = 3 from the covariance matrix and selecting the major semi-axis, its distribution was studied to build an appropriate tolerance interval. This tool allowed us to estimate, from a sample, the extremes that contain a certain percentage of a population (p) with a specific level of confidence (α).

The appropriate construction of tolerance intervals takes into account the type of distribution, making it possible to compare different statistical models, involving several steps: (i) test for normality, which, if satisfied, leads to the calculation of normal tolerance limits; (ii) searching for normalising transformation, to be implemented when the distribution is not normal. If it deviates only slightly, an acceptable

transformation is found, and normal tolerance limits can be calculated from transformed data; (iii) alternative distributions to be performed when the transformation approach fails by searching for a good fit so that tolerance limits from that distribution can be calculated; (iv) non-parametric tolerance limits when the others approach fails. In any case, it must be ensured that the sample size is adequate for the statistical treatment. All intervals are computed for a population percentage of p = 95% and a confidence value of α = 95%. It should be borne in mind that, in the case of non-parametric tolerance limit calculations, only one of these two features can be defined, the other being estimated downstream of the procedure. In that case, preventive treatment of the distributions may be necessary to eliminate possible outliers, e.g., by constructing a box-plot diagram. Precisely the latter approach was applied to the case study fixing α = 95%, and Figure 5 shows the actual distribution of the major semi-axes of the ellipsoids with k = 3. The approach, therefore, seems reasonable, considering that the tie points will constitute only a part of the final photogrammetric cloud.

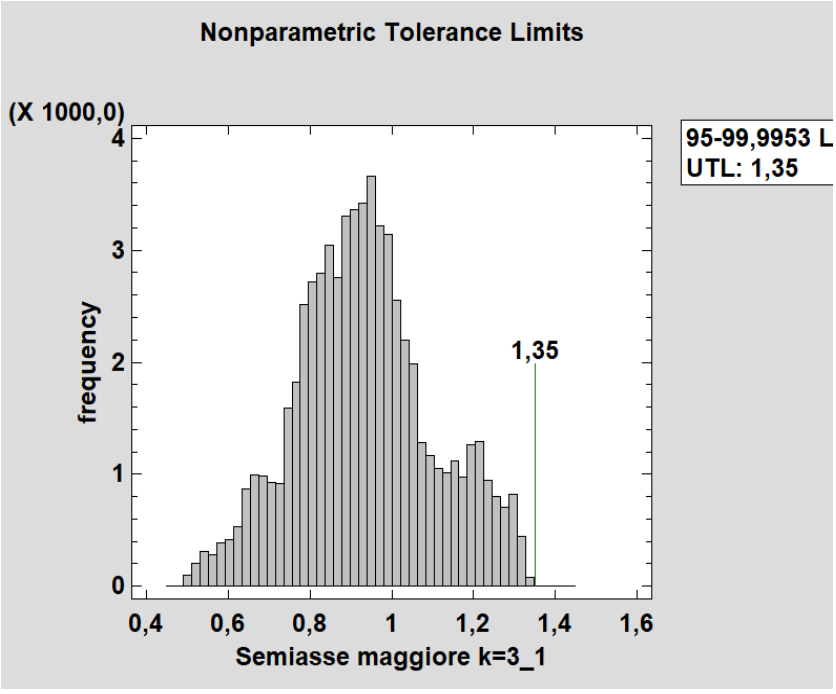

Figure 5. Distribution of lengths of major semi-axes with k = 3 and upper tolerance limit.

To be fair, the dense image-matching phase and its algorithms should also be involved, but this would become too complicated. Thus, we chose to employ the Structure from Motion classic workflow for the subsequent steps. Since the semi-axis length is a positive definite quantity, we outlined a one-sided interval, obtaining an upper tolerance limit of 1.35 mm, which can be used as an indicator of the accuracy of the entire photogrammetric process.

4. Conclusions

The question of photogrammetric survey data traceability is becoming more relevant than ever. There is still ambiguity about how to define the error, given the numerous parameters that control the processing workflow and the countless factors that can affect it. In the absence of more reliable analyses, the error on GCPs and CPs is not representative and does not justify any defects in the modelling, leaving the reasons for deficiencies hidden and not allowing for process improvement.

This study aimed to address this demand by attempting to achieve accuracy traceability while also providing maximum adaptability and flexibility to the requirements of the potential case studies and proposing possible solutions. In fact, to define the project requirements and assess the accuracy of geometric features, a procedure has been proposed. This is based on the reliability of the data processing that was observed to create source-based virtualisation.

One advantage of the suggested methodology is that it ensures a level of accuracy in the modelling phase can be easily traced. Thus, making the framework repeatable and compatible with data from various sensors. In detail, the procedure is robust, as it involves all tie points that survive the filtering phase. For them, it examines the covariance matrix, deriving the error ellipsoid and analysing the distribution of the lengths of the major semi-axes. This study was conducted in a rigorous manner. The distribution hardly ever follows the normal curve; therefore, position and dispersion indicators, such as mean and standard deviation, do not always describe the phenomenon effectively. In contrast, statistical tolerance intervals make it possible to overcome this ambiguity and derive a representative indicator that can be compared with the results of other photogrammetric processes.

Future developments will concentrate on a more detailed description

of the survey-related uncertainty components and the opportunity to specify accuracy levels during a preliminary design phase in accordance with the client's desired tolerances.

References

1. Brusaporci, S., 2017. The Importance of Being Honest: Issues of Transparency in Digital Visualization of Architectural Heritage. In Ippolito, A. (ed), *Handbook of Research on Emerging Technologies for Architectural and Archaeological Heritage*. IGI Global: Hershey, Pennsylvania, USA, pp. 66-93.
2. Remondino, F., Del Pizzo, S., Kersten, T., Troisi, S., 2012. Low Cost and open-source solutions for automated image orientation – A critical overview. *Lecture Notes in Computer Science,* 7616, 40-54.
3. Morena, S., Barba, S., Álvaro-Tordesillas, A., 2019. Shining 3D Einscan-Pro, application and validation in the field of Cultural Heritage, from the Chillida-Leku Museum to the Archaeological Museum Of Sarno. *Int. Arch. Photogramm. Remote Sens. Spatial Inf. Sci.*, XLII-2/W18, 135-142.
4. Puerto, P., Heißelmann, D., Müller, S., Mendikute, A., 2022. Methodology to Evaluate the Performance of Portable Photogrammetry for Large-Volume Metrology. *Metrology* 2, pp. 320-334.
5. Dai, F., Feng, Y., Hough, R., 2014. Photogrammetric error sources and impacts on modeling and surveying in construction engineering applications. *Visualisation in Engineering* 2(2), pp. 1-14.
6. Chetverikov, D., Svirko, D., Stepanov, D., Krsek, P., 2002. The Trimmed Iterative Closest Point algorithm. *Object recognition supported by user interaction for service robots* 3, pp. 545-548.
7. Lague, D., Brodu, N., Leroux, J., 2013. Accurate 3D comparison of complex topography with terrestrial laser scanner: Application to the Rangitikei canyon (N-Z). *ISPRS Journal of Photogrammetry and Remote Sensing* 82, pp. 10-26.
8. Luhmann, T., 2010. Close range photogrammetry for industrial applications. *ISPRS Journal of Photogrammetry and Remote Sensing* 65, pp. 558-569.
9. Nocerino, E., Menna, F., Remondino, F., 2014. Accuracy ff typical photogrammetric networks in Cultural Heritage 3D modeling projects. *The International Archives of the Photogrammetry, Remote Sensing and Spatial Information Sciences*, Volume XL-5, pp. 465-472.
10. Barazzetti, L., 2017. Network Design in Close-Range Photogrammetry with Short Baseline Images. *Int. Arch. Photogramm. Remote Sens. Spatial Inf. Sci., IV-2/W2*, 17-23.
11. Luhmann, T., Robson, S., Kyle, S., Boehm, J., 2014. *Close-Range photogrammetry and 3D Imaging*. De Gruyter: Boston, Massachusetts, USA.
12. Marino, M., 2010. *Le Sirene di Kroton*. Museo Archeologico Nazionale di Crotone: Crotone, Italy, p. 23.
13. Parrinello, S., La Placa, S., 2019. Vectorialization practices of the image drawing of the floor mosaics of the Basilica of Nativity in Bethlehem, *SCIRES-IT, SCIentific RESearch and Information Technology*, Volume IX (II), 95-104.

14. Nex, F., Remondino, F., 2014. UAV for 3D mapping applications: a review. *Applied Geomatics*, *6(1)*, 1-15.
15. Over, J.R., Ritchie, A.C., Kranenburg, C.J., Brown, J.A., Buscombe, D., Noble, T., Sherwood, C.R., Warrick, J.A., and Wernette, P.A., 2021. *Processing Coastal Imagery With Agisoft Metashape Professional Edition, Version 1.6 - Structure From Motion Workflow Documentation*. U.S. Geological Survey: Reston, Virginia, pp. 23-25.
16. Gujski, L.M., di Filippo, A., Limongiello, M., 2022. Machine Learning Clustering for Point Clouds Optimisation via Feature Analysis in Cultural Heritage. *Int. Arch. Photogramm. Remote Sens. Spatial Inf. Sci.*, *XLVI-2/W1-2022*, 245-251.
17. Creagh, L.T., McDonald, M., 2003. Design and Performance of Inkjet Print Heads for Non-Graphic-Arts Applications. *MRS Bulletin, 28*, 807-811 (2003).
18. Remondino, F., Fraser, C., 2006. Digital camera calibration methods: considerations and comparisons. *The International Archives of the Photogrammetry, Remote Sensing and Spatial Information Sciences*, *36(5)*, 266-272.
19. Tang, R., 2013. *Mathematical Methods for Camera Self-Calibration in Photogrammetry and Computer Vision*. Deutsche Geodätische Kommission: München, Germany.

In *Optical 3D Metrology (O3DM), Würzburg, Germany, 15-16 December 2022*.

in press

Approfondimenti

A chiusura di questo lavoro si presentano tre approfondimenti con il duplice scopo di: esaminare e chiarire alcuni aspetti dei processi descritti nelle precedenti pubblicazioni, non trattati per ragioni di sintesi; e aggiornare il lettore sugli ultimissimi sviluppi e su aspetti della ricerca che possono risultare ancora inediti.

Il primo approfondimento riguarda la teoria della fotografia e l'analisi della profondità di campo, in quanto una consapevole messa a fuoco del manufatto che ci si accinge a riprodurre è un parametro imprescindibile poiché influente sul dato input del processo fotogrammetrico. Mettere a fuoco significa – a seconda della distanza dal soggetto – regolare la distanza fra il centro del sistema ottico e il piano immagine su cui giace il sensore, al fine di riprodurre un'immagine nitida.

Teoricamente, si parla di nitidezza quando un una fonte luminosa puntiforme nello spazio oggetto è proiettata nello spazio immagine degenerando in un punto; tuttavia, nella realtà ciò si traduce in una piccola area circolare. Parimenti, estendendo il ragionamento agli infiniti punti costituenti un oggetto, si osserverà che questi saranno proiettati in un numero infinito di microscopiche aree circolari – le cui circonferenze risulteranno sovrapposte – definite come "cerchi di confusione" (CoC). Quanto più piccoli sono i cerchi di confusione, tanto maggiore apparirà nitida l'immagine (funzione della distanza da cui si si osserva la stessa), ragion per cui si parla di nitidezza 'apparente', in riferimento alla dimensione del CoC ritenuta accettabile in base alla distanza di osservazione. Inoltre, mettere a fuoco equivale a garantire la nitidezza – apparente – non solo del punto dato, ma di un certo intervallo spaziale definito "profondità di campo" (DoF): uno spazio caratterizzato da un'estensione enormemente variabile in relazione a più parametri quali lunghezza focale, distanza dal soggetto, distanza principale, apertura di diaframma e diametro del cerchio di confusione.

La comprensione dei rapporti geometrici che legano queste grandezze

è fondamentale per la gestione della DoF, per la scelta dell'ottica, funzione a sua volta dell'oggetto da acquisire e delle condizioni al contorno e, in sostanza, per l'impostazione della campagna di rilievo e la qualità del modello digitale finale.
Il secondo approfondimento riguarda l'ingrandimento nei microscopi USB, un parametro che ne definisce le prestazioni, ma che non trova una chiara definizione per questa nuova tipologia di strumenti. L'ingrandimento è la capacità di un microscopio di produrre un'immagine di un oggetto a una scala più grande (o anche più piccola) della sua dimensione effettiva.
Nonostante i microscopi tradizionali e i microscopi USB utilizzino entrambi una serie di lenti per fornire una visione ingrandita di un campione, il relativo potere di ingrandimento è definito spesso in modo diverso. Infatti, i microscopi digitali utilizzano sensori elettronici (quelli di una fotocamera) per sostituire gli oculari dei microscopi tradizionali e restituiscono l'immagine a monitor, attraverso l'interfaccia software del microscopio, con la possibilità di più dimensioni fisiche e risoluzioni pixel. Quindi, a causa della varietà delle dimensioni del sensore e delle risoluzioni dei display elettronici, determinare l'ingrandimento nel campo della microscopia digitale può risultare un po' più difficoltoso.
Il terzo approfondimento, infine, riflette sulla necessità – ancora non soddisfatta per chi voglia condividere e far circolare modelli digitali di oggetti, con particolare riferimento alla piccola scala – di avere accesso a un sistema di acquisizione tridimensionale efficiente e a basso costo.
Tenendo conto della diffusione su larga scala della fotografia digitale e delle sue applicazioni fotogrammetriche, la customizzazione di accessori dedicati può permettere un controllo del processo fotogrammetrico nel caso di strumentazioni professionali e financo migliori risultati nel caso di strumentazioni più entry-level. Inoltre, con particolare riferimento all'impiego di microscopi USB, l'utilizzo di una componentistica progettata ad hoc è ulteriormente motivato da fattori specifici, quali il campo visivo estremamente ridotto, il difficoltoso controllo delle vibrazioni, la necessità di condurre acquisizioni per prese convergenti e l'elevato numero di scatti da realizzare in tempi auspicabilmente contenuti.

1. La profondità di campo

Assumendo come sufficientemente valide le semplificazioni dell'ottica geometrica in ipotesi di lenti sottili[1], per definire una generica ottica fotografica (detta anche semplicemente lente) è necessario conoscerne lunghezza focale[2] (*l*) e apertura massima[3] (f/N). Ad esempio, relativamente alle ottiche utilizzate in questo lavoro, si chiarisce che sono state impiegate due ottiche macro, l'*AF-S VR Micro-Nikkor 105 mm f/2.8G IF-ED* e l'*AF-S Micro NIKKOR 60 mm f/2.8G ED*, di lunghezze focali rispettive di 105 mm e 60 mm e apertura massima pari a f/2.8.
È quindi quasi d'obbligo avanzare una prima riflessione, specifica per la fotografia ravvicinata, spesso omessa dalle case produttrici e che non sempre si riscontra nella letteratura della disciplina del disegno: la cosiddetta lunghezza focale dichiarata, il cui valore, nella maggior parte dei casi, è valido solo a elevate distanze di messa a fuoco. A mano a mano che ci si avvicina alla minima distanza di messa a fuoco (nel nostro caso F = 314 mm per il 105 mm e F = 185 mm per il 60 mm), la lunghezza focale si riduce, di poco nelle ottiche fisse, di più negli zoom, di più ancora in quelle macro; una riduzione della lunghezza focale alle brevi distanze negli obiettivi è, quindi, da considerare fisiologica, complice la progettazione IF, a lenti flottanti (che in molte ottiche contribuisce a mantenere una buona qualità anche a distanza ravvicinata). Ciò risulta di grande importanza per il calcolo dell'ingrandimento desiderato e dunque per la quantificazione del GSD del progetto fotogrammetrico. A tale proposito, si osservino i libretti a corredo degli obiettivi impiegati (Figura 1 e Figura 2). Le riportate "focused distance", tradotte in italiano come distanza di messa a fuoco, non si devono intendere quali "working distance", ovvero una distanza di lavoro (spazio utile tra ottica e oggetto) e neppure quale distanza tra il centro ottico e l'oggetto (*d*).

[1] Dal momento che un obbiettivo fotografico diventa assimilabile a una lente, anche se composto da un gruppo di più lenti, i termini 'lente', 'ottica' e 'obbiettivo' possono essere utilizzati alla stregua di sinonimi, ad esempio ai fini della descrizione della DoF.
[2] Distanza caratteristica, espressa in millimetri, che il centro ottico della lente (anche detto centro di proiezione del sistema) assume rispetto al suo fuoco quando la messa a fuoco è regolata su un oggetto infinitamente lontano.
[3] Massimo valore che assume il rapporto tra la lunghezza focale (*l*) dell'obbiettivo e il diametro dell'apertura del diaframma (*dd*), espresso sottoforma di frazione (f/N) in cui valore numerico N fa riferimento a una progressione (stop) il cui passo è tale da raddoppiare (o dimezzare) il flusso luminoso.

■ 被写界深度表 ■ Depth of field ■ Schärfentiefentabelle ■ Profondeur de champ
■ Profundidad de campo ■ Profondità di campo ■ Βάθος πεδίου ■ 景深刻度表 ■ 景深刻度表 (m)

•撮影距離 •Focused distance •Eingestellte Entfernung •Distance de mise au point •Distancia de enfoque •Distanza messa a fuoco •Απόσταση εστίασης •对焦距离 •聚焦距離			•被写界深度 •Depth of field •Schärfentiefe •Profondeur de champ •Profundidad de campo •Profondità di campo •Βάθος πεδίου •景深 · 景深				•撮影倍率 •Reproduction ratio •Abbildungsmaßstab •Rapport de reproduction •Relación de reproducción •Rapporto di riproduzione •Λόγος αναπαραγωγής •成像率 •成像率		
	f/2.8*	f/4*	f/5.6*	f/8*	f/11*	f/16*	f/22*	f/32*	
0.314	0.31 — 0.32	0.31 — 0.32	0.31 — 0.32	0.31 — 0.32	0.31 — 0.32	0.31 — 0.32	0.31 — 0.32	0.31 — 0.32	1/1.0
0.33	0.33 — 0.34	0.33 — 0.34	0.33 — 0.34	0.33 — 0.34	0.33 — 0.34	0.33 — 0.34	0.33 — 0.34	0.33 — 0.34	1/1.3
0.35	0.35 — 0.35	0.35 — 0.35	0.35 — 0.35	0.35 — 0.35	0.35 — 0.35	0.35 — 0.35	0.35 — 0.35	0.35 — 0.35	1/1.4
0.37	0.38 — 0.38	0.38 — 0.38	0.37 — 0.38	0.37 — 0.38	0.37 — 0.38	0.37 — 0.38	0.37 — 0.38	0.37 — 0.38	1/1.7
0.4	0.40 — 0.40	0.40 — 0.40	0.40 — 0.40	0.40 — 0.40	0.40 — 0.40	0.39 — 0.40	0.39 — 0.40	0.39 — 0.40	1/2.0
0.45	0.45 — 0.45	0.45 — 0.45	0.45 — 0.45	0.45 — 0.45	0.45 — 0.46	0.45 — 0.46	0.45 — 0.46	0.44 — 0.46	1/2.5
0.5	0.50 — 0.50	0.50 — 0.50	0.50 — 0.50	0.50 — 0.50	0.50 — 0.51	0.49 — 0.51	0.49 — 0.51	0.49 — 0.51	1/3.0
0.6	0.59 — 0.60	0.59 — 0.60	0.59 — 0.60	0.59 — 0.60	0.59 — 0.60	0.59 — 0.61	0.58 — 0.61	0.58 — 0.62	1/3.9
0.8	0.79 — 0.80	0.79 — 0.80	0.79 — 0.80	0.78 — 0.80	0.78 — 0.81	0.77 — 0.82	0.77 — 0.82	0.75 — 0.84	1/5.8
1	0.99 — 1.00	0.99 — 1.01	0.99 — 1.01	0.98 — 1.02	0.97 — 1.02	0.96 — 1.04	0.95 — 1.05	0.93 — 1.08	1/7.8
1.5	1.49 — 1.52	1.48 — 1.53	1.47 — 1.54	1.46 — 1.55	1.45 — 1.57	1.42 — 1.61	1.39 — 1.65	1.34 — 1.72	1/12.7
3	2.94 — 3.08	2.91 — 3.11	2.87 — 3.15	2.82 — 3.22	2.75 — 3.31	2.65 — 3.48	2.54 — 3.70	2.37 — 4.14	1/27.1
∞	116.20 — ∞	81.39 — ∞	58.19 — ∞	40.79 — ∞	29.71 — ∞	20.48 — ∞	14.94 — ∞	10.33 — ∞	1/∞

Figura 1. Valori di distanza di messa a fuoco, profondità di campo e rapporto di riproduzione per l'ottica AF-S VR Micro-Nikkor 105 mm f/2.8G IF-ED (dichiarati dal produttore).

■ 被写界深度表 ■ Depth of field ■ Schärfentiefentabelle ■ Profondeur de champ ■ Profundidad de campo
■ Skärpedjup ■ Глубина резкости ■ Scherptediepte ■ Profondità di campo ■ Hloubka ostrosti
■ Hĺbka ostrosti ■ 景深刻度表 ■ 景深刻度表 ■ 초점 심도 (m)

•撮影距離 •Focused distance •Eingestellte Entfernung •Distance de mise au point •Distancia de enfoque •Fokusavstånd •Дистанция съемки •Scherpstelafstand •Distanza messa a fuoco •Ostřící vzdálenost •Zaostriteľná vzdialenosť •对焦距离 •對焦距離 •초점비			•被写界深度 •Depth of field •Schärfentiefe •Profondeur de champ •Profundidad de campo •Skärpedjup •Глубина резкости •Scherptediepte •Profondità di campo •Hloubka ostrosti •Hĺbka ostrosti •景深 •景深 •심도			•撮影倍率 •Reproduction ratio •Abbildungsmaßstab •Rapport de reproduction •Relación de reproducción •Reproduktionsratio •Масштаб съемки •Reproductieverhouding •Rapporto di riproduzione •Poměr reprodukce •Reprodukčný pomer •成像率 •重現比率 •복사율		
	f/2.8*	f/4*	f/5.6*	f/8*	f/11	f/16*	f/22*	f/32*	
0.185	0.19 – 0.19	0.19 – 0.19	0.19 – 0.19	0.19 – 0.19	0.19 – 0.19	0.18 – 0.19	0.18 – 0.19	0.18 – 0.19	1/1.0
0.2	0.20 – 0.20	0.20 – 0.20	0.20 – 0.20	0.20 – 0.20	0.20 – 0.20	0.20 – 0.20	0.20 – 0.20	0.20 – 0.20	1/1.3
0.23	0.23 – 0.23	0.23 – 0.23	0.23 – 0.23	0.23 – 0.23	0.23 – 0.23	0.23 – 0.23	0.23 – 0.23	0.23 – 0.23	1/1.85
0.3	0.30 – 0.30	0.30 – 0.30	0.30 – 0.30	0.30 – 0.30	0.30 – 0.30	0.29 – 0.31	0.29 – 0.31	0.29 – 0.31	1/3.06
0.5	0.50 – 0.50	0.49 – 0.51	0.49 – 0.51	0.49 – 0.51	0.48 – 0.52	0.48 – 0.53	0.47 – 0.54	0.46 – 0.56	1/6.43
1	0.97 – 1.03	0.97 – 1.04	0.95 – 1.05	0.93 – 1.08	0.91 – 1.11	0.88 – 1.12	0.84 – 1.26	0.78 – 1.45	1/14.78
∞	38.01 – ∞	27.37 – ∞	19.56 – ∞	13.69 – ∞	9.96 – ∞	6.86 – ∞	4.99 – ∞	3.44 – ∞	1/∞

Figura 2. Valori di distanza di messa a fuoco, profondità di campo e rapporto di riproduzione per l'ottica AF-S Micro NIKKOR 60mm f/2.8G ED (dichiarati dal produttore).

Con "focused distance" (F) si intende, infatti, la distanza tra l'oggetto e il sensore, esprimibile come somma delle distanze oggetto-centro ottico (d) e centro ottico-sensore[4] (c):

$$F = d + c \ . \tag{1}$$

Per la verifica dell'ingrandimento di un dato o desiderato, occorre calcolare il valore effettivo di lunghezza focale. A partire dalla definizione geometrica di ingrandimento[5] e sfruttando l'equazione delle lenti sottili, tale valore è calcolabile in funzione delle variabili d e c come segue:

$$\frac{1}{d} + \frac{1}{c} = \frac{1}{l} \rightarrow l = \left(\frac{1}{d} - \frac{1}{c}\right)^{-1}, \tag{2}$$

in cui $d = F/(R + 1)$ e $c = F - d$.

Una considerazione meno banale riguarda la quantità c; come noto, tale distanza in fotogrammetria costituisce uno dei parametri dell'orientamento interno, calcolato in fase di calibrazione. Di norma è approssimata ad l dichiarata, poiché la variazione tra le due – nonché la differenza tra la l dichiarata e la l calcolata – è trascurabile, sia per gli ordini di grandezza della scala architettonica sia per le distanze assunte rispetto all'oggetto. Si può dimostrare però che in fotogrammetria macro tale approssimazione non è più accettabile: si noti dalle tabelle alla pagina seguente che valori sia di c che di l prossimi alla lunghezza focale dichiarata, per le due ottiche fisse macro prese in considerazione, si ottengono solamente per una distanza del sensore dall'oggetto di 3 m per il 105 mm e di 1 m per il 60 mm (Figura 3 e Figura 4), valori per i quali il rapporto di riproduzione non risulta adatto per applicazioni macro.
Per il calcolo della profondità di campo è necessaria un'ulteriore considerazione: sulla dimensione del cerchio di confusione. È banale osservare che una volta messo a fuoco l'oggetto, i suoi punti, rifratti sul piano focale (sensore) vadano a ricomporre l'immagine che apparirà nitida perché correttamente ricostruita come punti, o meglio come cerchi apparentemente puntiformi.

[4] Quest'ultima anche nota in ambito fotogrammetrico come "distanza principale".
[5] Rapporto tra le dimensioni dell'immagine di un oggetto (sul sensore) e le relative dimensioni reali dello stesso oggetto: relazione espressa anche come il rapporto tra le distanze c e d (triangoli simili).

Tabella 1. Valori di distanza oggetto-centro ottico (*d*), distanza centro ottico-sensore (*c*) e lunghezza focale (*l*), in mm, per l'AF-S VR Micro-Nikkor 105 mm f/2.8G IF-ED, sulla base dei valori di F e R dichiarati dal produttore.

Focused distance (F)	Reproduction ratio (R)	*d*	*c*	*l*
314	1,000	157,00	157,00	78,50
330	0,794	183,98	146,02	81,41
350	0,690	207,14	142,86	84,55
370	0,588	232,96	137,04	86,28
400	0,500	266,67	133,33	88,89
450	0,400	321,43	128,57	91,84
500	0,333	375,00	125,00	93,75
600	0,256	477,55	122,45	97,46
800	0,172	682,35	117,65	100,35
1000	0,128	886,36	113,64	100,72
1500	0,079	1390,51	109,49	101,50
3000	0,037	2893,24	106,76	102,96

Tabella 2. Valori di distanza oggetto-centro ottico (*d*), distanza centro ottico-sensore (*c*) e lunghezza focale (*l*), in mm, per l'AF-S Micro NIKKOR 60mm f/2.8G ED, sulla base dei valori di F e R dichiarati dal produttore.

Focused distance (F)	Reproduction ratio (R)	*d*	*c*	*l*
185	1,000	92,50	92,50	46,25
200	0,769	113,04	86,96	49,15
230	0,541	149,30	80,70	52,39
300	0,327	226,11	73,89	55,69
500	0,160	432,71	67,29	58,24
1000	0,068	936,63	63,37	59,36

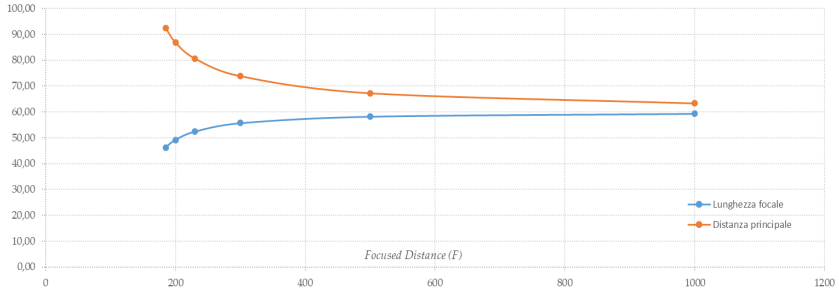

Figura 3. In ordinate i valori assunti [in mm] dalla lunghezza focale e della distanza principale rispetto alla distanza di messa a fuoco in ascisse [in mm] per l'AF-S Micro NIKKOR 60mm f/2.8G ED (sulla base dei valori di distanza di messa a fuoco e rapporto di riproduzione dichiarati dal produttore).

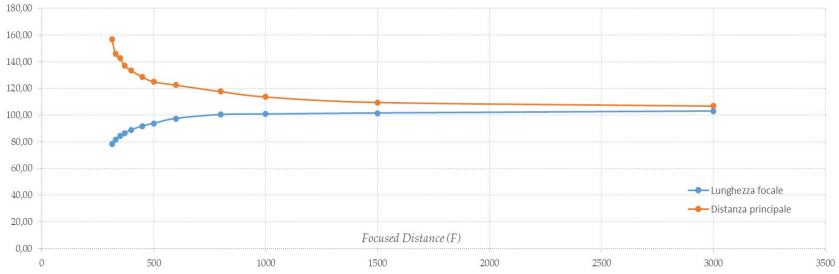

Figura 4. In ordinate i valori assunti [in mm] dalla lunghezza focale e della distanza principale rispetto alla distanza di messa a fuoco in ascisse [in mm] per l'AF-S VR Micro-Nikkor 105 mm f/2.8G IF-ED (sulla base dei valori di distanza di messa a fuoco e rapporto di riproduzione dichiarati dal produttore).

Quando la dimensione di questi cerchi – cerchi di confusione – raggiunge valori tali che l'occhio umano non sarà più in grado di distinguerli o discriminarli come cerchi, si ottiene apparentemente la migliore messa a fuoco: di conseguenza, la dimensione del diametro del cerchio di confusione ne rappresenta la discriminante.

Si ammetterà, quindi, che se si vuole rendere un'immagine estremamente nitida, sarà necessario ridurre il valore del diametro del cerchio di confusione. In altre parole, ciò significa garantire che le proiezioni dei punti di un oggetto siano ancora percepibili come puntiformi, ovvero da cerchi – di confusione – sufficientemente piccoli. In generale, il valore di riferimento accettabile per tale diametro corrisponde convenzionalmente al seguente principio empirico:

osservando una stampa delle dimensioni di 20×25 cm da una distanza di 32 cm, l'occhio umano sarà mediamente in grado di distinguere linee distanti tra loro non meno di 0,2 mm. A ciò si fa corrispondere, dunque, un cerchio di confusione pari a 0,2 mm, valore che allude alla linea più sottile che sia possibile distinguere. Un sensore FX, tuttavia, non misura 20×25 cm, ma 24×36 mm; ciò significa che per riprodurlo su un formato 20×25 cm la sua diagonale dovrà essere ingrandita di circa 7,4 volte. Ne deriva che, ricorrendo a una semplice proporzione sia possibile stimare il diametro accettabile del cerchio di confusione sul sensore:

$$d_{print} : d_{sensor} = \emptyset CoC_{print} : \emptyset CoC_{sensor} , \quad (3)$$

in cui le quantità note saranno: d_{print}, che corrisponde alla misura della diagonale della stampa; d_{sensor}, che corrisponde alla misura della diagonale del sensore, e $\emptyset CoC_{print}$, che corrisponde al valore del cerchio di confusione assunto per la stampa 20×25 cm. L'incognita sarà $\emptyset CoC_{sensor}$ che rappresenta il valore del diametro del cerchio di confusione sul sensore, pari quindi a: 0,20/7,4 = 0,027 mm.

Questo valore si trova in numerosi programmi di calcolo online e App per smartphone che, appunto, per sensori di 24×36 mm, propongono un diametro del cerchio di confusione pari a circa 0,03 mm.

Questa stima del valore del CoC però è funzione delle dimensioni del supporto e della distanza di osservazione; analisi sulla nitidezza, che trascendono la distanza di osservazione, possono risultare più restrittive, tendendo a invalidare il metodo empirico. A tale proposito, il problema si rivela più oneroso quando, ad esempio, diamo questi dati in pasto ad algoritmi che ragionano sul singolo pixel e non sulla distanza di osservazione dell'immagine, come ad esempio i software SfM. Per essere più precisi, allora, è sufficiente avanzare una stima più esatta del cerchio di confusione: in pratica, si può assegnare al CoC non più una quantità misurata in millimetri, ma una quantità misurata in pixel, il cui valore in millimetri diventerà più o meno restrittivo a seconda del sensore utilizzato. Ad esempio, nel caso del sensore FX di una Nikon D800E, con una diagonale di 43,18 mm a cui corrisponde una diagonale di 8849 px, è facile calcolare la dimensione del singolo pixel: *pixel size* = 0,0049 mm. Quindi, il valore sulla base del quale sarà possibile determinare il cerchio di confusione non sarà funzione di una

prefissata dimensione in millimetri, ma dipenderà dal numero di pixel sul sensore, corrispondenti alla dimensione minima distinguibile, pari ad almeno 3 px[6]. Da ciò si ricava un valore più oggettivo da attribuire al diametro del cerchio di confusione per il sensore specifico:

$$ØCoC = pixel\ size \cdot 3 = 0{,}0049 \cdot 3 = 0{,}015mm \quad (4)$$

Nel caso si osserva un valore più piccolo, all'incirca la metà del valore convenzionalmente proposto. A partire da una stima più consapevole di questo valore, si disporrà di un set di dati input più solido da utilizzare per il successivo calcolo della profondità di campo.

Considerando che il cerchio di confusione rappresenterà il 'limite' entro il quale sarà contenuta la dimensione dell'immagine di un punto spaziale, esisteranno due piani immagine posti alle distanze c_1 e c_2 a cavallo della distanza principale c, tali che le immagini dei punti ricompresi all'interno di questo intervallo spaziale avranno grado di sfocatura sempre inferiore – e al massimo uguale – al cerchio di confusione (perché proiettati all'interno o degeneranti nella circonferenza). Geometricamente questa condizione è garantita imponendo il passaggio dei raggi provenienti dallo spazio oggetto e rifratti nello spazio immagine per il limite superiore e per il limite inferiore del diametro del cerchio di confusione (Figura 5).

Per semplicità, si metta a fuoco un punto appartenente all'asse ottico alla distanza d e si ottenga la sua immagine – ovviamente sempre appartenente all'asse ottico – nello spazio immagine alla distanza c rispetto al centro di proiezione. Nota l'apertura di diaframma, i raggi in ingresso passeranno per gli estremi del diaframma e convergeranno quindi sul piano del sensore. A tale piano appartiene anche il cerchio di confusione, per cui è possibile tracciare i raggi che, passando per i suoi estremi e per gli estremi del diaframma, individuano univocamente la posizione dei due piani immagine posti alle distanze c_1 e c_2. Alle distanze c_1 e c_2, secondo l'equazione delle lenti sottili corrispondono, le distanze d_1 e d_2.

Tutto quello che è posto tra queste due distanze risulterà di nitidezza equivalente a quella di un soggetto alla esatta distanza di messa a fuoco d.

[6] Geometrie ottiche e profondità di campo nelle fotocamere reflex digitali: www.nikonschool.it/experience/geometrie3.php.

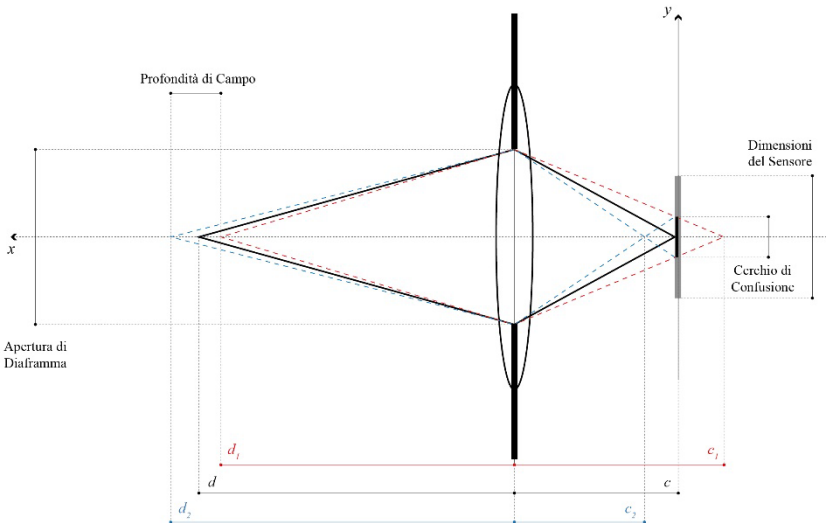

Figura 5. Schema ottico per la determinazione dell'area nitida (compresa tra d_1 e d_2) rispetto alla dimensione del cerchio di confusione.

Si può quindi concludere che la profondità di campo sia la porzione di spazio a cavallo della quale è eseguita la messa a fuoco; tale spazio è delimitato da due piani (limite anteriore e limite posteriore) all'interno dei quali tutti i punti hanno un diametro inferiore al diametro del cerchio di confusione. Se riduciamo il diaframma, gli angoli formati dalle rette tratteggiate in rosso e in blu si stringono (Figura 6). Continuando a fare passare tali rette per i margini del cerchio di confusione si otterranno nello spazio immagine punti di intersezione con l'asse ottico a distanze maggiori rispetto a c. Corrispondentemente, nello spazio oggetto, si allontaneranno tra di loro anche le distanze d_1 e d_2, incrementando quindi la DoF (Figura 6). Le distanze d_1 e d_2 sono ricavate analiticamente dalla equazione delle lenti sottili per formula inversa:

$$d_n = \left(\frac{1}{l} - \frac{1}{c_n}\right)^{-1}. \tag{5}$$

Si può quindi notare che quando la distanza c_2 coincide con la distanza l, ovvero coincide con la lunghezza focale, il piano limite corrispondente alla distanza d_2 va all'infinito. In queste condizioni, cioè con una DoF che includa l'infinito, la distanza d viene detta distanza iperfocale ed inoltre il punto d_1 si troverà a metà strada tra d e il centro ottico della lente.

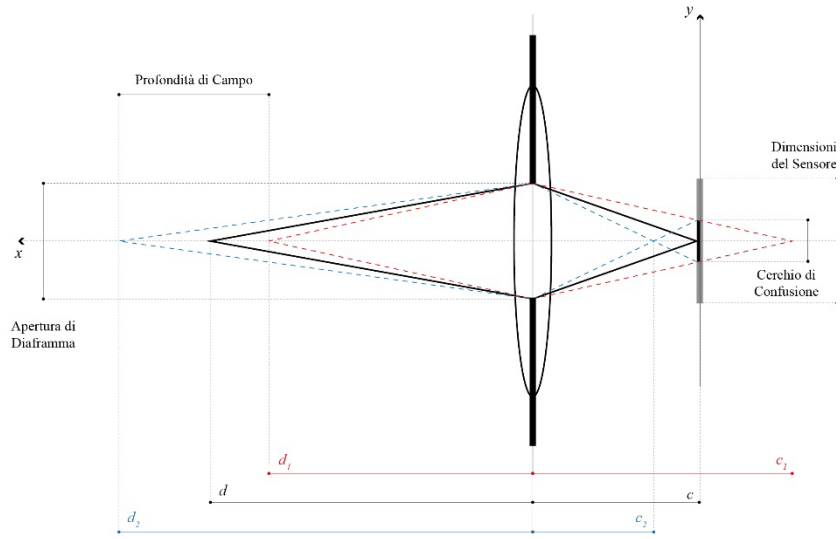

Figura 6. Schema ottico per la determinazione dell'area nitida (compresa tra d_1 e d_2) rispetto alla dimensione del cerchio di confusione.

Si propone, alla fine delle seguenti dimostrazioni, una serie di formule pratiche per ricavare immediatamente le incognite fondamentali del problema. Tali formule sono state riversate in un foglio di calcolo digitale progettato dall'autore (qui raggiungibile: http://bit.ly/3E6ZjOi). Considerando lo schema grafico in Figura 7, la prima operazione da fare è calcolare le immagini c_1 e c_2 a partire dai dati noti.

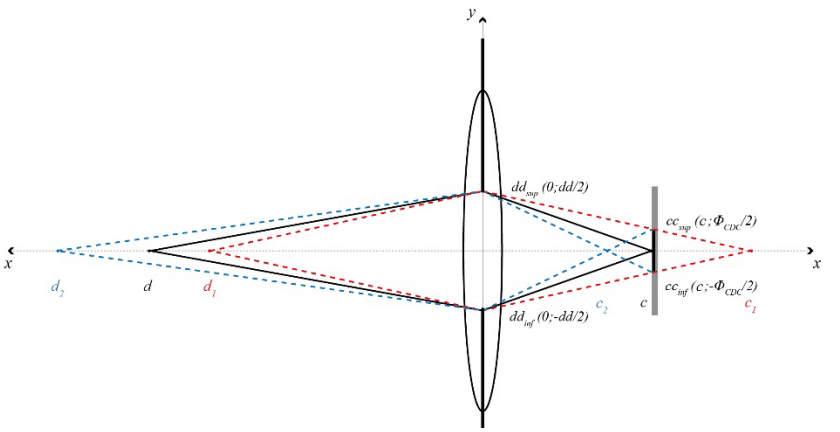

Figura 7. Schema ottico per la determinazione della profondità di campo.

Si imposta allora l'equazione di una retta passante per due punti, che nel caso di c_1 possono essere ad esempio DD_{sup} e CC_{sup} e nel caso di c_2 possono essere ad esempio DD_{sup} e CC_{inf}:

$$\frac{y-\frac{dd}{2}}{\frac{\emptyset_{CDC}}{2}-\frac{dd}{2}} = \frac{x}{c}, per\ x = c_1\ , \tag{6}$$

$$\frac{y-\frac{dd}{2}}{-\frac{\emptyset_{CDC}}{2}-\frac{dd}{2}} = \frac{x}{c}, per\ x = c_2\ . \tag{7}$$

Da cui si ottengono:

$$y = x\left(\frac{(\frac{\emptyset_{CDC}}{2}-\frac{dd}{2})}{c}\right)+\frac{dd}{2}, per\ x = c_1\ , \tag{8}$$

$$y = x\left(\frac{(-\frac{\emptyset_{CDC}}{2}-\frac{dd}{2})}{c}\right)+\frac{dd}{2}, per\ x = c_2\ . \tag{9}$$

Imponendo y = 0, si ottiene l'intersezione di queste rette con l'asse delle ascisse (che rappresenta l'asse ottico):

$$c_1 = \frac{dd\cdot c}{dd-\emptyset_{CDC}}\ , \tag{10}$$

$$c_2 = \frac{dd\cdot c}{dd+\emptyset_{CDC}}\ . \tag{11}$$

A questo punto è possibile ricavare dall'equazione delle lenti sottili la posizione di d_1 e d_2:

$$d_1 = \left(\frac{1}{l}-\frac{1}{c_1}\right)^{-1}\ , \tag{12}$$

$$d_2 = \left(\frac{1}{l}-\frac{1}{c_2}\right)^{-1}\ . \tag{13}$$

Per la seguente trattazione il sistema di riferimento ha origine nel centro ottico, per cui la (12) rappresenta la distanza più vicina al centro ottico da considerare accettabile in termini di nitidezza, mentre la (13) rappresenta la distanza più lontana al centro ottico da considerare accettabile in termini di nitidezza.

La profondità di campo è data quindi da:

$$d_1 - d_2 \,. \tag{15}$$

Calcolare la distanza iperfocale H è banale se si considera che, se $c_2 = l$, allora $d_2 \rightarrow \infty$ e $d_1 = H$. È sufficiente allora imporre:

$$c_2 = \frac{dd \cdot \mathrm{c}}{dd + \emptyset_{CDC}} = l \,. \tag{16}$$

Da cui si ricava:

$$c = \frac{l(dd + \emptyset_{CDC})}{dd} \,. \tag{17}$$

E per applicazione dell'equazione delle lenti sottili:

$$H = \left(\frac{1}{l} - \frac{1}{c}\right)^{-1} \,. \tag{18}$$[7]

A valle di queste considerazioni sulla 'natura' della profondità di campo è opportuno non trascurare il peso della varietà, per dimensione e soprattutto densità di pixel, di sensori digitali disponibili; ciò obbliga a una revisione delle indicazioni tabellate di profondità di campo – così come degli altri parametri discussi, che nel panorama attuale perdono una loro assolutezza – e, di conseguenza, a una maggior attenzione alla progettazione delle acquisizioni.

2. Microscopi USB e ingrandimento

Un microscopio USB è un sistema costituito da un ottica zoom macro collegata a una fotocamera che si interfaccia, mediante un software, direttamente con il display di un computer (senza la necessità di un oculare). Anche con queste attrezzature, la qualità dell'immagine finale dipenderà ancora dalla qualità dell'obbiettivo e del sensore, nonché dall'illuminazione aggiuntiva (sorgenti luminose LED integrate che circondano l'obbiettivo). In particolare, alcuni modelli della casa produttrice Dino-Lite consentono anche una regolazione dell'esposizione; il diaframma, invece, è sempre fisso (in Tabella 3, si riportano, inoltre, le dimensioni del sensore del microscopio Dino-Lite AM7013MZT).

[7] La forma della (18) è equivalente a quella proposta da Allen R. Greenleaf, 1950. *Photographic Optics*. The MacMillan Company, New York.

Tabella 3. Caratteristiche dimensionali del sensore del microscopio Dino-Lite AM7013MZT.

sensor size [px]		**sensor size [mm]**		
X_S	Y_S	X_S	Y_S	Pixel Size
2592	1944	3,67	2,74	0,00142

Una delle caratteristiche principali di questi strumenti – oltre il campo visivo, "Field Of View" (FOV), ovvero l'area visibile attraverso l'interfaccia software del microscopio in funzione dell'ingrandimento – è la distanza di lavoro, "Working Distance" (WD), definibile come la distanza tra l'estremità del microscopio e l'oggetto visualizzato. Una terza caratteristica riguarda, invece, la profondità di campo, "Depth Of Field" (DoF), intesa sempre come lo spazio tra i punti più vicini e più lontani che appaiono più nitidi durante la visualizzazione di un dato oggetto. Questi microscopi USB dispongono di una ghiera numerata che ha la funzione di regolare il grado di ingrandimento, azionando il sistema di lenti per la messa a fuoco. In base a tale funzionamento, per utilizzare questi dispositivi si possono seguire due approcci. Il primo è definito "Distance-based": il dispositivo è utilizzato a una distanza prestabilita, di conseguenza è regolata la messa a fuoco e l'ingrandimento che ne deriva. Il secondo è definito "Magnification-based": il dispositivo è utilizzato a un ingrandimento prestabilito, di conseguenza è posizionato poi manualmente alla distanza che consente di osservare il campione (o una sua porzione specifica) alla nitidezza sufficiente. L'ingrandimento dei microscopi USB costituisce, quindi, un'ulteriore discriminante per le applicazioni fotogrammetriche: un parametro non 'assoluto' ma 'relativo' alla dimensione della finestra di visualizzazione dell'interfaccia software del microscopio (a sua volta dipendente dalle specifiche del monitor che si sta utilizzando e che prende il nome di ingrandimento digitale[8]). Per esempio, nel caso dei microscopi Dino-Lite, il software proprietario DinoCapture 2.0, presenta un'interfaccia con una finestra di visualizzazione delle acquisizioni, delle dimensioni 213×157 mm (così auto-settata per il monitor di un Alienware m15 Ryzen Edition R5 alla risoluzione di 2560×1440 px).

[8] Some Useful Guidelines for Understanding Magnification in Today's New Digital Microscope Era: https://leica-microsystems.com/science-lab/what-does-300001-magnification-really-mean/.

Figura 8. Dimensioni in millimetri della finestra di cattura in DinoCapture 2.0 (con un monitor 15" e risoluzione di 2560×1440 px).

Come suggerito dalla stessa Dino-Lite USA, l'ingrandimento utilizzato – che può discostarsi dai valori riportati sulla ghiera – può essere verificato confrontando le dimensioni effettive del campione con la dimensione occupata sullo schermo. Allo scopo, in Figura 8 (in cui si opera con una regolazione, sulla relativa ghiera, dell'ingrandimento pari a 50×) è inquadrata una scala graduata che può facilitare il calcolo del suddetto rapporto. Si può osservare che 5 mm reali corrispondono a un segmento di 135,5 mm visualizzato sullo schermo, da cui si ricava un ingrandimento di circa 27× (≅135,5/5). Un calcolo equivalente si può sviluppare conoscendo il campo inquadrato, per esempio lungo la direzione orizzontale (X_F), in funzione della relativa dimensione della finestra di visualizzazione (X_W). Dalle specifiche riportate dal produttore, è allora banalmente desumibile per ciascuno step (Tabella 4), l'ingrandimento definibile come 'effettivo' (M_{eff}).

C'è da osservare che le differenze con gli ingrandimenti dichiarati (gli step della ghiera in Figura 9) sono da imputare, quindi, a valutazioni del produttore in funzione di una visualizzazione a monitor di risoluzione di 1280×720 px, all'epoca considerata come standard. Questo perché i valori in discussione fanno riferimento a un ingrandimento digitale, che sfrutta la visualizzazione a monitor e che può 'ingannare' il rilevatore nel valutare la qualità dell'immagine acquisita in relazione a un dato ingrandimento (digitale).

Tabella 4. Ingrandimento 'effettivo' calcolato per il microscopio Dino-Lite AM7013MZT sulla base dei valori di FOV dichiarati dal produttore (in funzione di un monitor di 15" con risoluzione di 2560×1440 px).

step	X_F [mm]	X_W [mm]	M_{eff}
20×	19,8	213	11×
30×	13,2	213	16×
40×	9,9	213	22×
50×	7,9	213	27×
60×	6,6	213	32×
220×	1,8	213	118×
230×	1,7	213	125×

Per essere più chiari, l'immagine visualizzata a monitor, prescindendo dalla risoluzione utilizzata, appare di qualità modesta nella finestra di interfaccia software, nonostante un valore di ingrandimento elevato. Ciò si nota anche con il file immagine salvato: questo, aperto e visualizzato al 100%, se osservato attentamente, svela la relativa maglia pixel. Quindi, ai fini della valutazione della qualità dell'immagine, oltre all'ingrandimento è da considerare l'interpolazione del segnale.

Figura 9. Step di ingrandimento per la regolazione manuale sui microscopi Dino-Lite.

Attualmente diffuso, specialmente per sensori molto piccoli (al di sotto di 1") è l'impiego del "pixel binning", un processo di combinazione dei dati di più pixel adiacenti in un unico pixel di dimensioni maggiori, al fine di aumentare il rapporto segnale/rumore a discapito di una riduzione della densità di campionamento e della risoluzione.

Per le ragioni sovraesposte, ai fini fotogrammetrici può essere utile riferirsi all'ingrandimento sul sensore (M_{sensor}), piuttosto che a quello digitale, che risulta infatti impiegabile ai fini di una stima a priori della distanza principale (cfr. § *Capitolo 6*). M_{sensor} definisce, dunque, un ingrandimento sul sensore in funzione dell'ottica ed è esprimibile come il rapporto tra la dimensione del sensore (X_S) e l'area inquadrata (X_F):

$$M_{sensor} = \frac{X_S}{X_F} \,. \tag{19}$$

Applicando tale relazione è possibile valutare l'ingrandimento dell'obbiettivo per ogni step della ghiera (Tabella 5).

Banalmente sarà poi possibile mettere in relazione la (19) con i valori di ingrandimento digitale.

Tabella 5. Valori dell'ingrandimento sul sensore comparati con gli step di ingrandimento sulla ghiera graduata del microscopio Dino-Lite AM7013MZT.

step	X_S [mm]	X_F [mm]	M_{sensor}
20×	3,7	19,8	0,2×
30×	3,7	13,2	0,3×
40×	3,7	9,9	0,4×
50×	3,7	7,9	0,5×
60×	3,7	6,6	0,6×
220×	3,7	1,8	2×
230×	3,7	1,7	2,2×

3. Target, calibratori e supporti

I target costituiscono, come risaputo, punti di coordinate spaziali note da introdurre nella scena fotografata per irrobustire la stima della struttura del modello di fotocamera, ovvero il calcolo dei parametri che

mappano la proiezione dalle coordinate spaziali a quelle immagine (processo anche noto come "Camera Calibration"). Sebbene questa fase possa essere condotta anche direttamente sulla base delle caratteristiche o trame naturali dell'oggetto, tempi di calcolo inferiori e maggiore accuratezza convalidano l'utilizzo dei target. Il loro scopo, infatti, oltre a definire un sistema di coordinate locali e la scala del modello, è teso a evidenziare corrispondenze reali per migliorare la procedura di allineamento delle prese fotografiche.

Il target sono punti univocamente riconoscibili ad alto contrasto con una particolare geometria e possono essere codificati o non codificati (Figura 10). Quelli codificati sono identificati automaticamente dall'algoritmo fotogrammetrico, limitando una certa ambiguità di posizionamento; il loro design e distribuzione tende a generare un gran numero di punti univoci minimizzando la dimensione del pattern. Tra le tipologie disponibili, i più comuni per un impego fotogrammetrico sono a codifica circolare e denominati Circular Coded Target - CCT (Figura 10a). Per essere rilevati con successo, questi target devono occupare un numero significativo di pixel sulle foto originali e nel caso di CCT si raccomanda che il raggio del cerchio centrale bianco sia almeno pari a 4-5 pixel; sono supportati anche bersagli circolari non codificati o a croce (Figura 10b), il cui rilevamento è possibile solo dopo che l'allineamento della camera è terminato. A titolo esemplificativo, il software di SfM Agisoft Metashape supporta quattro tipi di CCT, a 12 bit, 14 bit, 16 bit o 20 bit; se il pattern a 12 bit è considerato decodificato in modo più preciso, i pattern a 14 bit, 16 bit e 20 bit consentono di utilizzare un numero maggiore di CCT all'interno dello stesso progetto. Il riconoscimento dei target codificati avviene tramite l'inserimento automatico di "marker" nelle catture a cui sono successivamente associate le coordinate per geolocalizzare le immagini.

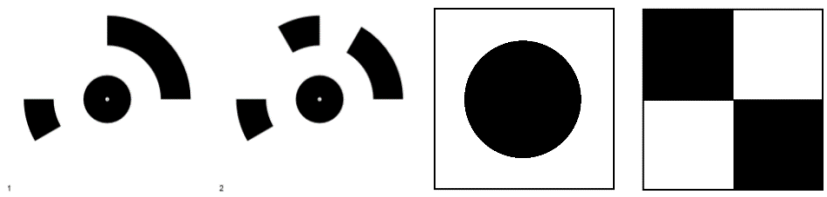

(**a**) (**b**)

Figura 10. Esempio di target: (**a**) target codificati; (**b**) target non codificati.

C'è da accennare che il rilevamento automatico dei target può condurre a sotto-stimarne o sovra-stimarne il numero effettivo. Anche per tale ragione, è sempre necessario un check da parte del rilevatore. La sovra-rilevazione, ad esempio, può essere risolta ordinando i marker per numero di proiezioni ed eliminando quelli 'estranei' al progetto, ovvero con un numero basso di proiezioni. In alternativa, in fase di importazione delle coordinate, l'utente può avere l'accortezza di assegnare ai marker importati la medesima nomenclatura di quelli rilevati – sapendo che in caso di sovra-stima quelli importati saranno in numero minore – e poi eliminare tutte quelli di cui non si evidenzierà una corrispondenza.
Nel caso di Metashape, il software distingue due 'tipologie' di marker: i "Control Points", che corrispondono a marker utilizzati per georeferenziare il modello; i "Check Points", che non partecipano al processo di ottimizzazione dell'allineamento delle camere ma sono utilizzati per controllare, come suggerisce il nome, o validare i risultati della stessa ottimizzazione. I valori (stimati) dei Check Points possono essere confrontati con i valori (misurati) dei Control Points, sempre tenendo in considerazione che i primi sono calcolati solo sulla base della minimizzazione dell'errore di riproiezione e non corrispondono a valori accomodati dal Bundle Adjustment.
Alla luce delle funzionalità dell'utilizzo di target codificati per la stima del modello di fotocamera, ne è stato implementato l'impiego attraverso la fabbricazione specifica di oggetti di calibrazione (calibratori o "reference object") bidimensionali o tridimensionali. La scelta dell'oggetto di calibrazione deve tenere conto dell'accuratezza progettuale richiesta e della precisione perseguibile nella produzione dei target. Generalmente, oggetti di calibrazione tridimensionali dovrebbero condurre a risultati migliori, per il disaccoppiamento dei parametri intrinseci ed estrinseci e per la presenza di informazioni distinte sulla profondità che riducono la correlazione tra la lunghezza focale e la distorsione della lente. Purtroppo, la realizzazione di un target 3D accurato si rivela un obiettivo più complesso e costoso. Per tale ragione, sono più comuni e accessibili modelli di calibrazione planari come schemi bidimensionali, solitamente stampati su carta, che includono punti rilevabili come centri dei target o angoli di scacchiera dislocati in posizioni note.

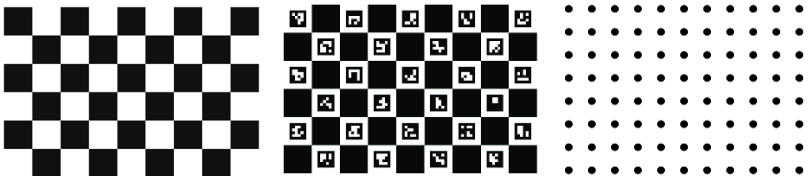

Figura 11. Esempio di modelli di calibrazione: (a) Motivo a scacchiera; (b) Modelli CharuCo; (c) Griglie circolari.

Tuttavia, stampare motivi di piccole dimensioni che siano adeguati alla scala di piccoli oggetti può comportare approssimazioni dovute alla scarsa risoluzione della stampante con la produzione di motivi di stampa imprecisi. Ciononostante, è dimostrata in letteratura la possibilità di validare modelli di calibrazione – al netto delle imprecisioni del motivo stampato – per ingrandimenti moderati e attraverso una misurazione con una macchina di misura a coordinate CMM del pattern realizzato[9]. Un fattore che influenza la tipologia del pattern di riferimento è relativo all'algoritmo di machine learning che si utilizzerà per il riconoscimento[10]; librerie come OpenCV, MVTec Halcon o libCalib e software come Calib Camera Calibrator, lasciano comunque una certa libertà per quanto riguarda i diversi modelli implementabili (Figura 11). Nel caso della calibrazione della camera dei microscopi USB sono stati progettati piccoli motivi a scacchiera su carta adesiva poi fissati a supporti rigidi orizzontali, con passo di 1 mm (Figura 12), dimensionati in funzione dell'area utile del microscopio a un predeterminato ingrandimento digitale (circa 19,8×14,9 mm a 20×). I "reference object" utilizzati in questo lavoro sono stati realizzati con tecniche differenti in funzione delle necessità operative e dei limiti strumentali. Nel caso dei calibratori "3Dino Plate" (Figura 13) l'intenzione è stata quella di avere un piano d'appoggio con punti noti per la scala, l'ottimizzazione del modello e l'agevolazione del riconoscimento di features omologhe in ambiente Agisoft Metashape.

[9] Percoco, G., Salmerón, A.J.S. *3D image based modelling for inspection of objects with micro-features, using inaccurate calibration patterns: an experimental contribution.* International Journal on Interactive Design and Manufacturing 2017, *11*, 415-425.

[10] Percoco, G., Lavecchia, F., Sánchez Salmerón, A.J.S. *Preliminary Study on the 3D Digitization of Millimeter Scale Products by Means of Photogrammetry*. In Proceedings of 9th CIRP Conference on Intelligent Computation in Manufacturing Engineering, Procedia CIRP Volume 33, Teti R. (Ed); Capri, Italy, 23-25 Luglio 2015, pp. 257-262.

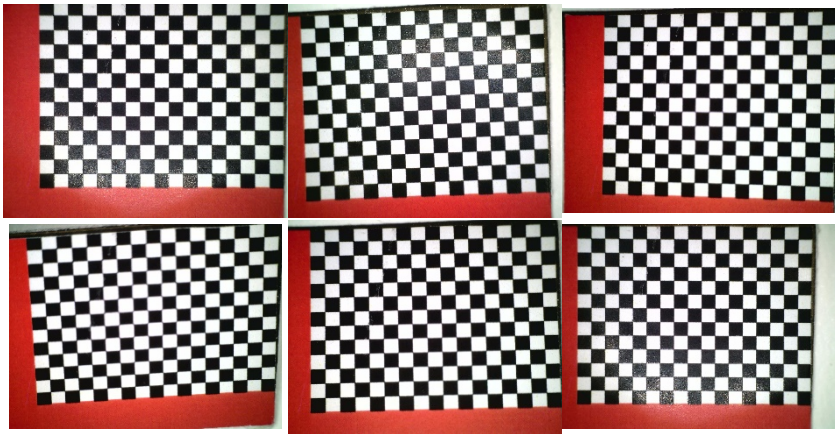

Figura 12. Alcuni scatti del motivo a scacchiera per la calibrazione della camera di un microscopio Dino-Lite allo zoom di 20×.

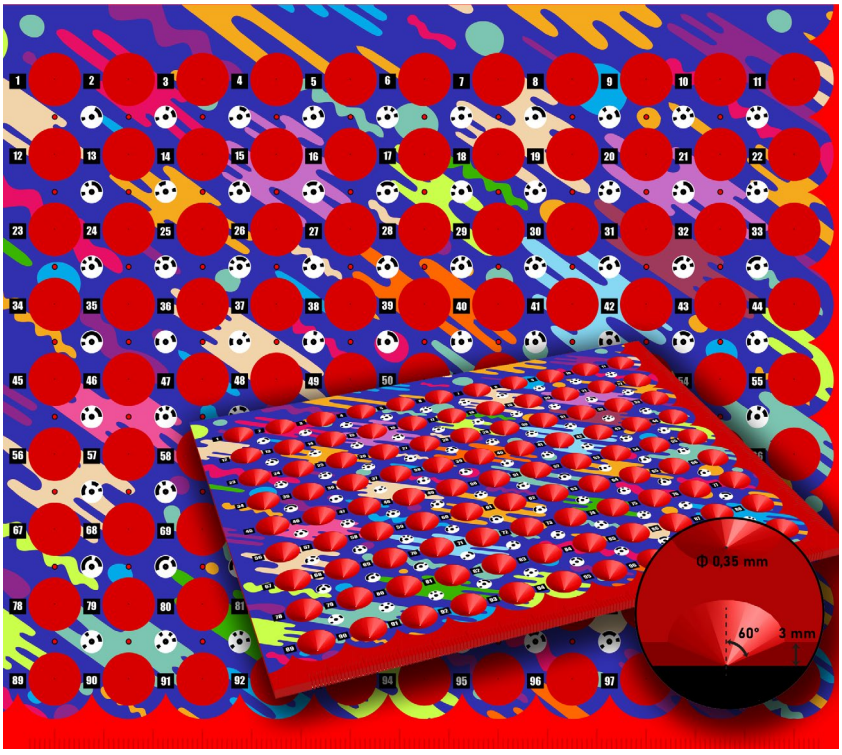

Figura 13. Il calibratore tridimensionale "3Dino Plate 1.0" (in PLA ottenuto con la stampante 3D Creality CR-10) con sovrapposto un pattern adesivo a target codificati.

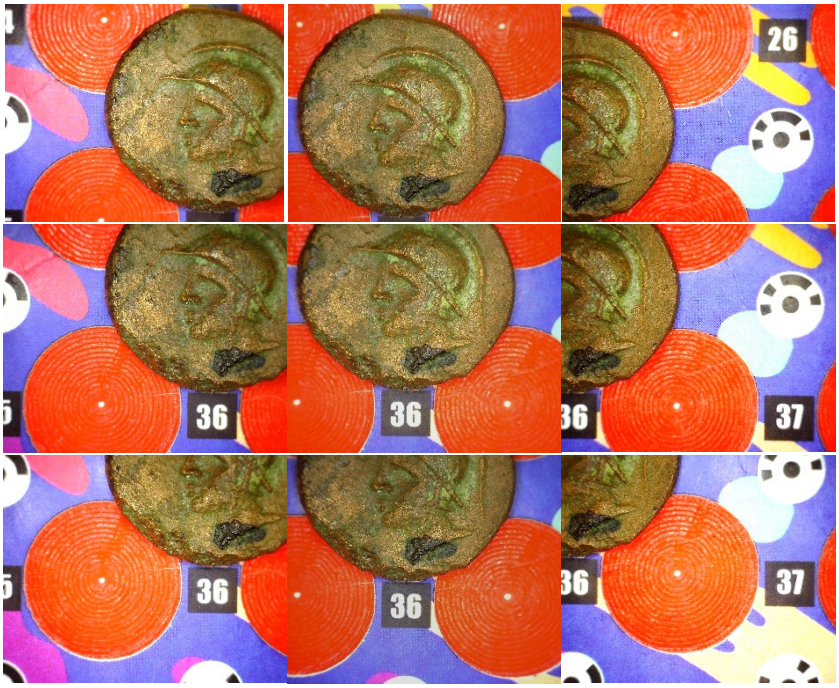

Figura 14. Una serie di acquisizioni con microscopio Dino-Lite a prese parallele con calibratore "3Dino Plate 1.0".

La presenza di fori a quota di -3 e -2mm, rispettivamente per la versione 1.0 e 2.0 del 3Dino Plate, è motivata dalla necessità di introdurre informazioni sulla dimensione Z, soprattutto per geometrie di acquisizione a prese prevalentemente parallele (Figura 14).
Il calibratore, una piastra 3D con fori troncoconici (dettaglio in basso a destra di Figura 13), è stato realizzato con processi di manifattura additiva (stampa 3D) a tecnologia FDM (Fused Deposition Modeling), ovvero per estrusione da ugello e successiva stratificazione di un filamento plastico fuso. La stampante utilizzata è una stampante a movimento cartesiano la 3D Creality CR-10 v 1.0, con le seguenti specifiche di stampa (il tempo occorso è stato di circa 13 ore): temperatura di letto (heatbed) pari a 50°C; temperatura dell'ugello (hotend) pari a 200°C; diametro dell'ugello di 0,3mm; materiale utilizzato, il PLA (poliacido lattico) con filamento di 1,75mm +/- 0,05mm di diametro; altezza di layer pari a 0,12mm; infill al 20% del tipo pattern cubic; velocità di stampa di 50mm/s.

Le caratteristiche intrinseche del PLA rendono le stampe realizzate con questo materiale soggette a un deterioramento relativamente rapido; ciò ha spinto a considerare inizialmente valida la scelta del PLA per la fase di codificazione della piastra e un suo uso immediato.
Si intende, inoltre, che l'impiego dei 3Dino Plate sia adatto a oggetti prevalentemente piani, dovendo la profondità di campo progettata attestarsi sui 5 mm per comprendere sia il calibratore che l'oggetto. In ambito micro, però, tale valore è incredibilmente alto da raggiungere in assenza di elaborazioni digitali delle immagini, quali la nota procedura di focus stacking, per cui le versioni successive del piatto calibrato sono state realizzate con profondità dei fori minori, fino ad arrivare ad 1 mm nell'ultimo prototipo.
Tale modello più avanzato di piatto calibrato (Figura 15), è stato realizzato con tecnica di fabbricazione additiva, a letto polvere con fascio laser, mediante la EOS M270, Xtended version. Il materiale impiegato è polvere di acciaio commercializzata come EOS GP1, corrispondente allo standard UNS S17400, anche identificato come 17-4 PH.
Per verificarne le eventuali criticità di stampa è stato realizzato un campione (Figura 16), con tre file e tre colonne di fori secondo le specifiche di progetto assegnate.
Da un'analisi macroscopica, il primo campione risultava deformato per effetto dei gradienti termici che si manifestano durante la fabbricazione; la problematica è stata risolta nella produzione del piatto prevedendo un trattamento termico post processo prima della rimozione del componente dalla piattaforma di costruzione. La superficie esibisce una rugosità media di 6.3μm, in linea con la rugosità attesa, ma con la superficie del foro troncoconico che non risulta regolare; quest'ultimo dato è comunque trascurabile poiché i coni hanno la sola funzione di non occludere la visione del fondo del foro nel caso di prese inclinate. A ogni modo, allo stato attuale, con le tecnologie descritte, la fabbricazione presenta piccole deviazioni dalle misure di progetto, valutabili nell'ordine dei decimi di millimetro, ad esempio: il diametro della direttrice al fondo dei fori misura mediamente 0,33mm (0, 35 da progetto), con un interasse medio fra i relativi centri di 14,939mm (15 da progetto). Ciò impone una misurazione a valle del processo produttivo per la determinazione delle coordinate effettive dei punti di controllo del calibratore tridimensionale, una sorta di certificazione del prodotto.

Figura 15. Il calibratore tridimensionale in acciaio "3Dino Plate 3.0".

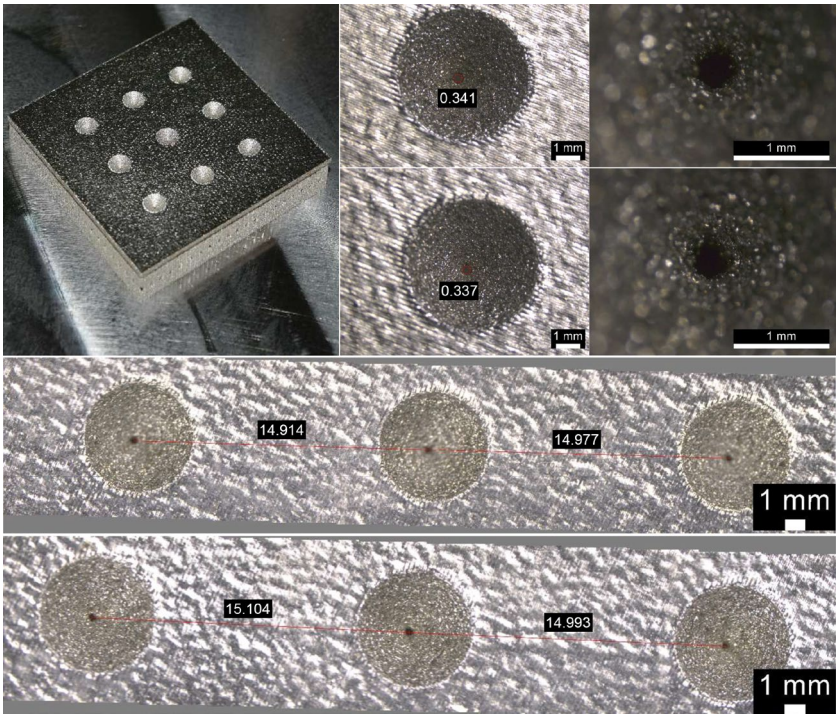

Figura 16. Analisi macroscopica dell'accuratezza del calibratore da fabbricazione additiva a letto di polvere d'acciaio a fascio laser con EOS M270.

Figura 17. Il calibratore bidimensionale, con pattern adesivo, per tavola rotante.

Come accennato, un'alternativa più accessibile e di facile realizzazione è rappresentata dalla progettazione di adesivi da disporre su piani rigidi, eventualmente tavole rotanti, caratterizzati da schemi bidimensionali. L'accortezza in questi casi riguarda principalmente la sola planarità del supporto, in alcuni casi invalidata da sbalzi di temperatura o variazioni di umidità, oltre che dalla fragilità del materiale. Un ulteriore fattore compromettente può essere la riflettività della carta utilizzata o, in caso contrario, il suo basso contrasto: è quindi buona norma utilizzare materiali opachi, impermeabili e non eccessivamente porosi. Infine, c'è da considerare – anche in questi casi – l'opportunità di controllare a priori l'accuratezza della stampa, anche da un punto di vista cromatico (così da avere in un solo oggetto anche un color-checker).
Il modello di riferimento in Figura 17 e in Figura 18 è caratterizzato da 56 target a 16-bit, codificati e circolari, generati automaticamente da Agisoft Metashape, omogeneamente distribuiti e di dimensioni crescenti all'allontanarsi dal centro della tavola (per meglio rispondere alle diverse dimensioni degli oggetti da digitalizzare).

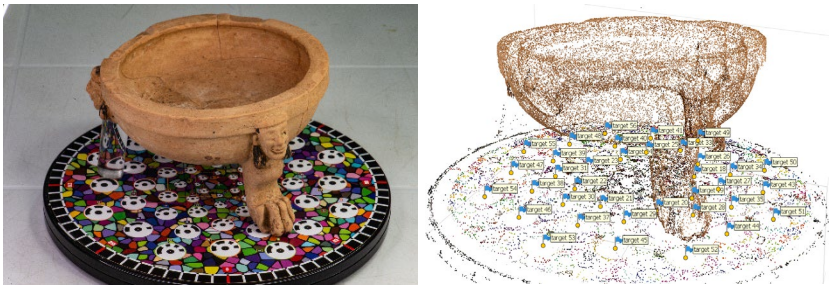

(**a**) (**b**)

Figura 18. Riconoscimento automatico dei target per un calibratore adesivo del diametro di 19 cm: (a) immagine fotografica dal set in input; (b) target sulla nuvola sparsa.

Come si può osservare il pattern è così finalizzato alla scalatura del modello, oltre al miglioramento delle prestazioni degli algoritmi di rilevamento/corrispondenza dei Key Points e, quindi, di calibrazione della camera; la grafica e le coordinate del calibratore sono state progettate ad hoc così da poter essere importate nel progetto fotogrammetrico (il modello e le coordinate da importare sono accessibili al seguente link: http://bit.ly/3E6ZjOi).

Per facilitare e velocizzare il processo di acquisizione, nonché inserire opportunamente i microscopi digitali USB nel workflow fotogrammetrico, è stato assemblato un primo prototipo per la sistematizzazione di un vero e proprio sistema di digitalizzazione low-cost basato sul paradigma fotogrammetrico, denominato "3DINO SYSTEM". Il sistema è costituito da una serie di supporti meccanici il cui telaio è completamente stampato in 3D e la cui componentistica accessoria è costituita anche da pezzi standard disponibili sul mercato. Il progetto è stato sviluppato con il supporto del Dipartimento di Ingegneria Industriale dell'Università di Salerno e ruota attorno al concetto di modularità; difatti, le singole componenti possono essere anche utilizzate separatamente e adattate a diverse specifiche esigenze. Il processo di realizzazione delle componenti è avvenuto per tecnologia FDM (Fused Deposition Modeling) con l'impiego di una stampante cartesiana, la Prusa i3 MK2.5S[11] (Figura 19). I filamenti utilizzati sono in PLA per le parti accessorie e ABS (acrilonitrile-butadiene-stirene), per i componenti meccanici strutturali da sottoporre a sollecitazioni più consistenti.

[11] Prusa, J. *3D Printing Handbook*, Prusa Research a.s.: Praga, Repubblica Ceca, 2020.

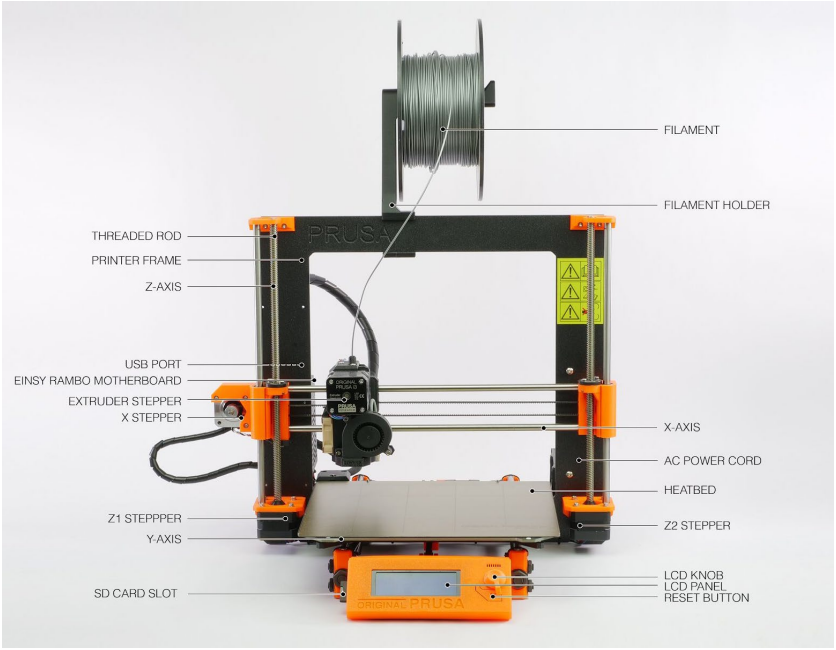

Figura 19. Schema della stampante cartesiana 3D Original Prusa i3 MK2.5S.

Infatti, il PLA ha un'ottima finitura superficiale, seppur tra i materiali più economici per la stampa 3D, abbinata a una bassa dilatazione termica rispetto agli altri materiali; le componenti realizzate in PLA però non sono progettate per poter essere soggette a sforzi meccanici, essendo il materiale duro e fragile, né per essere esposte a più forti fonti di calore (si registrerebbe un processo di ammorbidimento oltre i 60°C) e, come prima accennato, non resistendo bene se esposto ad agenti atmosferici. Quindi, per ottenere le parti necessariamente più durevoli si è fatto ricorso all'ABS, pur essendo questo più difficile da stampare a causa della maggiore flessibilità, è impiegato per ottenere parti durevoli. Il diametro dei filamenti, dettato dalle specifiche della stampante, è stato di 1,75 mm per entrambi i materiali impiegati.
Queste le specifiche di stampa: temperatura di estrusione (hotend) pari a 210°C e quella del letto riscaldato (heatbed) pari a 60°C per il PLA e 100°C per l'ABS; altezza di layer di 0,15 mm; infill 10% con pattern a nido d'ape; velocità di stampa media pari a 60 mm/s. Valori che hanno portato a un tempo complessivo di stampa di circa 7 giorni (comprensivo delle rifiniture).

Le diverse parti, la base (Figura 10 ai numeri 1-5), la costola (7-10) e il supporto (6), possono essere opportunamente collegate e movimentate (Figura 20, 21 e 22), garantendo, in primis, la rotazione del supporto per gli oggetti, indipendentemente dall'inclinazione dell'ottica che potrà così rimanere fissa durante il processo di digitalizzazione (corrispondente, ad esempio, a rotazioni a 360° dell'oggetto rispetto all'asse z 'secondario' a ciascuna delle quali è associata una particolare inclinazione dell'asse ottico).

La base di appoggio si compone di due pezzi: un rettangolo inferiore (1, in verde), dove è allocata una slitta (4, in grigio) vincolata allo scorrimento lungo una guida in direzione longitudinale (secondo la direzione di un asse z 'principale'). Il movimento della slitta avviene tramite un ingranaggio meccanico (5, in viola e ciano) del tipo vite-madrevite (anche detto chiocciola-vite senza fine). Il rapporto di trasmissione di tale ingranaggio è pari a:

$$\frac{2mm}{giro} \Leftrightarrow \frac{2mm}{2\pi\, rad}\,. \tag{20}$$

La madrevite di tale ingranaggio è attualmente fissata alla base tramite una squadretta avvitata; la vite senza fine è, invece, vincolata in estremità assialmente alla slitta, permettendo di conservare il grado di libertà rotazionale della stessa vite. Sulla slitta, mediante filettature, è apposta la costola dentata che costituisce la parte principale dell'attrezzatura (10, in grigio, descritta in seguito). La base presenta, poi, una zona circolare di raggio pari a 180 mm formata da due parti concentriche (1, in verde e 2 in rosa). Tra queste è stato creato un vano tecnico necessario per l'inserimento di tre ruote dentate (3, in giallo) di modulo 2, (parametro su cui si basa il dimensionamento dell'ingranaggio, definito come il rapporto tra il diametro primitivo[12] e il numero di denti della ruota) con rapporto di trasmissione (rapporto tra le due velocità angolari) pressocché unitario. La prima (posizionata al centro del sistema) e la terza (sporgente a destra), che consente all'operatore di azionare la rotazione alla base del supporto centrale (6, in viola), sono parzialmente visibili.

[12] Il diametro associato alla circonferenza lungo la quale avviene il contatto della coppia di ruote dentate, corrispondente alla ruota di frizione fittizia atta a trasmettere il moto (C. Pidatella, G. Ferrari Aggradi, D. Pidatella, *Corso di Meccanica*, Zanichelli: Bologna, Italia, 2010).

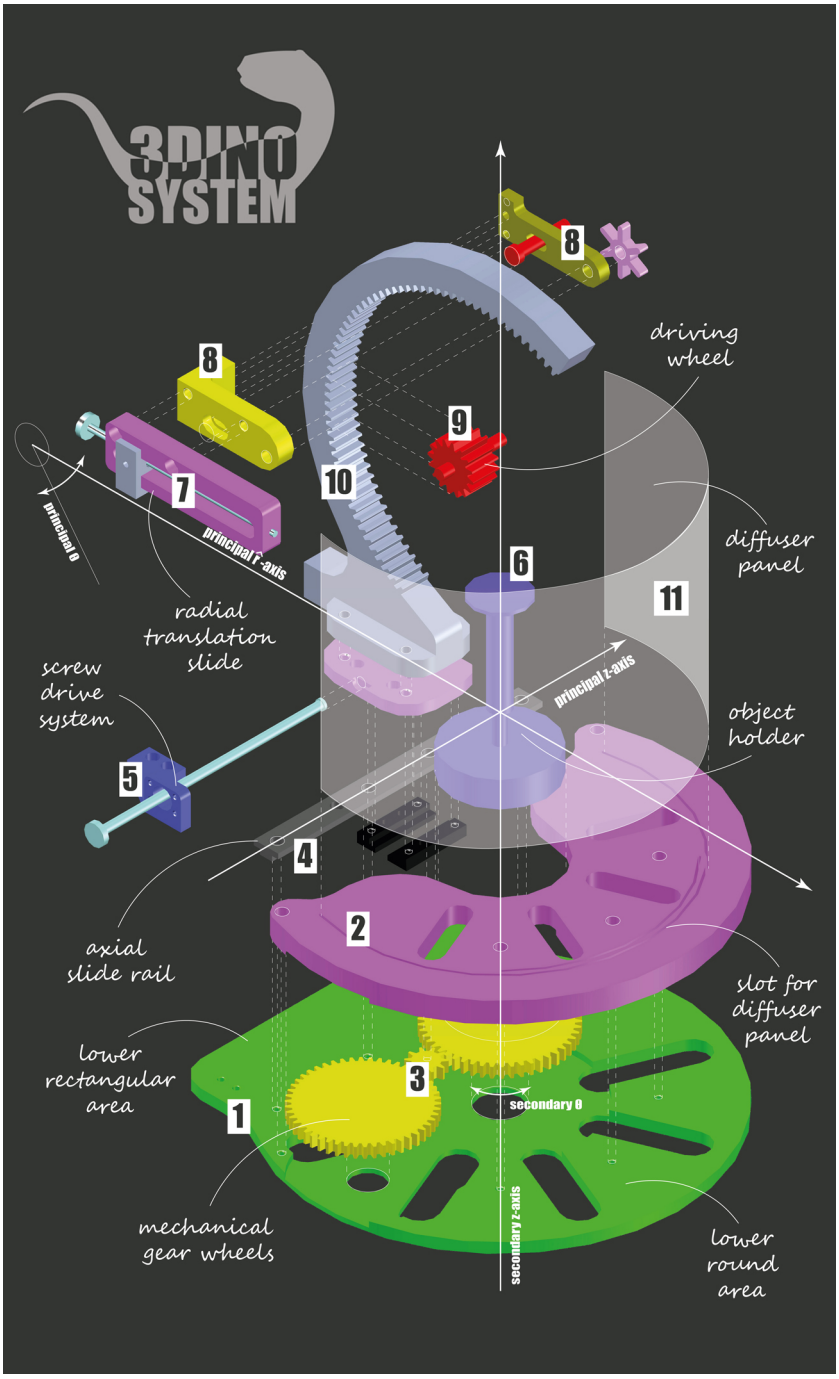

Figura 20. 3DINO SYSTEM, esploso assonometrico.

Le tolleranze di questo ingranaggio sono legate alla precisione tecnologia di stampa 3D utilizzata nella fase di prototipazione (fino a 0,2 mm). L'asse di rotazione della ruota centrale sarà indicato come asse z 'secondario'; il relativo angolo di rotazione rappresenta la coordinata θ secondaria. Al centro di tale ruota è possibile fissare un supporto (6, in viola), ad altezza regolabile (proprio lungo l'asse z 'secondario'); supporto che rappresenta la terza componente dell'attrezzatura.
In corrispondenza della zona periferica della base, per esattezza presso il limite circolare, è presente un piccolo canale atto all'inserimento di un pannello diffondente (11, in bianco semitrasparente).
La già introdotta costola è composta da una semi-ruota con dentatura interna di raggio primitivo pari a 150 mm, e una piccola ruota dentata motrice (9, in rosso) alla quale è connessa una slitta (7, in rosa) atta alla traslazione radiale dell'ottica. A tale traslazione radiale assoceremo l'asse $\hat{r}$ principale; invece, l'angolo che la slitta dell'ottica forma con l'orizzonte rappresenterà la coordinata θ 'principale'. Il modulo delle su esposte ruote dentate è analogo al precedente (pari a 2).
L'attrezzatura in definitiva presenta tre gradi di libertà per l'ottica e due gradi di libertà per l'oggetto. La coordinata θ 'principale' è legata alla rotazione della piccola ruota dentata motrice (9, in rosso), il pignone:

$$\theta = \frac{raggio\ pignone}{150\ mm} \cdot 2\pi \cdot (giri\ del\ pignone)\ . \qquad (21)$$

Dal primo prototipo sono emersi alcune imperfezioni i limiti, come ad esempio le dimensioni del piatto della stampante, in virtù del quale banalmente non era possibile stampare oggetti del diametro superiore ai 20cm. Ciò ha comportato la divisione dei pezzi più grandi in più parti, con verifiche nelle zone di giunzione. Un altro aspetto migliorato ha riguardato il peso della base, aumentato per una maggiore la stabilità del sistema e limitazione delle vibrazioni. Come ulteriori sviluppi futuri è da auspicare lo snellimento generale delle componenti massicce, quali il sistema di fissaggio della slitta micrometrica dell'ottica alla costola. Inoltre, il movimento di quest'ultima, determinato da un meccanismo vite-madrevite che spinge il sistema lungo un binario T-shape, risulta in alcuni casi faticoso per l'operatore. L'introduzione di una vite a ricircolo di sfere potrebbe aumentare la precisione (assenza di giochi interni), faciliterebbe l'operatore e risolverebbe

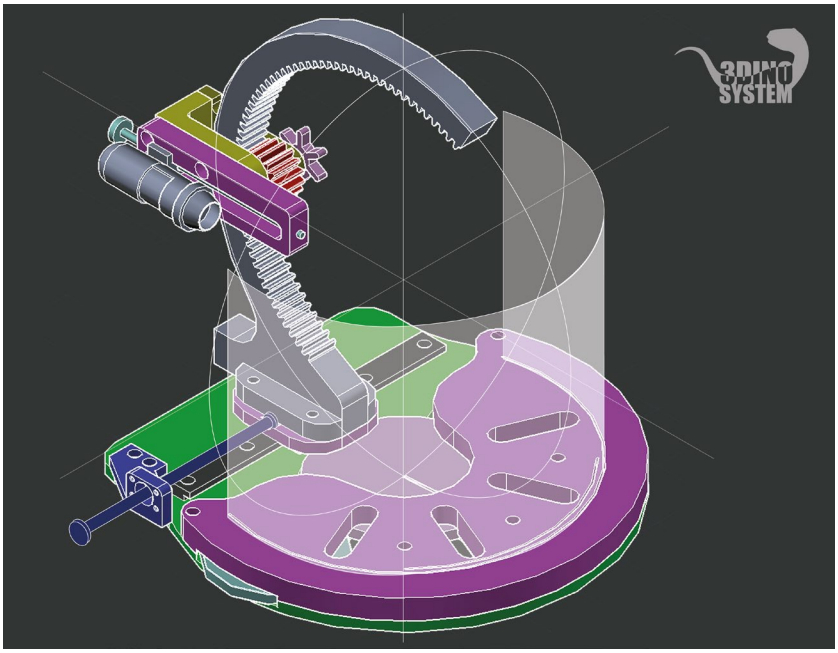

Figura 21. Assonometria del "3DINO SYSTEM" con pannello diffondente per l'illuminazione.

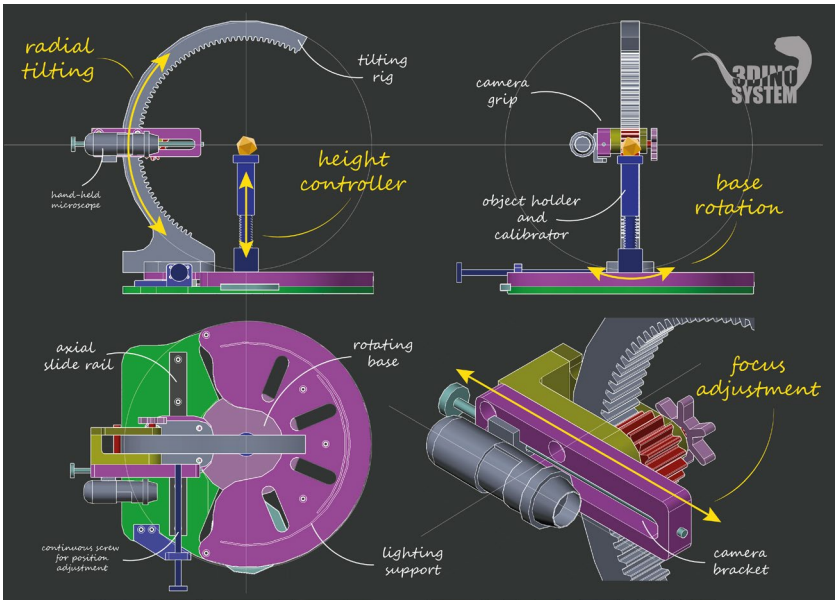

Figura 22. Schemi grafici del primo prototipo del "3DINO SYSTEM" con dettaglio (in basso a destra) del sistema di alloggiamento dell'ottica.

l'asimmetria e l'instabilità causati dallo sbalzo dell'attuale vite. Ciò consentirebbe anche di incassare il meccanismo nello spessore della base così da abbassare il baricentro del sistema e nascondere il binario. Ulteriori rettifiche potrebbero riguardare il meccanismo della costola, che, seppur valido allo stato attuale, gioverebbe di un serraggio assiale più preciso e di un meccanismo di scorrimento più fluido.

Final notes and future developments

Photographic images are enjoying a moment of particular glory and wide-ranging interdisciplinarity, possessing a number of exceptional qualities, such as speed of production and high descriptive power. In the field of surveying and representation, the widespread use of high-performance hardware at relatively low costs and the continuous implementation of new software are the reasons for the wide and frequent recourse to image-based surveying techniques.
However, extreme conditions may arise - in photogrammetry as well as in photography - breaking the current enthusiasm fuelled by the trend of miniaturisation, automatisms and instantaneous data sharing. In addition, alongside cases of exceptional complexity, the need can and must become that of controlling and refining the quality of the data, in order to obtain a greater richness of geometric description and the necessary levels of research.
Starting from these considerations, a study of the photogrammetric acquisition process for detailed survey was defined. The problems of representing small and very small objects with complex surfaces and features of less than a millimetre in size were thus addressed.
In particular, the use of new hardware for photogrammetry, the USB microscopes, and the customisation of accessories designed ad hoc for the insertion of these instruments in the photogrammetric procedure, constitute the most innovative part of the experimentation, whereby the various case studies provided an opportunity to validate what was proposed. Furthermore, the idea of implementing USB microscopes paves the way for new lines of research. In addition, the accessibility of surveying is enhanced, constituting a significant step in the transfer of knowledge and practices.
From the point of view of the surveyor, what emerges is confirmation of a complex framework in which specialised theoretical foundations and strong practical experience are required. Moreover, the topic's affiliation to several sectors accentuates the challenges in absence of contextualisation and systematic approach to both data acquisition and processing. Nevertheless, the continuous search for completeness,

manifested in the identification of significant case studies and the iterative refinement of processes, reflects the original nature of the theme, making this thesis one of the first on the international scene to deal with photogrammetric microscopic surveying.
It is desirable to imagine that the proposed methodology could be adapted to new scenarios, for example by including computational photography techniques and the development of remote control of optics according to designed acquisition plans, as is the case nowadays with flight plans for UAV devices, which would allow us to increasingly objectivise our work as imaging technicians.
Research is moving towards the structuring of rigorous close-range procedures that go through the entire representation process, from project planning to model generation, with the inclusion of different knowledge. The intention is to draw attention to the need not to fall into the simplistic use of software: indeed, attention must be paid - pursuing the teachings of Professor Vito Cardone - to avoiding that the infographic themes of surveying and representation are reduced to a mere execution of commands or tools already available with approaches disconnected from any theoretical framework or context.

Note finali e sviluppi futuri

Le immagini fotografiche godono di un momento di particolare splendore e di ampia interdisciplinarità, raccogliendo una serie di eccezionali qualità, come la rapidità di realizzazione e l'elevata capacità descrittiva. Nell'ambito del rilievo e della rappresentazione la grande diffusione di hardware performanti a costi relativamente contenuti e l'incessante implementazione di nuovi software costituiscono le ragioni dell'ampio e frequente impiego di tecniche di rilievo image-based.

Tuttavia, possono determinarsi condizioni limite – in fotogrammetria così come in fotografia – che spezzano l'incanto attuale alimentato dal trend della miniaturizzazione, degli automatismi e dell'istantanea condivisione del dato. In aggiunta, accanto a casi di eccezionale complessità, l'esigenza può e deve divenire quella di controllare e perfezionare la qualità del dato, per ottenere una maggiore ricchezza della descrizione geometrica e dei necessari i livelli delle ricerche.

A partire da queste considerazioni si è definito uno studio del processo di acquisizione fotogrammetrica per il rilievo di dettaglio. Sono state così affrontate le problematiche della rappresentazione di piccoli e piccolissimi oggetti con superfici complesse e caratteristiche di dimensioni inferiori al millimetro.

In particolare, l'impiego di nuovi hardware per la fotogrammetria, i microscopi USB, e la customizzazione di accessori ideati ad hoc per l'inserimento di tali strumenti nel procedimento fotogrammetrico, costituiscono la parte più innovativa della sperimentazione, con i diversi casi studio che hanno costituito l'occasione per validare quanto proposto. Inoltre, l'idea di implementare microscopi USB apre la strada a nuovi filoni di ricerca. A ciò si aggiunge il rafforzamento dell'accessibilità al rilievo, il che costituisce un passo significativo per il trasferimento di conoscenze e di pratiche.

Dal punto di vista del rilevatore, quello che emerge è la conferma di un quadro complesso in cui sono necessarie basi teoriche specialistiche e forti esperienze pratiche. Inoltre, l'afferenza del tema a più settori, accentua le difficoltà in assenza di una contestualizzazione

e di un approccio sistematico sia all'acquisizione che al trattamento dei dati. Ciononostante, la continua ricerca della completezza, manifestata nell'identificazione di casi studio significativi e nel perfezionamento iterativo dei processi, riflette la natura originale del tema, che posiziona questo lavoro di tesi tra i primi nel panorama internazionale ad occuparsi di rilievo microscopico fotogrammetrico.
È auspicabile immaginare che la metodologia proposta possa essere adattata a nuovi scenari, ad esempio includendo tecniche di fotografia computazionale e lo sviluppo di un controllo remoto delle ottiche secondo dei piani di acquisizione progettati, come accade oggi coi i piani di volo per dispositivi UAV, il che consentirebbe di oggettivizzare sempre più il nostro lavoro di rappresentatori.
Le ricerche si stanno muovendo verso la strutturazione di procedure close-range rigorose che attraversino tutto il processo di rappresentazione, dal project planning alla generazione dei modelli, con l'inclusione di saperi differenti. L'intento è quello di porre l'attenzione sulla necessità di non cadere nella semplicistica utilizzazione di software: l'attenzione, infatti, deve essere riposta – perseguendo gli insegnamenti del professore Vito Cardone – nell'evitare che le tematiche infografiche del rilevamento e della rappresentazione siano ridotte a una mera esecuzione di comandi o strumenti già disponibili con approcci avulsi da qualsiasi impianto o contesto teorico.

Ringraziamenti

A conclusione dei lavori desidero ringraziare tutti coloro che hanno gravitato attorno a questa tesi, docenti, ricercatori, studiosi, amici, ma soprattutto persone profondamente curiose, appassionate e ispirate quotidianamente dalla ricerca.

Porgo un sentito ringraziamento al mio tutor, il professore Salvatore Barba, che mi ha offerto la possibilità di avviare questa ricerca e che non ha mai perso occasione per valorizzarla. Il dialogo continuo ed estremamente proficuo, l'attenzione riposta e la disponibilità dimostrata sono solo alcuni dei motivi che mi hanno spinto a riporre completa fiducia in lui sia durante la stesura della tesi di laurea magistrale che per il percorso di dottorato.

Un ringraziamento particolare va anche al mio co-tutor, il Dott. Massimo Leserri, che con attenzione e interesse ha supervisionato sul lavoro in questi anni.

Ringrazio la IDCP Digital Innovation, nelle persone di Jan Boers, Danielle van Duijvendijk e Ivo Manders, distributore di Dino-Lite Microscopes in Europa per aver stipulato un accordo di trasferimento tecnologico con il Laboratorio Modelli dell'Università di Salerno, consentendo l'impiego fruttuoso dei microscopi USB per le sperimentazioni fotogrammetriche.

Un ringraziamento particolare a: Diego Ronchi, ISPC – Consiglio Nazionale delle Ricerche, le cui intuizioni hanno gettato le basi di questo lavoro e a Fausta Fiorillo, Politecnico di Milano, grazie alla cui esperienza e alle opportunità fornitemi con l'organizzazione di un tirocinio formativo la ricerca si è potuta perfezionare.

Grazie a tutti i co-autori dei contributi scientifici pubblicati, la cui collaborazione ha ampliato le possibilità del lavoro e arricchito i contenuti: Francesco Di Paola e Sara Morena, Università degli Studi di Palermo; Mirko Surdi, Ghent University; Marco Limongiello, Andrea di Filippo, Anna Sanseverino, Luigi Vecchio, Francesco Villecco e Nicola Cappetti, Università degli Studi di Salerno; Anna Dell'Amico, Università degli Studi di Pavia. Ringrazio, inoltre, il Dipartimento di

Scienze del Patrimonio Culturale – DISPAC dell'Università degli Studi di Salerno, in particolare, Renata Cantilena, Giacomo Pardini e Federico Carbone per avere aperto le porte del proprio laboratorio alle sperimentazioni della mia ricerca; il Dipartimento di Ingegneria Industriale – DIIN dell'Università degli Studi di Salerno, nelle persone di Fabrizia Caiazzo, Vittorio Alfieri e Paolo Argenio per la prototipazione del calibratore circolare in acciaio e Francesco Villecco, Damiano Fortuna e Vincenzo Russo per la progettazione e la stampa del primo prototipo del sistema di sostegni per la scansione fotogrammetrica denominato "3DINO".
Grazie a La Unidad de Investigación, Desarrollo y Transferencia - Grupo de Ingeniería Gráfica Aplicada de la Facultad de Ingeniería de la Universidad Nacional de La Plata (Argentina) che ha seguito con crescente interesse gli sviluppi di questa ricerca, in particolare a Gabriel Horacio Defranco.
Grazie ai musei che hanno accolto con entusiasmo l'iniziativa, quali il Museo Archeologico Nazionale di Vibo Valentia, il Museo Archeologico Nazionale di Crotone e il Museo Archeologico Nazionale di Capo Colonna, in particolare al Direttore Gregorio Aversa, nonché a Naos LAB, nell'ambito dei progetti V.I.S.A. e Kroton LAB. Ringrazio, inoltre, Katrien De Graef (Ghent University), Catherine Mittermayer (University of Geneva), Marinella Levi (+LAB, Politecnico di Milano) e 3D SurveyGroup per la condivisione di set di dati e materiali.
Un ringraziamento particolare per il lavoro di attenta revisione va a Laura Lopresti, Universidad Nacional de La Plata e a Francesco Fassi, Politecnico di Milano. Ci tengo, infine, a ringraziare il Laboratorio Modelli del Dipartimento di Ingegneria Civile dell'Università degli Studi di Salerno che, da oltre quattro anni, ormai, costituisce un riferimento fondamentale per lo sviluppo scientifico del mio lavoro.

Sara Antinozzi


ATICA CIVITAS
UM SALERNI